GIS-BASED MULTI-CRITERIA DECISION MAKING UNDER SILICA SATURATION INDEX (SSI) FOR SELECTING THE BEST DIRECT USE SCENARIOS FOR GEOTHERMAL RESOURCES IN CENTRAL AND SOUTHERN RIFT VALLEY, KENYA

ニェテ, ジョン

九州大学
KYUSHU UNIVERSITY

GIS-BASED MULTI-CRITERIA DECISION MAKING UNDER SILICA SATURATION INDEX (SSI) FOR SELECTING THE BEST DIRECT USE SCENARIOS FOR GEOTHERMAL RESOURCES IN CENTRAL AND SOUTHERN RIFT VALLEY, KENYA

By

NGETHE John

A thesis submitted to Kyushu University
For a degree of Doctor of Engineering

Department of Earth Resources Engineering
Graduate School of Engineering
Kyushu University
Fukuoka, Japan.

March, 2023

KYUSHU
UNIVERSITY

九州大学

A DOCTORAL DISSERTATION

By

NGETHE John

January, 2023

GIS-BASED MULTI-CRITERIA DECISION MAKING UNDER SILICA SATURATION INDEX (SSI) FOR SELECTING THE BEST DIRECT USE SCENARIOS FOR GEOTHERMAL RESOURCES IN CENTRAL AND SOUTHERN RIFT VALLEY, KENYA

Submitted by

NGETHE John

Dissertation Submitted in Partial Fulfilment of the

Requirements for The Degree of

Doctor of Engineering

(Earth Resources Engineering)

Supervised by

Associate Professor Dr. Saeid Jalilinasrabady

Energy Resources Engineering Laboratory

Department of Earth Resources Engineering,

Graduate School of Engineering, Kyushu University, Japan,

January, 2023

Abstract

Geothermal energy is ubiquitous in the earth's crust, and its utilization has increased rapidly recently, anchored on its primary merits of low carbon emissions, renewability, and reliability. Using renewable energies is one of the fundamental strategies for decarbonizing the energy sector. The primary aim is to mitigate global warming by limiting global temperature rise to 2°C by 2100, as stipulated in the Paris Agreement of 2015. The world economies need to shift their energy sources for thermal needs to include renewables, more so geothermal, solar, and bioenergy, to attain the Paris Agreement of 2015 goal. The utilization of geothermal energy is conventionally categorized into two major classes: the production of electricity (indirect use) and heating (direct use). Electric generation involves the use of steam and hot brine at temperatures ranging from 120 – 200°C, while thermal uses utilize hot brine at 30 – 150°C. Using geothermal resources to meet thermal needs such as heating water for bathing, horticultural greenhouse warming, residential/space heating, aquacultural pond heating, and industrial heating is defined as the direct use (DU) of geothermal energy. Although geothermal energy is best suited to address some modern thermal needs, in 2021, DU of geothermal energy only accounted for 0.77 percent of all thermal energy use worldwide. DU of geothermal energy is site-specific and majorly dictated by economics. Even with the availability of high enthalpy geothermal fluids, DU could still be curtailed by fluid pH, salinity, and silica content. Selecting economically viable best DU scenarios for a given geothermal resource needs meticulous matching of geothermal resource characteristics to the nearby economic activities and local infrastructure. Silica saturation index (SSI) analysis should also be factored in to avoid silica scaling of DU facilities and reinjection well. There is a lack of a visual framework for incorporating all the necessary criteria for selecting the best DU scenarios, hence the motivation of this research. The current study employed a GIS-based Multi-Criteria Decision-Making (MCDM) method: a hybrid of the analytical hierarchy process (AHP) method with the weighted aggregated sum product assessment (WASPAS) method. The model analyzed nine utilization scenarios against eleven criteria to select the best DU scenarios for six high-enthalpy quaternary volcanoes and ten low-enthalpy resources in the central and southern Kenyan rift. The best typical DU schemes identified were horticultural greenhouse warming, spa/bathing, and crop drying. The model was validated with existing DU case studies to gauge its ability to predict suitable utilization methods. There was a good match between the model's selection and existing case studies implicating the synergistic merger of GIS-based MCDM methods and SSI as a robust tool for planning and carrying out the feasibility study for DU of geothermal energy.

The outcome of this research will contribute to the overall understanding of selecting the best direct-use scenarios for each geothermal resource based on its fluid characteristic, local economic activities, and enabling local infrastructure. The study also characterizes high, medium, and low enthalpy geothermal resources, with or without productive deep wells or hot springs. The contents of the dissertation consist of seven chapters below:

Chapter 1 introduces the background of the study, the introduction of direct use of geothermal energy in high and low enthalpy geothermal resources, the geothermal status in Kenya. This chapter describes the research objectives and methodology.

Chapter 2 reviews geothermal state-of-the-art methods of classifying geothermal resources according to geology, temperature, and developmental status. Also reviewed in the chapter are the multi criteria decision making (MCDM) methods, criteria weighting, 2D inverse distance weighted and ordinary kriging interpolation methods of point vector data. Provided herein are brief reviews

of the relevant prior works on Geographic Information Systems (GIS), Remote Sensing (RS) of satellite images for land use classification, and location selection. Additionally, the innovative concept of enhancing silica solubility for moderately to highly alkaline geothermal resources by raising pH above 8.5 is presented.

Chapter 3 introduces the procedures of using MCDM methods in QGIS are expounded on, where the specific MCDM methods being (AHP-WASPAS hybrid) are outlined. The reasons and the procedures of selecting the 2D interpolation methods. Remote sensing, creation of criteria map layers and rasterization of vector data are given. Finally, the chapter summarizes the model for selecting the best use scenarios.

Chapter 4 expounds on the novel method of identifying and characterizing high enthalpy geothermal resources for direct use. The chapter analyzes six high enthalpy geothermal resources in central and southern Kenyan Rift Valley: Menengai, Elementaita, Eburru, Olkaria, Longonot and Suswa. The heat demands at the Olkaria, Eburru, and the Menengai geothermal fields were 180 MWt, 650 MWt, and 2050 MWt, respectively. Hence, Menengai and Eburru geothermal fields have more heat demands than Olkaria, while Olkaria has more volumes of disposable steam and brine compared to them.

Chapter 5 focuses on selecting geothermal resources in medium to low enthalpy geothermal resources with no deeper wells. The chapter identifies the significant role hot springs play by providing warm to hot fluids for direct use. The chapter expounds on hydrogeochemistry analysis of hot spring water and the use of resultant data to do exergetic classification of medium to low enthalpy geothermal resources in Kenya. Finally, the chapter selects best direct use scenarios for hot spring using GIS-based hydrogeochemistry data and economic enabling factors near the geothermal resource. The hot springs were discovered to provide approximately 275 MWt of heat, which is significant for direct usage.

Chapter 6 reviews all the direct use case studies in Kenya and tries to use them to validate the GIS-based MCDM selection model introduced in this study. The validation identified some case studies in high suitability areas while others were in areas classified as medium suitability. Even though those case studies that coincided with high suitability locations were financially viable, their establishment did not consider the results of the current study. The rest are of smaller scale and not economically sustainable.

Chapter 7 summarizes the overall conclusions and recommends future work optimizing geothermal resources in Kenya for direct use.

Acknowledgement

I would like to express my sincere gratitude and appreciation to my supervisor Associate Professor Saeid Jalilinasrabady for his guidance, encouragement, and support during my study life in Japan. I also wish to thank all the members of Energy Resources Engineering laboratory for their contribution to my research in their various capacities. More so Rie Yamashiro for her immeasurable help with laboratory geochemical analysis of water samples. I also want to appreciate Dr Eri Inou for his guidance in collection of field samples and interpreting results of geochemical analysis. I will forever remain indebted to Dr. Kiprono Alvin for making my publishing life easier. I also extend my appreciation to Prof. Yasuhiro Yamada and Arata Kioka for making the laboratory life feel like home.

Sincere appreciation goes to JICA, for the Kizuna scholarship which catered for overseas field trips and conferences. And for financing my studies at Kyushu University and life in Fukuoka.

I also want to thank the management of Jomo Kenyatta University of Agriculture and Technology (JKUAT) for granting me study leave for three years to study.

Great appreciation goes to Kenya Electricity Generating Company (KenGen) represented by Mr. Apondo Kizito for availing the data for research. Likewise, I want to acknowledge the invaluable help of Oserian Development Company Limited (ODCL) for availing geothermally heated fresh cut rose flowers greenhouses data. Specifically, I want to thank Mr. Apollo Opondo for his advice and suggestion.

Finally, I want to thank my family; Kamau, Freddie, Lucy, Christabel, and my mum for all their prayers, encouragements and help during my stay in Japan. Finally, much love goes to Sofia and Flynn for their perseverance during my absence.

Dedication

For my daughter Sofia, and son Flynn.
And their mother, Christabel.

“It always seems impossible until it is done.” Nelson Mandela.

Table of Contents

List of Figures

List of Tables

CHAPTER ONE

1. INTRODUCTION

The world is striving to cap global temperature rise to 2°C by 2100, as stipulated by the Paris Agreement 2015. A pathway to this goal is to replace the fossil fuels with renewable energy, such as solar, wind, hydropower, geothermal, ocean power and bioenergy. Unfortunately, solar, wind, hydropower, ocean power and bioenergy are susceptible to weather variations. They also have lower energy densities compared to fossil fuels. Geothermal energy excels as key renewable energy because it is reliable, emits lower greenhouse gases (CO_2, H_2S, CH_4) and ubiquitous in the earth's crust. Unlike the aforementioned renewable energy sources, geothermal energy can provide thermal energy directly with a temperature range of 25 – 200°C.
Utilization of geothermal energy is conventionally categorized into two major classes: production of electricity (indirect use) and heating (direct use), as shown in Figure 1.1. Electric generation involve use of steam and hot brine at temperatures ranging from 120 – 200°C, while thermal uses utilize hot brine at 25 – 150°C.

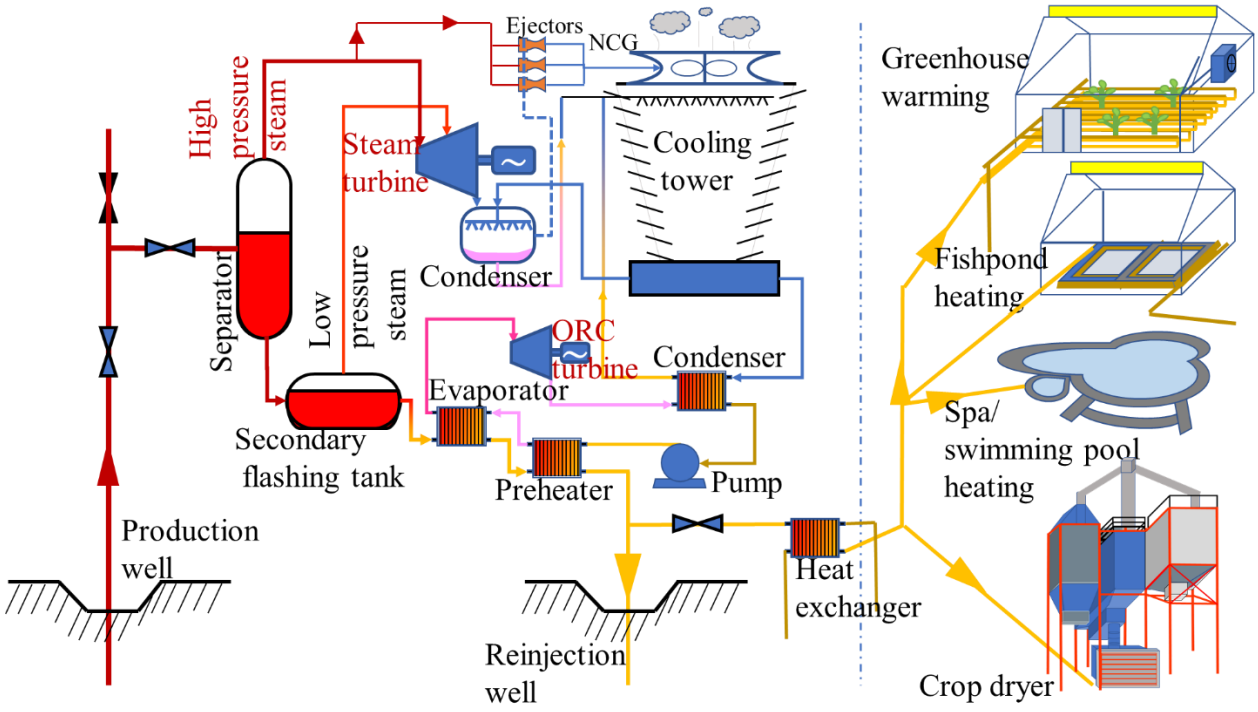

Figure 1.1 Electric power generation and direct use of a conventional high enthalpy geothermal resource for maximu utilization efficiency.

Using geothermal resources to meet thermal needs such as heating water for bathing/swimming, horticultural greenhouse warming, residential/space heating, aquacultural pond heating, and industrial heating is defined as the direct use (DU) of geothermal energy. In the last two and half decades, DU of geothermal energy has enjoyed a steady annual growth, especially in residential/space heating and bathing/swimming, by 8.3% and 6.6%, respectively, as shown in Figure 1.2 (Lund & Toth, 2021a).

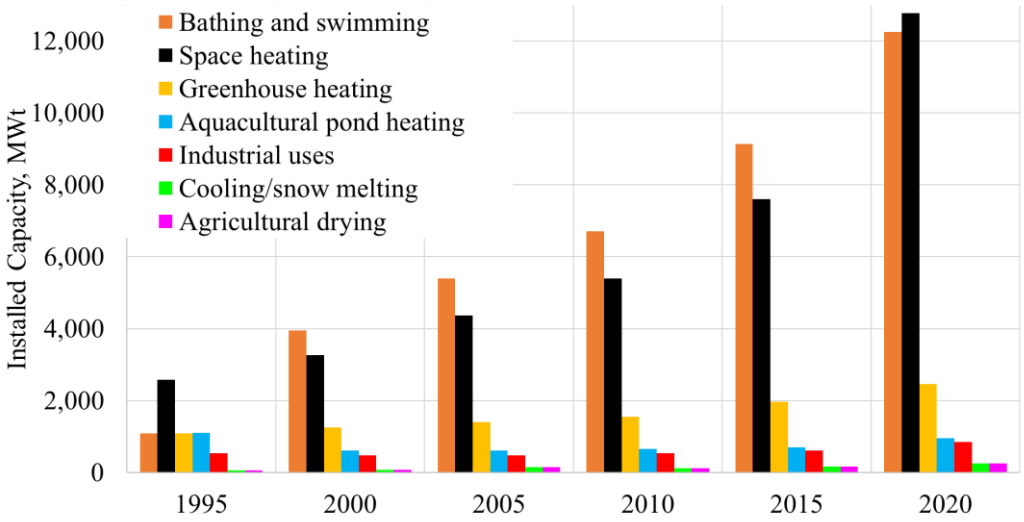

Figure 1.2 The global growth of different direct use scenarios over time in MWt, (excluding ground heat pumps) (Lund and Toth, 2021).

Although geothermal energy is best suited to address some modern thermal needs, in 2021 DU of geothermal energy only made up 0.77 percent of all thermal energy use worldwide (Lund & Toth, 2021a). Inclusion of ground source heat pumps boosts DU of geothermal energy to 1.55% of the total global thermal energy usage (REN21, 2022). The low percentage of global geothermal usage could be attributed partly to the sparse distribution of high enthalpy geothermal resources, compounded by the high risks and costs associated with developing geothermal fields.

1.1 Background of the study

Kenya lies in the equator, to the east of African continent. It is neighboured by South Sudan to the northwest, Ethiopia to the north, Somalia to the northeast, Tanzania to the south and Uganda to the west, as depicted by **Error! Reference source not found.**. Kenya covers an area of 581,309 k m^2 and experiences tropical climate, which often include prolonged droughts. Kenya uses energy from various sources for both generation of electricity and heating. For generation of electricity, Kenya has installed capacity of 678Mwe fossil fuels (diesel), 863 MWe geothermal, 838 MWe hydro, 436 MWe wind, 2 MWe biomass, and 173 MWe solar, by end of 2021. In homes, cottage businesses including firing bricks, bakeries, industrial processing of sugar, tea, vegetable oils, pharmaceuticals, as well as in schools and restaurants, bioenergy (firewood) predominates cooking and heating by over 90%. LPG, charcoal, and kerosene supply 30% of thermal needs for the Kenyan urban population, though still dwarfed by firewood usage. The harm caused by bioenergy derived from forests extends beyond the devastation of ecosystems, soil, biodiversity, and carbon sequestration systems. It also causes rivers to dry up, which hinders the production of hydropower and forces the impacted countries to use more fossil fuels to make up for lost hydroelectric capacity (Njenga et al., 2021; Tchobsala et al., 2022). Kenya imposed a ban on logging and other wrong forestry practices in 2018. Kenya's forest cover has now increased to 8.83 percent in 2021 from 5.9 percent in 2018, although additional efforts are needed to increase the tree cover to 10% mandated under Article 69, Section 1 (a) of the Kenyan constitution. (Kenya Forest Service, 2021). The transportation sector in Kenya is predominantly 100% fueled by petroleum sources.

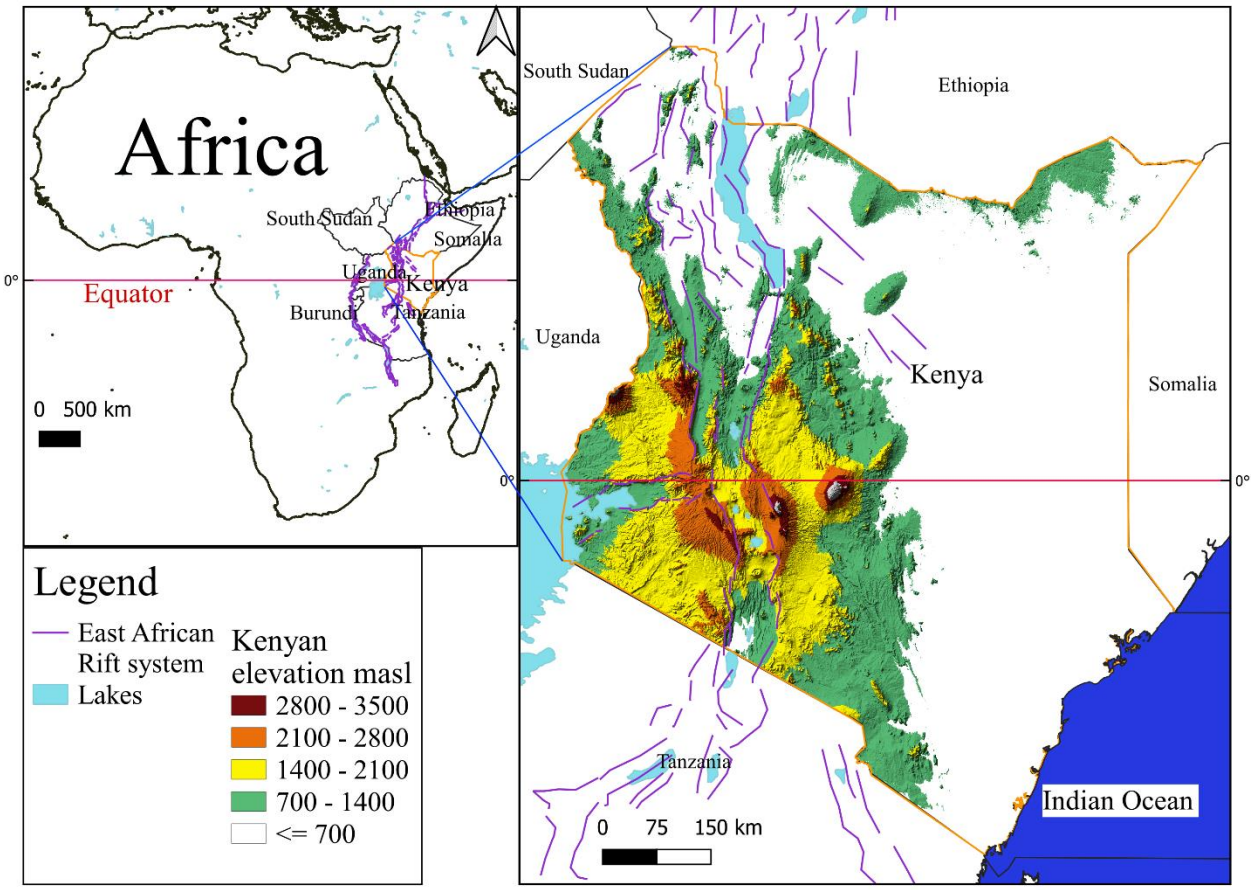

Figure 1.3 Location of Kenyan in African continent and its elevation in meters above sea level.

Though geothermal energy constitutes 29% of the installed electricity capacity, it contributes up to 44% of the daily dispatched power. Almost the entire 863 MWe. is generated from Olkaria geothermal field except for 1.8 MWe generated from Eburru geothermal field. Menengai, Paka, and Korosi geothermal fields have production wells in place though power plants are yet to be installed to actualize more geothermal capacity. To this end, several research works have been dedicated to optimizing geothermal reservoirs and power plants for power production (Bett & Jalilinasrabady, 2021a; Kanda et al., 2019; Maithya et al., 2020).

The densely populated parts of Kenya have an altitude of 700 – 3500 m above sea level, as shown in **Error! Reference source not found.**. The high altitude renders most regions with cooler c limates despite Kenya straddling the equator. In addition, Kenya's economy heavily depends on agriculture, more so on export of tea, coffee, fresh-cut flowers, vegetables, fish, as well as international tourism. These economic activities present heating demands in form of heat for drying crops, heat for warming horticultural greenhouses, aquacultural ponds, and swimming pools/spas. As forementioned, Kenya heavily relies on firewood and fossil fuels for heating especially in industries, crop drying (tea, maize, wheat, beans), and greenhouses. For instance, processing of one tonne of brown tea requires felling 14 trees. This research seeks to carry out a feasibility study on how geothermal energy can replace the firewood and fossil fuels in greenhouse warming, aquacultural pond heating, heating of spas/ swimming pools, crop drying, water desalination, just to name a few.

This research encompasses six high enthalpy geothermal resources (Menengai, Elementaita, Eburru, Olkaria, Longonot, Suswa) and ten low enthalpy geothermal resources (Homa Hills, Kipsegon, Olchorro, Majimoto, Narosura, Lake Magadi, Kijabe, Kariandusi, Lake Bogoria, and Arus), as shown in Figure 1.4.

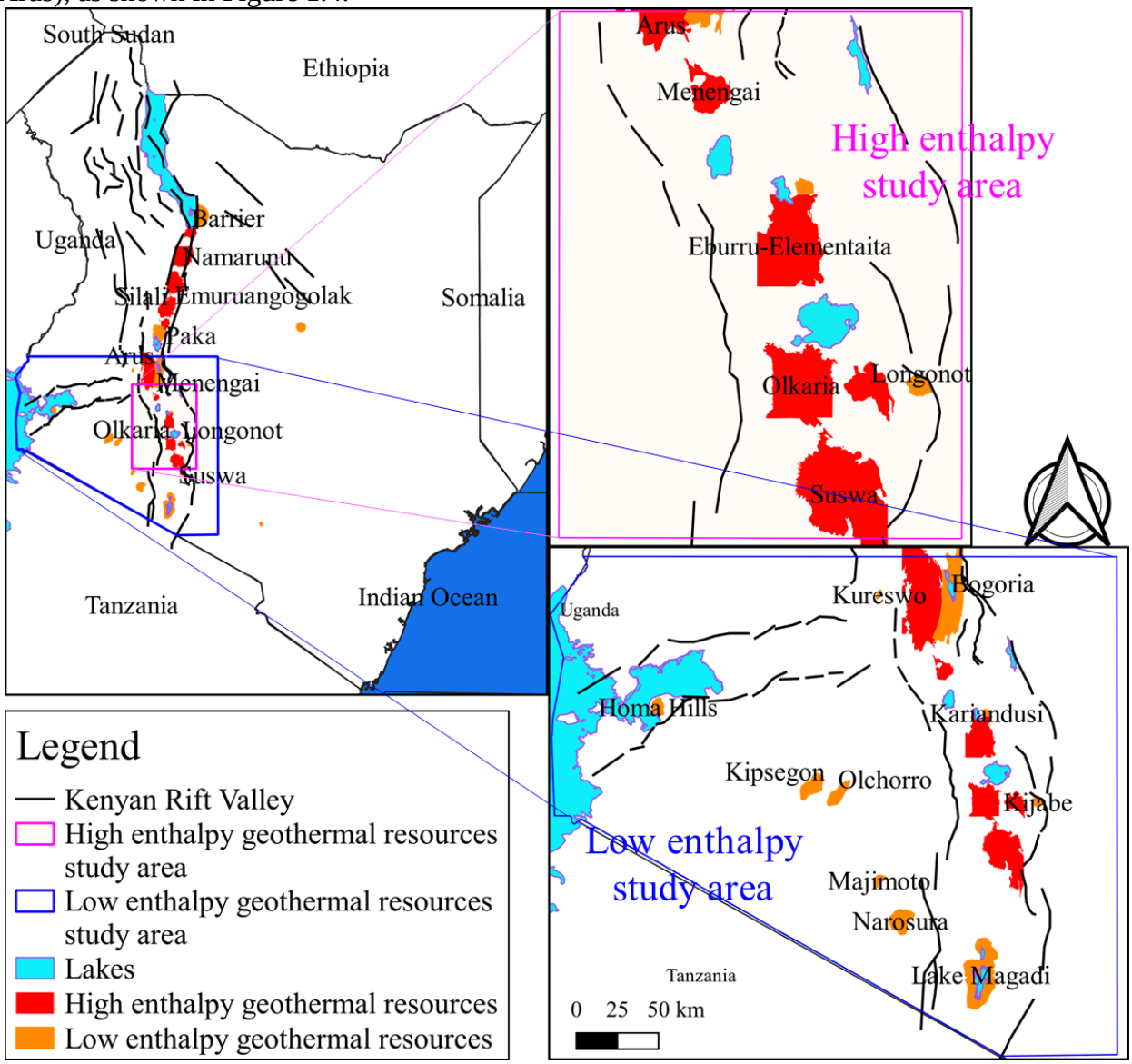

Figure 1.4 Maps showing high (in red) and low (in brown) enthalpy geothermal reouces considered under the current study and the boundaries of their respective study areas within Kenya.

1.2 Geothermal energy

Geothermal is considered a renewable form of energy generated and stored within the earth's core. Low temperature geothermal energy is accessible almost everywhere in the earth's crust, while high temperature resources are associated with active volcanic areas close to plate tectonic boundaries (DiPippo, 2016; Magnus and Victor, 2012). The high enthalpy geothermal energy resources are mainly distributed along the rim of major tectonic subduction zones (Shortall et al., 2015). Geothermal has been identified in over 90 countries and utilized in at least 88 nations (Lund

and Toth, 2021b). Geothermal capacity in the world has been growing since its first industrial application in 1912 in Italy (Watson, 2013). The total installed electricity capacity from worldwide geothermal power plants is currently around 16 GWe and direct use of over 59GWt, without inclusion of ground source heat pumps (REN21, 2021).

A hydrothermal system thrives when three elements exist in unison: a heat source, high permeability, and water for recirculating the heat (Huenges, 2010). There are four major types of heat sources for hydrothermal systems: magmatic intrusions, chemical reaction (hydration of peridotite ("serpentinization reaction")), radioactive decay and geothermal gradient (Erfurt, 2021; Lowell and Rona, 2005).The aqueous liquid in hydrothermal systems originate from descending meteoric water, though magmatic/connate waters may be present in small quantities. Caprock, mostly composed of kaolinite, calcite, illite-smectite minerals as mixed layers, help to contain fluids at temperatures above 100°C which are then exploited for power production after deep drilling (Corrado et al., 2014). For the sustainable development of any geothermal system, there should be a reliable recharge mechanism (Jalilinasrabady, 2011). To access the geothermal resource, the geological and hydrological frameworks should be studied and understood (DiPippo, 2016; Glassley, 2012). Surface manifestations such as hot springs, fumaroles, geysers or warm pools, and volcanoes indicate geothermal energy availability (Erfurt, 2021). The majority of high temperature geothermal prospects are primarily located in active volcanic regions, such as those along tectonic plate boundaries (plate convergent zones) like the Pacific Ring of Fire, which circles the Pacific Ocean, or continental plate rifting regions, like the African Rift Systems (Masum and Akbar, 2019). Between the earth's surface and the crust, the average temperature gradient and heat fluxes are 2.5 - 3.1ºC/100 m and $1.2x10^{-6}$ cal/cm^{2}·s, respectively (DiPippo, 2016). The rocks in the crust are responsible for natural conduction of heat to the surface at a rate of 1.8 to 5 W (m°C) (Lowell and Rona, 2005).

Best scenario utilization of geothermal energy depends on the nature and characteristics of the hydrothermal system. For the optimal exploitation of geothermal energy, investment is required from conception to project retirement. The main exploration techniques include geochemistry, geophysics, and environmental and/social-economic studies.

1.3 Uses of geothermal energy

Utilization of geothermal energy is conventionally categorized into two major classes: production of electricity (indirect use) and heating (direct use). Electric generation involve use of steam and hot brine at temperatures ranging from 120 – 200°C, while thermal uses utilize hot brine at 25 – 150°C. These uses are described in detail in the Lindal's chart, Figure 1.5, depending on temperature and site of utilization. While many studies have majored on either flash technology and/or organic Rankine (ORC) techniques of electricity generation, the current study majors on direct use. Direct use of geothermal energy encompasses use of both deep and shallow geothermal resources for heating and cooling. The nature of use is quite site-specific with most renowned uses being district heating in Iceland, spa/bathing in Japan, greenhouse warming in Kenya, space warming and cooling in China, heated swimming pools and hot spring geotourism in USA. Hot spring tourism, aquacultural pond heating, greenhouse warming, space heating, crop drying, and snow melting are common to many nations that have geothermal resource. The major regions that have invested in direct use of geothermal energy are the Europe, Asia, North America, and the Common Wealth Independent States, as shown in Figure 1.6.

Figure 1.5 Uses of geothermal energy depending on temperature of fluid conveyed to the surface, modified from Dipippo (DiPippo, 2012)

The major merit of direct use is its ability to use low enthalpy resources such as hot springs, fumaroles, geysers, and cascaded use of hot water from power plants.

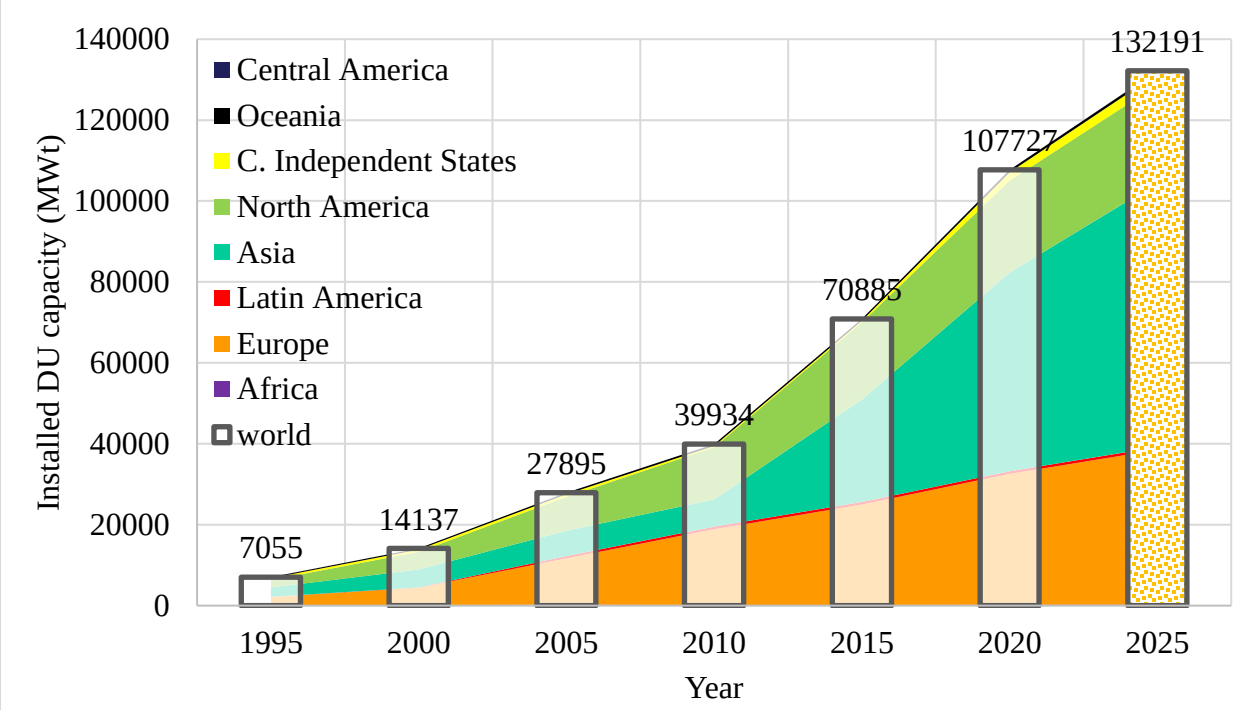

Figure 1.6: World DU of geothermal energy status by region (1995-2025) (Lund et al., 2005, 2011; Lund and Boyd, 2016; Lund and Freeston, 2001; Lund and Toth, 2021b).

1.4 Energy situation in Kenya

Electricity, petroleum, and biomass account for 6%, 19%, and 75% of Kenya's key energy sources, respectively. In remote areas, biomass serves as the primary fuel source (Kiplagat et al., 2011). The food and agricultural processing industries such as tea, vegetable oil, baby food processors, and cosmetic factories use firewood boilers to generate processing steam. Kenya's installed electricity capacity consists of about 70% renewables The target is to have at least 65% of electricity penetration by 2022 (Takase et al., 2021). The government is focused on encouraging more renewable power plants (Power Africa, 2016). The primary sources of electricity are geothermal and hydropower, which account for 25% and 35% of installed generation capacity, respectively. Geothermal is ranked first in installed capacity out of the total installed capacity of 3 GWe, having a capacity of 1,193 MWe. With 336 MWe of installed capacity, wind energy dominates as the largest installed in the continent of Africa. (Murage and Anderson, 2014; Takase et al., 2021).

Table 1.1: Electricity installed capacity in Kenya 2014 - 2020 (Kazimierczuk, 2019; Kiplagat et al., 2011; Omenda et al., 2020; Omenda, 2010).

Sources	**2014**	**2015**	**2016**	**2017**	**2018**	**2019**	**2020**
	Installed capacity (MWe)						**Forecasted Capacity (MWe)**
Hydro	822	828	829	834	837	837	921
Geothermal	366	619	663	673	847.4	1,193	1,984
Wind	6	26.1	26.1	26.1	336.1	336.1	786
Solar	17	31	32	38	93	95	430
Thermal	-	833.6	801.6	806.9	807.7	749.3	751
Cogeneration	-	26	28	28	28	28	28
Bioenergy/Bagasse	67	38	88	88	88	88	108
Gas turbine	60	60	60	60	60	60	60
Total renewable	1,211	1,504.1	1,550.1	1,571.1	2,113.5	2,461.1	4,121
Total non-renewable	60	919.6	889.6	894.9	895.7	837.3	839
Total capacity	**1,271**	**2,423.7**	**2,439.7**	**2,466**	**3,009.2**	**3,298.4**	**4,960**

Between 2014 and 2020, Kenya's energy sources are depicted in Table 1.1 and Figure 1.7. In comparison to non-renewable energy sources, renewables have grown quickly as their installed capacity has increased. The main source of new renewable energy is geothermal. Noteworthy observation is that no significant capacity has been added to diesel fueled power plants since 2015 and a significant number of them are expected to be decommissioned by 2035. The frequent and prolonged droughts exacerbated by deforestation and climate change have curtailed expansion of hydropower since 2014. Commissioning of a 340 MWe of wind energy in 2020 at Lake Turkana was a major step towards commitment of going green by the Kenyan power sector. Kenya has committed towards going green in electric power sector, but the heat energy sector is predominantly dominated by firewood and fossil fuels. However, expansion of direct use has been minimal, as depicted in Figure 1.8.

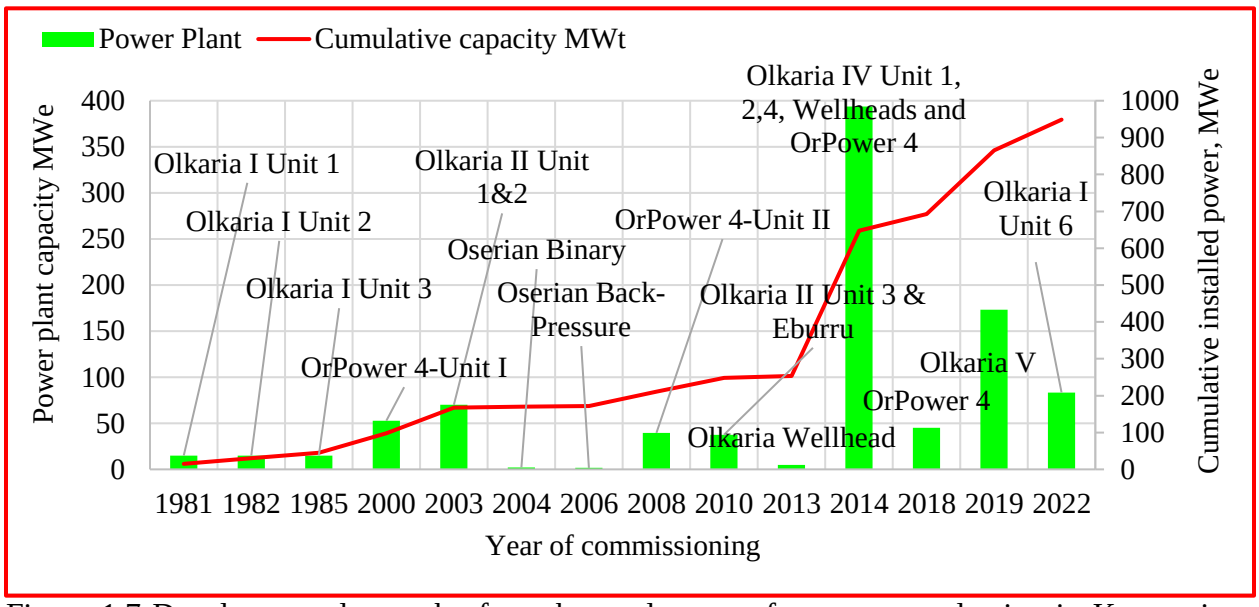

Figure 1.7 Developmental growth of geothrermal energy for power production in Kenya since 1981.

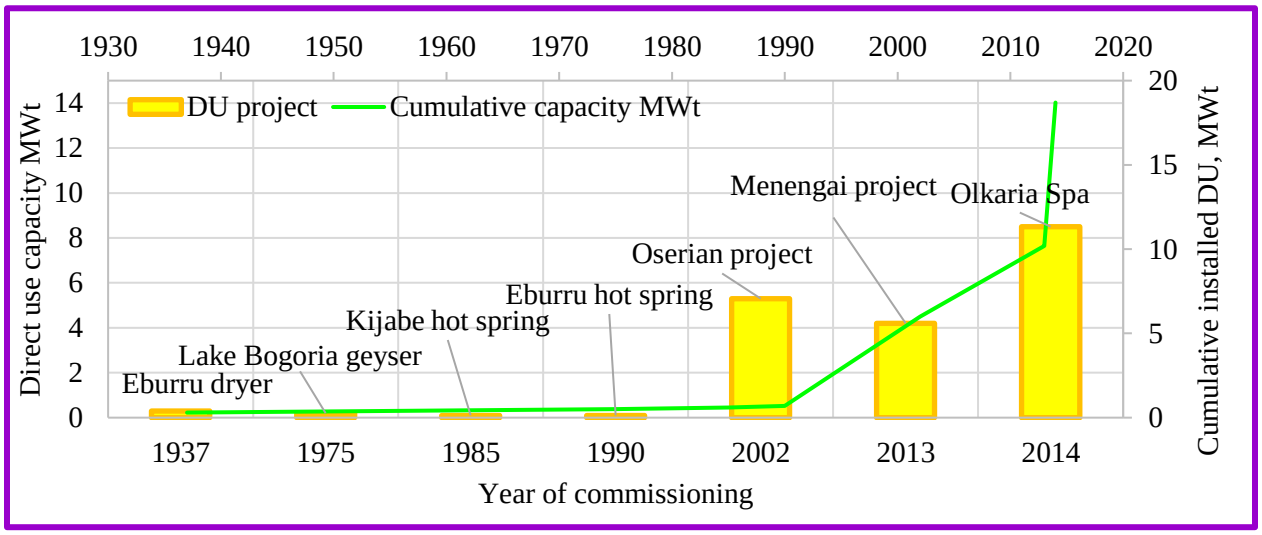

Figure 1.8 Developmental growth of direct use of geothermal energy in Kenya since 1937.

In 2020, it was anticipated that the installed electrical capacity will reach about 4.2 GWe. One of the renewable energy sources that is anticipated to displace fossil fuels is wind energy. Reduced greenhouse gas emissions, fewer imports of fossil fuels, and cheaper energy costs are all advantages of renewable energy sources. Geothermal has the desired baseload properties among renewable sources.

1.5 Research objectives

The research's objectives are to characterize geothermal resources for direct use, estimate thermal demands near the geothermal resources and select their best direct use scenarios.

1.5.1 Main objective

This study's main goal is to develop a visual structured framework for selecting the suitability sites for direct use and best direct use scenarios for the geothermal resources.

1.5.2 Specific objectives

For a successful selection of optimal direct use sites and selection of best direct use scenarios of geothermal resources, several other steps are requisite:

1. Characterization/classification of geothermal energy in terms of enthalpy and developmental status.
2. To set up a GIS-based MCDM (QGIS-based AHP-WASPAS). method for analyzing direct use scenarios.
3. To modify silica saturation index (SSI) for mild to moderately alkaline geothermal resources by pH modification through degassing of CO_2 and H_2S to allow more heat extraction from geothermal resources.
4. Land use classification of grain farms in the vicinity of geothermal resources through remote sensing (RS) of satellite images.
5. Selection of relevant direct use scenarios and selection criteria for high, medium and low enthalpy geothermal resources.
6. To estimate themal demands near geothermal resources and to select hot brine/water piping routes.

1.6 Problem statement

Many studies on the DU of geothermal energy are based on case studies There hasn't been a single solution that offers a clear, organized framework for matching regional thermal needs to the available geothermal resources. The goal of this research is to create a structured framework for identifying thermal needs close to Kenyan geothermal resources and matching them to resource features in order to choose the most suitable DU scenarios. Since high enthalpy geothermal resources set their separation pressures at a saturation index (SSI) equal to one, cooling the brine below this temperature would create conducive conditions for silica scaling. However, for moderately alkaline geothermal resources with high content of non-condensable gases (CO_2 and H_2S), degassing shifts pH to above 8.5, which causes monomeric silica to disassociate to silicate ions, which are more soluble. This allows SSI to be modified to above SSI = 1 without causing silica deposition. In addition, medium and low enthalpy geothermal resources lack productive wells and are thus considered unsuitable for direct use. This study took advantage of hot springs in these geothermal resources to characterize them for direct use.

1.7 Justification

Geothermal energy sector has witnessed steep growth in Kenya in the las three decades, from 45 MWe in 1992 to 863 MWt in 2022. That is an average growth of 27 MWe per year. This growth has been focused on electric power generation only. However, efficiency of power production range from 10 – 17.5% (Bett & Jalilinasrabady, 2021b). This implies that the circumspect utilization of Olkaria, Eburru, and Menengai geothermal fields' based on SSI = 1 limit them to less than 20% utilization efficiency. The lower the utilization efficiency, the longer the payback on investment period. On the other hand, the efficiency of direct use ranges from 80 – 90% due to the lower sink temperatures and less parasitic load. Hence, a field with cascaded use from power production to direct use increases its utilization efficiency and revenues. Kenya direct use capacity since 2014 has been 18.5 MWt, yet demand for heat provided by the agricultural, industrial, and tourism industry is immense. Besides, the medium to low enthalpy geothermal resources in Kenya are considered high risk and have no deep productive wells. However, some have hot springs with moderate to high flow rates of warm to hot waters that can sustain small scale direct uses. Currently worldwide, there lacks a study that links heat demand to the geothermal resources for economically sustainable direct uses. This study established a structured framework to link high, medium, and

low enthalpy geothermal resources to the local thermal demands and select the best direct use scenarios for each resource. This study establishes that Kenya can increase its direct use capacity from 18.5 MWt to 300 MWt by using hot springs alone and further 163 MWt from utilizing brine at Olkaria, Menengai and Eburru.

1.8 Methodology

Figure 1.9 shows the research flow chart of GIS-based MCDM framework for characterizing and linking geothermal resources to local demands in Kenya. It also shows the sources and flow of data and the various scientific analysis tools used in the study to meet the objectives. The results were direct use scenarios, location and estimate of heat demands and reclassification of geothermal resources for direct use.

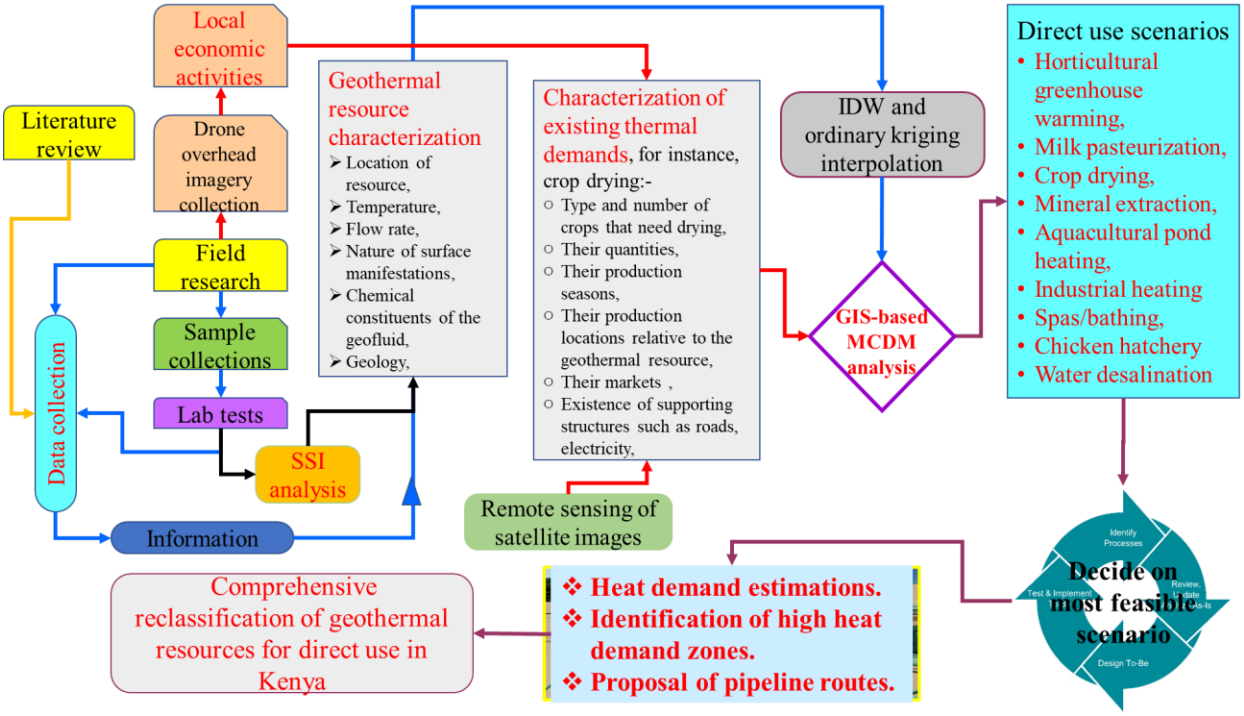

Figure 1.9: The research flow chart shows the study conception, tools and results. The red coloured text is the motivating concept for the dissertation, while the black coloured text is the requisite steps.

Figure 1.9 shows the stages and studies in geothermal research, while Figure 1.10 shows the desired results graphical model.

Figure 1.10 shows the details of a rasterization of point data from geothermal fields (Temp, flow rates, silica concentration) using 2D inverse distance weighted (IDW) and ordinary kriging interpolation methods. It also shows proximity analysis of rasterized polygon and line data (roads, rivers, grain farms, national parks, cities) and their GIS-based MCDM recombination to produce direct use scenarios' suitability zones. From Figure 1.11, it is noted that suitability for direct use is highly influenced by a spatial analysis of the local economic activities, enabling infrastructure and geothermal characteristics.

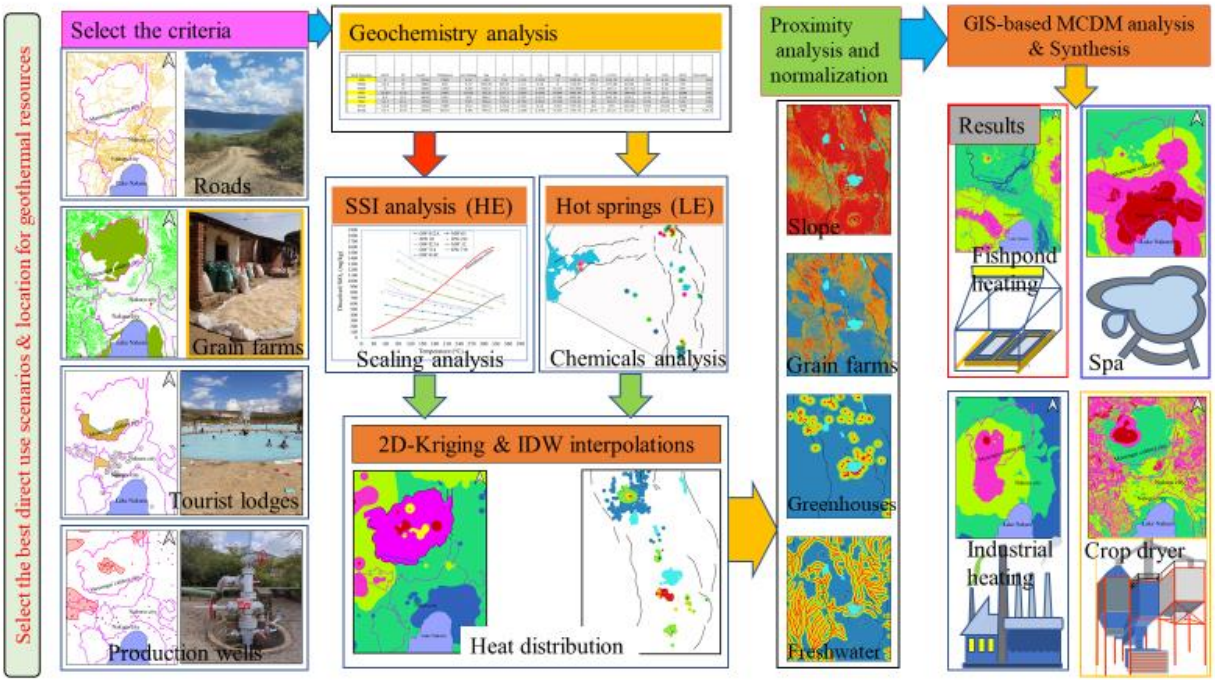

Figure 1.10: A schematic diagram showing a GIS-based MCDM system linking local heat demands and geothermal characteristics.

1.8.1 Hydrogeochemistry of medium to low enthalpy geothermal prospects in Kenya

Water samples were collected in polythene bottles and sealed with tape tightly on site. Figure 1.11 shows the 17 locations of the hot springs. six hot springs are located outside the Rift system, while Homa Hills, (Abundu and Bala), is on the Nyanza rift, which relates to the East Africa Rift System. The samples were treated or untreated on-site, depending on the analysis to be conducted in the lab. The treated samples had 2 ml of 0.1M HCl added to preserve cations. Untreated samples were used for anions determination, laboratory pH and conductivity. On the site, pH, temperature, and conductivity were recorded. Atomic Absorption Spectrometry analyzed cations after filtering through 0.45 µm Millipore membrane. Chloride analysis was performed using Mohr's (argentometric titration) method. Quartz and total silica analysis were done using silicomolybdate, a photometric method. The back titration method was used for the analysis of carbonate alkalinity.

Geochemistry is essential in geothermal exploration. The most contributing factor is hydrogeothermometry to infer the reservoir estimated temperatures from the chemical compositions of the geothermal fluids. Temperature equilibria control the concentration of the dissolved constituents (Fridriksson and Ármannsson, 2007). Geochemical exploration also gives information on the origin, flow directions and helps to identify the sub-surface reservoirs. Chemical compositions, isotope analysis, and hydrogeothermometry were applied to estimate the reservoir temperature of the thermal springs in Kenya. QGIS tool shows the location of developed geothermal fields and prospects in Kenya. The thermal manifestations sampled are shown in Figure 1.11. The sampling methods and analysis are outlined by Arnorsson (2000) and Ellis and Mohan (1977), where they gave detailed geochemical procedures specifically for geothermal

waters. The ternary diagrams were plotted using the liquid analysis spreadsheet developed by Powell and Cunning (2010).

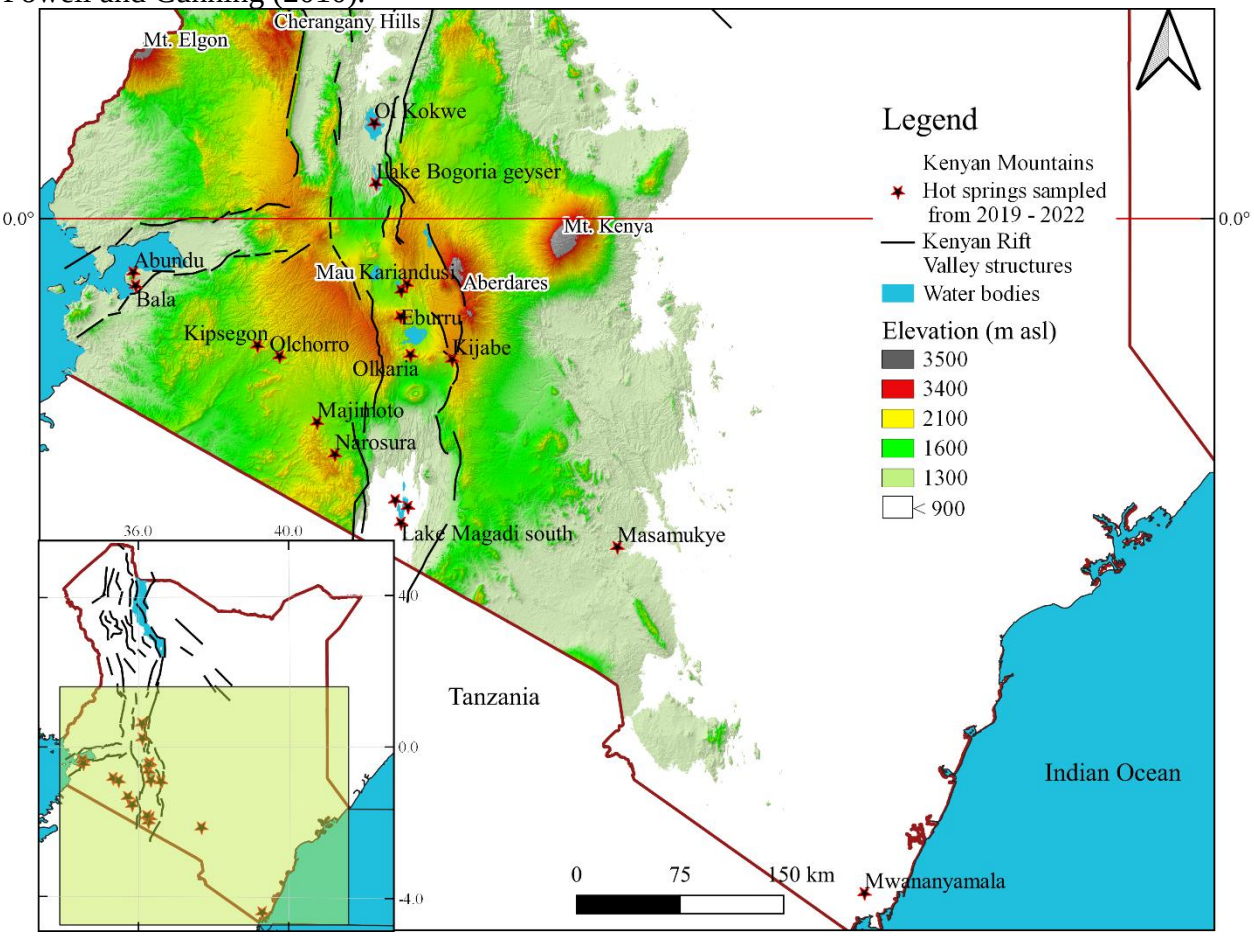

Figure 1.11: Map of Kenya showing the hot springs that were sampled for analysis from 2019 - 2022 The elevation data shows most hot springs are located in areas wth an elevation of 900 - 2100 m above se level (asl).

1.8.2 GIS and direct use of geothermal

A geographic information system (GIS) is defined as a map-based visual representation of geographical topological data, such as locations, distances, distribution, and other descriptive data, on the surface of the planet. GIS is a potent tool for manipulating and analyzing data for decision-making because it enables the collection, storing, and retrieval of data. Most of geothermal data is spatial, especially locations of deep wells, hot springs, fumaroles, steam and brine pipelines, production and reinjection zones in a field, length, orientation, and tilt angles of major and minor faults, the depth of the reservoir and caprock. For direct use, GIS is used to map areas of high thermal demands and hence help in decision making of interlinking these heat demands to the nearest geothermal resource. The distances that raw materials must travel to be processed and the distances that processed commodities must travel to be sold also affect the economic sustainability of direct use initiatives. Thus, before making investments, GIS enhances economic analysis of direct use projects.

1.8.3 MCDM methods

Multi-criteria decision making (MCDM) methods is a science of decision making domiciled in operations research. The merits of MCDM methods are their propensity to combine various incommensurate variables and conflicting objectives by allowing tradeoffs in decision making. MCDM methods potential to significantly improve decision making in engineering, especially in geosciences, where most decisions involve vagueness and tradeoffs. In this research, MCDM methods were used in weighting criteria and overlaying them in GIS to provide a systematic method of site selection. MCDM methods have been used before in geothermal sciences for deep well drilling site selection and exploration (Noorollahi et al., 2015; Prol-Ledesma, 2000). However, none of these studies have considered suitability selection for direct use.

1.8.4 Classification of geothermal resources

The classification of geothermal energy is crucial before committing to the development of a geothermal prospect. This is partly due to differences in reservoir characteristics for high, medium, and low enthalpy geothermal resources. Hence, hydrogeochemistry is carried out first to establish fluid chemistry and estimate reservoir temperatures. Classification of geothermal energy helps in prioritizing the most favourable resources and the ones closest to established infrastructures such as roads, piped water, transmission lines and close to urban areas. This used classification to select medium and low enthalpy geothermal resources for small-scale direct use scenarios facilitated by hot springs. The large-scale direct use scenarios requiring deep wells and fluid piping were tailored to the high enthalpy geothermal resources.

1.8.5 Silica saturation index (SSI)

Silica is abundant in earth's crust and its solubility in hydrothermal systems depends on temperature and is controlled by solubility of quartz and chalcedony. Low enthalpy alkaline geothermal resources contain low concentration of dissolved silica as witnessed by hot springs of Kenyan rift valley system. However, deep fluid from high enthalpy resources may contain high concentrations of dissolved silica, >300 mg/litre. The solubility of silica on the surface decreases as temperature decreases and polymerization may take place necessitating silica deposition (scaling). Silica scaling clogs pipes, reinjection wells, turbine blades, and heat exchangers causing downtimes and high operational costs. Silica saturation index (SSI) is the ratio of total amount of silica contained in a litre of brine at a given temperature to the maximum amount of silica that can be dissolved in a fluid at that temperature. SSI > 1.0 would cause oversaturation of silica and initiate polymerization process of excess monomeric silica. A problem is presented regarding how that nearly oversaturated brine can be used to supply heat for direct usage since most power facilities in Kenya separate brine and steam at SSI = 1.0 and reinject the separated brine when hot to avoid supersaturation conditions. In order to increase the solubility of monomeric silica and hence enable additional brine cooling with minimal hazards of silica scaling, this research presents a novel method for modifying the pH of brine from moderately alkaline geothermal resources to allow direct use.

1.9 Thesis outline

The contents of the dissertation consist of seven chapters below:

Chapter 1: Introduces the background of the study, the introduction of direct use of geothermal energy in high and low enthalpy geothermal resources, the geothermal status in Kenya. This chapter describes the research objectives and methodology.

Chapter 2: This chapter reviews geothermal state of the art methods of methods of classifying geothermal resources according to geology, temperature, and developmental status. Also reviewed are the multi criteria decision making (MCDM) methods, criteria weighting, 2D inverse distance weighted and ordinary kriging interpolation methos of point data. The previous relevant studies on geographic information systems (GIS) and remote sensing of satellite images for land use and selecting suitability locations were summarized in brief. The novel idea of increasing silica solubility by raising pH above 8.5 for mildly to moderately alkaline geothermal resources is also introduced.

Chapter 3: The procedures of using MCDM methods in QGIS is expounded, the specific MCDM methods (AHP-WASPAS hybrid), are outlined. The reasons and the procedures of selecting the 2D interpolation methods. Remote sensing, creation of criteria map layers and rasterization of vector data are given. Finally, the chapter summarizes the model for selecting the best use scenarios.

Chapter 4: The chapter expounds on the novel method of identifying and characterizing high enthalpy geothermal resources for direct use. The chapter analyses six high enthalpy geothermal resources in central and southern Kenya rift valley: Menengai, Elementaita, Eburru, Olkaria, Longonot and Suswa. All are defined by trachytic volcanism and central calderas, except Elementaita. Nine direct use scenarios were analyzed against eleven criteria. The criteria used was influenced by local economic activities, local infrastructure and geothermal characteristic. The best direct uses for Olkaria were discovered as horticultural greenhouse warming with a heat demand of 84 MWt, Spa/bathing/swimming with a heat demand of 6.3 MWt, and industrial heating with an unknown heat demand. The best direct use scenarios for Menengai were found to be crop drying with a heat demand of 1227 MWt, milk pasteurization with a heat demand of 800 MWt, industrial heating with a demand of 21 MWt, and spa/bathing/swimming with a heat demand of 6 MWt. The best direct use scenarios at Eburru were found to be crop drying with a heat demand of 395.5 MWt, milk pasteurization with a heat demand of 256 MWt, and water desalination with uncertain heat demand. Hence, Menengai and Eburru geothermal fields have more heat demands than Olkaria, while Olkaria has more volumes of disposable steam and brine compared to them.

Chapter 5: Focuses on selecting geothermal resources in medium to low enthalpy geothermal resources with no deeper wells. The topics identifies the important role hot springs play by providing warm to hot fluids for direct use. The topic expounds geochemical analysis of hot spring water and the use of resultant data to do exergetic classification of medium to low enthalpy geothermal resources in Kenya. Finally, the chapter selects best direct use scenarios of hot spring based on GIS-based hydrogeochemistry data and economic enabling factors near the geothermal resource. It is discovered that the hot springs provide over 275 MWt of heat that has significant effects on direct utilization. The hot springs suitable for domestic use and aquaculture were identified as Narosora, Majimoto, Kijabe, Eburru and Kipsegon. Those best suited for spas/bathing/swimming and hot spring tourism were identified as Lake Bogoria, Kariandusi, Homa Hills, Lake Magadi north, and Arus hot springs.

Chapter 6: This chapter reviews all the direct use case studies in Kenya and tries to use them to validate the GIS-based MCDM selection model introduced in this study. The validation was able to identify some case studies in high suitability areas while others were in areas classified as medium suitability. This is because establishment of these case studies was not based on the current study, though those which coincided with high suitability areas are commercially viable. The rest are of smaller scale and not economically sustainable.

Chapter 7: Summarizes the overall conclusions and recommends future work optimizing geothermal resources in Kenya for direct use.

CHAPTER TWO

2. LITERATURE REVIEW

2.1. Overview

This chapter describes the conventional use of geothermal energy in Kenya. Kenya is Africa's leading geothermal user with an installed capacity of 863 MWe and 18.5 MWt for electricity generation and direct use, respectively (Omenda et al., 2021). Exergetic optimization of geothermal resources for electric power generation has been conducted, by proposing a bottoming organic Rankine cycle (ORC) units (Bett et al., 2019; Bett & Jalilinasrabady, 2021b; Jalilinasrabady et al., 2021; Kwambai, 2010). There are few, inconclusive research studies on optimizing geothermal resources for direct use (DU), and those studies mostly focused on the Olkaria or Menengai geothermal regions. (Kiruja, 2017; Ronoh, 2020). This chapter describes direct use, its merits and previous studies aimed at optimizing it. Exergetic re-classification of reservoirs is hereby described as the initial stage of optimizing geothermal energy resources. The geographic/geospatial information system (GIS)-based multicriteria decision-making (MCDM) methods are introduced to interlink the resources to the local heat demands, and the best applicable models chosen. For high enthalpy geothermal fields, silica scaling is introduced by further cooling geothermal fluids below the silica saturation index (SSI) of 1, hence a silica saturation index (SSI) analysis is utilized to extend the heat extraction temperature downwards to between 100 and 120°C . Furthermore, crop drying generates heat demands for geothermal resources, and pinpointing the locations and dimensions of grain farms is essential for determining the quantity of heat demand. To determine the sizes and distribution of grain farms close to geothermal energy sources, this chapter introduces remote sensing (RS) using satellite images. State of the art methods of classifying geothermal energy resources is also expounded upon in the chapter.

2.2. Introduction

Geothermal energy has been proposed as one form of clean renewable to replace fossil fuels in power production in an effort to decarbonize energy production. Nations endowed with high enthalpy geothermal resources have accelerated their efforts to explore, develop and exploit these resources. Power production from geothermal energy has tripled in the last three decades from 5 GWe to the current 15 GWe in 2021 (REN21, 2022). The growth has even been faster on the direct uses, 107.7 GWt, which has seen it double in usage in 5 years from 300 TJ/yr in 2015 to 600 TJ/yr in 2020 (Lund & Toth, 2021a). Despite, the high demand for thermal energy from geothermal sources, many relevant research studies concentrate on optimizing the exploration, development and management of reservoirs for electric power generation (Bett and Jalilinasrabady, 2021b; Kanda et al., 2019; Kipngok et al., 2019; Maithya et al., 2020). No studies characterize geothermal resources for direct use (DU) (GreenMax, 2020). A significant amount of heat applicable to direct use (DU) is underutilized due to limited knowledge of demand matching these resources. Direct use (DU) has the potential to transform local agricultural and tourism sectors and spur economic growth.

By leveraging its reliability, compared to solar, wind, ocean power and hydropower, geothermal's ability to contribute more to global thermal needs relies on overcoming the challenges of matching local thermal demands to the available energy sources. These challenges emerge from the fact that it is costly to transport thermal energy farther from geothermal sources. Besides, different local economic activities, proximity to urban centres, and road infrastructure complicate the issue of matching thermal energy demands to the available geothermal resources. Many studies on the DU

of geothermal energy are based on case studies. None has provided a visual, structured framework for matching local thermal needs to the available geothermal resources. This research seeks to establish a structured framework to identify thermal needs near Kenyan geothermal resources and match them to the resource characteristics for selecting the best DU scenarios.

Each geothermal resource is unique in terms of location, terrain, heat and fluid chemical properties. The distinctiveness of each geothermal resource is further enhanced by variations in transportation infrastructure (roads), regional economic activity, distribution of fresh surface water, and proximity to protected zones and populated areas. Characterizing geothermal resources for direct use (DU) is challenging because of these various criteria. However, by carefully evaluating these factors, it may be possible to choose the geothermal locations that are best suited for direct use (DU) as well as the optimal direct use (DU) scenarios for any specific geothermal resource. Currently, there does not exist a framework of combining and analyzing these criteria to characterize suitability of a geothermal resource to direct use (DU).

To characterize geothermal resources in Kenya for direct use (DU), this study used geospatial information systems (GIS). In order to protect high enthalpy geothermal resources from silica scaling and to determine the safety level for the community's use of hot springs, geochemistry analysis was used. New low enthalpy geothermal resources were also mapped in Quantum Geographic Information System (QGIS), and the geochemistry of their hot springs was introduced. Additionally, the thermal distribution of geothermal resources was estimated using 2-D inverse distance weighted (IDW) and ordinary kriging interpolation techniques. Finally, remote sensing (RS) was employed to categorize grain fields by analyzing agricultural activity close to geothermal resources.

2.3. Development of geothermal energy and direct use (DU)

Geothermal development has six broad stages: 1) Pre-feasibility study, 2) Exploration, 3) Resource delineation and appraisal, 4) Production wells drilling, 5) Construction of power plant facilities, and 6) Operations and maintenance, as shown in Figure 2.2. Risk and uncertainty are ubiquitous snags that constantly affect the reservoir, capital, operations, maintenance, and the environment in all geothermal development stages. Risk is the probability of success, while uncertainty is the fuzziness of explicitly characterizing a parameter (Witter et al., 2019). Figure 2.1 shows that multiple criteria describe the deep well-siting and utilization. The outcome of the well drilling is characterized by multiple attributes, which in turn help to select the best application scenario.

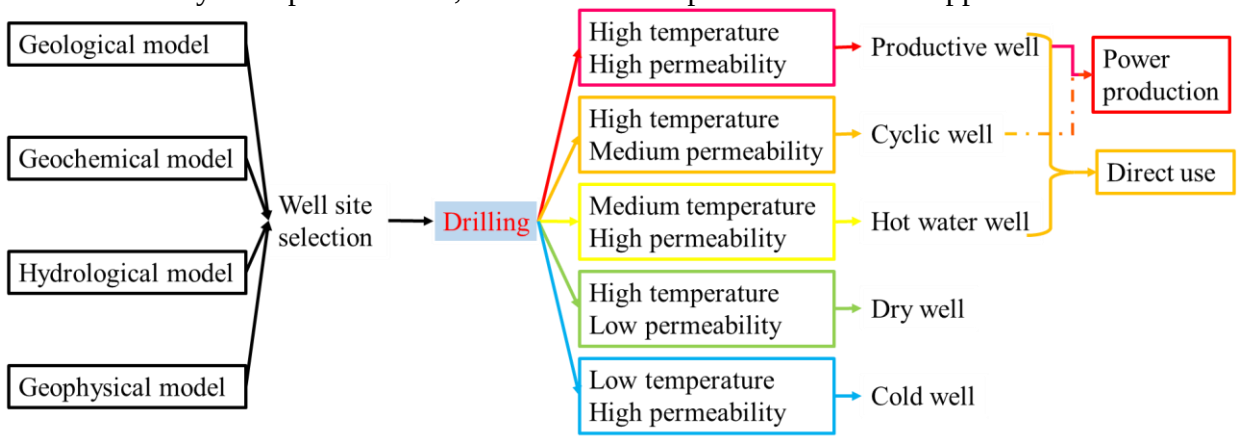

Figure 2.1 Multi-attribute nature of geothermal development and utilization.

Geothermal reservoirs are located in the subsurface and depend on the interaction of underlying inferred fractures, magma intrusions, host rock, and well-established pathways for the passage of

meteoric and magmatic waters. Uncertainty involves locating the precise location where all of the above criteria interact, hosting high enthalpy geofluids with high well permeability (Witter et al., 2019). In a geothermal development project, drilling production and reinjection wells is the most capital-intensive undertaking, consuming over 40% of the total budget. The uncertainty of locating an optimal drilling location leads to an increased risk of drilling an unproductive well and thus losing the well drilling capital. For electricity generation using flash technology, the risk of drilling an unsuccessful well is $5.83 million on average, in Kenya and Iceland (Okwiri, 2017). Comprehensive subsurface studies, numerical simulation, long-term monitoring, and detailed resource characterization can help mitigate resource risk. Besides, concrete market assessment helps improve the project's financial viability (Traineau et al., 2015). On the other hand, the DU of geothermal energy is less affected by low enthalpy, high concentration of non-condensable gases (NCG) and low permeability of the well. This is because DU can utilize cyclic and low enthalpy wells, including wells experiencing high NCG concentrations, as experienced by Olkaria well OW-101. Dry wells can also be converted into ground source heat pumps by pumping in water after plugging the production casing. Consequently, the risk curve in geothermal development for DU is lower than that of electric power production, as depicted in Figure 2.3.
DU can be set up downstream of an existing geothermal power plant without requiring costly construction and operation of steam lines, power plants, steam separators and reinjection wells, thus making DU cheaper by 40% and less risky by 30%, as shown in Figure 2.2. Other merits of DU over electric power production from geothermal energy are its ability to utilize surface manifestations such as fumaroles and hots springs for small-scale bathing, aquacultural pond heating, geotourism, heating and other related uses way ahead of drilling wells. However, the wells increase utilization capacity and cater for medium to high enthalpy DU uses such as industrial heating.

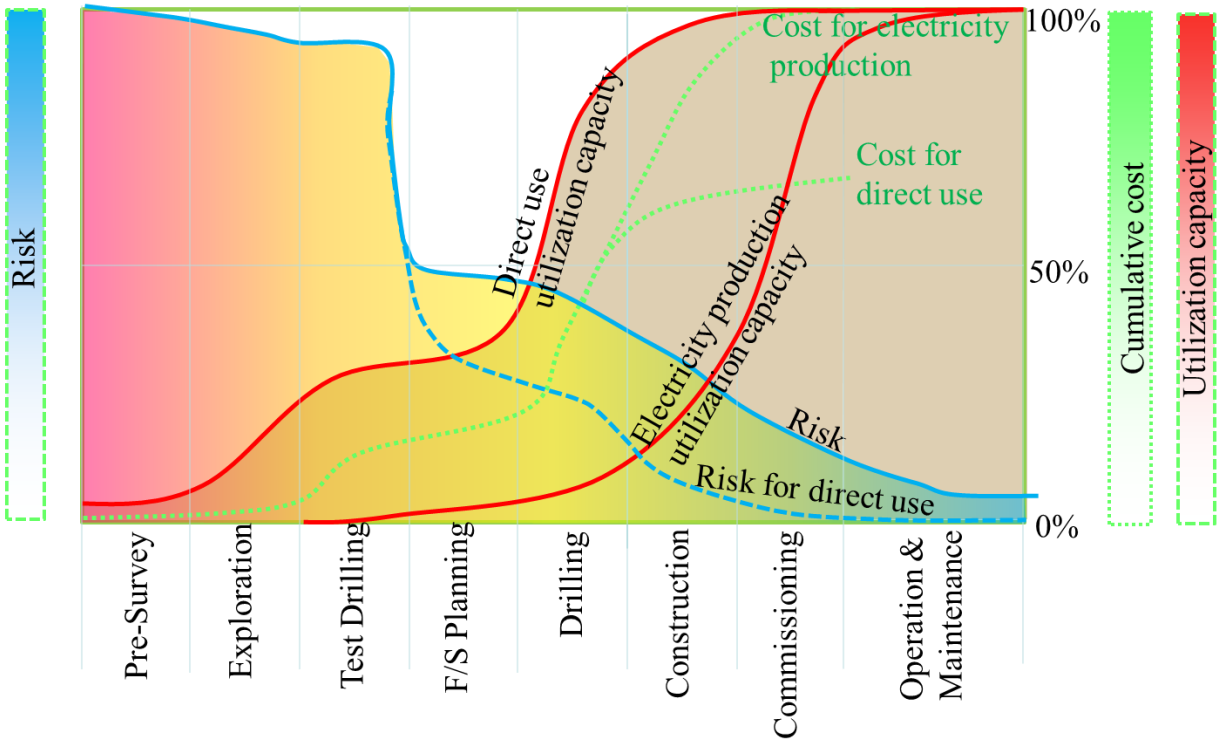

Figure 2.2. Risks and costs in percentages for geothermal development for both direct use and electric power generation.

2.3.1 Previous studies on direct use (DU)

Unlike other clean energy sources such as solar, wind and wave energy, geothermal energy in up-flow zones with a temperature gradient above 50°C/km is denser; hence, it is easier to transport via pipes and transfer the heat to fluids by heat exchangers. DU involves using thermal energy in geofluids for heating purposes or exploiting chemical constituents of the geofluid or geofluid itself for domestic and industrial use. Unfortunately, geothermal fluids are constrained to the vicinity of the production well due to the high cost of transporting the fluids, exergy destruction and subsequent silica scaling. Iceland is exemplary in DU (district heating and bathing) and has an extensive hot water piping network with the most prolonged hot water pipeline of 23 km (Ragnarsson, 2021). The longest brine pipelines at Olkaria and Menengai geothermal fields are 3.7 km and 4.6 km respectively. Figure 2.3 shows that estimated total cost of installing hot water piping for the nominal diameter range of 250 - 350 mm as $1000/m based on Equation (2.1). Hence, with an installation cost of more than $ 1million/km, it is paramount to limit hot water usage from geothermal resources to industries, farms, resorts and homes closest to the production wells.

$$Ct = Cc + Cp + (Ce + Co)\left(1 - \frac{1}{(1+i)^T}\right) \times \frac{1}{i} \qquad (2.1)$$

Equation (2.1) is a simplified estimation of the total updated cost of brine and hot water piping, where Cc is the capital cost, Cp is the pump installation cost, Ce is the annual energy cost, Co is the pump and pipe maintenance cost, i is the rate of interest, and T is the number of years the pipeline will be operated. This estimate may increase when the cost of land and pipe supports are factored in. Hilly rugged terrain may increase the piping cost by affecting pipe length and pumping head. To overcome these challenges, it is crucial to match geothermal resources with local thermal needs and settle with applications requiring minimal brine piping and pumping.

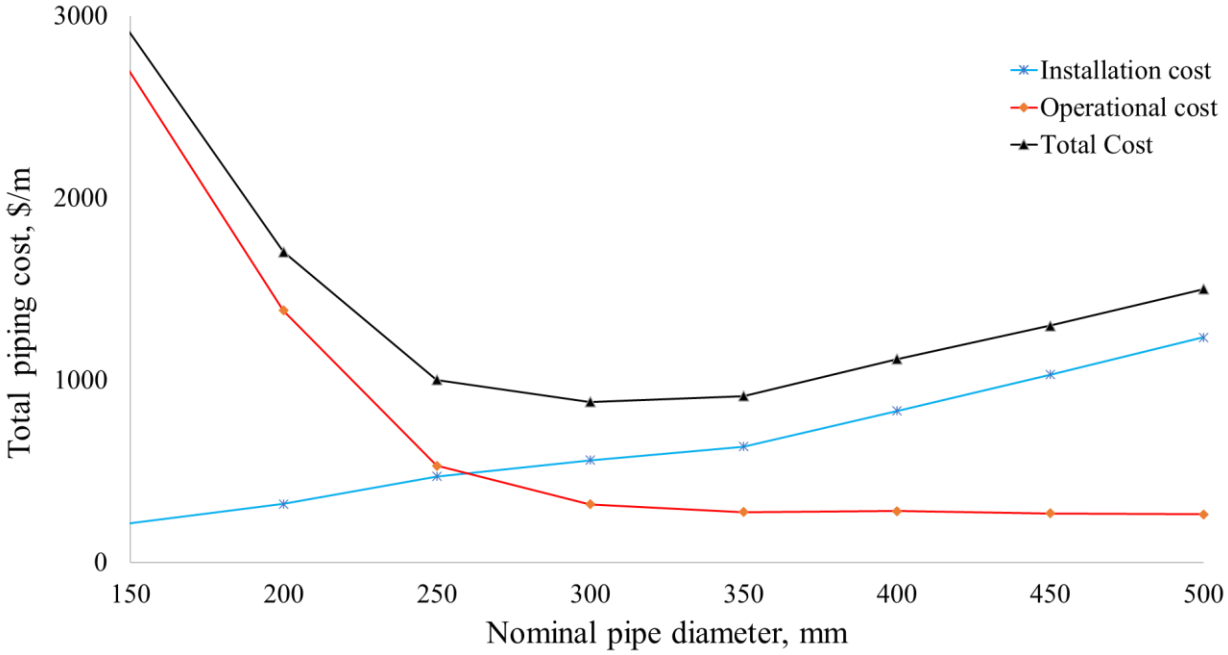

Figure 2.3. The installation and operational cost of brine and hot water piping based on nominal diameter.

Conventional DU includes horticultural greenhouse heating, crop drying, milk pasteurization, spa and balneotherapy, mineral extraction and many more depending on their optimal temperature needs as outlined in the Lindal chart. The uses below 120℃ are considered low enthalpy, while those that require temperatures above 120℃ are classified as moderate to high enthalpy needs.
Lund and Toth (2021) highlighted worldwide DU statistics and trends since 1995 to 2019. Their research revealed acceptance of DU of geothermal resources by countries from 28 in 1995 to 88 in 2019. The most accepted applications are space heating, bathing, aquacultural pond heating, horticultural greenhouse warming, crop drying and industrial heating in the order of percentage of utilization, as shown in Figure 1.2.
Few studies have been conducted to select DU scenarios for a given geothermal resource. Roe et al. (2015) conducted a feasibility study for DU of hot spring water at Adak, Akutan and Atka, Alaska, USA. The criteria they considered critical for a successful district heating project were temperature, flow rate and chemistry of hot spring water as resource assessment. Climatic conditions, distance, and terrain from hot springs to residential areas were the main variables influencing pipeline design and cost. They used the Lindal diagram to match water temperatures with possible DU scenarios. Tole (1988) used the chemistry of hot springs in Kenya to characterize reservoir temperatures and suggest possible DU scenarios based on temperatures and flow rates.
Several studies have also been conducted to establish DU scenarios for Kenyan high enthalpy geothermal resources to encourage DU related ventures as alternative revenue streams. Ronoh (2020) conducted a feasibility study of an industrial heating park to utilize cheap steam, electricity and more than 2127 t/h of brine available at Olkaria Domes and was faced with a decisional challenge locating the green park within Olkaria field. Kinyanjui (2014) conducted a feasibility study of having a spa and a crop drier at Menengai geothermal field to utilize 55 kg/s and 2 kg/s of brine and steam at 130°C, respectively. He used the brine piping cost to choose an ideal location for the spa. Kiruja (2017) conducted a feasibility study to establish the viability of providing hot brine to an industrial zone located within the Menengai caldera on the southern fringes. This author considered five attributes: profitability, available energy, resource reliability, resource temperature, possibility of future growth, and water requirement to evaluate whether a geothermally powered industrial zone utilizing 8.8 to 36.3 MWt will be profitable. These earlier DU studies both failed to take into account heat demands presented by the local economic activities and local enabling infrastructure to provide a framework for choosing sustainable DU scenarios for a particular geothermal resource.

2.4. Classifications of geothermal energy

Geothermal resources vary in terms of geological settings, depth of the reservoir, geochemistry of their fluids, state of heat carrying fluid, temperature, enthalpy, exergy and in levels of complexity when exploiting them. This wide substantial heterogeneity creates several disagreeing classification techniques (Rezaie and Aghajani, 2013). Geothermal classification has no globally agreed standards, guidelines, or codes to assess, quantify and classify the resources (Falcone et al., 2017). Hence the following classifications methods are conventionally used either as stand-alone or in combination with others to characterize geothermal resources for assessment, exploration, development, and reporting:

1. Thermodynamic properties of reservoir fluids: temperature, enthalpy, exergy (high, medium, low), as in Figure 2.4. Depending on the temperature and pressure distribution of the geofluids in a hydrothermal system, the geofluid could be liquid or vapour dominated, with most systems falling somewhere in the middle (Jalilinasrabady, 2022).

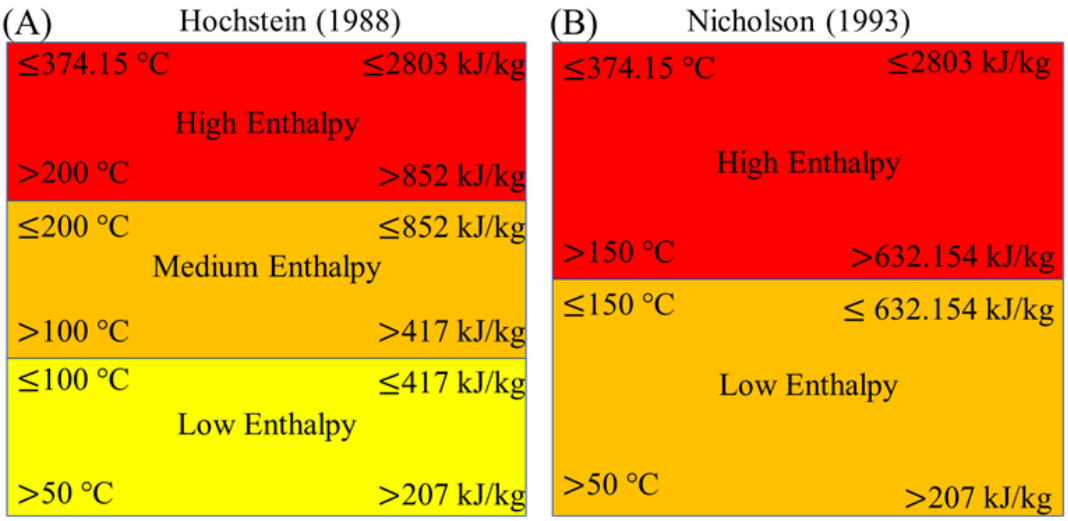

Figure 2.4 The thermodynamic fluid parameters that are typically employed to characterize a hydrothermal system (Williams et al., 2011).

2. Geological setting fundamentally affects locations, heat sources, mode of heat transfer, geofluid chemical composition, reservoir depth, temperature characteristics, and size of the geothermal resource. Continental plate movements and natural geothermal gradient play significant roles in hydrothermal systems' occurrence. Convergent and divergent plate borders create major strike slips, arcs, orogenic belts, mid-oceanic ridges, and active rifts which allow lithospheric thinning and magma intrusions, thus introducing magma as the primary heat source for the associated geothermal resources (Hermant et al., 2019). In intra-cratonic basins, the lithosphere may be thin enough to allow upwelling of the aesthenosphere and subsequent conduction and convection of heat via rock layers and faults with fluids. In conclusion, the geological setting affects the variables that make geothermal energy development feasible in the depth of interest; the amount of heat stored at a drillable depth (5km) and the capacity to recover this heat at the surface at an economically viable rate for a given purpose (Jalilinasrabady, 2022).
3. Degree of confidence of resource extraction: This encompasses setting pragmatic boundaries on resource recoverability, assessment status, accessibility, and sustainability based on available technology and capital for exploration and extraction of hot geofluids. The Australian Geothermal Energy Group's Geothermal Lexicon and Canadian Geothermal Code for Public Reporting of geothermal energy resources distills the eight stages of geothermal project development status into two data-driven broad categories of geothermal resources: resource and reserve. The resource category encompasses inferred, indicated and measured resources. The inferred resource is represented by little geological knowledge of the resource and low confidence in the estimation of heat recoverability, while measured resource is inconclusively explored resource (using geochemistry, geological, gravity, magnetotellutic (MT), and transient electromagnetics (TEM) surveys in addition to monitoring wells) in trying to delineate the resource and improve confidence on the estimation of thermal recovery. On the other hand, the geothermal reserves are divided into probable and proven reserves. The probable reserve's reservoir is well delineated by advanced geophysics, geochemical and geological exploratory surveys and has several productive wells in existence. The

proven is a geothermal field has several production wells that have been producing electricity or hot water sustainably for a given period (AGRCC, 2008; Deibert et al., 2010; Lawless et al., 2010). In addition to geological limitations, thermal extraction factors from proven geothermal reserves could be curtailed by environmental protection policies, land access, technological progress, competitive costs, sustainable production levels, and proximity to markets. This led to the geothermal reclassification into four potential zones: theoretical, technical, economic and developable as shown in Figure 2.5 by Rybach (Rybach, 2015). The developable reserve portion is the easily bankable resource able to produce electricity and hot water for direct use at a competitive market price for a reasonable return on investment.

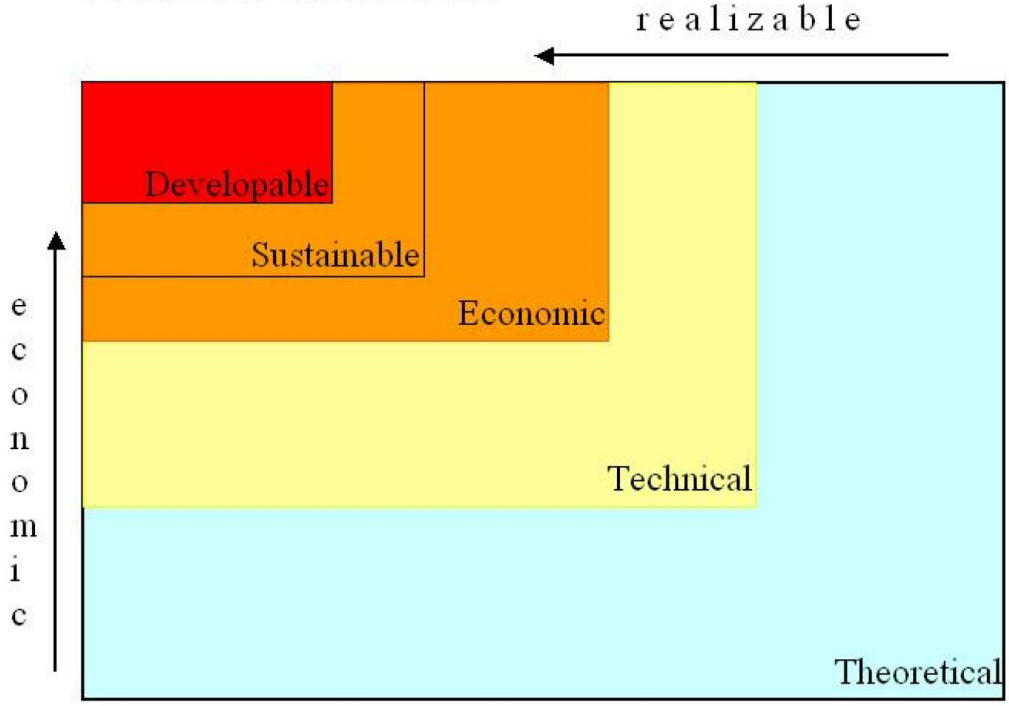

Figure 2.5 Classification of geothermal resources based on economics, environmental constraints, and technical ability to extract and utilize the resource (Rybach, 2015).

2.5. Previous studies on MCDM methods and geothermal energy

MCDM methods are used to systematize evaluation and selection in decision-making. MCDM methods utilize pairwise comparison and the least Euclidean distance from the ideal solution to select and rank available choices. They are categorized into subjective-based MADM methods and continuous objective-based MODM methods (Zavadskas et al., 2016). MADM methods are applied in decision optimization, while MODM methods are used to optimize design equations subject to design constraints. MADM methods available in the literature are, analytical hierarchy process (AHP), elimination et choix traduisant la realité (ELECTRE), technique for order preferences by similarity to an ideal solution (TOPSIS), preference ranking organization method for enrichment of evaluations (PROMETHEE), analytic network process (ANP), VIKOR, potentially all pairwise rankings of all possible alternatives (PAPRIKA), weighted aggregated sum product assessment method (WASPAS), weighted sum method (WSM), just to name a few (Bozorg-Haddad et al., 2021; Zavadskas et al., 2016). AHP, ANP, TOPSIS, WASPAS, and VIKOR are popular for selecting alternatives, while OWA, ELECTRE and PROMETHEE are suitable for outranking alternatives (Oukil and Govindaluri, 2020; Simić et al., 2021). MADM

methods have been used to select alternative sustainable pathways for decarbonizing energy systems (Hottenroth et al., 2022). The critical benefit of MCDM methods is providing a structured framework for working with heterogenous and incommensurable criteria as is encountered when characterizing geothermal resources for DU.

Previous applications of MCDM methods include the selection of renewable energy alternatives best fitted for particular regions. However, geothermal energy was considered as one of the alternatives, though not the best alternative (Karaşan and Kahraman, 2020; Xu et al., 2020). These studies dealt with intangible criteria such as social-political, technological, environmental impact, job creation, quality of energy and economic considerations, which are hard to quantify (Budak et al., 2019). Broad intangible criteria fail to describe in detail the developmental and exploitation aspects of geothermal energy, more so as far as DU is concerned. For instance, Kenya's decision to fast-track geothermal development was due to the disruption of the baseload hydroelectricity by the frequent droughts. These frequent and prolonged droughts caused load shading (electricity blackouts) in many parts of the country. Accordingly, geothermal energy was prioritized as an affordable and reliable indigenous energy source to replace hydroelectricity. Environmental, land acquisition, social-political, and technological criteria played a minor role when selecting geothermal energy as a suitable renewable energy. Therefore, there is a research gap of the in-depth characterization of geothermal resources and the selection of their best utilization scenarios, especially for DU. A few studies utilizing MADM methods to describe and analyze geothermal reservoirs exist in the literature. However, none is dedicated to the DU of high enthalpy geothermal energy resources.

Duan et al. (2011) used a merger of AHP and fuzzy synthetic evaluation (FSE-AHP) to quantify the sustainability of two geothermal reservoirs, Tianjin and Xiaotangshan geothermal fields, based on the quantity of fluid discharged from the reservoirs and the quantity of brine reinjected back. This method provided a cost-effective way of managing decision making on geothermal reservoirs. Mostafaeipour et al. (2020) used MCDM methods to rank provinces in Afghanistan for geothermal suitability. They used nine criteria: hot spring density, fault density, hot mineral spring density, volcanic dome density, fault density, drainage density, intrusive rock density, population density, university density and area of the province. Though these criteria are quantifiable, they do not provide confidence in geothermal exploration since they are deficient of geological, geochemical and geophysical exploration data. Raos et al. (2022) applied MCDM methods to quantify the sub-criteria of the geological settings, technology, society, environment, and economy when evaluating enhanced geothermal systems. In detail, they endeavored to provide parametric equations for reservoir flow rate, permeability, and wellhead temperature, among others. They also faced the same challenge of uncertainty in quantifying parameters such as social and environmental impacts. Unfortunately, this research work did not evaluate thermal demands, hence used a modified Lindal diagram to select DU scenarios based on reservoir temperatures.

2.6. Previous studies on GIS-based MCDM methods

A geographic information system (GIS) is defined as a visual representation of spatial topological data such as locations, distances, distribution, and other descriptive information on the earth’s surface as a map, as shown in Figure 2.6.

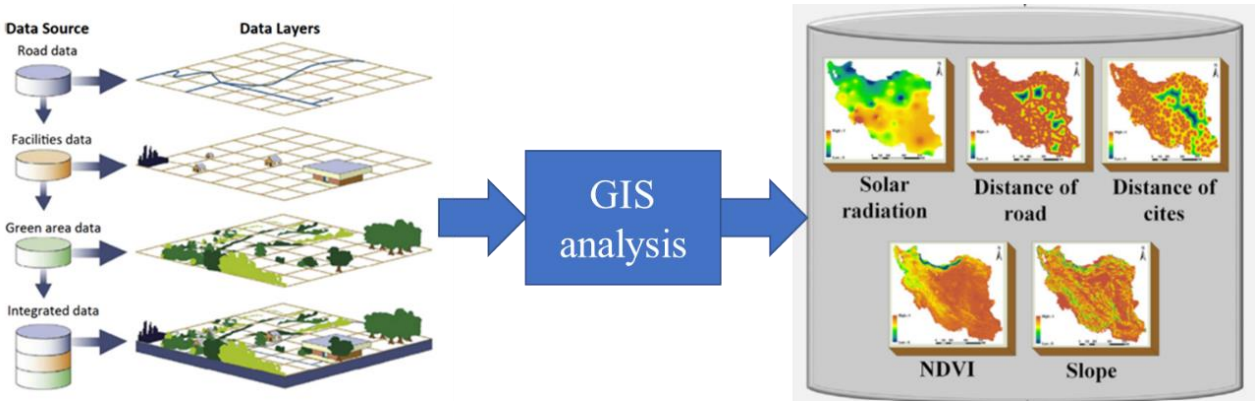

Figure 2.6 GIS allows the representation of information as map layers which can be manipulated and combined to help in better decision making (Firozjaei et al., 2019; Lepuschitz, 2015).

GIS's ability to allow capture, storage and retrieval of data makes it a powerful tool for manipulating and analyzing data for decision making. Some available GIS platforms, such as ArcGIS and QGIS-SAGA, are incorporated with limited analytical MCDM algorithms such as WLC, AHP, OWA, MOLA and CA. The synergistic merger of AHP and GIS is most preferred in spatial decision making involving optimal site selection and suitability mapping (Kabak et al., 2018; Arabameri et al., 2019). Yalcin and Kilic Gul (2017) used GIS-based MCDA methods to conduct a pre-feasibility study of the availability of geothermal resources by considering locations of hot springs, fault lines, land surface temperatures and proximity to geological indicators at Afyonkarahisar, Turkey. Ramos-Escudero et al. (2021) used AHP to develop suitability map for shallow geothermal energy utilized by closed-loop ground source heat pumps. Their research employed the criteria of thermal conductivity of hosting rocks, ground surface temperature, heating and cooling degree days, annual temperature amplitude, and consolidation grade rock. The selection resulted in three classes of suitability for the Murcia region of Spain. Kiavarz and Jelokhani-Niaraki (2017) used OWA as MCDM method for prospecting geothermal resources in Iwate and Akita. As criteria, the authors used heat degrees and distances from volcanoes, faults, hot springs, alteration grounds, and fumaroles. ORness values ranging from 0-1.0 were used to control risks in choosing suitability. Additional research works on GIS-based MCDM involving shallow and deep geothermal resources are highlighted in Table 2.1.

2.6.1 Choice of MADM methods to use and weighting method

Development of geothermal energy entails manipulation and linking of spatial data such as proximity to subduction and divergent zones, location of eruption centres, proximity to surface manifestations, well-drilling directions, geofluid piping routes from the wells to the power plant, fault locations and inclinations, as well as mapping of reservoir characteristics. Table 2.1 shows previous studies incorporating GIS-based MADM methods in selecting optimal sites where the AHP method emerged as the most frequently used MCDM method in GIS.

Table 2.1. Summary of state-of-the-art applying synergistic GIS-based MADM methods on geothermal energy.

Year	Objective	MADM method(s)	Purpose of MADM	References
2000	Optimal siting of geothermal wells	Fuzzy, Boolean, Index Overlay models	Weighting	(Prol-Ledesma, 2000)
2008	Optimal siting of geothermal wells	Boolean, Index Overlay	Weighting	(Noorollahi et al., 2008)

2011	Geothermal reservoir management	FSE, AHP	Weighting	(Duan et al., 2011)
2017	Exploring geothermal resources	GIS, AHP	Weighting	(Yalcin and Kilic, 2017)
2017	Prospecting geothermal resources	OWA status updates	Weighting	(Kiavarz and Jelokhani-Niaraki, 2017)
2018	Selecting areas with optimal drilling conditions for GSHP	AHP	Weighting,	(Tinti et al., 2018)
2020	Selection of geothermal projects	SWARA, ARAS, VICKOR, TOPSIS	Weighting, Ranking	(Mostafaeipour et al., 2020)
2021	Spatial analysis for shallow geothermal energy	GIS, AHP TOPSIS	Weighting, Ranking	(Ramos-Escudero et al., 2021)
2021	Selection of suitability for geothermal potential	Fuzzy AHP	Weighting	(Şener and Şener, 2021)
2021	Assessment of geothermal potential	AHP	Weighting	(Meng et al., 2021)
2022	Quantification of parameters for enhanced geothermal systems	GIS, AHP	Weighting	(Raos et al., 2022)
2022	Suitability selection for shallow geothermal energy (GSHP)	AHP	Weighting,	(Dong et al., 2022)
2022	Suitability for exploitation of geothermal energy in Africa	AHP	Weighting,	(Elbarbary et al., 2022)

Table 2.1 shows that GIS-based MCDM research works on geothermal energy are few and based on selecting suitable locations for exploiting geothermal resources (exploration stage). The AHP is popular since it is incorporated into common GIS platforms like ArcGIS and QGIS-SAGA. The primary reason the AHP is the most popular approach for weighting criteria is that it can translate verbal expressions of judgment to the subset of rational numbers by using the basic AHP scale given in Table 2.2 (Özkan et al., 2019). AHP is also robust in weighting incommensurate variables and was thus adopted in the current research. This research extends hybrid AHP-WASPAS into GIS to select the best DU application scenarios for high enthalpy geothermal resources in Kenyan central and southern rift valley. The WASPAS method combines the weighted sum model (WSM) and weighted product model (WPM). This GIS-based MCDM method works with incommensurate data, mainly numerical data, making it the best suited for this research.

Table 2.2. Fundamental AHP scale for quantitative comparison of alternatives (Saaty, 1980).

Intensity of importance	Verbal expression	Explanation
1	Indifference	Two choices contribute equally to the objective
3	Moderate preference	Judgment slightly favors one choice over another
5	Strong preference	Judgment strongly favors one choice over another
7	Very strong preference	One choice is favored very strongly over another
9	Extremely strong preference	The importance of one choice over another is of the highest possible order of affirmation
2,3,4,8	Intermediate values	Values to reflect compromise

2.7. Silica saturation index (SSI) for controlling alkaline geothermal reservoirs

Once the geothermal resource is proven, the main constraints to resource exploitation and reservoir management are the deposition of precipitated amorphous silica and the volume of reinjected brine (Brown, 2011). Solubility of amorphous silica is influenced by temperature, pH and ionization of silicic acid in that order (Fleming & Crerar, 1982). At any given temperature and pH, the brine has a maximum concentration of dissolved amorphous silica it can accommodate before onset of

polymerization (at equilibrium). Silica concentration above equilibrium results in oversaturation. The degree of oversaturation or undersaturation of brine with respect to dissolved silica is called the silica saturation index (SSI), defined by Equation (3.19. Undersaturation and oversaturation conditions are determined by SSI<1.0 and SSI>1.0, respectively. Oversaturation causes the excess monomeric silica to polymerize, leading to silica deposition depending on the brine's temperature, pH and chemistry (Krauskopf, 1956). Four principal methods of reducing the oversaturation of silica in geothermal brine exist: hot-brine reinjection, pH adjustment, dilution with condensate and passing oversaturated brine in ageing tanks at pH 7 - 8 to encourage the deposition of polymerized silica. Kenyan geothermal fields have adopted the hot-brine reinjection methodology. pH adjustment to 5.0 - 6.0 retards polymerization kinetics of monomeric silica and is well suited for acidic reservoirs (Kiyota & Uchiyama, 2011). Tank ageing of brine is effective for brines with pH values above 7.0 (Gunnarsson & Arnórsson, 2005), and is sometimes accelerated by adding silica seeds to the ageing tank (Setiawan et al., 2019).

At Olkaria and Menengai geothermal fields, the steam separation pressure is highly dictated by SSI to a range of 4.6 - 11.0 bara for Olkaria and 6.0 - 10.0 bara for Menengai geothermal fields. The brine is reinjected at separation conditions to avoid the oversaturation of silica in the brine, hence evading silica scaling to surface facilities and the subsurface. At this stage, the separated brine at 150 - 187°C has considerable exergy that can support various thermal applications. Power production from geothermal energy using high-pressure flash technology evade silica oversaturation in brine by separating the steam at the point of SSI equal to 1.0. Low pressure flashing of brine, binary systems, and DU, are obliged to use brine with the SSI exceeding 1.0 to achieve economic benefits. Olkaria and Menengai geothermal fields have conservatively designed brine separators at SSI≈1.0, evading silica scaling in the brine flow systems as a trade-off for heat extracted from the reservoir. This compromise reduces geothermal utilization efficiency, thus necessitating drilling more wells to produce the same amount of electric power and thermal energy compared to a similar system with a final utilization of $1.0 \geq SSI \leq 2.0$.

Previous studies show silica oligomerization increases with pH from 3 to 8 for brine with silica concentrations exceeding SSI≤1. The peak pH for forming nano colloids occurs at 7 to 8. However for alkaline brines with a pH above 8.5, the ionization of monomeric silica into silicate anions lowers the SSI (Alexander et al., 1954; Okamoto et al., 1957). Fleming and Crerar (1982) were the first to suggest that degassing of CO_2 from alkaline brines with pH > 8.5 could be used to improve the solubility of amorphous silica and retard the polymerization process. This research seeks to extend this method in Kenyan alkaline geothermal fields to allow DU of geothermal energy in the range of $1.0 < SSI < 2.0$. The majority of hot brine reinjection wells at Olkaria and Menengai geothermal fields have pH values of 8.0 - 10.0 at 25°C, which creates a challenge in pH control of silica scaling through acidification. Luckily, they also conveniently have zero or very low concentrations of Al, Fe, Mg and Ca, which encourage the formation of metal silicates in neutral and alkaline brines (Okamoto et al., 1957).

2.8. Comparison of the current research with previous similar works

The current research seeks to characterize Kenyan geothermal resources' suitability for direct applications in horticultural greenhouse warming, crop drying, industrial heating, spa/bathing, geotourism, milk pasteurization, water desalination/water condensing and aquacultural pond heating. The aim is to improve existing knowledge and acceptance of financially viable DU opportunities available at each geothermal resource and evaluate which projects to prioritize for maximum positive impacts on the surrounding community. It is believed such understanding will fast-track DU to catch up with electricity generation from geothermal resources: reduce

postharvest losses of grains and fish hence improving food security. Besides, it will increase the utilization factor of the resource development investment.

This research presents a novel method of matching thermal needs for different DU projects to the available energy in geothermal resources through GIS-based MCDM methods and thermal efficiency optimization by applying SSI as a trade-off tool. In addition, the calculated field and project rankings are incorporated into GIS through the AHP-WASPAS hybrid method to show the best site for DU projects in Kenya.

Currently, none of the existing research captures DU of geothermal energy, hence the motivation to apply GIS-based MADM methods in open access Quantum-GIS (QGIS) software to characterize the best DU scenarios for Kenyan high enthalpy geothermal resources hosted in Quaternary volcanos emplaced within the floor of Kenyan rift. To link MADM methods and QGIS, kriging and inverse distance weighted (IDW) spatial interpolations were combined with AHP and WASPAS (weighted aggregated sum product assessment) to give synergistic benefits. The innovation of the current study is captured in Table 2.3.

Table 2.3. Difference between the current research work and previous studies on GIS-based MCDM methodology in classifying geothermal resources for DU.

Research aspects	**Current work**	**Previous studies**	**Reference**
Provide a framework for linking thermal demand to the available high enthalpy geothermal resources for DU	Yes	No	-
Application of actual reservoir data to inform decision making	Yes	Yes	(Duan et al., 2011)
Strategic use of AHP for weighting of criteria	Yes	Yes	(Duan et al., 2011; Yalcin & Kilic, 2017)
The GIS-based WASPAS provides a visual framework for ranking and selection	Yes	No	-
Use of modified SSI as a tradeoff tool for calculating hot brine reinjection temperature	Yes	No	-
Linking of East African Rift (EAR) system geothermal resources to their closest farms, cities, industries and communities to spur DU	Yes	No	-

With the highlights of previous studies, the subsequent chapters present results and discussions on the exploration method (geochemistry and QGIS update). New hot springs mapped in Kenya and reservoir temperature estimated using geothermometers.

2.9. Contributions of the current study

When selecting ideal places for DU, this study stands out because of its unique method of dealing with the many challenges that characterize geothermal resources. The novel approach is broken down as follows.

1. No existing studies characterize high, medium and low enthalpy geothermal energy for DU. Prior studies on DU concentrate on case studies in different countries without analyzing the criteria and attributes that make the geothermal resource best suited for the DU scenarios. This research aims to match and link thermal needs to existing geothermal resources by prioritizing heat quantity, geochemistry of geofluid, local economic activities and proximity to local infrastructure.
2. Previous GIS-based studies used AHP to calculate criteria weights and select suitability. However, the pairwise comparison in AHP is effective in weighting criteria but results in

implicit data (verbal), which introduces uncertainty in selection and ranking. This research combines the analytical hierarchy process (AHP) method with the weighted aggregated sum product assessment (WASPAS) method to overcome this challenge.

3. Unlike prior studies that use implicit data, this research employs actual field data based on geothermal wells, boreholes, hot springs, fumaroles, and their geochemical properties to make decisions. This perspective is crucial to constrain the results as closely as possible to reality.
4. This research employs the ionization of monomeric silica into silicate anions when the pH is shifted above 8.5 through degassing CO_2 and H_2S. The shift of pH to values ranging from 8.5 to 10.0 increases the solubility of amorphous silica at lower temperatures ranging from 110 - 120°C, thus allowing DU to operate in temperatures of 110 to 180°C with reduced chances of silica deposition. This method has not been employed before to control silica deposition in heat exchangers.

CHAPTER THREE

3. METHODOLOGY

3.1. Overview

This chapter describes the research methods utilized to optimize and match/link Kenyan geothermal resources to heat demands in their vicinity. More specifically, the chapter describes applied Multi-Criteria Decision Making (MCDM) methods: analytical hierarchy process (AHP) and Weighted Aggregated Sum Product Assessment Method (WASPAS). Details on 2D Inverse Distance Weighted (IDW) and ordinary kriging interpolation methods are also expounded in this chapter as methods for estimating heat distribution within and around geothermal resources. Described herein is modification of Silica Saturation Index (SSI) by ionization of monomeric silica ions into silicate ions by degassing of CO_2 and H_2S from alkaline brines with pH > 8.5 to improve the solubility of amorphous silica and retard the polymerization process. Finally, land use classification in the study area via remote sensing of Sentinel-2 (A and B) images is described in detail for delineating grain farms and their distributions. The classification criteria for Kenyan geothermal resources are given, and data acquisition methods and sources are explained.

3.2. Introduction

The methodology of the current study is conceptualized in Figure 3.1. The present study identified nine DU scenarios: horticultural greenhouse warming, crop drying, aquacultural pond heating, chicken hatchery, milk pasteurization, industrial heating, water desalination, spa and bathing, and mineral extraction, as thermal needs within the vicinity of the geothermal resources under the study. Eleven criteria strongly affect the nine DU scenarios were chosen as outlined in Figure 3.1, with one level of sub-criteria. Though there are eleven criteria, each utilization scenario is impacted by a few criteria. For instance, horticultural greenhouse warming is affected by proximity to roads for timely transportation of perishables to the market, proximity to markets, proximity to a perennial source of surface water for irrigation and near-flat land for construction of the greenhouse structures, as well as temperature and quantity of brine available. On the other hand, crop drying is affected by the proximity of grain farms and road networks to enable smooth transport of grains to the geothermal drier and then to the market in addition to temperatures and quantity of brine available. Proximity to the road network, topography, market proximity, temperatures, and flow rates of geothermal fluids seem to cut across most utilization scenarios.

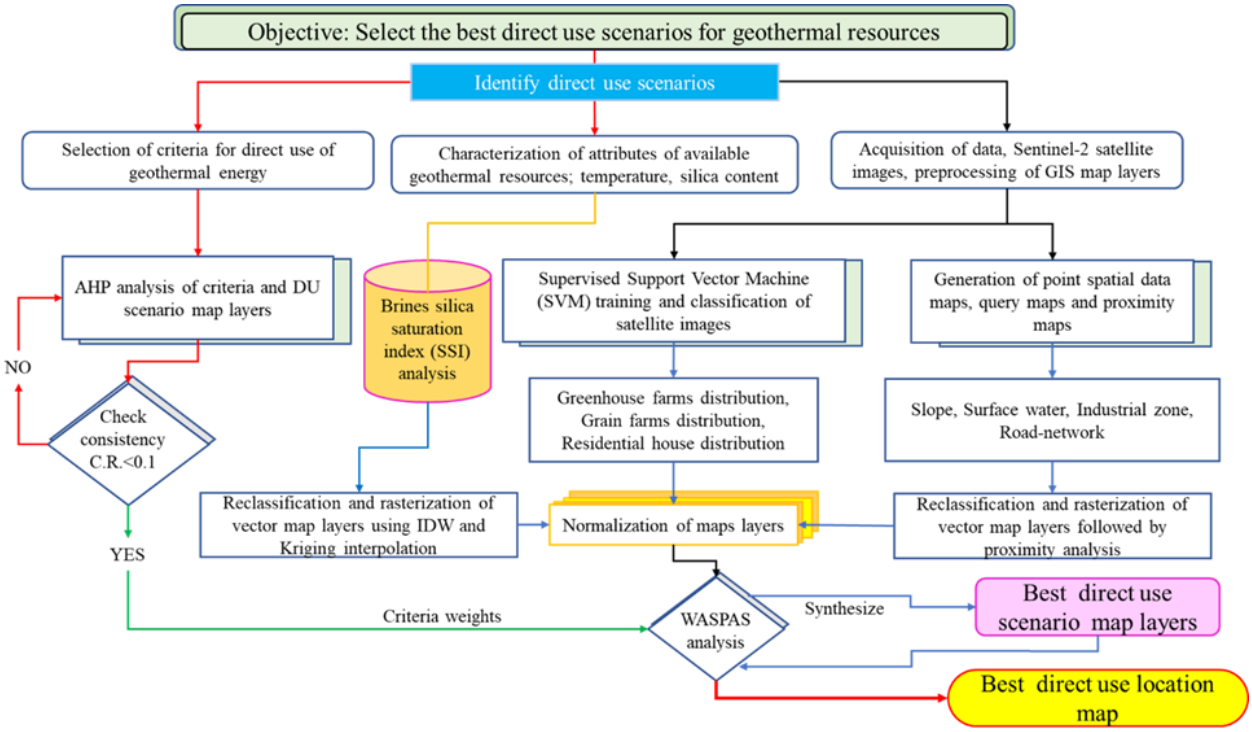

Figure 3.1 The GIS-based hybrid AHP-WASPAS MCDM methodology used for the selection of best utilization scenarios for direct utilization of geothermal energy.

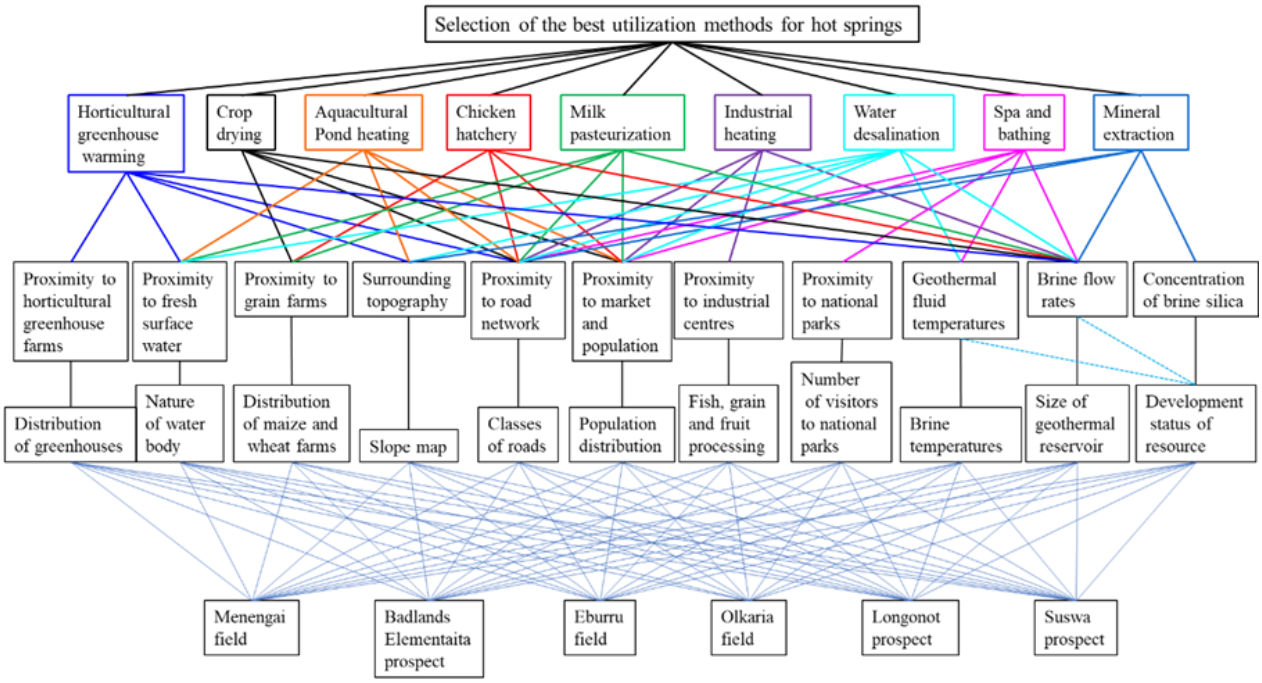

Figure 3.2 Hierarchical breakdown of objective and criteria to match with available geothermal resources.

The basic approach to the methodology outlined three broad segments geared towards realizing the main objective: identifying relevant criteria, characterization of geothermal resources, and

definition of thermal demands. The requirements of the nine DU scenarios expounded in Figure 3.2 were influential in determining the criteria. Every criterion had varying degrees of influence on each DU scenario and the overall selection of the best location for DU. For instance, geothermal fluid temperature and flow rate were considered critical in achieving the main objectives. Owing to the sheer number of criteria, a systematic method of bestowing each criterion with a meriting weight was necessary. AHP was adopted in the current research because it has been applied in most previous studies because of its robustness and consistency in weighting criteria (Zavadskas et al., 2016). The weights were helpful in the synthesis of DU scenario map layers.

Characterizing geothermal resources involved mapping locations of geothermal heat resources accessible to surface. Liquid and vapour phases convey the heat to the surface. The lowest exergy is derived from warm boreholes at 30°C and the highest from geothermal wells (steam and brine at 210°C). The various properties of boreholes, fumaroles, hot springs, and geothermal wells were mapped in QGIS as point vector layers. To avoid silica deposition in surface facilities and reinjection wells, a modified SSI analysis was used to establish the lowest possible hot brine reinjection temperatures. Since the geothermal resource is captured in spatial point data, interpolation is necessary to cover certain encompassed regions. This research employed Kriging and inverse distance weighted (IDW) interpolation methods depending on distribution density and variability of point data.

Thermal needs were identified as those economic activities that require thermal energy input to achieve maximum productivity. Such activities are indicated in Figure 3.2 as DU scenarios. Land use classification of the study area was performed through remote sensing to establish the location, acreage and distribution of grain farms, horticultural greenhouses, and settlements. Supervised classification of Sentinel-2 satellite's images of the study area helped produce the current land use maps. Rasterizing other relevant line and polygon vector data such as rivers, lakes, road networks, national parks, and urban centres provided proximity analysis map layers. The map layers representing the criteria were normalized and synthesized for each DU scenario. The MCDM method, WASPAS, availed a befitting framework for combining different criteria map layers to achieve DU classification.

3.3. Analytical Hierarchy Process (AHP)

Saaty conceptualized AHP in 1971 to solve issues of planning and prioritization (Saaty, 1980). The AHP's backbone is the fundamental AHP scale and the pairwise comparison that allows judgement to be translated to rational numbers which assign weights to the criteria. The main merits of AHP are its ability to integrate verbal expressions of judgement and different incommensurable variables into a decision matrix that helps to rank and select available choices. The consistency ratio (CR) threshold of 0.1 is calculated to assess the distribution of weight coefficients in the decision matrix, increasing the weighting process's reliability (Saaty, 1980). AHP involves four primary steps (Saaty & Müjgan, 2005);

1. *Decomposition of the main objective/goal into hierarchical components,*
2. *Assigning rational numbers from the fundamental AHP scale to the judgmental linguistic variables while performing a pairwise comparison to obtain the decision matrix,*
3. *Computing local weights and consistency ratio of the judgement,*
4. *Aggregation of local weights.*

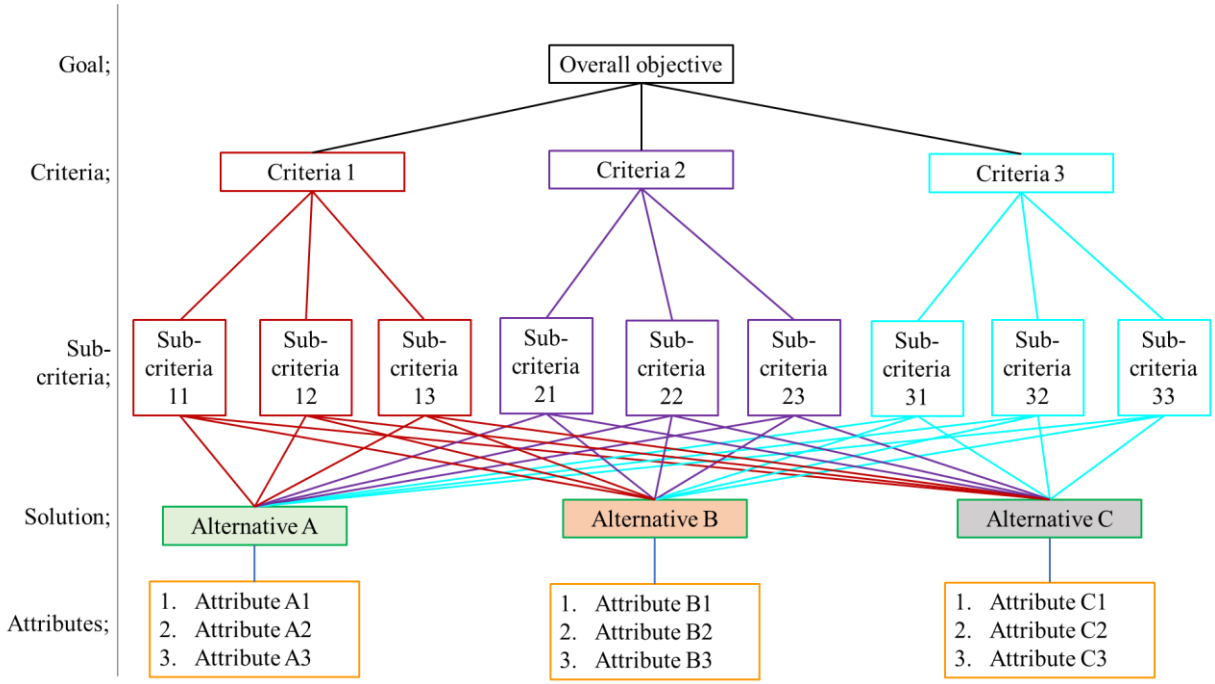

Figure 3.3 Graphical representation of the AHP model

Figure 3.3 shows a simplified AHP model in which different aspects of the objective are compartmentalized, while alternatives are characterized by their inherent attributes. This hierarchical decomposition simplifies assigning judgmental weights and carrying out the pairwise comparison. Equation (3.1) displays the decision matrix and the resultant maximum eigenvector, on the right-hand side, representing the decision weights.

$$\begin{bmatrix} 1 & \frac{a_1}{a_2} & \frac{a_1}{a_3} \\ \frac{a_2}{a_1} & 1 & \frac{a_2}{a_3} \\ \frac{a_3}{a_1} & \frac{a_3}{a_2} & 1 \end{bmatrix} \times \begin{bmatrix} w_1 \\ w_2 \\ w_3 \end{bmatrix} = \lambda_{max} \begin{bmatrix} w_1 \\ w_2 \\ w_3 \end{bmatrix} \tag{3.1}$$

Where $a_1, w_1 \; and \; \lambda_{max}$ represent pairwise judgement, criteria weight, and the maximum eigen value of the decision matrix, respectively. The assessment of the sound judgement is done by computing consistency ratio (C.R) expressed by Equations (3.2) and (3.3) by the help of Table 3.1 that defines random index (RI_n) for a square matrix of dimension (n) of one to eleven.

$$C.I = \frac{\lambda_{max} - n}{n - 1} \tag{3.2}$$

$$C.R = \frac{CI}{RI_n} \tag{3.3}$$

Table 3.1 Random index (RI_n) for square matrices.

n	1	2	3	4	5	6	7	8	9	10	11
RI_n	0	0	0.58	0.9	1.12	1.24	1.32	1.41	1.45	1.49	1.51

Sound judgement is assumed when C.R<0.1, otherwise the pairwise comparison is re-assessed until the C.R is lowered below 0.1 (Saaty, 1980).

3.3.1. **Criteria weighting**

The weighting of criteria map layers was performed based on AHP as outlined in Figure 3.2 and Figure 3.3. The criteria map layer weighting was divided into two main nested levels: the specific DU scenario maps level (micro-level) and the global DU suitability maps (macro-level). Firstly, the reference criteria map layer weights were generated based on their relevance to the general DU suitability. The reference weights, displayed in Table 3.2 columns two, were then used as a basis for generating micro criteria weights for generating DU scenarios, displaced in Table 3.2 column three to eleven. The resultant local criteria weights were then used to manipulate and combine criteria map layers in WASPAS to produce each specific DU scenario, based on the interlinkage shown in the Figure 3.2. Secondly, DU scenario maps were weighted, as shown in Table 3.3, at a global level using the AHP method depending on the economic importance of the DU scenario to the study area. For instance, the criteria that linked the direct utilization of geothermal resources to agriculture and food security, such as horticultural greenhouse warming, crop drying, aquacultural pond heating, milk pasteurization, chicken hatchery and industrial heating, were given more weight due to their positive contribution to food security. Since Kenyan alkaline geothermal brines have a lithium concentration of < 2.0 ppm, mineral extraction was given the least weight. The synthesized DU scenario map layers were combined using the WASPAS method to produce global DU suitability maps for SSI at zero and SSI at two.

Table 3.2. Micro-level criteria weights.

Local criteria weights as determined by the AHP method										
Criteria map layers	Reference weights	Horticultural greenhouse warming	Crop drying	Aquacultural pond heating	Chicken hatchery	Milk pasteurization	Industrial heating	water desalination	Spa and bathing	Mineral extraction
Proximity to horticultural greenhouses	0.05	0.19								
Proximity to surface freshwater	0.041	0.11		0.19		0.11				
Proximity to grain farms	0.06		0.22		0.306	0.19				
Proximity to the road network	0.12		0.07	0.15	0.167	0.19	0.07	0.08	0.19	0.2
Population distribution	0.026			0.15	0.167		0.04	0.15	0.08	
Proximity to national parks	0.017								0.09	
Proximity to tourist resorts	0.005								0.18	
Proximity to industrial zones	0.055						0.11			0.1
Slope	0.026	0.06		0.07				0.05		
Brine flow rate	0.19	0.24	0.25	0.15	0.19	0.17	0.26	0.24	0.21	0.4
Brine temperature	0.24	0.28	0.35	0.2	0.12	0.21	0.31	0.31	0.2	
Brine silica concentration	0.17	0.12	0.11	0.09	0.05	0.13	0.21	0.17	0.05	0.3
$C.I$	0.143	0.06	0.033	0.04	0.072	0.063	0.049	0.022	0.047	0.051
$C.R$	0.055	0.048	0.029	0.031	0.058	0.051	0.039	0.018	0.036	0.056

Table 3.3. Global weights generated by the AHP method for the DU scenarios.

DU scenarios	Horticultural greenhouse warming	Crop drying	Aquacultural pond heating	Chicken hatchery	Milk pasteurization	Industrial heating	water desalination	Spa and bathing	Mineral extraction
Weights	0.16	0.18	0.13	0.09	0.14	0.12	0.05	0.11	0.02
Consistency	C.I. 0.046					C.R. 0.032			

3.4. Weighted aggregated sum product assessment method (WASPAS)

WASPAS method is a synergistic interaction of the weighted sum model (WSM) and weighted product model (WPM) in a compensatory manner introduced by (Zavadskas et al., 2012). Aggregation of the two models improves ranking accuracy compared to working with either model. WASPAS has three significant steps: normalizing the decision matrix, weighting and final recombination using Equation (3.8). The decision matrix (DM) is normalized by Equation (3.4) for beneficial criteria and Equation (3.5) for nonbeneficial criteria with $\min\ x_j > 0$.

$$\bar{r_{ij}} = \frac{x_{ij}}{\max\ x_j} \tag{3.4}$$

$$\bar{r_{ij}} = \frac{\min\ x_j}{x_{ij}} \tag{3.5}$$

Where $\bar{r_{ij}}$ depicts normalized criteria map layers in micro-level synthesis and normalized DU scenario map layers in macro-level synthesis. The normalized DM is then weighted for both the weighted product and sum models using Equations (3.6) and (3.7).

$$WPD\ weighting = \prod_{j=1}^{n} \left(\bar{r_{ij}}\right)^{w_j} \tag{3.6}$$

$$WSD\ weighting = \sum_{j=1}^{n} \bar{r_{ij}}.w_j \tag{3.7}$$

The WASPAS method ranking is performed by combining the two weighted methods by including a multiplier λ in the joint generalized criterion, Q, in Equation (3.8).

$$Q_i = \prod_{j=1}^{n} \left(\bar{r_{ij}}\right)^{w_j} \times \lambda + (1-\lambda) \times \sum_{j=1}^{n} \bar{r_{ij}}.w_j \tag{3.8}$$

Zavadskas et al. (2012) proposed $\lambda = 0.5$ for improved accuracy in ranking.

3.5. Interpolation method

Interpolation in GIS is performed to estimate missing discreet data of a spatial point based on values of other neighbouring points and its proximity to them within a given boundary. Interpolation is based on the autocorrelation of data, and is highly enhanced by both numbers and the distribution of known points (Firozjaei et al., 2019). This research only performed interpolation on geothermal resources because their dataset is presented in vector point format, such as geothermal wells, fumaroles, hot springs, warm to hot water boreholes, etc. Within the study area, several geothermal resources, such as Eburru-Elementaita and Olkaria-Longonot-Suswa, show some correlation in heat distribution as evidenced by boreholes dug within their proximity producing warm to hot water or steam. This distribution of high geothermal gradient justifies the use of interpolation tools to estimate geothermal gradient and heat distribution. QGIS is equipped with kriging and inverse distance weighted (IDW) spatial interpolations methods.

3.5.1. Inverse distance weighted (IDW) interpolation

The IDW interpolation's popularity stems from its simplicity. The unknown data point is expressed in terms of points with known values and the inverse of distances from that point to the others, as in Equation (3.9. This relationship implies that the closest neighbours impose more influence than those far away within a given bounded area (Setianto and Triandini, 2015).

$$y_0 = \frac{\sum_{i=1}^{n} x_i w_i}{\sum_{i=1}^{n} w_{ij}} \tag{3.9}$$

Where y_0 is the point with an estimated value, x_i is the point with a known value, n is the number of points with known values, w_i is the respective weight based on the inverse distance between y_0 and x_i. w_i is given as $w_i = d_i^{-u}$ where d_i is the distance between y_0 and x_i and u is the decay function. In this investigation, it was discovered that a decay function of 2.0 provided a more accurate forecast than values of 1 and 3.

Larger distances within a boundary system and fewer data points dramatically reduced the accuracy of IDW interpolation. Thus, point vector data layers such as clusters of hot springs that occurred in close proximity within a smaller area were interpolated using IDW. Less variation was observed in the discharge, temperatures, and chemical composition of hot spring clusters. As a result of interpolation, the point source data was converted to rasters, which are more easily manipulated in GIS platforms. The output layers' pixels were 50 m x 50 m in size.

3.5.2. Kriging interpolation

Kriging estimation is a probabilistic multi-step process commonly used to estimate values of subsurface resources such as water, heat flow and concentration of chemical constituents in soil. Kriging interpolation considers the distance from the point with unknown data values to the other known data points, including the degree of variability of the sampled data (Senapathi et al., 2019). Equation (3.10) shows the general formula for the kriging interpolation:

$$Z(y_0) = \sum_{i=1}^{n} \lambda_i Z(y_i). \tag{3.10}$$

Where, $Z(y_i)$ is the value of known data point at i_{th} location, $Z(y_0)$ is the estimation value at location 0, λ_i is the unknown weight for the known data point at i_{th} location, n is the number of known data points (Cressie, 1989).

Since kriging estimation is anchored on the best linear unbiased estimator, the local spatial dependency of sampled known data points is crucial for calculating the weights. This dependency relationship between known data points and the distances separating them is quantified by

semivariograms and covariances. This study utilized the ordinary kriging interpolation method, represented in Equation (3.11), which is widely used for geospatial data analysis. Firstly, the statistical distribution of the data was analyzed to determine whether it needed to be transformed to fit the normal distribution. The semivariogram was then curve fitted using the following parameters: model function, lag size, nugget, sill, and determination of whether the data are anisotropic or isotropic. The best fitting of the theoretical model to the empirical semivariogram (observed data from geothermal fields) served as the basis for selecting the model. This heavily depended on data trends with respect to distance and distributional variability within the study area. The cross-validation of the predicted data was compared to the observed data with the primary goal of reducing the root mean squared error (RMSE) as much as possible (Bilewu and Sule, 2015). The data set presented in this study fitted well with the gaussian, spherical and exponential valid model functions and predicted values with standard errors ranging from 0.0% for points closer to the known data points and 5.7% for points further from measured data points. Only areas with prediction errors below 5% were utilized for selecting suitable regions.

$$Z(y_0) = \mu + \varepsilon(y_0). \tag{3.11}$$

Where μ is an unknown constant (Lagrange parameter) and $\varepsilon(y_0)$ represents random spatially autocorrelated errors (Zimmerman and Zimmerman, 1991).

Figure 3.4 shows some semivariograms used to provide temperature distribution of hot fluids accessible to the surface around the Menengai caldera and within the greater Olkaria geothermal field. When fine-tuning the fitting of the various variogram models, the root mean squared error (RMSE) was employed as a statistical indicator in the cross-validation technique to compare estimated/predicted values with observed sample readings. The variograms show a sampling of conventional kriging interpolation models that accurately predicted the empirical data and had the lowest root mean squared error (RMSE). Locations for DU suitability were chosen using temperature distributions as a key factor.

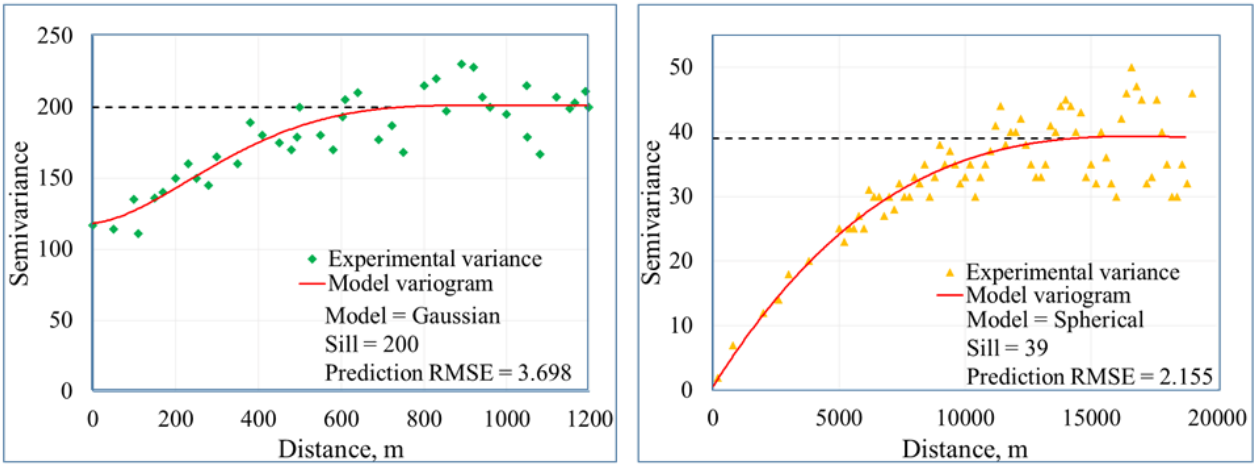

Figure 3.4 (a) Shows a semivariogram of Olkaria geothermal wells based on temperature data, while (b) a semivariogram of shallow warm boreholes distributed around the Menengai caldera.

3.6. Remote sensing for land use classification

Remote sensing for land use classification is the analyzes aerial images to map out a part of the earth's surface into classes such as vegetation, agriculture, populated areas, surface water, bare soil and their changes over time (Jenicka, 2021). This research sort to classify grain farms, horticultural greenhouses, and human settlements near geothermal resources in the central and

southern Kenyan Rift Valley from satellite images. In comparison to field surveys, remote sensing provides a significantly faster and less expensive way to estimate grain yields over an extensive study area (Khanal et al., 2017). The satellite imagery, a sample listed in Table 3.4, used for land use classification was freely obtained from the European Space Agency's Sentinel missions website, https://scihub.copernicus.eu/dhus/#/home. The Sentinel-2 MSI data was chosen due to its moderate spatial resolution of 10 m and high frequency of imagery capture (every five days), providing a dense time series of images for each area of interest (Chastain et al., 2019).
The land use classes were then created by reconstituting the satellite imagery bands into pixel composites (false-colour images) and running them through a supervised pixel-based support vector machine (SVM) classifier. In classifying remote sensing data, the SVM classifier is effective and efficient (Varma, 2016).

Table 3.4 Sentinel-2 satellite immagery.

No.	List of sentinel-2 satellite images used in the study	Date accessed
1	S2A_MSIL2A_20200725T074621_N0214_R135_T36MZE_20200725T111115.SAFE	9/23/2020
2	S2A_MSIL2A_20200605T074621_N0214_R135_T36MZE_20200605T111207.SAFE	9/23/2020
3	S2B_MSIL1C_20200630T074619_N0209_R135_T36MZE_20200630T100725.SAFE	9/14/2020
4	S2A_MSIL1C_20200526T074621_N0209_R135_T36MZE_20200526T100641.SAFE	9/24/2020
5	S2A_MSIL2A_20200605T074621_N0214_R135_T36MYE_20200605T111207.SAFE	10/1/2020
6	S2A_MSIL2A_20200107T075311_N0213_R135_T36MYE_20200107T103344.SAFE	9/18/2020
7	S2A_MSIL1C_20200403T073611_N0209_R092_T36MZE_20200403T095545.SAFE	9/26/2020
8	S2A_MSIL1C_20200801T073621_N0209_R092_T36MZE_20200801T094857.SAFE	9/15/2020
9	S2A_MSIL1C_20200831T073621_N0209_R092_T36MZE_20200831T094106.SAFE	9/26/2020
10	S2A_MSIL1C_20200513T073621_N0209_R092_T36NZF_20200513T095757.SAFE	9/21/2020
11	S2A_MSIL1C_20201212T075321_N0209_R135_T36NYG_20201212T091533.SAFE	2/11/2021
12	S2A_MSIL1C_20210108T074311_N0209_R092_T37NBA_20210108T091312.SAFE	2/11/2021
13	S2A_MSIL1C_20210128T074201_N0209_R092_T36MZE_20210128T091232.SAFE	2/12/2021
14	S2A_MSIL1C_20210128T074201_N0209_R092_T37MBV_20210128T091232.SAFE	2/11/2021
15	S2A_MSIL1C_20210131T075141_N0209_R135_T36MZE_20210131T091559.SAFE	2/14/2021
16	S2A_MSIL1C_20210131T075141_N0209_R135_T36NXF_20210131T091559.SAFE	2/11/2021
17	S2A_MSIL2A_20201212T075321_N0214_R135_T36MYE_20201212T105613.SAFE	2/16/2021
18	S2A_MSIL2A_20201212T075321_N0214_R135_T36NXF_20201212T105613.SAFE	2/13/2021
19	S2A_MSIL2A_20210128T074201_N0214_R092_T36MZD_20210128T105900.SAFE	2/18/2021
20	S2A_MSIL2A_20210131T075141_N0214_R135_T36NYF_20210131T110009.SAFE	2/12/2021
21	S2B_MSIL1C_20200211T074959_N0209_R135_T36MZE_20200211T100642.SAFE	5/3/2020
22	S2A_MSIL1C_20200513T073621_N0209_R092_T37MBU_20200513T095757.SAFE	9/12/2020
23	S2A_MSIL1C_20210806T073621_N0301_R092_T37NBA_20210807T003646.SAFE	12/13/2021
24	S2A_MSIL1C_20210829T074611_N0301_R135_T36MZE_20210829T090242.SAFE	11/3/2021
25	S2A_MSIL1C_20211028T075031_N0301_R135_T36MYE_20211028T085304.SAFE	11/28/2021
26	S2A_MSIL1C_20211224T074331_N0301_R092_T36MZE_20211224T085543.SAFE	1/11/2022

3.6.1. **Importance of use of remote sensing for grain farm mapping**

In Kenya, post-harvesting grain loss is a significant issue, particularly for maize, where it is claimed that 30% of the harvested grains are lost due to inadequate drying and storage (Dudi, 2014). The loss has an adverse financial impact on the farmers and worsens food security in a

nation with a surplus of demand for maize (Onono et al., 2013). Areas near geothermal resources should use the low-grade energy in brine for sanitary and quicker crop drying with fewer grain loss chances to reduce grains' post-harvest loss. There are some industrial diesel-fired maize dryers, according to a study conducted by VEGA for USAID and GDC on the demand for energy for crop drying. One is located in Nakuru, which handles grains transported within a radius of 250 km (Land O' Lakes, 2014). These grain dryers demonstrate the viability of the idea of centralized drying facilities. Compared to fossil and biomass fuels, the drying centres can reduce their energy expenditures by up to 50% by using the thermal energy contained in geothermal brine (Ngethe & Jalilinasrabady, 2020).

Additionally, an item of significant capital expenditure like a high-capacity crop dryer needs drying earnings to pay for itself. Dryer capacity and utilization parameters affect the payback period. To make the most of the crop dryer, choosing a location in the center of a grain-growing area is essential. This study used remote sensing to detect land use near geothermal resources, concentrating on grain farming, horticultural greenhouses, and population dispersal. To accomplish this, sentinel-2 images were downloaded from Corpernicus Scientific Data Hub and processed to track grain farms from land preparation and planting to growing seasons, revealing critical information regarding crop calendars and farm sizes. Sentinel-2 images were downloaded twice monthly from 2020, January to 2021, December and the crop growth was monitored.

3.6.2. **Satellite image processing procedure**

The following order of preprocessing steps was followed after downloading the images:

1. Atmospheric correction through dark object subtraction (DOS)
2. Cloud cover masking
3. Band B11 was resampled from 20 m resolution to 10 m resolution using nearest neighbour interpolation.
4. Consequently, bands B11 (SWIR), B08 (NIR) and B02 (Blue) were combined to create a false-color composite image. The false-colour composite image highlights rigorously growing crops, such as maize, as bright green, bare soil and sparse vegetation as mauve, buildings and roads as light purple, lakes and rivers as bluish and mature trees as dull green to dark green (Lemenkova, 2020).
5. Sentinel-2's B11, B08, and B02 false-color multiband photos were afterward put through supervised image classification. Support Vector Machine (SVM) algorithms were utilized through segmentation and classification techniques to retrieve data on horticultural greenhouses, maize plantation seasons, farm distribution, and cluster sizes of neighbouring human populations.

Change detection was applied to processed photos from several dates in order to verify the distribution and sizes of maize farms. Between the maize farms, the areas that saw little to no change over the whole growing season were referred to as the woodlands, bushland, and grasslands. The counterchecked categorized photographs were merged to create a coherent, distinctively paletted image highlighting maize farms in their precise proportions and distribution.

3.7. Direct use and silica scaling management in alkaline geothermal resources

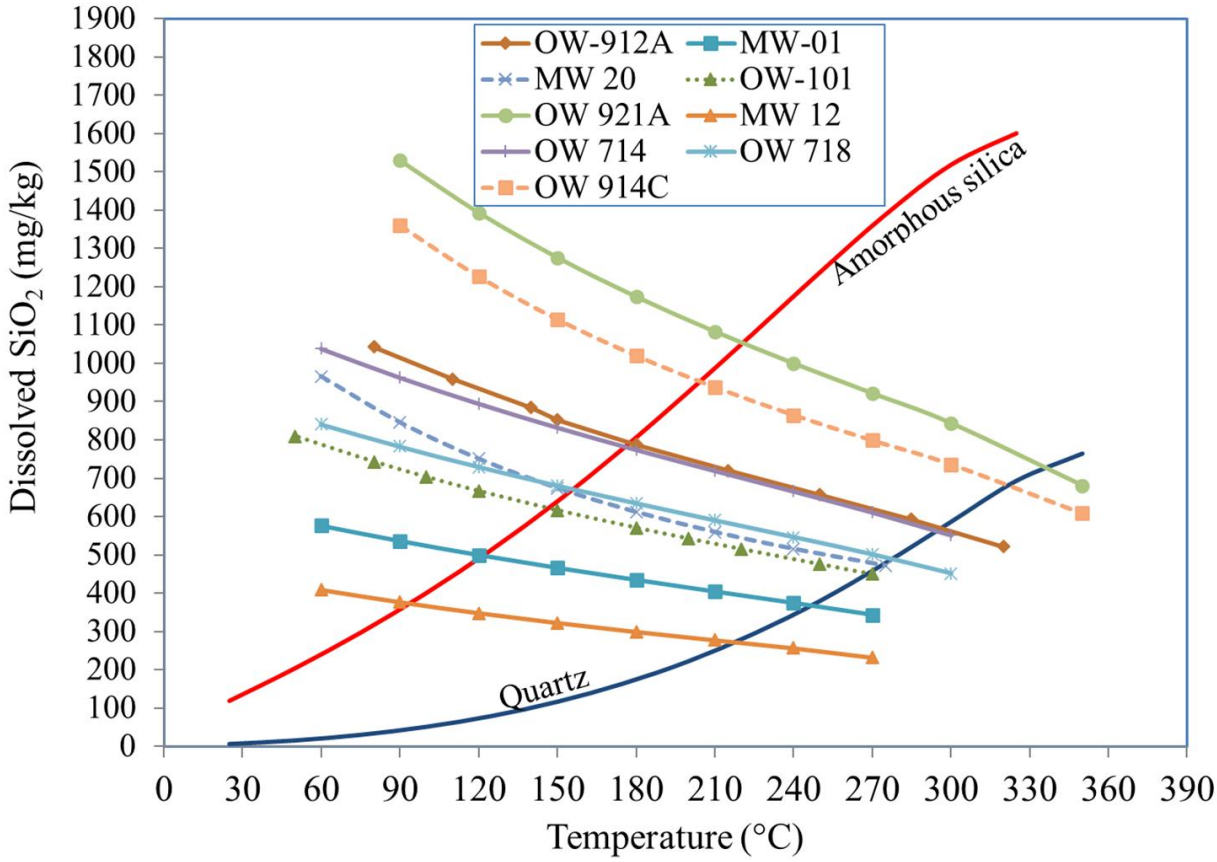

Figure 3.5 Silica solubility curves for some of the production wells from Eburru, Olkaria and Menengai geothermal fields, calculated from the Program WATCH, version 2.4 / 2010 based on adiabatic boiling to reservoir conditions and pH 7.0.

The solubility of silica is dependent on temperature in a reversible chemical equilibrium shown in Equation (3.12). At the reservoir, the solubility of silica is in equilibrium. However, as geofluids rise to the surface, changes in temperature and pH may cause amorphous silica to precipitate.

$$SiO_{2_{(s)}} + 2H_2O \rightleftharpoons H_4SiO_{4_{(aq)}} \tag{3.12}$$

The dissolved amorphous silica is weak silicic acid and its concentration, C, can be calculated in mg/kg using Equation (3.13) as amorphous silica solubility curve in Figure 3.5 for $0℃ \leq T \leq 250℃$ (Fournier & Rowe, 1977).

$$\log C = \frac{-731}{T} + 4.52 \tag{3.13}$$

Where T is the temperature (K). Using Equation (3.13), the silica saturation index (SSI) is calculated as

$$SSI = \frac{C_{(meas)}}{C}. \tag{3.14}$$

Whereas $C_{(meas)}$ is the measured total silica concentration in the geofluid. As the pH increases above 8.5, the silicic acid dissociates to a charged hydrogen cation and silicate anion, as in Equation (3.15), which is more soluble than the silicic acid (Fleming & Crerar, 1982).

$$H_4SiO_4 \rightleftharpoons H^+ + H_3SiO_4^- \quad (3.15)$$

To account for th pH and temperature effect on the solubility of silica, Equation (3.15) is modified to Equation (3.16) by using the Debye-Hückel equation (Fleming & Crerar, 1982).

$$S = C \times \left[1 + \left\{\frac{10^{pH} \times K_1}{\gamma_{(H_3SiO_4^-)}}\right\}\right] \quad (3.16)$$

Where S is the concentration of both silicic acid and silicate anions in mg/kg, C is the same as in Equation (3.13), K_1 is the silicic acid dissociation constant given in Equation (3.17) and $\gamma_{(H_3SiO_4^-)}$ is the activity coefficient of $H_3SiO_4^-$ (Brown, 2011).

$$K_1 = \frac{-2549}{T} - 15.36 \times 10^{-6}T^2 \quad (3.17)$$

For precipitation of silica to take place at pH>8.5, the pH change has a more substantial effect compared to the temperature change and hence, the concentration of amorphous silica is liable to precipitate, $C_{Modified}$, is obtained from concentration of $H_3SiO_4^-$ as in Equation (3.18).

$$C_{Modified} = [S - C] \times \frac{m_{SiO_2}}{m_{H_4SiO_4}} \quad (3.18)$$

Where m_{SiO_2} and $m_{H_4SiO_4}$ are the molecular weights of silica and silicic acid, respectively. It follows that for the modified silica saturation index for moderately alkaline geothermal brine, is calculated as in Equation (3.19).

$$SSI_{Modified} = \frac{C_{(Modified)}}{C} \quad (3.19)$$

The difference between SSI and $SSI_{Modified}$ provides a safe zone where heat for DU can be extracted from alkaline brines with minimal risk of silica scaling. For DU, it is safer to extract brine from production wells with less silica content and higher pH values, >8.5, to reduce the risks of amorphous silica oversaturation. However, suppose the wells are already connected to centralized steam separators. It is prudent to work with brine from more neutralized reinjection wells in terms of silica content such as OW-703, OW-708, OW-901, and OW-911 from Figure 3.6. Steam separation also allows degassing of CO_2 and H_2S hence shifting the pH of the brine towards alkalinity to encourage first-order dissociation of silicic acid into silicate ions once pH exceeds 8.5. For DU to utilize high enthalpy alkaline brines like encountered at Olkaria Domes, OW 914C and 921A, in Figure 3.5, an additional steam flashing is required from 184℃ to 150℃ to encourage more degassing or/with NaOH dosing to shift the pH to 10 for both the first and second-order dissociation of silicic acid to take place and deter the precipitation of silica on surface facilities. By analyzing the degassing and pH effect on the Eburru, Menengai and Olkaria geothermal fluids, it was established that heat could safely be extracted from various percentages of brine to a minimum temperature of either 100℃ or 130℃, shown in Table 3.5, for alkaline brines with low and high silica content, respectively. At an average temperature of 150℃, these fluids are accessible close to hot reinjection pipelines, evaporation ponds or hot reinjection wells.

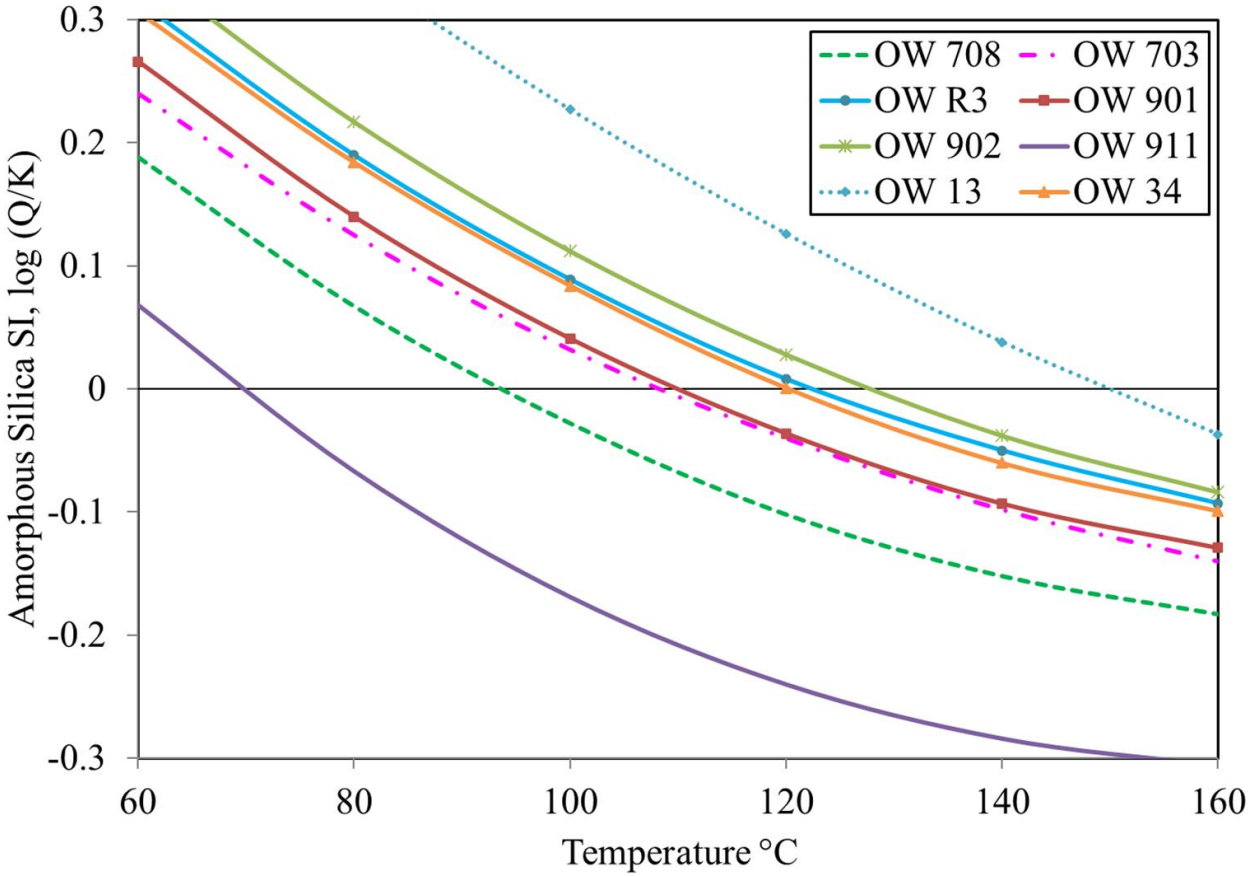

Figure 3.6 The modified silica saturation index, $SSI_{Modified}$ for some of the hot brine reinjection wells at the Olkaria geothermal field based on conductive cooling at a degassing coefficient of 1.0 calculated using the Program WATCH, version 2.4 / 2010.

Table 3.5. Brine quantity by percentage for heat extraction for DU.

Geothermal field	Quantity of brine to be cooled to 130℃	Quantity of brine to be cooled to 100℃
Eburru	100%	-
Menengai	30%	60%
Olkaria	21%	41%

3.8. Classification of geothermal resources

Except for details of specific case studies, the three geothermal energy classification methods listed above are nearly conclusive for the assessment, exploration, development, exploitation, and reporting of geothermal resources. However, the classification based on thermodynamics fluid properties is best appropriate to describe the geothermal resource for exploitation Temperature, enthalpy and exergy are some of the properties used to calculate work done and energy conversion efficiency (Jalilinasrabady and Itoi, 2013; Lee, 2001). Well-logging data at Olkaria and Menengai geothermal fields indicate that the reservoir's temperature and depth do not necessarily

significantly influence the fluids' enthalpy flowing into the wells. The main factors affecting enthalpy, in addition to temperature, are pressure, permeability distribution within the reservoir, and the make-up of the feed zones into the well.
One or two high enthalpy feed zones may coexist in a well with shallow low enthalpy feed zones. For instance, a well could combine shallow low enthalpy feed zones with one or two high enthalpy feed zones. Some wells have medium enthalpy feed zones at the onset of production casing and zero permeability at the bottom despite very high temperatures or vice versa. These combinations make it difficult to predict the enthalpy values of fluids within the reservoir. Lee (2001) introduced a stable method of classifying geothermal energy on the surface based on exergy normalized to the maximum exergy of the corresponding sink condition. The normalized exergy ratio, referred to as the specific exergy index (SExI), has values ranging from zero to a unit and is based on Equation (3.20).

$$SExI = \frac{(h - 273.16s)}{1192} \tag{3.20}$$

Where h and s stand for enthalpy (kJ/kg) and entropy (kJ/kgK), respectively. Lee used saturated steam at 100°C as the lower boundery of high-quality steam for power production with SExI = 0.5 and hot water at the same temperature as the upper boundary for low-quality resource with SExI = 0.05. The resources with SExI above 0.5 are regarded as high enthalpy. In contrast, those with SExI lower than 0.05 are regarded as low enthalpy and those who fall in between as medium enthalpy geothermal resources. Kenyan geothermal resources were classified in this manner, as shown in Figure 3.7.

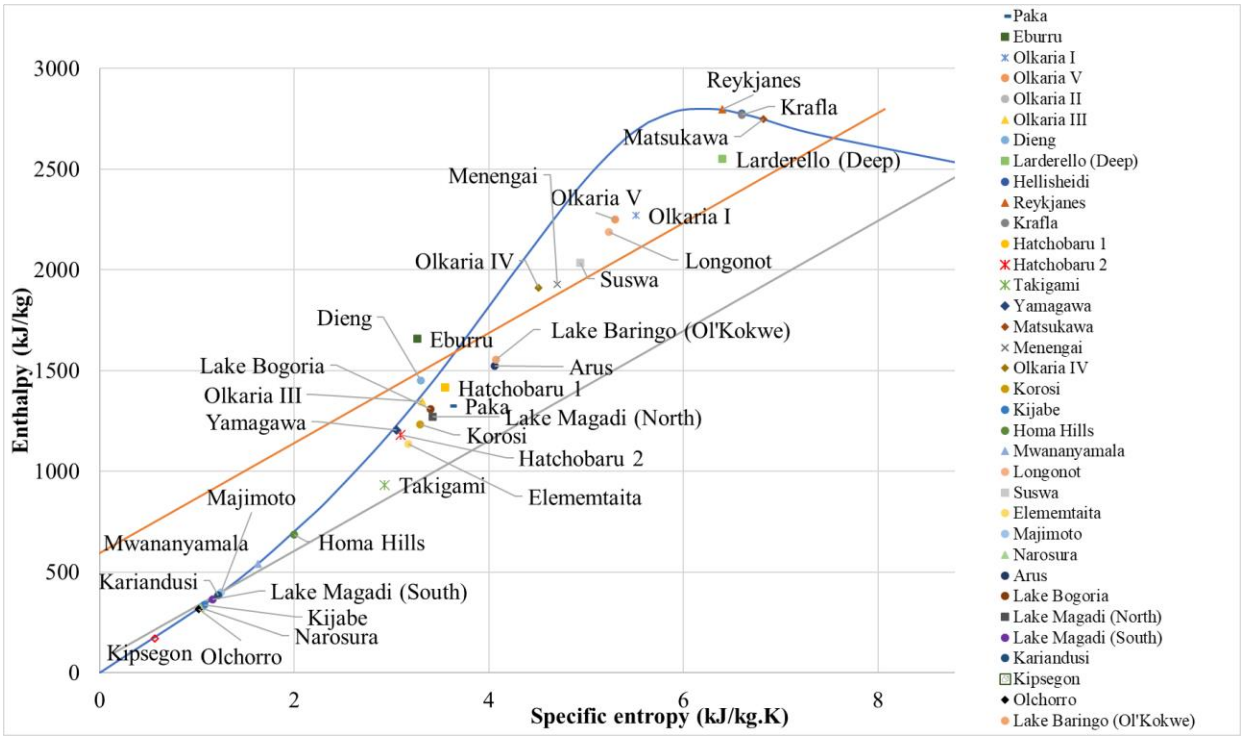

Figure 3.7 SExI plot classifying geothermal resources from Kenya, Japan, Iceland, Italy and Indonesia.

From Figure 3.7, most geothermal resources in Kenya are mapped as medium and high enthalpy. East Olkaria is mapped as high enthalpy, while west Olkaria falls into medium enthalpy category.

Most of Japan's most reliable geothermal fields, including Takigami, Hatchobaru, and Yamagawa, fall into the liquid-dominated category of medium enthalpy geothermal fields. A recent study on their sustainability indicates that their production zones will remain stable for more than 15 years. (Jalilinasrabady et al., 2021).

3.9. Data acquisition

Direct use of geothermal energy is site-specific since it depends on both favourable characteristics of the geothermal resource and the economic activities of the surrounding communities. This research obtained well production data on fluid chemistry and enthalpy from developed geothermal resources in Kenya such as Eburru, Olkaria, and Menengai geothermal fields. In addition, we collected warm/hot water boreholes data and surface manifestation data on fumaroles and hot springs from undeveloped geothermal resources such as Longonot, Suswa and Elementaita during field research. This study used data from 134 geothermal wells, 128 boreholes, 41 fumaroles, and three hot springs within the study area to create brine flow rate, brine temperature and brine silica concentration criteria maps. The geothermal wells data were acquired from geothermal development companies, Kenya Electricity Generating Company (KenGen) and Geothermal Development Company (GDC). The fumarolic, hot springs, and boreholes data were acquired during a field survey of these geothermal fields and prospects. The data was mostly in point data format (production wells, hot reinjection wells, fumaroles, hot springs). To establish geothermal heat flow to the surface within vicinities of geothermal fields, warm water boreholes data, with 50 – 500 m depth, was used. Supplementary data on all geothermal resources under the current study was also collected from the literature (C. W. Karingithi et al., 2010a; Kipngok et al., 2019; Saitet & Rop, 2015).

The Sentinel-2 (A and B) imagery for remote sensing agricultural land-use classification was obtained from the European Space Agency open-source website called Copernicus Open Access Hub, https://scihub.copernicus.eu/dhus/#/home (Macarringue et al., 2022). The website shares global satellite images captured every five days from two satellite platforms A and B (Chastain et al., 2019). Sentinel-2 images are categorized into 12 bands distinguished by wavelength and spatial resolution differences. The visible light bands (B2, B3, B4) and near-infrared (NIR) band (B8) have a spatial resolution of 10 m. Visible and near-infrared (VNIR) bands (B5, B6, B7) and short-wave infrared (SWIR) bands (B8A, B11, B12) have a resolution of 20 m (Park et al., 2017). The rest of the bands (B1, B9, B10) have a spatial resolution of 60 m. For agricultural classification, the image bands SWIR (B11), NIR (B8),and B2 were combined into a multiband false-colour composite virtual raster that highlights rigorous growing crops, such as maize, as bright green, bare soil and sparse vegetation as mauve, buildings and roads as light purple, lakes, and rivers as bluish and mature trees as dull green to dark green (Lemenkova, 2020). The land use classes from remote sensing analysis yielded the grain farms, population distribution and horticultural greenhouse distribution criteria maps. The surface freshwater, road networks, and industrial zones vector criteria map layers were extracted from Google Satellite base maps in QGIS and field surveys. The slope criteria map layer was generated by analyzing the slope on a SRTM 1 Arc-Second Global digital elevation model (DEM) file downloaded from the USGS Earth Explorer website, https://earthexplorer.usgs.gov/. The national parks maps were extracted from a national wildlife census 2021 report provided by the Kenyan Ministry of Tourism and Wildlife (Waweru et al., 2021).

CHAPTER FOUR

4. SELECTION OF BEST DIRECT USE SCENARIOS FOR HIGH ENTHALPY GEOTHERMAL RESOURCES LOCATED WITHIN CENTRAL AND SOUTHERN KENYAN RIFT VALLEY

4.1 Introduction

This chapter will investigate suitability of direct use within vicinity of high enthalpy geothermal resources. To accomplish this objective, this study used data from 134 geothermal wells, 128 boreholes, 41 fumaroles, and three hot springs within the study area to create brine flow rate, brine temperature and brine silica concentration criteria maps. The geothermal wells data was acquired from geothermal development companies, Kenya Electricity Generating Company (KenGen) and Geothermal Development Company (GDC). The fumarolic, hot springs, and boreholes data were acquired during a field survey of these geothermal fields and prospects. This study established a novel framework structure for analyzing geothermal resources for direct use. The model used was based on GIS-based AHP-WASPAS hybrid method to show the best site for DU projects in Kenya. Heat demands for sustaining commercial-sized geothermally heated projects were estimated and their locations discovered.

4.2 History of development of high enthalpy geothermal resources in Kenyan rift valley

Exploration of geothermal energy in Kenya began earnestly in 1956 as a collaboration of the Kenyan government and the United Nations, and by 1959, two shallow exploration wells: OW-X1 and OW-X2, were drilled. They failed to discharge, and the exploration work halted. Further work resumed in the 1970s with the drilling of OW-01 and OW-02. OW-02 successfully discharged steam and set the stage for the development of geothermal energy in Kenya (Ofwona, 2000). Olkaria one power plant was commissioned for 45 MWe in three stages of each 15 MWe in 1981, 1982 and 1985 (Ofwona, 2010). The first 3-D natural state model was developed by Bodvarsson et al. (1987). In 1990, a detailed geological and hydrogeochemical survey of Elementaita, Eburru, Olkaria, Longonot and Suswa regions was done by Clarke et al. (1990) They detailed geological maps and gas geothermometer estimations for the hydrothermal systems inside the volcanic complexes. In 1993, Dunkley et al. (1993) conducted a detailed geological and hydrogeochemical survey of geothermal recourses located in northern Kenya rift valley, encompassing Lake Baringo to Lake Turkana. Since the 1980s, the Ministry of Energy tasked Kenya Power Company (KPC) with developing geothermal resources. Kenya Electricity Generating Company (KenGen) was formed in 1996 by separating the responsibilities of generating electricity from those of distribution. After separation from the mother company (Kenya Power Company) in 1996, KenGen renamed itself and began operating independently in 1997, though fully government owned. In 2006, the government sold a 30% stake through an Initial Public Offer (IPO) to make KenGen partially private. KenGen continued as solely responsible for assessing, exploring, and developing geothermal resources in Kenya, especially at the Greater Olkaria complex and Eburru geothermal fields. Geothermal Development Company (GDC) was later formed in 2011 to produce steam for independent power producers (IPPs) and accelerate resource development in Kenya by absorbing the risks involved when drilling geothermal wells. Kengen and GDC have prioritized the development of high enthalpy resources, and currently four fields have been proven to

sustainably produce steam: Olkaria, Eburru, Menengai, and Paka. Development of Korosi is ongoing. By 2022 December, the Greater Olkaria Complex produces about 863 MWe from single flash and organic rankine cycle (ORC) power plants, as shown in Figure 4.1. High enthalpy geothermal resources in Kenya are characterized by their colocation with dormant caldera volcanoes located on the floor of the Kenyan rift valley. They are controlled by trachytic structures of the Pleistocene to the Holocene eras and have reservoir temperatures of above 200°C, either measured directly or estimated from geothermometers.

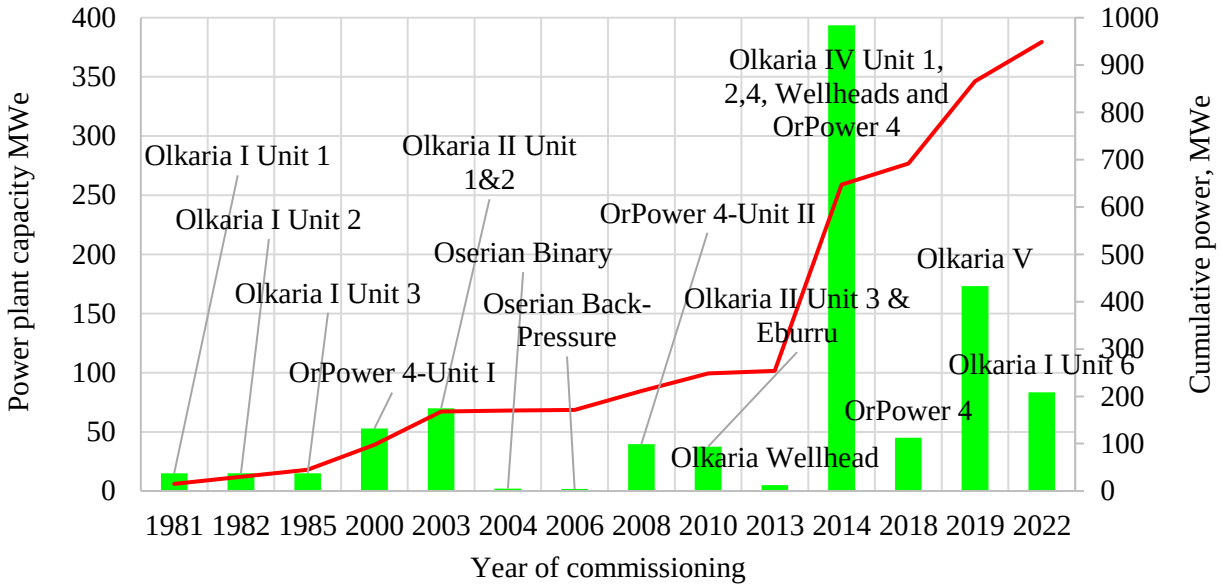

Figure 4.1 Year progression of Kenyan geothermal energy development for power production.

4.3 The need for direct use of high enthalpy geothermal resources

Kenya produces about 863 MWe from the 948.72 MWe installed geothermal resources at the Greater Olkaria Complex and Eburru geothermal field. The power generation process has availed a total of about 4700 t/h of hot brine to the surface with an average temperature of 158 – 190°C from the three geothermal fields, as summarized in Table 4.1. Almost all this high temperature brine is reinjected back into the reservoir. However, brine from Olkaria and Eburru wellhead units is normally not reinjected back to the reservoir since it is dumped into evaporation ponds. This implies that a potential of over 790 MWt of direct heat is lost by evaporating or reinjecting the brine back to the reservoir, when considering a sink condition of 30°C. This heat could be utilized in greenhouse warming, aquacultural pond heating, Spa/bathing and swimming, industrial heating, milk pasteurization, and crop drying.

Table 4.1 Figures of hot brine availabe at Olkaria, Menengai, and Eburru geothermal fields showing their flow rates in tonnes per hour and temperatures (Gitonga, 2016; Ouko and Mangi, 2020).

Geothermal field	Brine flow rates (tph)	Separation pressure (bara)	Brine Temperature (°C)
Olkaria I	258	6	158
Olkaria II	566	6	158

Olkaria I AU	524	12	188
Olkaria IV	814.7	12	188
Olkaria V	1020	13	191
Olkaria Wellheads	589	7	165
Eburru	60	6	158
Menengai	910	6	158

Besides, the high separation pressures at Olkaria and Menengai prevent self-discharging wells with wellhead pressures below 4 bara from generation of electricity. Such wells, as well as those with cyclical discharges, are closed and regarded as being unproductive. Direct usage is best suited for high enthalpy geothermal resources with production wells since they provide fluids with high flow rates and temperatures that can support large-scale commercial operations.

At same time, Kenyan agricultural sector grapple with lack of thermal energy for grain drying, tea drying, aquacultural pond heating, swimming pools heating and industrial heating. White maize/corn is the main staple food in Kenya with a per capita consumption of 70 kg (Gitonga and Snyder, 2022). Post harvesting grain loss is a serious problem in Kenya, especially for maize where it is estimated that 30% of the harvested grains are lost through poor drying and storage (Dudi, 2014; Kamar et al., 2018). Kenya's indigenous maize production is unable to satisfy demand, necessitating imports, particularly in years with protracted drought. Therefore, food security in Kenya might be increased by implementing clean and effective grain drying facilities, such as those driven by geothermal brine. Besides, vegetable oil processing industries and tea drying companies in Kenya use firewood to run steam boilers for heating and drying purposes, causing accelerated deforestation and destruction of water catchment systems. It is estimated that 4 – 10 trees are felled to process one tonne of brown tea leaves. Kenya exports over 400,000 MT of processed tea annually from over 66 drying factories. Furthermore, due to their high demand for irrigation water, fresh-cut flowers are farmed close to permanent freshwater rivers and lakes and are Kenya's second-largest export. The high altitudes (1000 – 3500 m asl) of the Kenyan rainfed agricultural lands cause them to experience colder nights (below 20°C) and chilly weather in June and July. This condition cause dew-point temperatures to drop inside greenhouses and encourage the proliferation of fungal diseases, such as Petal Botrytis and Downy Mildew (Ngethe & Jalilinasrabady, 2021). Therefore, the demand for thermal energy is significant in Kenya and several research studies have tried to suggest how to interlink these demands to the available geothermal energy. In 2013, geothermal Development Company (GDC) and USAID enlisted Land O'Lakes to do prefeasibility studies for geothermally heated greenhouses and aquacultural ponds (Land O' Lakes, 2013; Land O'Lakes, 2013). Through a Strengths-Weaknesses-Opportunities-Threats (SWOT) analysis, they concluded that the potential for geo-greenhouse and geo-aquaculture development in Kenya has a high probability of success if stable electric power is connected to the farms and quality fish feed production companies are established. In 2014, Land O' Lakes conducted the th1rd prefeasibility study on geothermally heated crop dryers, and they concluded that geo-drying of grains and tea offered a competitive edge provided the wet products were transported to the geothermal centres (Land O' Lakes, 2014). These studies identified potential thermal demands but failed to characterize the geothermal resources to these demands. They also failed to produce maps assessing grain farming land, horticultural greenhouses, road infrastructure and other technical and economic enabling factors for direct use. Hence, their study can be termed inconclusive and too removed from reality. In 2020, Climate Technology Centre & Network (CTCN) enlisted GreenMax Capital Advisors to conduct a study of identifying the most

suitable direct use applications and technologies in low to medium temperature geothermal systems in six African countries: Djibouti, Ethiopia, Kenya, Rwanda, Tanzania, and Uganda (GreenMax, 2020). In Kenya, the study chose to work with Menengai, Eburru, and Olkaria geothermal fields, despite these geothermal fields being categorized as high temperature as shown in Table 4.1. They concluded that the best direct use scenarios for Olkaria, grain drying, fish drying and water desalination. For Eburru, grain drying, milk pasteurization and chicken hatcheries were chosen as the top heat demands. For Menengai, grain drying, milk pasteurization, water desalination and balneotherapy were chosen as the top heat demands. These heat demands were estimated from forums and questionnaires to the local community. However, the study failed to identify the grain catchment zones, sources and destinations of milk and water to be cleaned. Still, geothermal characterization was not done to ascertain a sustainable heat provision to the direct uses. The demand for greenhouse heating was also somehow ignored.

The forementioned studies failed to conduct a conclusive feasibility study since direct use involves various geothermal characteristics and enabling economic factors which need a structured framework for analysis. For high enthalpy geothermal resources, it is crucial to factor in the location of production and hot reinjection wells, their temperatures and flow rates, their chemistry and production history. For economic factors, it is important to understand the size and distribution of grain farms, roads for ease movement of goods, proximity to fresh surface water, proximity to the urban areas, and local economic activities for a realistic matching of heat demands to the heat resources provided by the geothermal resources. This study used a GIS-based MCDM methods to analyze and interlink local thermal demands to the available geothermal characteristics. More specifically, this study used AHP-WASPAS hybrid in weighting and overlaying criteria map layers in QGIS to produce best direct use scenarios for six high enthalpy geothermal resources in central and southern Kenyan rift valley: Olkaria, Eburru, Menengai, Longonot, Suswa and Elementaita.

This study chose to analyze the suitability of these high enthalpy geothermal resources for horticultural greenhouse warming, aquacultural pond heating, grain drying, water desalination, milk pasteurization, chicken hatchery warming, industrial heating, spa/bathing/swimming, and mineral extraction (silica). For analysis, eleven criteria relevant to the study area were chose: (1) distribution of horticultural greenhouses, (2) fresh surface water, (3) grain farms, (4) slope map, (5) road network, (6) population distribution, (7) industrial zones, (8) national parks, (9) brine temperature, (10) brine flow rates, and (11) brine silica concentration.

4.4 Description of the study area

Kenya shares the eastern branch of East African Rift (EAR) with Djibouti, Ethiopia, and Tanzania. In this region, the African continent is gradually splitting into two tectonic plates: the Somali plate to the East and the Nubian Plate to the west (Kanda et al., 2019). The Kenyan rift valley is a zone of crustal spreading with a N-S trend that is marked by volcanic activity, normal faulting, and the development of large-scale graben structures (Ofwona, 2010). Fourteen high enthalpy geothermal resources, three saltwater lakes, and five freshwater lakes are emplaced within the Kenyan rift graben's floor (Biggs et al., 2021). These high enthalpy resources are associated with rifting-related volcanic activity, which gave rise to several Quaternary volcanic complexes that host geothermal reservoirs in Kenya (Kanda et al., 2019). This study's high enthalpy geothermal resources are Menengai, Eburru, Badlands Elementaita, Olkaria, Suswa, and Longonot, shown in Figure 4.2 (a), located within the central and southern Rift Valley. Menengai, Eburru and Olkaria fields are categorized as proven geothermal resources since they have production wells.

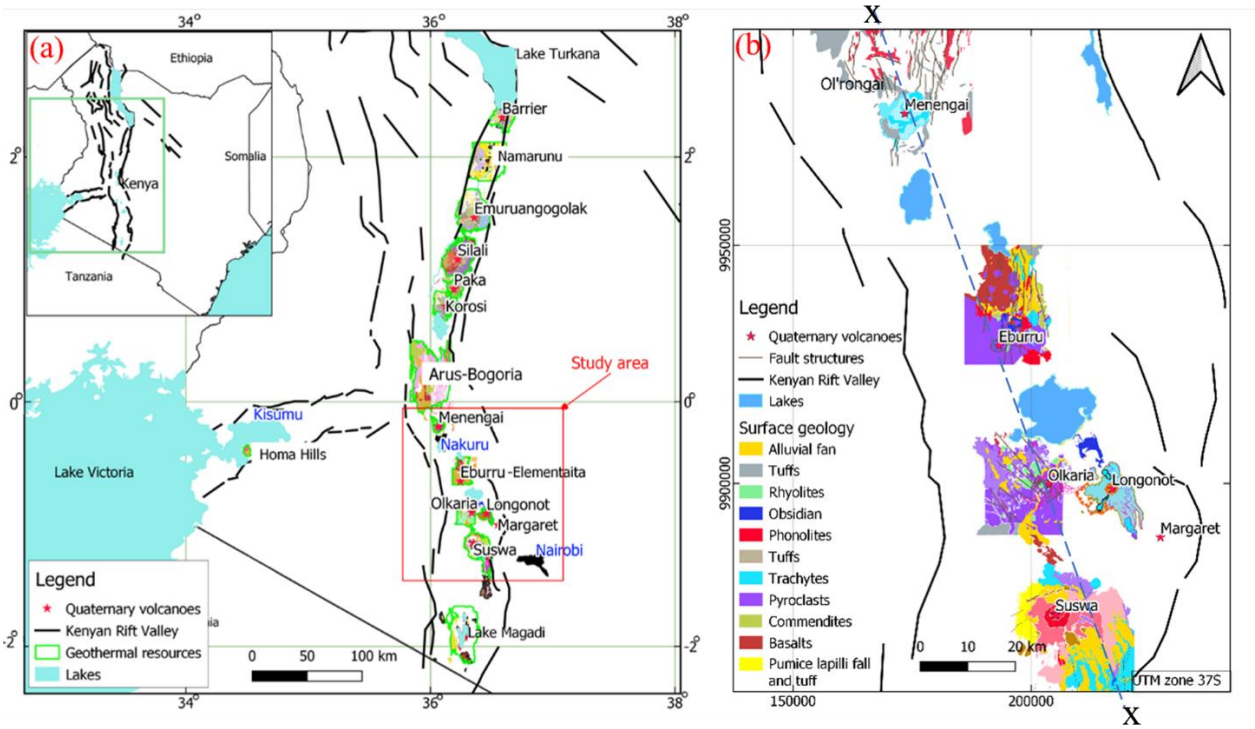

Figure 4.2 (a) Map of locations of geothermal resources in Kenya emplaced within the rift system and (b) the surface geology of resources within the study area.

The study area covers an area of 110 km (west to East) and 144 km (north to south), resulting in a total area of 14840 km^2. The width and length of the study area were determined by a catchment radius of 35 km from each geothermal resource for providing raw materials and customers for the DU scenarios. The 35 km reach was settled on from DU case studies in Iceland with a maximum brine reach of 23 to 35 km (Ragnarsson, 2021). The study area's six high enthalpy geothermal resources are aligned in an NW-SE trend, stretching the overall study area width to 110 km.

4.4.1 Characterization of geothermal resources in central and southern Kenyan Rift Valley

The Quaternary volcanoes that host high enthalpy geothermal reservoirs vary in many aspects such as geological make-up, structural setting, and topography, as shown in Figure 4.2 (b), which influence the DU of geothermal energy in one way or another. Menengai caldera reservoir is located within a partially collapsed caldera with high southern rim walls. In contrast, Ol'rongai reservoir, adjacent to the Menengai reservoir, is located outside the caldera to the northwest beneath Ol'rongai hill. The caldera's surface is covered by rugged terrain of trachytes while tuffs and ignibrites overlie the Ol'rongai region. The Rongai plain lies to the west of the caldera, where boreholes drilled to <200 m depth have struck warm water with varying temperatures, 25-54°C, implying a shallow, lateral up-flow zone at which high geothermal gradient beyond 3°C/100 m is experienced (I. Kanda et al., 2019). Geothermal drilling began in 2011 at Menengai geothermal field with over 20 production wells completed with mass flow rate capacity of 840 t/h and 910 t/h for steam and brine, respectively (Khaemba, 2015). Menengai geothermal reservoir lies at an average depth of 2000 m below surface elevation, of about 1900-2100 masl, and is controlled by

a shallow lying magmatic body at 4-5 km below surface elevation (A. M. Wamalwa et al., 2013). Menengai caldera is distinguished as the hottest reservoir with the fluid discharge of bicarbonate facies to the south and bicarbonate-chloride waters to the north. Well bottom temperatures of up to 400°C have been reported (Kipngok et al., 2019). Both Nakuru city and Lake Nakuru lie 2 km to the south and 6 km to the southeast of Menengai caldera, respectively.

Olkaria geothermal field is the most developed and studied rhyolitic Quaternary volcano hosted within Hell's Gate National Park, located about five kilometres south of Lake Naivasha. Olkaria region is characterized by undulating rugged terrain carpeted by the Longonot tephra layer. It is cleft by a deep Olnjoroa gorge which separates the greater Olkaria region into two; Olkaria East and Northeast fields to the north and Olkaria Domes to the south. The greater Olkaria complex is divided into seven fields for ease of development and exploitation. The greater Olkaria is believed to be underlain by a deep magmatic chamber with shallower intrusions that give rise to the four main up-flow zones in the Olkaria geothermal field (Axelsson et al., 2013; Saitet and Rop, 2015). The up-flow zones feed the Olkaria West field, Olkaria East, Olkaria Northeast and the Olkaria Domes field with both bicarbonate and bicarbonate-chloride waters. The Olkaria geological setting features the Ololbutot fault, Gorge Farm fault, Olkaria fault and Suswa fault (Bonyo, 2020). The lithological stratigraphy reveals almost horizontal layering Olkaria rhyolites and basalt tuffs that host the reservoir, overlain by younger upper rhyolites and unconsolidated pyroclasts. Since the accelerated development in 1981, the Olkaria field has been subject to advanced geophysical and geochemistry investigation to characterize and manage the reservoir for sustainable heat extraction. Currently, 6230 t/h and 2729 t/h of steam and brine are responsible for over 864 MWe and 13.8 MWt utilized in Kenya from geothermal energy. The Olkaria East production field discharges dilute sodium chloride waters, Olkaria West discharges sodium bicarbonate waters, while Olkaria Domes produces both sodium bicarbonate and sodium chloride waters to the northeast and southwest of the field, respectively (Bonyo, 2020; R. N. Wamalwa et al., 2016). Since Olkaria Domes discharges hot geofluids at temperatures above 184°C, they have high silica content 623-1832 ppm that discourage heat extraction below 184°C to avoid silica scaling.

Eburru is another rhyolitic Quaternary volcano located about 25km to the northwest of Olkaria geothermal field with a peak of 2820 masl, as shown in Figure 4.3. The pyroclastic deposits cover the Eburru forest region to the west, while the northern part is carpeted by recent basalts that extend through Badlands to Lake Elementaita. Rhyolites, trachytes and comendites are also present in a few secluded regions (Maithya & Fujimitsu, 2019).

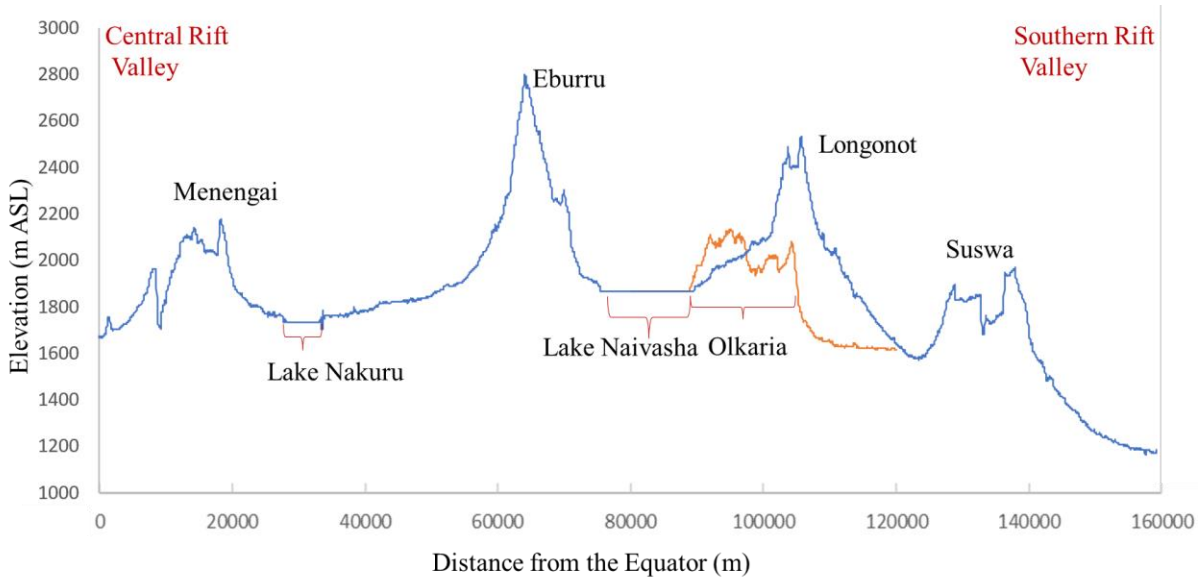

Figure 4.3. Elevation profile (a cross-sectional view X - X) for the Quaternary volcanoes drawn from equator line southward within the study area, as indicated in Figure 4.2 (b).

Eburru field has conspicuous surface manifestations as evidenced by numerous steaming and hydrothermally altered grounds, near-boiling fumaroles and one hot spring. The hydrothermal activity in the region is believed to be structurally controlled by the older regional rift faults, and younger local fissures oriented N-S and NW-SE, serving as conduits for lava ascent and fluid pathways towards the magma intrusions (Maithya et al., 2020). The reservoir is hosted in pantelleritic rhyolites with a volume of about 3 km^3 with sodium bicarbonate waters (Kiende & Kandie, 2015). The few geophysical and geochemical studies conducted on this field indicate that Eburru, a small reservoir, can support the production of 10-25 MWe for 30 years (Maithya et al., 2020; Mwarania, 2014). Eburru geothermal field has one productive well with a discharge of 23 t/h of steam and 60 t/h of brine coupled to a 2.4 MW single flash power plant. The DU at Eburru include condensing of steam from fumaroles for domestic use, geothermally heated crop drier, and hot spring waters for bathing.

Badlands-Elementaita is a geothermal prospect that lies between Eburru and Lake Elementaita. It is characterized by faults and mini-grabens oriented N-S, pyroclastic cones jutting from basaltic carpet (F. Mwaura, 2000). The prospect has near boiling, 87.1-97.2°C, fumaroles to the south and several warm springs, 44°C, to the north that discharge into the Lake Elementaita. The geological survey conducted on resource assessment concluded that southern parts of Elementaita near Eburru volcano have up-flow zones that could provide steam. These regions are close to the high-temperature fumaroles and the local fissures. Kenya Electricity Generating Company (KenGen) plans to drill three exploratory wells in this region to guide future exploration, development, and exploitation of these fields. It is also noted that advanced geophysical and geochemical studies are required to characterize this resource further. It is therefore prudent to classify this resource as an indicated resource.

Longonot geothermal prospect is hosted by a trachytic Quaternary volcano within central rift graben with a conspicuous elliptical caldera/crater with the highest point at 2740 masl. The Longonot pyroclastic cone is a recent eruption about 9150±150 years BP hosted on a previous composite trachytic cone that collapsed 21000 yrs BP. The younger cone formation was followed by a large explosive eruption of pyroclastic ash and the possible collapse of the “pan” crater on

the top of the volcano (Clarke et al., 1990). Due to the recent Longonot ash that overlies previous volcanic deposits, fault structures are implicitly implied as buried structures through such studies as CO_2 degassing, which links recent volcanic structures to the controlling fluid pathways, especially around the crater rim (Robertson et al., 2016). Recent geophysical studies targeting Longonot's geothermal reservoir indicate that the up-flow zones are located on the south to southwestern flanks of the volcano (Ambunya, 2017). The up-flow zone coincides with the two boreholes drilled to 250-500 m below the surface in this region that struct hot water. One borehole produced steam, thus categorizing Longonot as a probable geothermal resource.

To the immediate south of Longonot volcano lies Suswa, another-trachytic phonolite volcano, with the highest point at 2356 masl. It is distinguished by two nested calderas at the summit, crowning a central volcano with both caldera rims exhibiting intense fumarolic activity. The calderas are overlain with tuffs and phonolite lavas, which are underlain by phonolitic trachytes as an indication of multi-phase eruption. MT and TEM geophysical studies show that the resistive bodies at 1000 masl to 0 masl that correspond to a hydrothermal reservoir are located on the northern to western regions of the Suswa volcano (Mohamud, 2013). Geothermal Development Company (GDC) did a conceptual model based on reviewed geophysical, geological, and geochemical studies. It indicated the inner caldera contains the reservoir with an outflow of moderately hot fluids to the north and south (Kipngok et al., 2017). South of the Suswa volcano, two water boreholes were dug to a depth of 500 m, but they didn't find any water and instead released steam that was over 100°C in temperature. The fumaroles on the southern flanks of the volcano are condensed to provide drinking water to the locals. Suswa is categorized as a probable geothermal resource with reservoir temperatures of more than 200°C.

The aforementioned high enthalpy geothermal resources are emplaced within Quaternary volcanoes with different criteria such as altitude, geological setting, surface topography, and water bodies. Five of the fourteen high enthalpy geothermal resources have either exploratory or production wells. In addition, these high enthalpy geothermal resources' varied proximity to transport infrastructure, cities, flower farms, grain farms, National Parks, and resorts generate additional criteria that need careful matching to ascertain the most suitable DU scenario. These criteria are best represented as topological spatial data for ease of visualization.

4.5 Challenge of silica scaling to direct use of high enthalpy geothermal resources

One main challenge that comes with utilization of hot brine from high enthalpy geothermal energy is high concentration of the amorphous silica. To maximize returns on investment, steam and brine separation pressure for liquid dominated reservoirs is always set at silica saturation index (SSI) of one. Separation at pressures where $SSI > 1$ could avail more steam for the power plant but will raise concentration of amorphous silica beyond its solubility at that temperature. This will set up the right conditions for precipitation of monomeric silica and eventually deposition of silica scale into brine pipes, heat exchangers, and reinjection well. Deposition of silica scale inside brine pipes and hot reinjection well is very detrimental to the reservoir and costly to plant operations. Table Table 4.2 to Table 4.4 show sampled wells at Olkaria, Menengai and their fluid chemistry which was used to analyze the wells with respect to silica saturation index (SSI), as explained in Chapter Three, section 3.7. From this data, it is noted that Kenyan deep reservoirs fluids can be categorized from mild to moderately alkaline with pH range 8.5 to 10.5. This condition is enables monomeric silica to dissociate to a charged hydrogen cation and silicate anion, as in Equation (3.15), which are more soluble than the silicic acid (Fleming & Crerar, 1982). This could explain why wells at Olkaria Domes with silica concentration of >1500 mg/kg have pH above 10, as shown in Figure 4.5. The low concentrations of aluminum, magnesium, iron and calcium could also be a benefit

since most silicate and calcite scales are based on complex reactions with these metal irons (Opondo, 2015). Though it was interesting to note a weak direct proportional relationship between

Table 4.2 Well characteristics data for sampled production wells used in this study from the Greater Olkaria Complex, Menengai and Eburru geothermal fields.

Well Number	WHP (bar-g)	TDS (ppm)	pH@20°C	Na	K	Li	Ca	Mg	Cl	SO4	t-CO_2	F	B	H2S	SiO2	Fe	Al	Enthalpy (kJ/kg)
OW-903A	9	937	9.81	397.9	59.51	1.048	5.052	0.584	506.93	53.1	89.23	14.62	1.7	0.17	796			1,675
OW-903B	10	1451	9.9	620.2	138.6	0.247	1.228	0	587.17	277.9	359.7	60.99	1.99	5.78	623			1,454
OW-904	7.85		9.49	509.7	124.1	1.463	0.069	0.482	278.43	92.7	592.02	50.84	1.43	9.18	952			1,297
OW-904A	9.66	1462	10.02	567.9	97.82	1.506	0	0.291	559.75	101.2	397.82	40.6	2.8	4.42	835			1,437
OW-904B	8	1140	9.63	455.92	131.1	1.166	1.372	0.3	303.59	206.5	278.08	52.86	2.96	6.936	924			1,619
OW-908	9	1360	9.32	424	150	1.39	2.329	0	638.05	233.4	246.79	45.53	1.05	6.12	896			2,162
OW-908A	10.3	940	9.77	482.04	98.34	1.21	0.25	0	316.07	79.4	277.86	82.08	2.59	2.38	727			1,402
OW-908B	9	1340	9.68	636.5	172.5	1.603	1.048	0.171	572.866	36.7	267.3	207.02	0.44	9.52	874			2,052
OW-909	13.83	1585	10.06	702.6	227.7	1.819	0.506	0.083	683.49	42	277.86	188.66	0.48	15.3	1088			2,054
OW-909A	6.5	1915	8.8	806.7	254.7	1.271	0.173	0.364	603.94	78	365.16	252.5	0.33	20.4	1326			1,677
OW-910	15.7	725	9.55	358.2	74.55	0.752	0.955	0.159	274.52	82	214.5	103.46	0.49	11.29	515			1,937
OW-910A	13.8	1380	10.2	659.3	173.6	1.163	0.21	0.04	547.36	93	275	215.96	0.69	31.69	1045			2,214
OW-910B	13.7	919.5	9.86	459.2	78.89	1.169	1.538	0.357	325.75	26.6	313.5	61.24	0.5	19.27	784			1,721
MW-01	10.45	8140	9.2	4577	303		1.98	0.21	789	154	7260	119	1.5	20	342	3.07		1,299
MW-03	1.84	6670	9.7/20.9	4370	98		0.13		999	431	4370	108	0.4	10	199	0.93	1.2	1,168
MW-04	5.04	7010	9.3/20.1	3242	131		2.59	0.09	1040	287	4960	141	1.8	118	348	0.58		1,413
MW-12	5.87	5820	8.7/22.9	3567	116		0.23	0.35	705.5	227	4554	64	0.326	74.8	480	0.28	0.35	1,653
MW-19	9.308	1312	9.6/23	683	23		0.1		314.7	226	407	71	1.141	20.4	589			1,976
MW-20	12.07	3240	8.8/19.9	2139	334		0.01		313.6	128	2836	272	0.657	73.1	740			2,406
EW-01		4796	9	1849	331	2.26		0.24	644	313	792	171	0.43	0.68	761			1250
OW-10	5.02	2016.5	8.75	8.55.1	129.7	0.99	3.91	0.176	1080	57	114.19	81.1	8.03	0.91	638	0.099	0.985	2,535
OW-15	5.61	1907.5	8.69	708.9	115.4	1.69	1.67	0.04	1040	40.6	72.07	62.4	8.73	22.6	604	<0.02	0.824	1,899
OW-16	5.86	1254.5	8.97	481.5	69	0.88	1.01	0.047	636	35.9	82.86	69.6	5.42	2.06	573	<0.02	0.686	1,384
OW-19	5.32	1261.5	9.1	527.3	97.3	1.62	1.08	0.032	700	39.2	65.47	63.8	8.85	9.48	622	<0.02	1.048	1,823
OW-23	6.11	830.5	9.44	369.9	52	0.7	0.9	0.051	221	42.4	131.93	74.8	4.03	7.88	653	0.037	0.71	2,193
OW-25	6.43	1289.5	9.15	522	94.5	1	1.2	0.106	671	28.4	149.57	70.1	5.47	2.12	641	<0.02	0.511	2,516
OW-101	5.3	0	9.5	660	112	2.9	0.3	0.2	357	57	1108	61	4	4.8	600			1,660

OW-202	3.1	1770	9	559	131	2.2	1.4	0.6	284	69	1031	60.3	1.4	3.1	388			1,061
OW-301	7.39	3241	8.67	1282.7	208.2	3.67	0.66	0.066	240	112	2465.38	104.8	6.77	3.96	855	<0.02	0.666	1,653
OW-302	5.66	1939.5	9.72	632.6	101.2	3.21	1.04	0.082	505	54.4	578.16	76.9	3.54	3.43	744	<0.03	0.784	1,237
OW-304D	3.9	1597	8.13	959.4	73.6	0.65	3.48	1.732	52	92.9	1752	23.8	3.33	0.97	364	0.139	0.521	1,672
OW-306	3.99	1427	9.15	850	96.4	0.96	1.2	0.081	251	50.4	1081	61.7	6.26	2.9	551	0.091	1.375	1,037
OW-307	0.35	2157	9.22	837.7	90.4	1.35	0.71	0.053	109	115.1	1553.26	57.4	2.04	3.49	312	<0.03	0.58	435
OW-308	6.3	6034	8.1	2530.1	244.1	6.89	1.84	0.294	109	140.8	9657.51	77.2	3.38	0.18	307	0.159	0.058	2,049
OW-709	7.06	2207.5	9.93	845.7	217.7	1.41	1.41	0.037	770	72.6	318.03	28	5.13	6.54	649	<0.02	0.892	1,921
OW-714	14.92	1766	9.54	557.1	108	1.51	0.88	0.056	682	35.2	135.02	66.4	3.63	8.44	739	0.014	1.053	1,303
OW-718	8.28		9.44	500	80				474	41	152	51	4.43	3.1	694			956
OW-719	8.02	1432.5	9.38	535.8	80.5	1.02	1.09	0.042	544	82.9	162.31	46.1	4.77	4.46	588	<0.02	1.511	1,259
OW-724A	5		8.77	450	50				477	68	144	38	3.2	4	538			1,446
OW-726	6.76		8.9	570	88				675	61	167	37	5	7.8	758			1,602
OW-727	5.52		8.54	500	67				576	77	147	37	4.2	5.1	818			1,720
OW-914	6.9		10.06	1569	461	2.73		0.01	514	87.5	1400	270	3.39	2.99	650			2,111
OW-914A	14		7.43	891	217	1.26	0.91	0.04	381	51.6	877		2.89	2.14	685			1,841
OW-914B	12.8		10.1	776	158	0.87	1.89	0.05	324	79.8	356	275	3.01	2.38	293			2,225
OW-914C	11.7		9.51	896	278	1.57			386	47.1	706	234	0.96	4.08	997			
OW-915	11.56	1345	9.93	653.5	189.8	0.671	2.672	0.047	480.64	16.1	246.62	187.41	3.17	17.88	682			2034
OW-915C	16		10.16	1338	264	1.63			619	110.6	847	235	1.19	11.56	1832			2,424
OW-915D	12		10.28	918	337	1.61			698	137	342	264	1.2	4.62	1535			2,326
OW-916B	10		9.69	711	171	1.89			352	83.1	434	230	0.98	3.74	1161			2,253
OW-921	14.5		7.76	563	153	0.671	0.36	0.084	339	79.8	273	70.6	2.03	2.04	1117			1,882

Table 4.3 Chemistry characteristics of hot reinjection wells at the greater Olkaria geothermal field.

Well	WHP	Cond (μΩ/cm)	Ph@20°c	B (ppm)	Cl (ppm)	F (ppm)	SO4 (ppm)	CO2 (ppm)	H2S (ppm)	SiO2 (ppm)	Li	Na (ppm)	K (ppm)	Ca (ppm)	Mg	Fe
OW-708	6	3507	9.48	3.44	602.7	55.26	43.3	140.1	8.568	676	1.704	590.2	88.32	2.591	0.241	0.522
OW R3	6	2637	9.54	1.614	493	71.79	17.5	254.8	23.8	575	1.519	515	105.9	1.526	0.284	1.391
OW 34	5.36	1205	5.25	1.3	484.9	52.38	57.6	431.2	120.7	770	1.27	178	40	1.17	0.07	

OW-713	9	1542	7.94	1.81	581.86	86.73	131.75	243.1	78.2	849	1.97	267	77	2	0.15
OW 13	8.9	1052	6.25	1.61	128.15		5.05	143	59.5	746	1.13	220.5	64.5	1.95	0.14
OW 7	10	4880	9.83/25	3.37	1448	144.15	14.64	167.42	129.2	771	1.773	823.05	375		
OW 911	11	1245	9.348/25		642.52	138.89	27.3	399.88	24.82	1025	1.3125	433.33	128.137		
OW 902	10.8	2890	9.86	2.76	437.98	36.9	28.67	346.0266	11.56	1043	1.275	538.03	164.94		
OW 703	5	2570	9.92/25		628.9	81.78	16.24	207.68	146.2		0.8636	473.25	187.5		
OW 12	6.6	1328	8.64		448.49	64.48	62.1	64.88	6.8	700	1.043	384.131	79.87		
OW 911A		2410	9.89		453.75	184.61	9.48	545.6	20.74	532	1.58	492.12	150		
OW 913A	4.6	1769	9.74		311.54	139.98	14.72	272.8	13.6	1124	1.5642	448.466	62.978		
OW 901	10.4	940	9.782/26	1.06	227	19.58	32.75	475.64	42.84	974	1.07	450	70.589		

Table 4.4 Gas phase chemistry data from the Greater Olkaria Complex and Menengai geothermal fields.

Gas in Steam mmoles/100moles									
Well Number	WHP (bar-g)	Enthalpy (kJ/kg)	Gas sampling pressure (bar-g)	CO2	H2S	CH4	H2	N2	O2
OW-903B	10	1,454	2.8	10134	32.2	3.4	22.3	10	
OW-904B	8	1,619	6.9	5631.2	164.9	7.8	2.3	370	0
OW-909	13.83	2,054	5.4	6163.2	38.1	1.1	2.5	267	
MW-01	10.45	1,299	2.76	6327	6	8.6	4	16.4	0
MW-03	1.84	1,168	0.38	910	1.6	14	5	7.8	0.9
MW-04	5.04	1,413	3.45	1900	34.4	4.4	78.1	16.6	0
MW-12	5.87	1,653	4.14	2862	33	11.7	115.8	4.3	0
MW-19	9.308	1,976	8.62	240	5.2	0.7	29.3	66.8	1.6
MW-20	12.07	2,406	12.1	2212	15.3	34.7	154.8	3.5	0
OW-10	5.02	2,535	4.53	142	7.87	1.11	6.37	6.24	1.31
OW-15	5.61	1,899	4.64	103	9.62	0.38	6.45	6.51	0.14
OW-16	5.86	1,384	4.66	111	11.16	0.43	5.65	2.9	0.01
OW-19	5.32	1,823	4.58	165	15.51	0.67	8.86	6.56	0.17
OW-23	6.11	2,193	5.04	146	13.13	0.31	9.53	4.49	0.12
OW-25	6.43	2,516	4.9	141	10.08	0.3	7.8	4.42	0.05
OW-202	3.1	1,061	1.46	280	1	0.5	0.02	1.57	0.07
OW-301	7.39	1,653	1.46	7675	6.4	1.47	1.9	20.3	0
OW-302	5.66	1,237	1.79	662	1.99	0.67	0.63	5.81	0.88
OW-304D	3.9	1,672	2.58	20650	4.76	3.05	1.69	31.26	0
OW-306	3.99	1,037	1.79	2048	5.23	1.69	0.97	14.12	0
OW-307	0.35	435	0	3027	4.82	2.23	4.38	383.24	83.65
OW-308	6.3	2,049	3.74	47812	0.91	4.08	0.05	50.17	9.3
OW-709	7.06	1,921	1.93	101	2.64	0.5	3.42	5.51	0
OW-714	14.92	1,303	2.76	146	7.89	0.6	2.22	6.05	0
OW-718	8.28	956	2.76	65	4.06	0.6	1.83	4.53	
OW-719	8.02	1,259	2.88	280	9.57	0.81	1.88	7.35	0
OW-726	6.76	1,602	2.97	256	21.22	1.36	9.63	2.52	
OW-727	5.52	1,720	3.03	302	12.14	1.4	7.35	3.51	
OW-914	6.9	2,111	3.8	498	0.91	0.61	12.3	18.1	
OW-914A	14	1,841	3.5	648	1.8	0.08	13.5	11.7	
OW-914B	12.8	2,225	5.7	328	1.57	0.71	6.8	5.9	
OW-914C	11.7		11	631	2.56	3.75	10.8	7.3	
OW-915	11.56	2034	10	329.8	5.03	0.25	19.5	2.58	0.35
OW-915C	16	2,424	16	137	1.3	0.07	27.8	5.9	
OW-915D	12	2,326	11	94	2.4	0.42	22.1	10.6	
OW-916B	10	2,253	9.8	494	5.46	3.13	38.8	6.7	
OW-921	14.5	1,882	14	394	2.71	0.87	6.4	22.3	

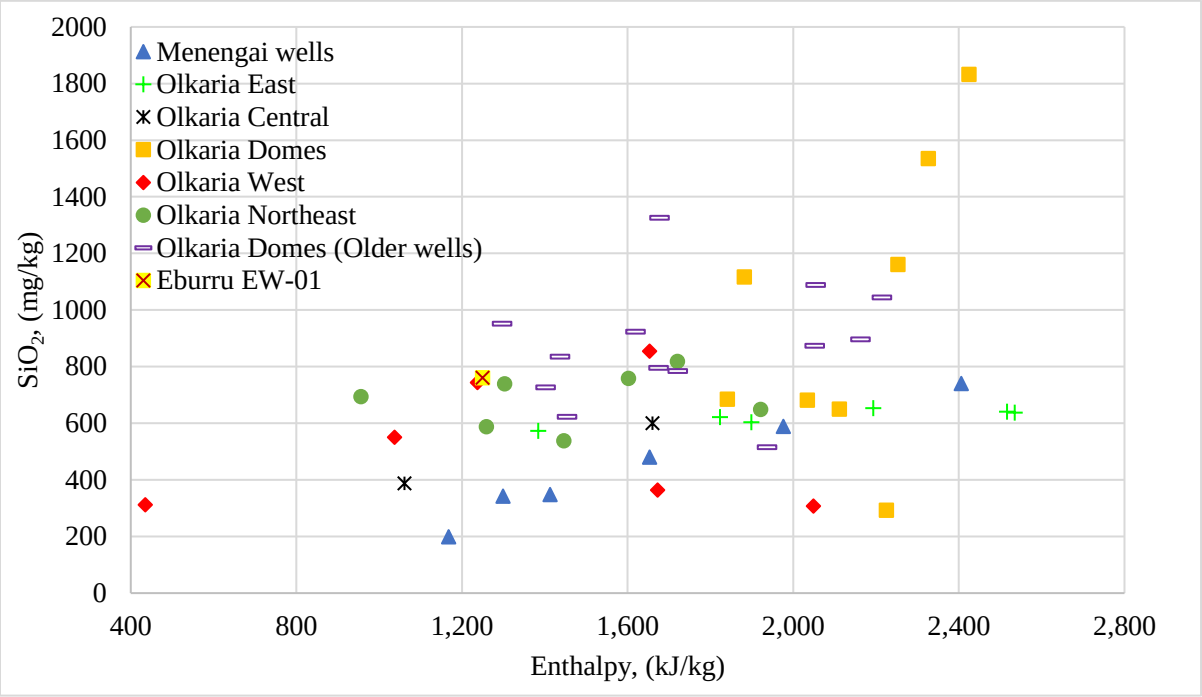

Figure 4.4 Correlation of well enthalpy to the concentration of total silica in the brine.

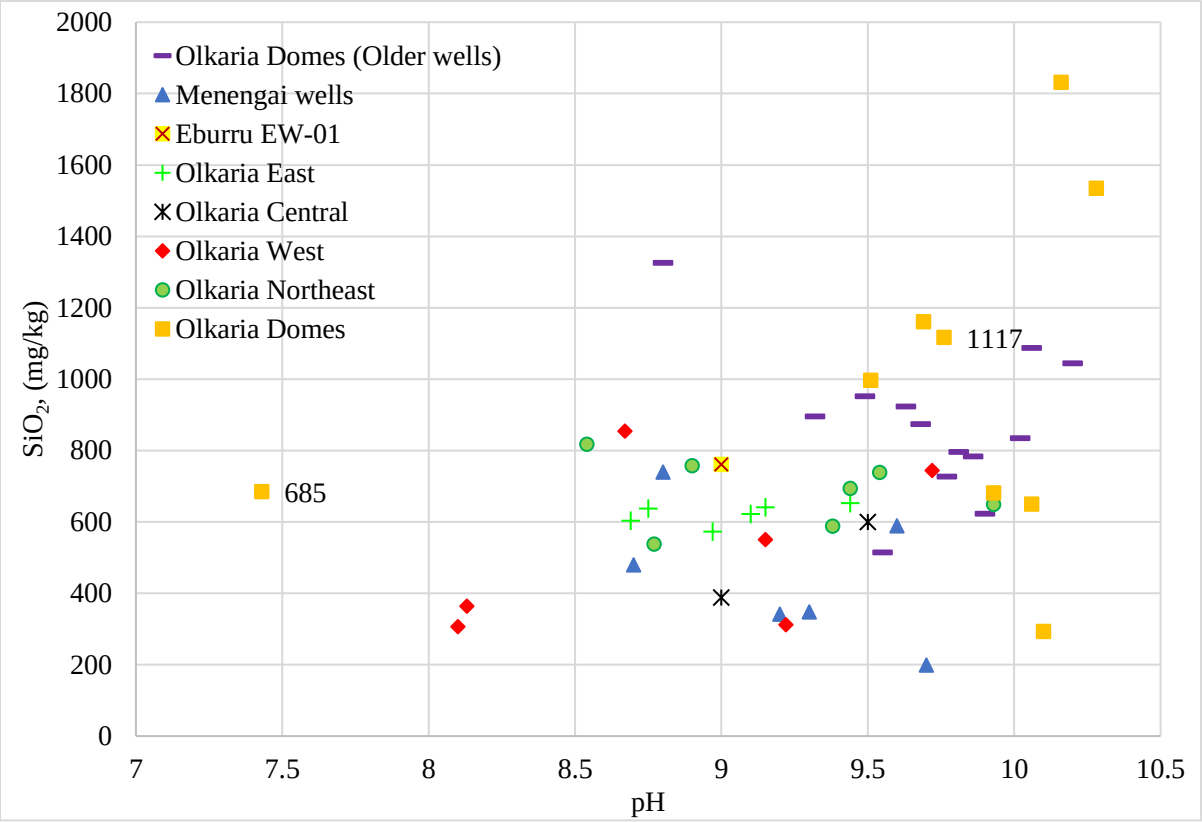

Figure 4.5 Correlation of production well brine pH to the concentration of total silica.

enthalpy and silica concentration, wells at Menengai, Olkaria East, Olkaria West and Olkaria Northeast had less silica concentrations despite their high enthalpy levels. These wells are ideal for direct use due to their reduced risks of silica scaling. This is evidenced at well OW-101 used by Oserian for greenhouse warming, which is cooled to 45°C and the heat exchanger only gets cleaned once annually. The brine and steam separation pressures are normally set at SSI equal to one based on total silica concentration alone. This leaves direct use of high enthalpy geothermal energy with no high temperature brine from separators to work with. By analyzing the effects of pH on amorphous silica, $SSI_{Modified}$ is recalculated, as in Equation 3.19, which allows brine temperatures to be cooled to SSI≥2 before hot reinjection. This extra heat is used in the various heating scenarios for direct use.

4.6 Distribution of grain farms

Kenya rainfed arable land is divided into three: Rift Valley and Western, which receive long rains in April to August, and Central and Eastern Kenya, which receive long rains in October to December. Rift Valley and Western Kenya cultivate maize and beans in one long planting season, while Eastern and Central Kenya have two planting seasons for maize, as shown in Figure 4.6.

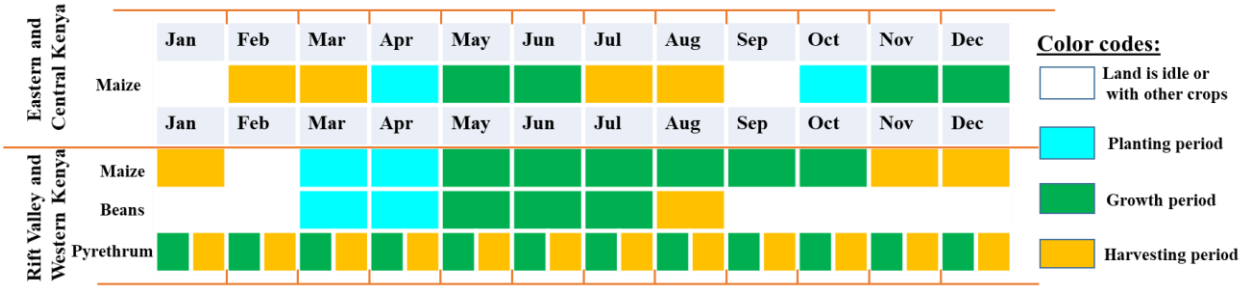

Figure 4.6 Crop calender for grain cultivation in Kenya (Ngethe and Jalilinasrabady, 2020).

The crop calendar is useful to estimate the periods in which the crop dryer will run in full capacity or idle. Besides the crop calendar, this study used remote sensing (RS) of Sentinel-2 (A and B) satellite images to estimate the size and distribution of grain farms. Sentinel-2 satellite images were chosen due to their relatively good spectral, spatial and temporal resolutions, as shown in Figure 4.7 and summarized in Table 4.5.

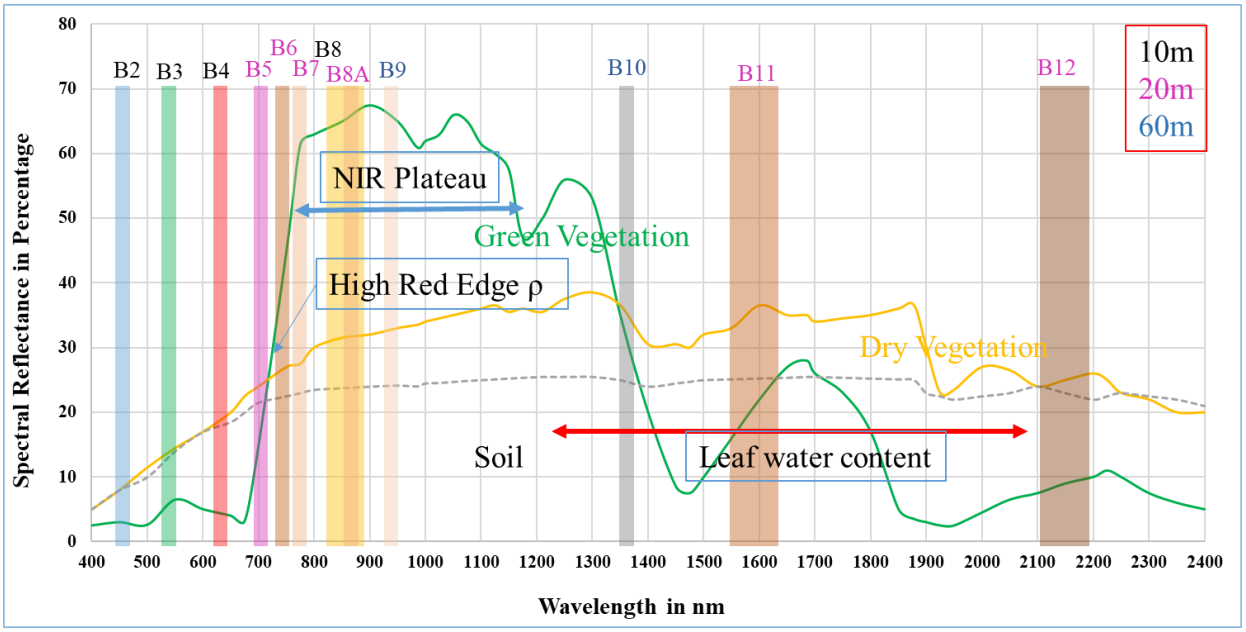

Figure 4.7 Spectral resolution of Sentinel-2 satellite images.

Table 4.5 Summary of satellite platforms offering free imagery for academic analysis.

Sensor	Spatial Resolution	Partitioned Spectra	Spectral Resolution	Temporal Resolution	Radiometric Resolution
MODIS	1Km/500m/250m	Yes	Excellent	1-2 days	Good
PALSAR-2	100m	No	Very Good	14 Days	Excellent
ETM+/OLI	30m	Yes	Fair	16 Days	Good
Sentinel-2	10m & 20m	Yes	Good	5 Days	Good
Weights	0.30	0.20	0.25	0.19	0.11

The images were downloaded and prepared as detailed in the methodology chapter, section 3.6 to obtained distribution maps of the grain farms and human settlements.

4.7 Interpolation and proximity analysis of spatial point, line, and polygon vector data

The geothermal resources spatial data, such as warm boreholes, hot springs, fumaroles and deep well temperatures, silica concentration and flow rates were represented as point vector in QGIS. In this format, the data needs interpolation to estimate heat distribution and in the process rasterize the data. This study used ordinary kriging and inverse distance weighted interpolation methods on point vector data.

The fresh surface water data such as rivers and economic factors such as roads distribution data was represented as spatial line vectors. They were then converted to polygons by assigning them 1.0 km buffer zone and then the polygon map layers were rasterized and analyzed for proximity. The spatial polygon data which represented economic activities such as horticultural greenhouses, national parks, and locations of industrial parks were rasterized, and proximity analysis performed.

All the vector map layers were rasterized to a resolution of 50 m x 50 m per pixel to shorten processing time and provide a reasonable selection resolution.

4.8 Criteria map layers

First, the topological spatial point data were mapped, as shown in Figure 4.8, and regions with no data were filled in using IDW and Kriging interpolation techniques. IDW was applied for point data with more than 10 points with global trend in variables, such as temperatures of clusters of hot springs. IDW interpolation relies on the distance between point data and the values of those points without considering their local variance, hence suitable for a denser group of point data (Setianto & Triandini, 2015). The ordinary kriging technique was used for map layers with more data points showing a high degree of local variabilities, such as geothermal wells, warm water boreholes, and clusters of fumaroles. Despite having the data required for manipulation on the GIS platform, raw vector map layers cannot be added to, multiplied by, or subtracted from one another because they include incommensurate data with distinct magnitudes. As a result, they must be rasterized to enable suitability map synthesis, as shown in Figure 4.9.

Each specific criteria map in Figure 4.8 has significance in selecting DU scenarios. Criteria map layer (1) displays the distribution and locations of fresh-cut flowers and vegetables ranging from 0.5 to 83.5 ha. The criteria map layer was generated from remote sensing of Sentinel-2 MSI data. The classes obtained were ground-truthed by google hybrid base maps in QGIS. Establishing a horticultural greenhouse infrastructure incurs significant capital investment and moving existing greenhouses closer to geothermal resources is not feasible. This criteria map was aimed to locate those horticultural greenhouses closer to geothermal resources, which may be served by shorter brine piping for horticultural greenhouse warming. Criteria layer (2) is a vector map representing the distribution of perennial rivers and freshwater lakes in the study area. The rivers and lakes were extracted from Google Satellite hybrid base maps in QGIS. Access to freshwater is crucial for irrigation of farms, aquacultural pond heating, and domestic use. Geothermal resources near freshwater sources are good candidates for horticultural greenhouse warming, fish drying and processing, and aquacultural heated ponds. On the other hand, those geothermal resources with scarce surface freshwater provide optimal locations for water desalination from boreholes and saline lakes. Criterial map layer (3) depicts the distribution of grain farms (maize). This criteria map layer was generated from classifying Sentinel-2 MSI data by supervised SVM classifiers in QGIS. The proximity of the densely distributed grain farms to geothermal resources provides a crop catchment to sustain a geothermally heated crop dryer. Besides, the grain farms provide animal and chicken feeds; hence, this map layer is influential in choosing optimal locations for geothermally heated chicken hatchery and milk pasteurization centres.

Map layer (4) is a topographical representation of the surface slope. This criteria map layer was generated by analyzing slope from SRTM 1 Arc-Second Global digital elevation model (DEM) image. The slope has a significant influence on agriculture, real estate, and the growth of urban centres. The optimal slope for grain farming, horticultural greenhouses, aquacultural pond heating, and animal husbandry is 0º to 8º. In the cases where brine piping is required, slope plays a major role in optimizing the pumping head. Criteria maps (5) and (6) represent the road network and distribution of houses. These criteria map layers were obtained from extracted from google satellite hybrid maps and remotely sensed data, respectively. Roads provide accessibility to geothermal resources, allowing a smooth exchange of customers, raw materials, and other products to and from the locations of the DU scenarios. Roads are vital to almost all the DU scenarios. Population

distribution help to identify the likely markets for the goods processed from DU scenarios and serve as a source of tourists for spas and geotourism.

Criteria map layer (7) represents the location of industrial zones. This criteria map layer was generated from Google Satellite hybrid maps and field survey. Two of the industrial zones located northwest of Nakuru city and Nairobi city (the southeast corner of the study area) deal with crop drying, cooking oil refinery, animal feeds, milk processing, and others. These processes require thermal energy and are the primary source of thermal needs for industrial geothermal heating. Industrial zones have also been proposed within the Menengai and Olkaria geothermal fields. Criteria map layer (8) represents the locations and size of national parks. The criteria map layer was extracted from wildlife census report from Kenyan Ministry of Tourism and Wildlife (Waweru et al., 2021). National parks are protected zones where economic activities such as the DU scenarios are disallowed. However, national parks receive domestic and international tourists who may be interested in geotourism and spa activities. Hence, locating some DU activities near national parks helps to popularize them. The larger the number of visitors a national park receives, the more popular the geothermal resources near them will become as visitors seek more collocated attractions.

Criteria map layers (9) and (10) represent locations with geothermal brine temperature in degrees celsius and flow rates in tonnes/hour, respectively. These criteria map layers were mapped from geothermal resources data (well data) obtained from Kenyan institutions in charge of developing geothermal energy (KenGen and GDC) as well as from field surveys of surface manifestation and warm water boreholes within the study area. Availability of brine in large quantities and at usable temperatures is paramount for all DU scenarios. The total sum implication of brine flow rate and brine temperature represents extractable heat which is the main resource from the geothermal fields and prospects. Criteria map layer (11) depicts silica content in brine produced by each geothermal well or hot spring. Silica concentration criteria map layer was generated from geochemical data of geothermal wells and hot springs data. Silica is a serious impediment to the DU of geothermal energy because it limits the amount of energy that can be extracted from geothermal brine. The high the silica content in geothermal brine, the harder it is to cool that brine below saturation temperature without incurring risks of silica deposition. Silica scaling clogs piping systems and reinjection wells resulting in significant financial losses. The silica concentration map layer impacts all DU scenarios negatively except mineral extraction, where silica is the main target. Further details on the map layers, such as resolution, data sources and the nature of the map layer, are expounded in Table 4.6

Table 4.6 Further details of the criteria map layers.

Criteria map layers	**Map layer type**	**Data source**	**Resolution (m)**
Proximity to horticultural greenhouses	Raster	Satellite images	10
Proximity to surface freshwater	Vector (line and polygon)	Google Satellite hybrid maps	10
Proximity to grain farms	Raster	Satellite images	10
Proximity to road network	Vector (line)	Google open street maps	10
Population distribution	Raster	Satellite images	10
Proximity to national parks	Vector (polygon)	Kenya Ministry of Tourism and Wildlife	10
Proximity to tourist resorts	Vector (point)	Field survey	10

Proximity to industrial zones	Vector (polygon)	Field survey and Google Satellite maps	20
Slope	Raster (digital elevation map)	www. asf.alaska.edu/ and https://earthexplorer.usgs.gov/	15
Brine flow rate	Vector (point)	Geothermal companies in Kenya and field survey	10
Brine temperature	Vector (point)	Geothermal companies in Kenya and field survey	10
Brine silica concentration	Vector (point)	Geothermal companies in Kenya and field survey	10

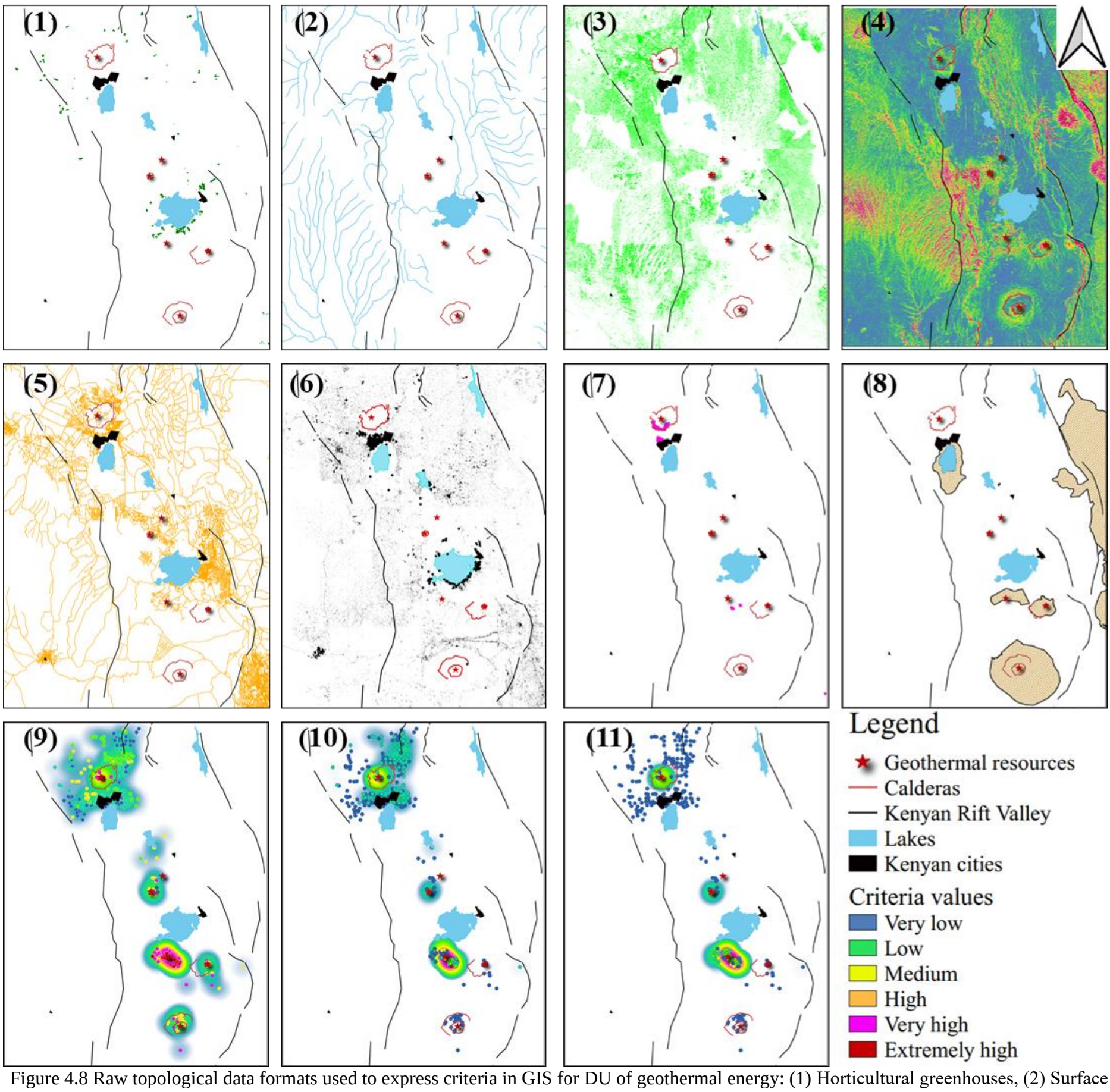

Figure 4.8 Raw topological data formats used to express criteria in GIS for DU of geothermal energy: (1) Horticultural greenhouses, (2) Surface freshwater, (3) Grain farms, (4) Slope map, (5) Road network, (6) Population distribution, (7) Industrial zones, (8) National parks, (9) Brine temperature, (10) Brine flow rates, and (11) Brine silica concentration. The dots in criteria maps nine to eleven indicate the locations of the geothermal wells, hot springs, fumaroles and warm water boreholes.

The vector layers (point, polygon, and line) were rasterized in Quantum Geographic Information System (QGIS) platform based on their relevant field data. The resultant raster layers' pixels were then normalized using Equations (3.4) and (3.5) based on whether the criterion was favourable or a constraint to DU of geothermal energy. In this case, the pixels for each criterion map layer ranged from 0 for low and 1 for very high DU scenarios, as shown in Figure 4.9. For visualization purposes, the normalized raster layers were segmented into four coloured data classes showing the suitability of a given spatial location to the DU scenarios: low, medium, high, and very high. The choice of four colours scheme is to provide demarcated regions of varying suitability from the "very high" (red) to the "low" (Blue). The colours representing "medium" and"high" demarcate the areas of compromise depending on the favourability of the region. The choice of the natural breaks Jenkins method (discrete interpolation) helps avoid ambiguity created by the continuous interpolation symbology in the suitability selection (Slocum & Kessler, 2014).

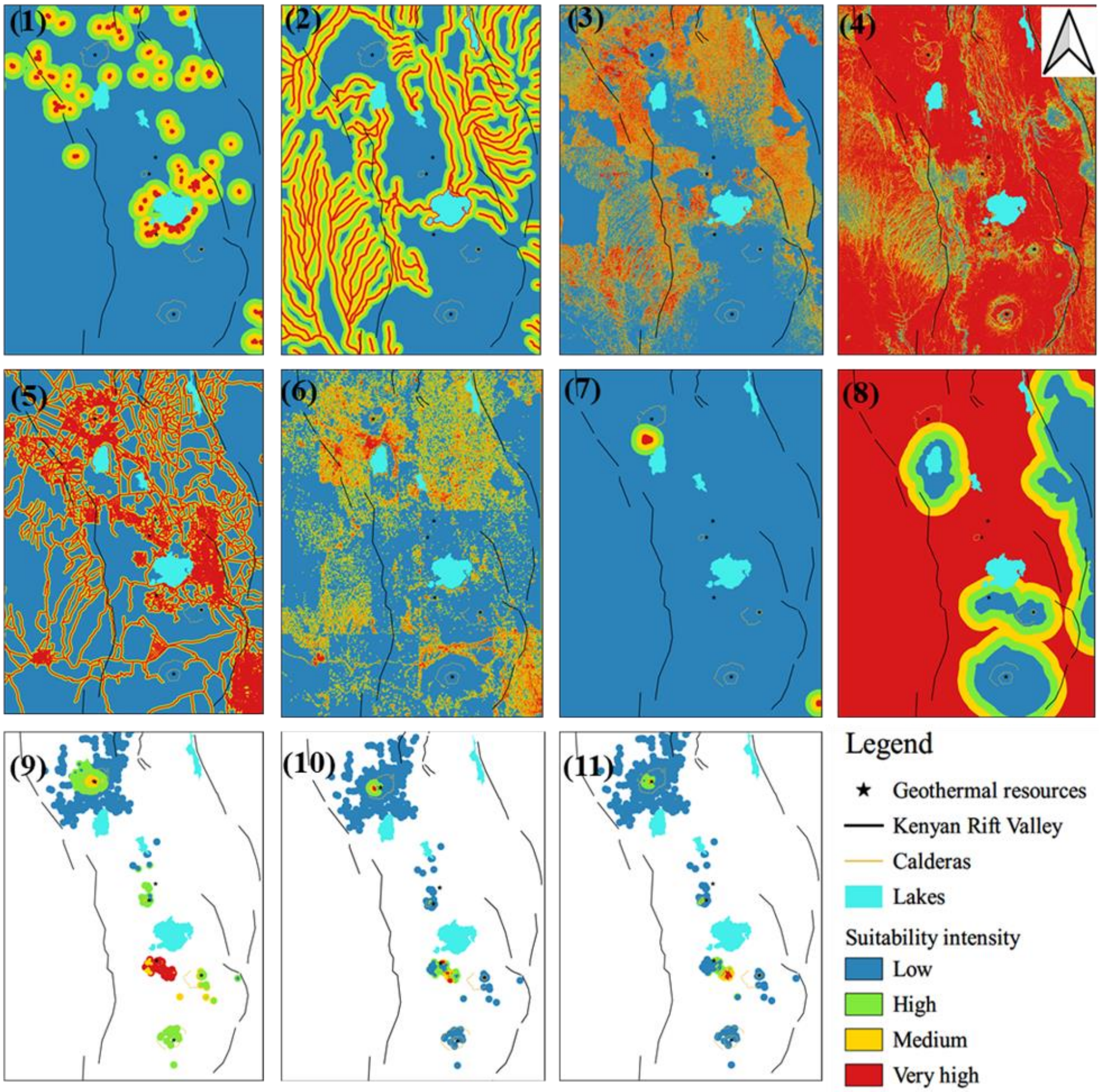

Figure 4.9 Normalized criteria maps showing regions of high suitability: (1) Horticultural greenhouses, (2) Surface freshwater, (3) Grain farms, (4) Slope map, (5) Road network, (6) Population distribution, (7) Industrial zones, (8) National parks, (9) Brine temperature, (10) Brine flow rates, and (11) Brine silica concentration.

All the normalized criteria maps were then weighted using the weights generated by AHP. Each pixel was weighted using Equations (3.6) and (3.7), and synthesized as in WASPAS Equation (3.8) to produce a resultant intensity map layer for each DU scenario. Lastly, the nine direct utilization scenario maps were combined using the WASPAS method by adding and multiplying pixels values to produce a final intensity ranking map. This final map was reclassified into six classes (very low, low, medium, high, very high and extremely high) using the natural breaks Jenks method (Yalcin & Kilic, 2017). The six colour codes break the classification data into six suitability classes for each DU scenario. The class breaks will aid decision-makers on which geothermal resources to prioritize in terms of DU investments.

4.9 Comparison of DU of geothermal energy to the local economic activities

The criteria maps in Figure 4.8 shows spatial representation of both natural resources, infrastructure and economic activities which need to be analyzed and matched to the available geothermal resources to produce DU scenario maps. The key economic activities are highlighted in Table 4.7

Table 4.7 Local economic activities helping to select the best DU scenarios.

DU scenarios	Local economic activities	Locations	Geothermal resource within proximity
Horticultural greenhouse warming	Fresh-cut flower and vegetable farming	Around Lake Naivasha and regions to the northeast and west of Menengai caldera	Olkaria, Menengai
Crop drying	Grain farming, pyrethrum and tea growing	Regions surrounding Menengai and Eburru calderas	Menengai, Eburru, Olkaria
Aquacultural pond heating	Aquaculture	Oserian farm to the northwest of Olkaria	Olkaria, Menengai
Chicken hatchery	Chicken and grain farming	To the most regions of the study area	Menengai, Eburru, Olkaria
Milk pasteurization	Dairy and grain farming	Around Menengai and Eburru calderas	Menengai, Eburru, Olkaria
Industrial heating	Crop drying, cooking oil refinery, animal feeds, milk processing, fish processing	To the southeast of Menengai caldera and southern shores of Lake Naivasha	Olkaria, Menengai
Spa and bathing	Tourist resorts, wildlife tourism, geotourism and hiking	Within Nakuru city and the shores of Lake Naivasha	Menengai, Eburru, Olkaria, Elementaita, Suswa, Longonot
Mineral extraction	Silica extraction (proposed)	Within Menengai caldera and Olkaria spa	Olkaria, Menengai

4.10 Results and discussions

The present study identified nine DU scenarios: horticultural greenhouse warming, crop drying, aquacultural pond heating, chicken hatchery, milk pasteurization, industrial heating, water desalination, spa and bathing, and mineral extraction. One of the objectives of the present study was to present a visual display of the best DU scenarios for the six quaternary high enthalpy geothermal resources on the central and southern Kenyan rift floor. The DU scenarios were synthesized by matching local economic activities, infrastructure, and available resource characteristics to provide the most suitable conditions for successfully implementing the respective DU scenarios. The heat energy extracted from geothermal resources for DU is highly dictated by the Silica Saturation Index (SSI). SSI dictates brine separation and reinjection temperatures as a conservative measure for preventing silica scaling.

4.10.1 Results under SSI equal to 1.0

DU of geothermal energy can make use of surface manifestations but on a small scale. A large amount of hot geothermal brine is necessary for energy-intensive DU situations, including industrial heating, crop drying, horticultural greenhouse warming, aquacultural pond heating, milk pasteurization, and water desalination. Suppose the geothermal brine is separated at a silica saturation index (SSI) of 1.0 and reinjected while hot. In that case, the geothermal field remains with a small quantity of brine on the surface at lower temperatures. This brine is barely enough to cater for energy-intensive cascaded uses. The normalized criteria map layers in Figure 4.9 were

weighted and synthesized through WASPAS methodology in QGIS, as shown in Figure 3.1, to produce direct use scenarios for SSI = 1.0 shown in Figure 4.10, Figure 4.11 and Figure 4.12. Figure 4.10 to Figure 4.12 show the suitability of the six geothermal resources for various DU scenarios at SSI = 1.0. At SSI = 1.0, almost the total separated brine is reinjected hot except for low-pressure wells and wellhead unit wells whose brine is not reinjected because it is dumped in shallow evaporation ponds. From Figure 4.10 to Figure 4.12, the suitability locations are much contracted and located within the geothermal fields. This is majorly caused by the fact that it is not feasible to transport brine at a low flow rate and enthalpy from the geothermal field to the neighbourhood with thermal needs. At SSI = 1.0, geothermal wells were reduced from 111 to 23 at Olkaria and from 23 to 6 at Menengai geothermal fields. Brine conditions at Eburru were not affected by SSI because it was not reinjected. Most of the wells not affected by SSI analysis at the Olkaria geothermal field are those coupled to the wellhead generators. Brine from wellhead generators is dumped into evaporation ponds and is therefore available for DU. From the DU scenarios in Figure 4.10 to Figure 4.12, the model failed to consider the surface manifestations without brine, such as fumaroles, hence suitability for DU at Elementaita, Suswa, and Longonot prospects is low since they have no production wells.

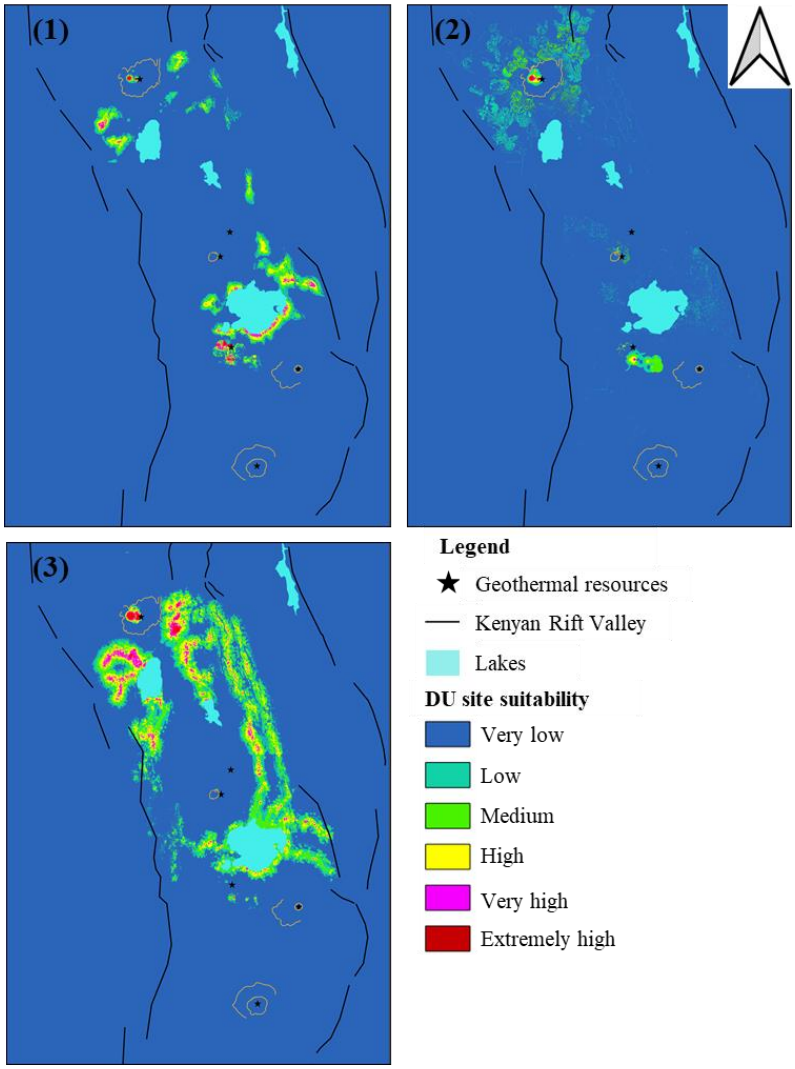

Figure 4.10 Best suited DU sites for (1) horticultural greenhouse warming, (2) crop drying, and (3) aquacultural pond heating scenarios for SSI equal to 1.0.

From Figure 4.10, (1) The horticultural greenhouse warming DU scenario was synthesized from weighted normalized proximity map layers of horticultural greenhouses, surface freshwater, slope map, road network, and brine characteristics (temperature, flow rate and silica concentration) from Figure 4.9. The clustering (placement) of existing horticultural greenhouses, the availability of irrigation water from the Lake Naivasha, road systems, and flow rates of hot brine are the main factors affecting the suitability for horticultural greenhouse warming. The areas suitable for warming horticultural greenhouses are highlighted in red, including the northwest field of Olkaria, the area northwest of the Menengai caldera, and the areas northwest of Lake Nakuru, where hot water can be obtained from shallow boreholes thanks to the high geothermal gradient experienced there. However, the model highlighted the densely clustered greenhouses and failed to pick the scattered horticultural greenhouse regions near Menengai caldera. (2) The crop drying DU scenario was synthesized from weighted normalized criteria maps layers of the grain farms, road networks, and brine characteristic. The proximity of grain fields to geothermal resources and the availability of a high enthalpy and voluminous brine flow rate determined the suitability for crop drying. The northwest region of Menengai geothermal field, Eburru geothermal field, and finally Olkaria East geothermal field were selected as the three most suitable regions. (3) The aquacultural heated ponds DU scenario was synthesized from weighted normalized criteria maps layers of the surface freshwater, road networks, population distribution, and brine characteristic. The availability of surface freshwater sources, such as Lake Naivasha and its inflowing perennial rivers, as well as the population density that provides a fish market, appear to be key factors in the suitability map layer for heated aquacultural ponds. The territories south of the Menengai geothermal field were chosen as the most suitable locations. Aquacultural heated ponds may be possible within the Menengai and Olkaria geothermal fields. The perennial rivers discharging into Lakes Nakuru and

Naivasha also provided feasible regions to the east of the geothermal resources. The best location is east of Nakuru city since there are warm boreholes there and population density is high.

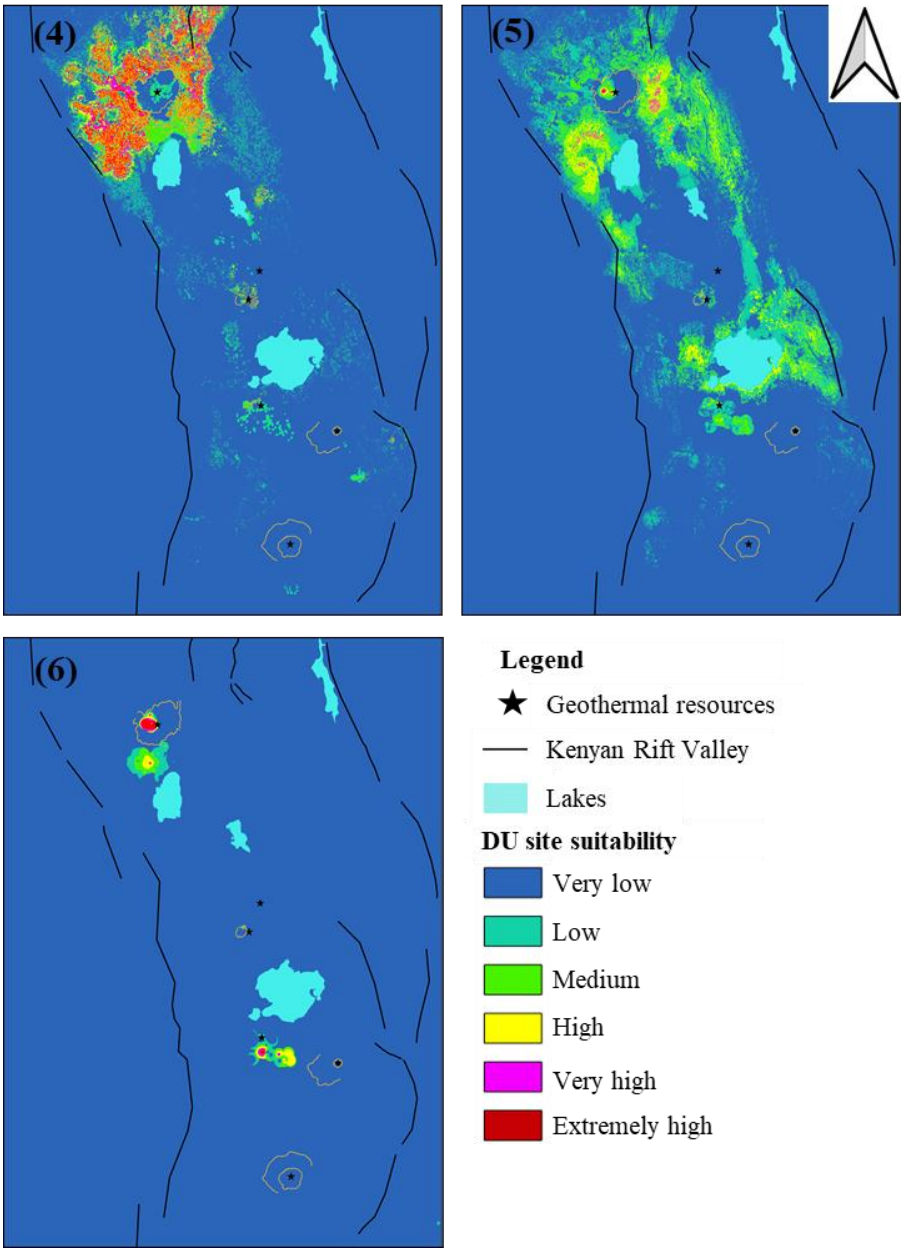

Figure 4.11 Best suited DU sites for (4) chicken hatchery, (5) milk pasteurization, and (6) industrial heating scenarios for SSI equal to 1.0.

From Figure 4.11, (4) the chicken hatchery DU scenario was synthesized from weighted normalized criteria maps layers of the grain farms, surface freshwater, road networks, population distribution, and brine characteristic. The suitability areas for chicken hatchery were heavily influenced by the availability of warm water boreholes, grain farms and high population density around Menengai and Eburru geothermal fields. (5) The milk pasteurization DU scenario was synthesized from weighted normalized criteria maps layers of the surface freshwater, grain farms, road networks, population distribution, and brine characteristic. The locations with grain fields, surface freshwater sources, high population densities, and roadways are highlighted on the milk

pasteurization suitability maps. The Menengai caldera, the Eburru and Olkaria geothermal fields, and regions to the east and southwest of the Menengai geothermal field are shown on the suitability map as the best appropriate places. (6) The industrial heating DU scenario was synthesized from weighted normalized criteria maps layers of the industrial zones, grain farms, road networks, population distribution, and brine characteristic. The Menengai caldera and, to a lesser extent, the Olkaria geothermal field appears to be the only viable regions due to the availability of significant flow rates of hot geothermal brine and their proximity to existing industrial zones that process grain, oil, milk, and timber.

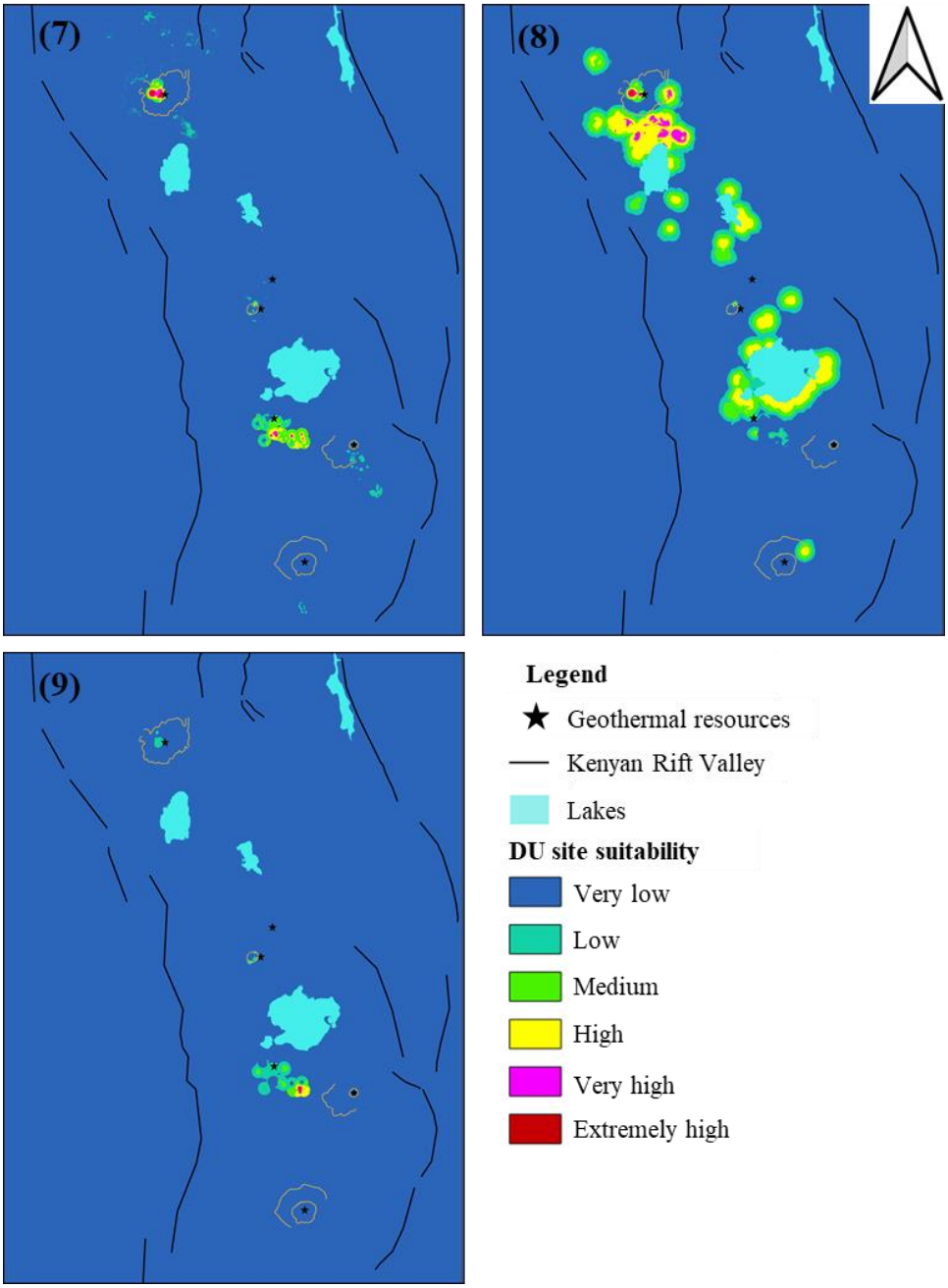

Figure 4.12 Best suited DU sites for (7) water desalination, (8) spa/bathing, and (9) mineral extraction scenarios for SSI equal to 1.0.

From Figure 4.12, (7) the water desalination DU scenario was synthesized from weighted normalized criteria maps layers of the surface freshwater, slope, road networks, population distribution, and brine characteristic. The absence of surface freshwater sources near the geothermal resources significantly impacted suitability selection for water desalination. The most suitable regions were Menengai, Eburru, and Olkaria geothermal fields, including Longonot and Suswa prospects. (8) The spa and bathing DU scenario was synthesized from weighted normalized criteria maps layers of the national parks, grain farms, road networks, population distribution, and brine characteristic. The places that were best suited for geothermally heated spas and swimming pools are those with high brine flow rates, tourist destinations, a good transportation system, and dense populations. Nakuru city, directly south of Menengai geothermal field, and Menengai crater are the finest appropriate regions. The lack of geothermal wells (brine) caused Lake Naivasha and Lake Elementaita's shorelines to be less suitable. (9) The mineral extraction DU scenario was synthesized from weighted normalized criteria maps layers of road networks and brine characteristic. The availability of high brine flow rates with high silica concentrations also had an impact on mineral extraction. The mineral that was targeted was silica, which has several industrial applications, including scouring, glass production, and the production of cosmetic goods. The Olkaria Domes, located southeast of the Olkaria geothermal field, was determined to be the best location for silica extraction.

At this state of limited brine for DU due to reinjection of brine at low SSI, the Menengai geothermal field shows the best DU scenarios as industrial heating, milk pasteurization, chicken hatchery and crop drying. Olkaria leads in spa and bathing, horticultural greenhouse warming, aquacultural pond heating, water desalination, and mineral extraction. Eburru comes third with its best DU scenarios: grain drying, chicken hatchery, milk pasteurization, and water desalination. The fields with no productive geothermal wells were rated less suitable due to lack of a reasonable volume of high enthalpy geofluid for DU.

4.10.2 Results under SSI equal to 2.0

Through SSI analysis of brine from various geothermal wells, the number of usable wells at Menengai and Olkaria geothermal fields increased to 18 and 77, respectively. Increasing both the flow rates and enthalpy of geothermal brine, consequently increasing the possibility of piping hot water to meet the thermal needs of economic activities in the neighbourhood of geothermal fields. SSI values above 1.0 allow the brine to be reinjected at lower than separation temperatures. This study found that pH modification by CO_2 and H_2S degassing could allow safe heat extraction and brine reinjection at SSI≈2.0. The DU scenario suitability maps shown in Figure 4.13, Figure 4.14 and Figure 4.15 are for SSI = 2.0. Likewise, to the case of SSI = 1.0, the normalized criteria map layers from Figure 4.9 were weighted and synthesized through WASPAS methodology in QGIS as shown in Figure 3.1 to produce direct use scenarios for SSI = 2.0 shown in Figure 4.13, Figure 4.14 and Figure 4.15. From the DU scenarios in Figure 4.13, Figure 4.14 and Figure 4.15, SSI

analysis did not affect surface manifestations, hence suitability for DU at Elementaita, Suswa, and Longonot prospects remained low since they have no production wells.

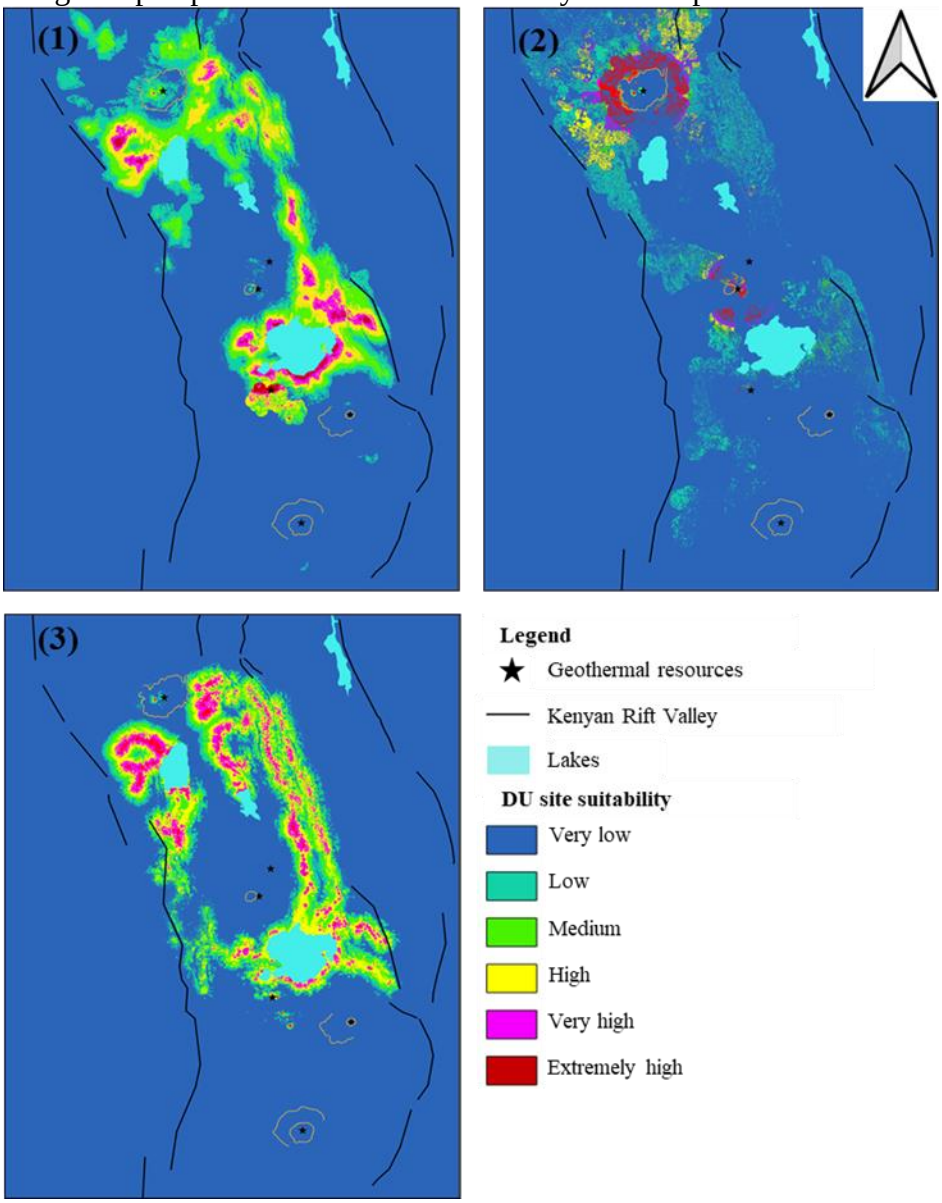

Figure 4.13 Best suited DU sites for (1) horticultural greenhouse warming, (2) crop drying, and (3) aquacultural pond heating scenarios for SSI equal to 2.0.

From Figure 4.13, the synthesis procedure for DU scenarios from criteria map layers in Figure 4.9 remained as in the case of SSI = 1.0. Hence, the significant changes in selection of suitability will be discussed from DU scenario one to nine as follows: (1) Highlights the suitability of northern Olkaria and the shores of Lake Naivasha to the horticultural greenhouse warming. The suitability is based on the availability of high flow rates of high-temperature brine from the Olkaria geothermal field with a possibility of brine transportation to the flower farms on the shores of Lake Naivasha. (2) Depicts the most suitable grain farms for geothermally powered crop dryers around Menengai and Eburru geothermal fields. (3) Suitability for aquacultural pond heating was less affected by SSI since the brine flow rates and temperatures requirement for fish culture are low.

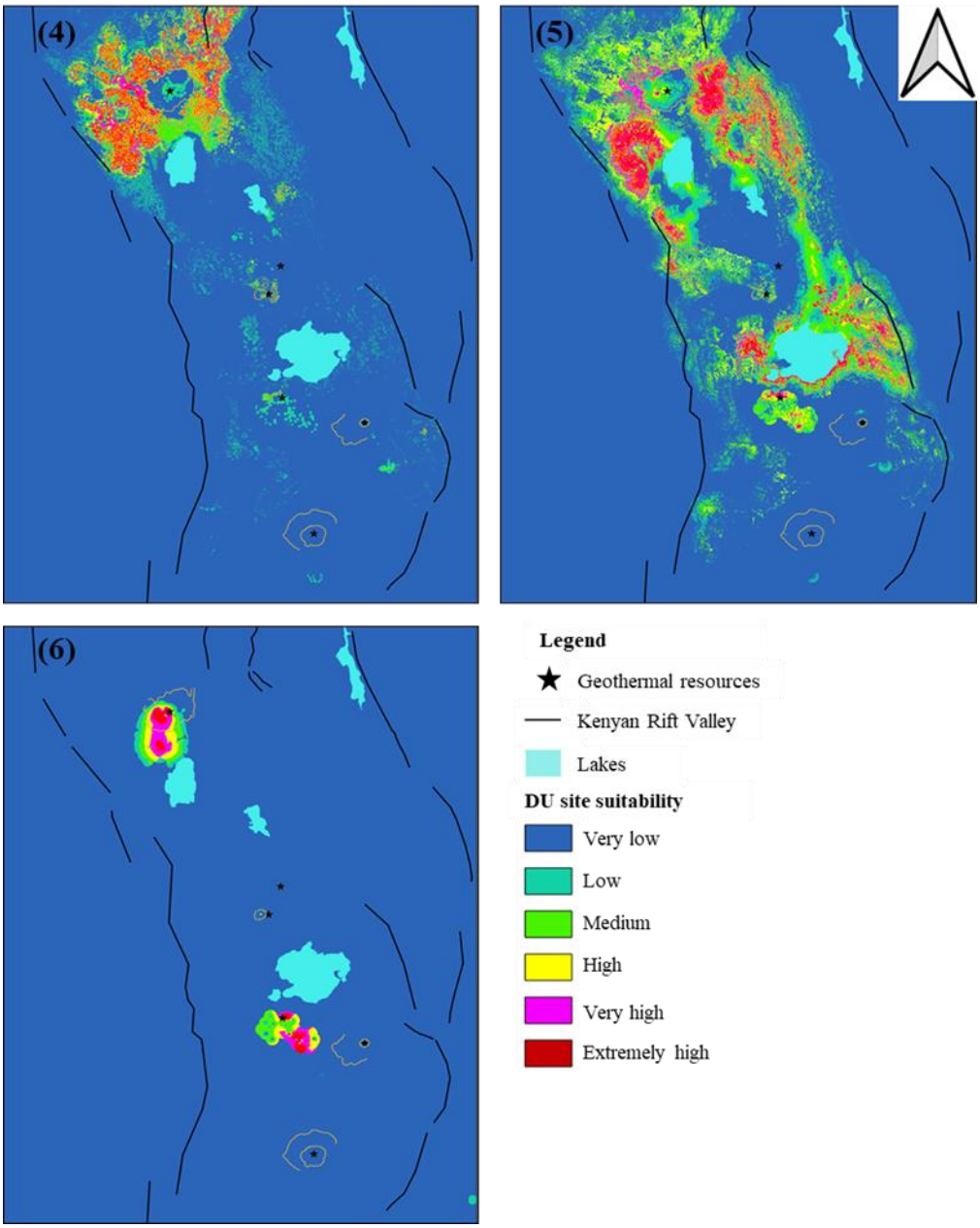

Figure 4.14 Best suited DU sites for (4) chicken hatchery, (5) milk pasteurization, and (6) industrial heating scenarios for SSI equal to 2.0.

From Figure 4.14, (4) the chicken hatchery requires low brine temperatures and flow rates; hence SSI effects were insignificant in this particular DU scenario. (5) Suitability map for milk pasteurization was affected positively by SSI modification since it requires high temperatures and brine flow rates. This shifted suitability regions to the east and southwest regions of the Menengai geothermal field, followed closely by Eburru and Olkaria geothermal fields. (6) The SSI analysis was vital since industrial heating requires high enthalpy brine. The SSI analysis allows brine transport from Menengai caldera to Nakuru city, while Olkaria domes provide the best region for industrial heating within the Olkaria geothermal field.

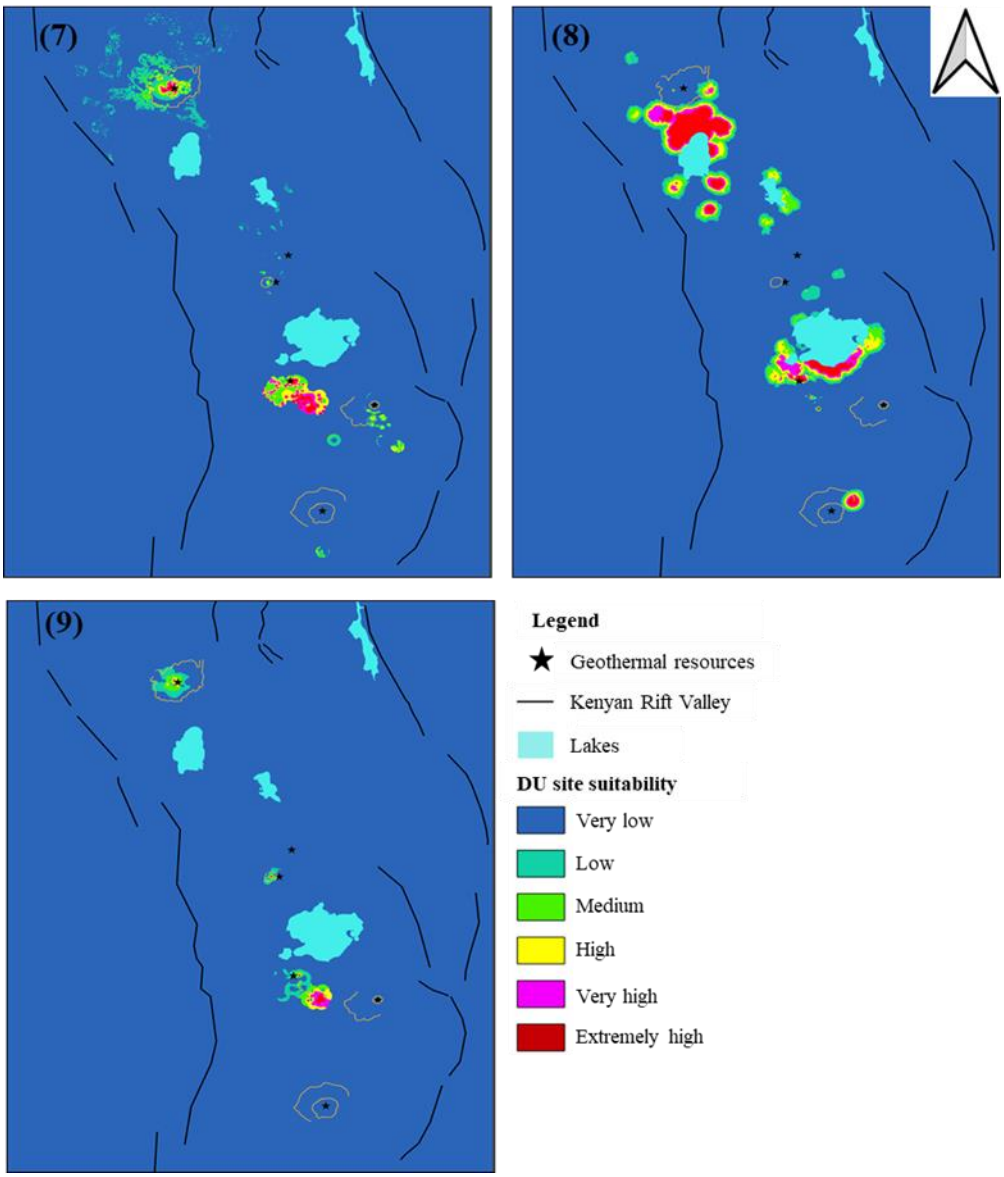

Figure 4.15 Best suited DU sites for (7) water desalination, (8) spa/bathing, and (9) mineral extraction scenarios for SSI equal to 2.0.

From Figure 4.15 (7) raising the SSI to 2.0 expanded the Olkaria geothermal field's suitability for water desalination to the Olkaria domes. The Menengai geothermal field suitability also expanded to the west of the caldera. (8) The suitability regions for geothermally heated spas and swimming pools expanded to Nakuru city and the south shore of Lake Naivasha, which have numerous tourist resorts. The expansion is based on the increase in brine temperature and flow rate when SSI is raised from 1.0 to 2.0. Besides, high brine flow rates and enthalpy provided the possibility of piping brine to Nakuru city and the south shore of Lake Naivasha. (9) At a higher SSI value, the amount of brine for mineral extraction increased, especially in Olkaria domes and Olkaria east fields.

The ability to access high flow rates and high enthalpy geothermal brine provides Nakuru city, located south of the Menengai geothermal field and the southern shore of Lake Naivasha, with ample opportunity for cascaded use. These two regions are highlighted red on the maps, especially

for spa and bathing. The southern shore of Lake Naivasha has collocated tourist lodges and fresh-cut flower greenhouses. Piping brine or hot water to this location will ensure economic cascaded use of geothermal energy, prioritizing the horticultural greenhouse warming and heated swimming pools.

4.10.3 Global (combined) DU suitability maps

When the DU scenario maps were synthesized together, they produced overall DU map for both scenarios, SSI=1.0 and SSI=2.0,Figure 4.16. At SSI=1.0, in Figure 4.16(a), DU is limited to within geothermal fields creating hot fluid accessibility challenges especially when such fields are located within protected areas such as national parks. For SSI=2.0, in Figure 4.16(b), piping of brine away from production wells become a possibility and DU can then be done at already existing facilities such as flower farms, tourist resorts and manufacturing industries. This research shows that, DU depend on higher SSI values for economic viability of projects. Figure 4.16 shows that geothermal resources with hot water boreholes, hot springs and productive geothermal wells were classified in detail compared to those that had none, hence highlighting the strength of the model in working with developed geothermal resources.

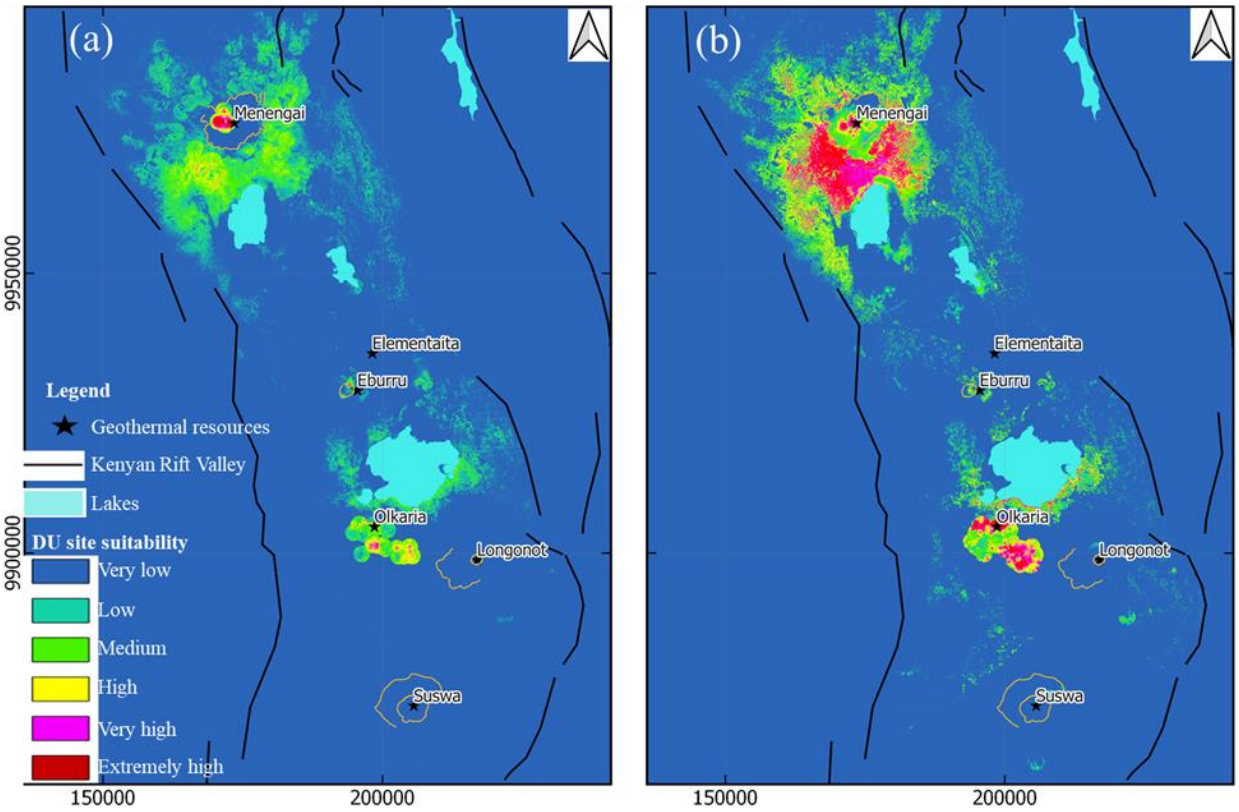

Figure 4.16. Best DU sites in southern and central Kenyan rift (a) for SSI = 1.0 and (b) SSI = 2.0.

From Figure 4.16, it seen that before factoring in SSI analysis, Olkaria geothermal field has more available brine at the surface to sustain direct uses inside the boundaries of the geothermal field compared to Menengai and Eburru geothermal fields. When SSI is increased to 2, Olkaria and Menengai geothermal fields increase their volume of usable hot brine and possibility of brine piping extends suitability zones to the neighbourhood. For Olkaria, the demand is spread along the southern shore of Lake Naivasha, while for Menengai, the suitability zone spreads southward to cover the Nakuru city.

The Menengai geothermal field was identified to be best suited in both cases of SSI ≈ 1.0 and 1.0>SSI ≤ 2.0. This might be explained by the Menengai caldera's deep wells' low silica concentration and the high thermal demands provided by the nearby grain farms and the city of Nakuru. Olkaria comes second with high volumes of disposable hot brine and moderate heat demands provided by the nearby flower greenhouse farms and tourist lodges. Although the grain and dairy farms near Eburru geothermal field provide high thermal demands, the available hot brine is insufficient to meet these needs.

4.11 Sensitivity analysis and validation

Sensitivity analysis evaluates a model's robustness concerning the parameters' variability (Lowry et al., 1995). Sensitivity analysis is performed at either the macro-level or the micro-level (Feizizadeh et al., 2015). The micro-level sensitivity analysis sought to determine the effect of each criterion on one of the related DU scenarios, as shown in the Table 4.8. At the macro-level, the global sensitivity analysis sought to determine the criteria weights which quantitatively affect overall suitability selection. The reference criteria weights were already determined using the AHP method, and the sensitivity analysis is for counterchecking the effect of variability of these weights on the overall selection. Global sensitivity analysis was performed by means of average shift in ranks (ASR) defined as:

$$ASR = \frac{1}{n}\sum_{a=1}^{n}\left|x\_rank_{ref} - x\_rank\right| \tag{4.1}$$

Where ASR is the average shift in ranks, x_rank_{ref} is the rank of alternative X with respect to a referenced ranking, and x_rank is the current rank of X (Feizizadeh et al., 2015). As summarized by the Equation (4.1), ASR captures summed differences in changes of ranking and divides it to the total number of alternatives. The results presented in Figure 4.17 indicate that the brine temperature, flow rate, silica scaling, and road networks had the greatest ability to reverse ranking, in that order.

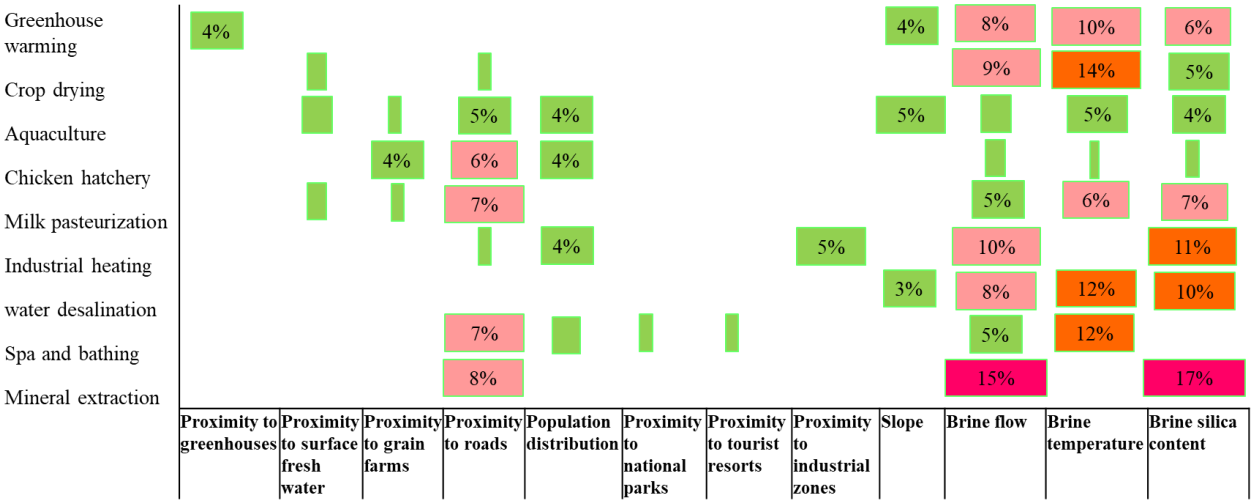

Figure 4.17. Micro-level sensitivity analysis showing the effect of variability of criteria weights on the DU scenarios in percentage.

Table 4.8 Global sensitivity analysis of criteria map layer weights.

	Decision weights												
Criteria map layers	Reference	Greenhouse warming	Crop drying	Aquaculture	Chicken hatchery	Milk pasteurization	Industrial heating	water desalination	Spa and bathing	Mineral extraction	Min	Max	Ranking variation %
Proximity to greenhouses	0.05	0.19	-	-	-	-	-	-	-	-	0.1	0.22	5
Proximity to surface freshwater	0.041	0.11	-	0.19	-	0.11	-	-	-	-	0.1	0.2	2.1
Proximity to grain farms	0.06	-	0.22	-	0.306	0.19	-	-	-	-	0.15	0.35	4.7
Proximity to roads	0.12	-	0.07	0.15	0.167	0.19	0.07	0.08	0.19	0.2	0.05	0.2	8
Population distribution	0.026	-	-	0.15	0.167	-	0.04	0.15	0.08	-	0.03	0.2	5
Proximity to national parks	0.017	-	-	-	-	-	-	-	0.09	-	0.07	0.1	2
Proximity to tourist resorts	0.005	-	-	-	-	-	-	-	0.18	-	0.15	0.2	4.5
Proximity to industrial zones	0.055	-	-	-	-	-	0.11	-	-	0.1	0.1	0.15	1.5
Slope	0.026	0.06	-	0.07	-	-	-	0.05	-	-	0.03	0.07	5.5
Brine flow	0.19	0.24	0.25	0.15	0.19	0.17	0.26	0.24	0.21	0.4	0.1	0.5	24
Brine temperature	0.24	0.28	0.35	0.2	0.12	0.21	0.31	0.31	0.2	-	0.1	0.4	17
Brine silica content	0.17	0.12	0.11	0.09	0.05	0.13	0.21	0.17	0.05	0.3	0.02	0.2	11

4.12 Calculated heat demands

Heat demands for each geothermal resource analyzed was estimated by evaluating its top three best direct use scenarios.

4.12.1 Olkaria - Naivasha region

For Olkaria, the top three direct use scenarios were found to be greenhouse warming, spa/bathing/swimming pools and industrial heating. The greenhouse warming estimates were calculated from the size of horticultural greenhouses overlapping the zones classified as very high and extremely high and within 10 km of the geothermal field, as shown in Figure 4.18. This gives about 700 ha of horticultural greenhouses with a total demand of 84 MWt, equal to 1470 t/h of hot brine/water provided at 95°C. The very high and extremely high zones also overlay about 30 lodges/restaurants specialized with food and lodging which have unheated swimming pools. Assuming each swimming pool has an area of 6 m by 12 m, its demand for hot water/brine is 6 t/h at 65°C, for self-cleaning pools without fluid recirculation. This provides a total of demand of 6.3 MWt, equal to 189 t/h of brine, based on brine provision at 65°C and disposal at 35°C. It is difficult to estimate the demand for industrial heating since it is process-specific, and no case study exists in Kenya. Hence it can be concluded that a demand of more than 90 MWt exists at the southern shores of Lake Naivasha, which can be augmented by geothermal energy.

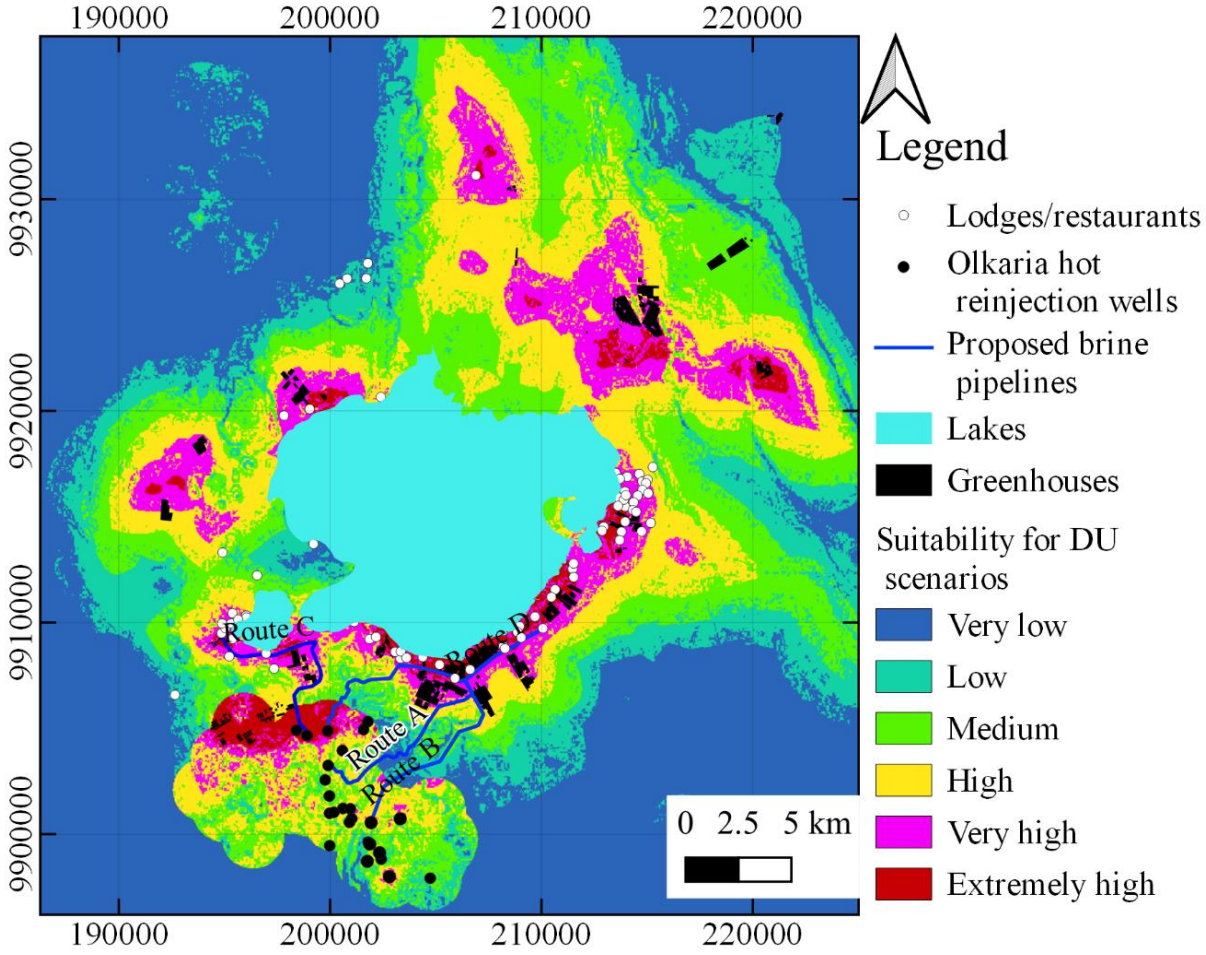

Figure 4.18 Locations of best direct use around Olkaria geothermal field and proposed brine/hot water pipe routes.

The demand was mapped to the south of Lake Oloiden, (the smaller lake in Figure 4.18), and the southern shore of Lake Naivasha. Three brine pipe routes, A, B and D, were selected to

supply brine from three different hot reinjection wells to the southern shore of Lake Naivasha, as shown in Figure 4.18 and Figure 4.19.

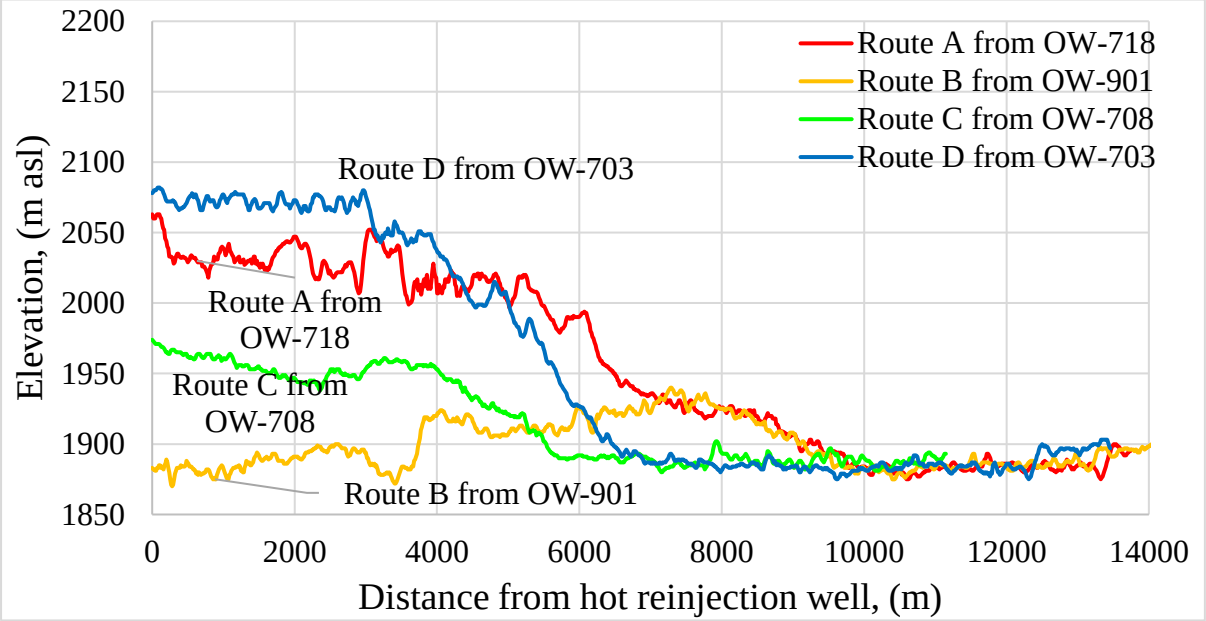

Figure 4.19 Proposed brine pipe routes at Olkaria geothermal field.

Routes A and D are more feasible since they require fewer pumping stations, while route B encounters higher pumping heads compared to the elevation of the hot reinjection well. Route C supplies hot water/brine to the southern shore of Lake Oloiden. This location has fewer greenhouses and more restaurants; hence route C's pipe would likely have a smaller diameter. However, if cascade use is adopted, hot fluids discharged from greenhouses heat exchangers may suffice to supply the lodges/restaurants with brine for spas and swimming pool warming. This study findings disagree with survey based study done on 2020 by GreenMax (2020) on behalf of Climate Technology Centre & Network (CTCN), which listed top direct use scenarios at Olkaria as crop drying, fish-drying and refrigeration, and meat processing. The farming and fishing activities around Olkaria geothermal field were in such small scale as to warrant an establishment of either geothermally powered drying or processing facilities.

4.12.2 Menengai - Nakuru region

Even though the Menengai geothermal field has fewer hot brine production wells than the Olkaria geothermal field, its close proximity to Nakuru City and the presence of shallow upflow zones about it make it the most suitable for commercial-scale direct-use scenarios. The shallow upflow zones of less than 300 m in depth can be accessed by boreholes for a temperature range of 30 - 55°C. The presence of large-scale grain farms and industrial zone in vicinity of the geothermal field create high thermal demands that can sustain economic viability of commercial direct use facilities such as crop driers, industrial heating facilities, and water desalination plants. From Figure 4.20, the few and scattered horticultural greenhouses are over 10 km farther from the geothermal field, do not present a significant heat demand to warrant a deep well or brine piping. However, this situation may change in future and the demand for greenhouse warming may increase. Besides, the greenhouses to the northeast of the region are large and close to the Bahati upflow zone, hence they may use shallow borehole warm waters with temperatures of 50 - 80°C. When the top three direct use scenarios for Menengai geothermal filed were listed as grain drying, milk pasteurization, spa/bathing/swimming pools,

and industrial heating, the “Very high” and “Extremely high” zones were located at the southwest of the Menengai caldera, as shown in Figure 4.20.

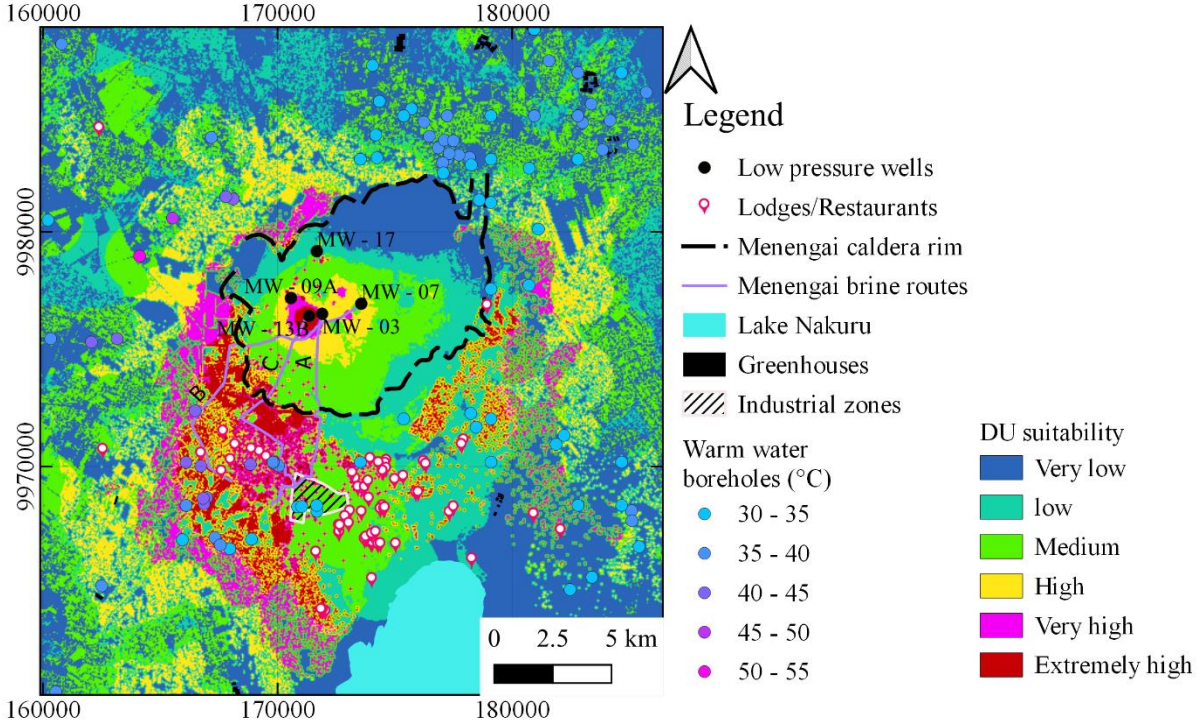

Figure 4.20 Direct use suitability map for crop dying, milk pasteurization, spa/bathing, and industial heating around Menengai geothermal field.

The suitability for direct use inside the caldera is smaller and concentrated around the high temperature geothermal wells. The region to the southwest region of the caldera has large grain farms, lodges/restaurants and an industrial zone which present a significant demand for hot brine/water. This region also has a shallow upflow zone accessible by boreholes with a depth of <200 m. These wells have warm water with temperature range of 30 – 45°C. The locations of the boreholes with warm water in Figure 4.20 seem to be oriented in two axes, NW – SE and NE – SW, intersecting at the hottest region inside the menengai caldera. This warm water boreholes within Nakuru city and its environs makes it suitable to many low heat requirements direct use scenarios. This shallow and easily accessible upflow zones is not witnessed at the vicinities of Olkaria, Suswa and Longonot geothermal resources since their water table is deeper, >500 m, and boreholes drilled there produce steam.

The study by GreenMax (2020) listed the top three direct use scenarios as grain (maize) drying, milk pasteurization, and water desalination. When these direct uses are factored in selecting suitability locations, the “Extremely high” zones migrate to the west of Menengai caldera, while the “Very high” zones surround the caldera, except at the location of Nakuru city, as shown in Figure 4.21. The suitability locations represented in Figure 4.21 fail to account for the heat demand associated with economic factors represented by Nakuru city, such as number and locations of lodges/restaurants, the location of industrial zone, and the proximity of Lake Naivasha national park. Although Figure 4.21shows a grain catchment zone for a crop dryer located within the Menengai caldera, it is not easy to select a region with a high density of heat demand to sustain an economically viable direct use facility or warrant hot brine or steam piping from the geothermal field. Hence, this study finds direct use scenarios dictated by the heat demands from the local economic activities such as grain farming, tourism, and vegetable oil processing to be more realistic, as represented by Figure 4.20.

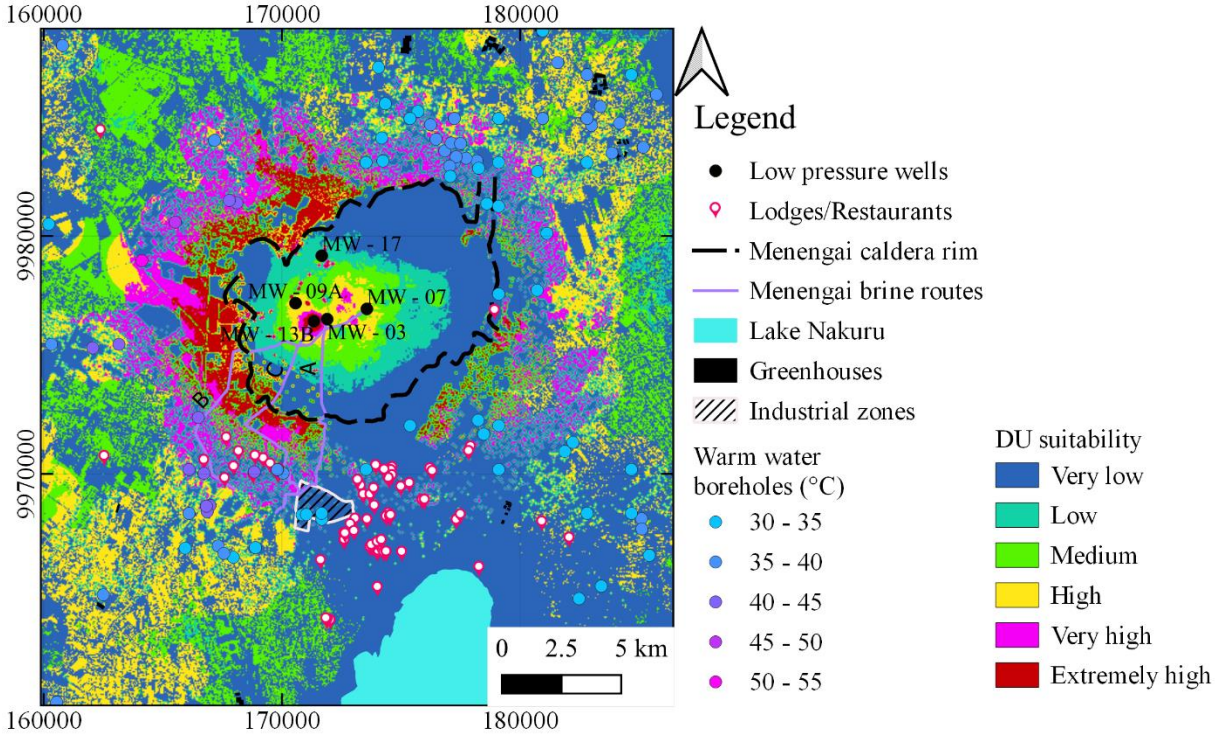

Figure 4.21 Direct use suitability map for crop dying, milk pasteurization, and water desalination around Menengai geothermal field.

From Figure 4.20, it is noted that suitability zone is concentrated to the southwest of Menengai caldera and to the west of Nakuru city, where a pool of tourist resorts and industrial zone dealing with vegetable oil processing and maize drying/storage provide an year round demand for high temperature heat. The heat could be transported from the Menengai caldera to the high demand region either as steam, hot water/brine or a combination of both. Three proposed hot brine/water pipe routes were selected as shown in Figure 4.22. The southern towering caldera wall impeded pipe routes by introducing a pumping head of 50 – 100 m. Routes A, B, and C in Figure 4.22 went over the caldera at the lowest elevation point, but in doing so, increased the overall pipe length.

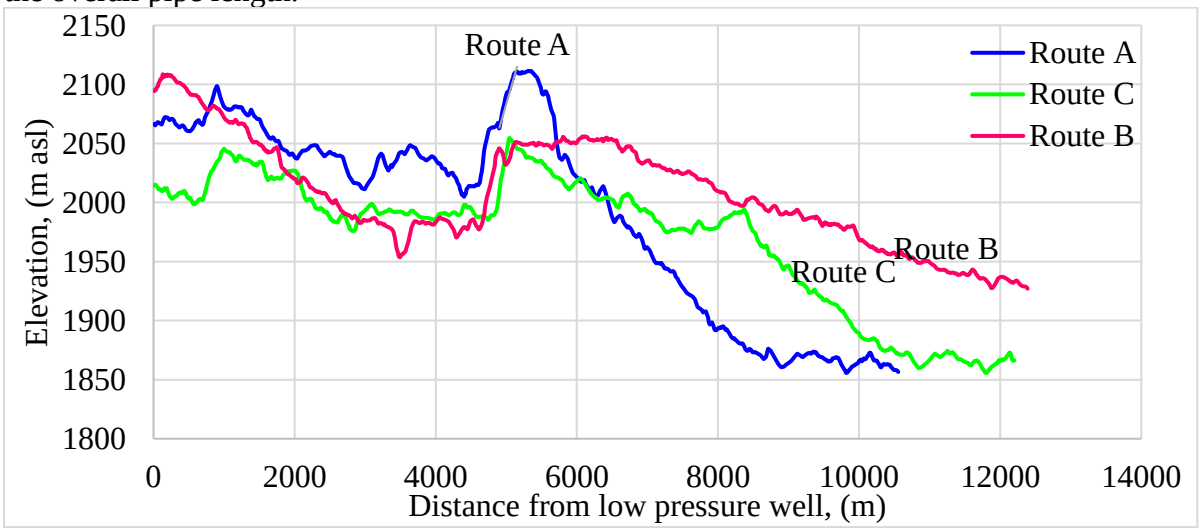

Figure 4.22 Brine pipe routes for from Menengai geothermal field to the west of Nakuru City.

The pipes targeted the region with concentrated heat demand in Figure 4.20. For corn drying demand, three fundamental conversion coefficients were used: maize yields in tonnes per hectare (ha), moisture shrink and maize dryer' energy efficiency. The maize yield in Kenyan rift valley is highly dependent on rainfall received per growing season, and varies from 3000 – 5000 t/h of dry maize at 13 – 14 % moisture content (Jin et al., 2019). At the end of maize growing season, the maize is harvested at 25% moisture content and requires to be dried to 13 - 14% moisture content for storage and commercial milling. Ideal maize dryer's energy efficiency is about 2.55 - 3.02 MJ/kg of water (Maier & Bakker-Arkema, 2002). Natural gas and biomass dryers' energy efficiency can range from 5.0 – 9.0 MJ/ kg of water evaporated (Mwaura et al., 1982). There is a 6-tonne batch dryer at Menengai geothermal heated by hot water at 60 – 90°C, with energy efficiency of 8.16 MJ/kg of water evaporated. Hence, this study adopted a high capacity cross-flow grain dryer with an energy efficiency of 7.0 MJ/kg of water evaporated and a moisture shrink of 12 % (Brooker et al., 1981; Maier & Bakker-Arkema, 2002). Hence using these coefficients, the grain drying heat demand about Menengai geothermal field is 1227 MWt, translating to 24,059 t/h or 1,748 t/h of brine or steam supplied at 90°C or 130°C, respectively, and dryer exhaust of 45°C. This translates to a supply of 33 t/h or 2.43 t/h of brine and steam for a month, respectively. This heat demand is within the Menengai geothermal field capacity. The industrial heating demand created by vegetable oil processing plants in industrial zone present a heat demand of 21 MWt, same as boiler capacity at Kapa Oil refineries, equal to 162 t/h of steam at 3 bara. The hospitality industry represented by resorts/lodges/restaurants was a less than that at Olkaria, at 6 MWt or 177 t/h of brine supplied at 90°C. In addition, the grain farms around Menengai caldera double as dairy farms and the region has a minimum dairy cattle head of 1200, representing a heat demand for milk pasteurization of 800 MWt. This translates to about 15,686 t/h of brine or1139.6 t/h of steam 90°C or 130°C, respectively.

4.12.3 Eburru region

The Eburru region is occupied by small-scale farmers cultivating maize and pyrethrum. The region has three productive wells, MW-01, MW-04 and MW-06, where only MW-01 produce about 21 t/h of steam and 60 t/h of hot brine. Wells MW-04 and MW-06 are liquid dominated wells with no steam, and hence were shut in. However, this region has a shallow upflow zone and shallow wells, <50 M deep, produce steam. This upflow zone is about 24 - 30 m deep near the old pyrethrum dryer, hence concentrating the suitability zones to the southeast, as indicated in Figure 4.23. Coincidentally the pyrethrum farms and grain farms are concentrated to the southeast, making this region the best suited to handle a grain dryer project.

The heat demand at Eburru is presented by grain farms which require drying and milk pasteurization. The dairy farming at Eburru region is closely tied to the grain farms since the wastes from the maize crop provides 80 – 90% of animal feeds used by dairy farmers. There are 372 ha of maize farms around Eburru, and assuming each ha has one dairy cow with a minimal daily milk production of 5 litres. The maize drying and milk pasteurization activities present a heat demand of 395.5 MWt and 256 MWt, respectively. The maize needs 1748 t/h or 560 t/h of brine or steam, provided at 90°C or 130°C, respectively. The milk needs 5019.6 t/h or 365 t/h of brine and steam provided at 90°C or 130°C, respectively.

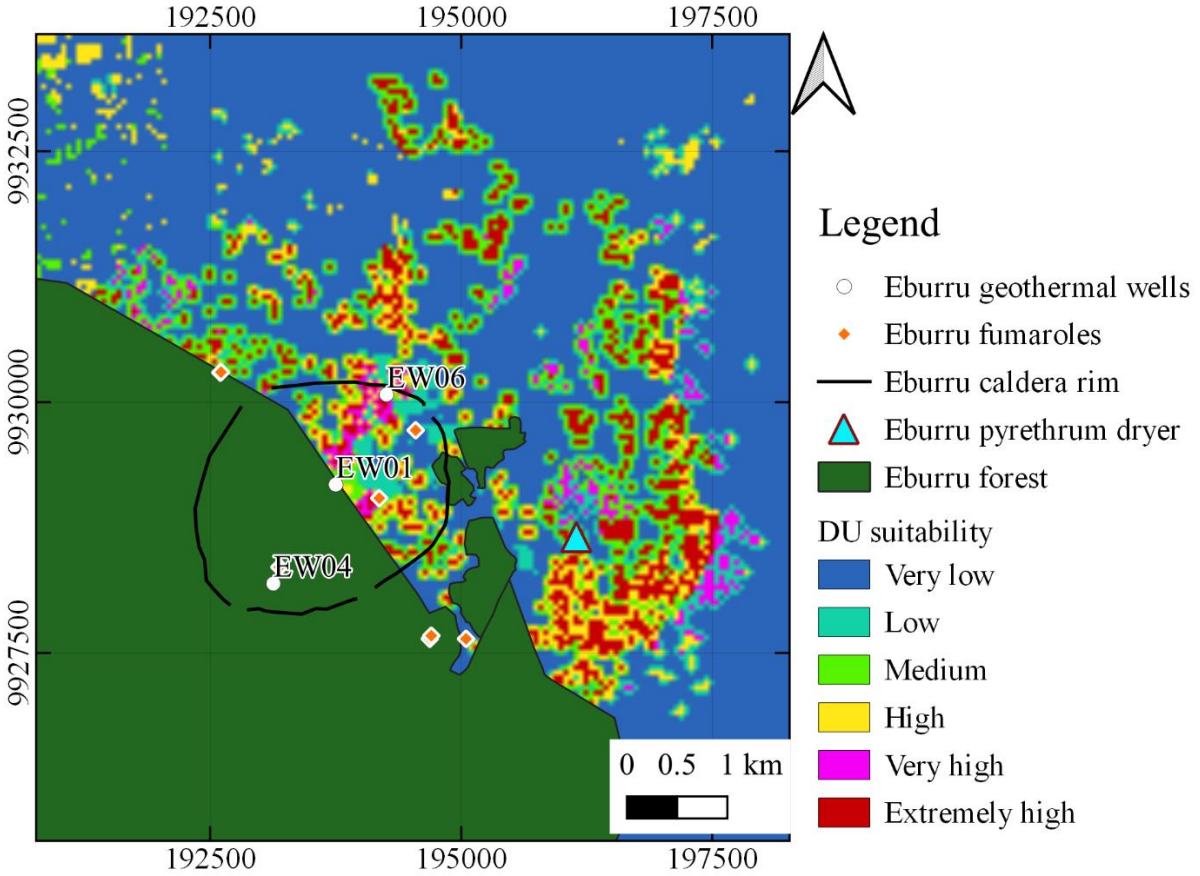

Figure 4.23 Direct use suitability map for crop dying, milk pasteurization, and water desalination around Menengai geothermal field.

4.12.4 Elementaita, Longonot and Suswa regions

These geothermal fields lack either shallow or deeper geothermal wells since they are still in the advanced stages of exploring for geothermal resources. Additionally, there are no significant heat-intensive commercial activity nearby. This is due to the absence of fresh surface water in the areas surrounding these geothermal sources and the insufficiency of rainfall to support extensive rain-fed or irrigated grain/dairy farming. Hence, the suitability selection for direct use ranked these geothermal resources poorly.

4.13 Design of "economic" pipeline diameter, insulation thickness, brine cost per m^3

It is desirable to estimate the minimum cost of hot brine conveyed to the consumers via pipelines from the Olkaria or Menengai geothermal reservoirs. Minimum brine cost per tonne would only result from the lowest cost of pipe installation characterized by economic pipe diameter, minimum effective insulation thickness, least annual pumping costs, and the shortest pipeline route to the consumers.

Previous feasibility studies at Olkaria and Menengai failed to propose the shortest brine routes, economic pipe diameter, and brine cost to the consumers (Kiruja, 2017; Mburu, 2010; Ronoh, 2020). Identifying locations of concentrated heat demands is a crucial prerequisite step, which directs route selection, selection of brine flow rate, and informs piping challenges to be encountered, as illustrated in section 4.12. Pipe design involves optimization of the parameters shown in Figure 4.24.

The Olkaria and Menengai geothermal fields have a demand of 120-300 t/h of hot brine located outside of the geothermal fields. This research chose to a pipeline conveying a flow rate of 300

t/h. When designing water piping, the main motivation is to reduce pumping cost by choosing an "economic" diameter with minimal frictional losses and piping material. One of the constraints is fluid velocity and flow rates.

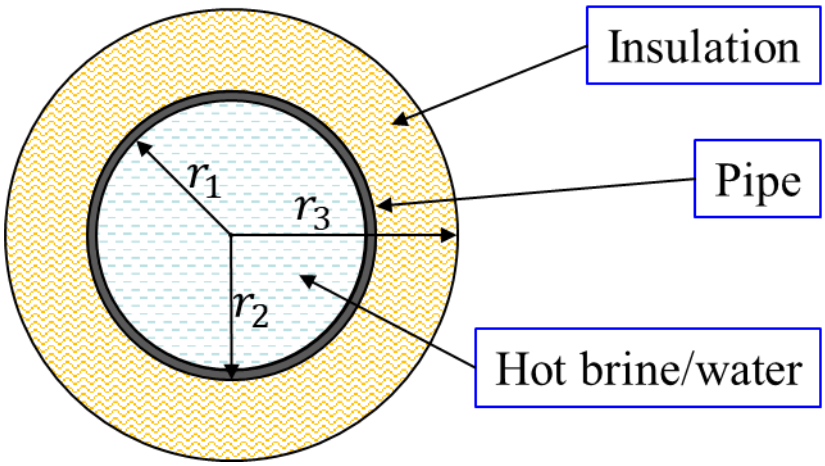

Figure 4.24 Insulated pipe parameters.

Pressure differences in the pipe are introduced by friction, elevation, and velocity of flow as shown in Equation (4.2, which is an aggregation of Bernoulli's and Darcy-Weisbach equations.

$$P_1 - P_2 = g(\rho_1 - \rho_2)(z_2 - z_1) + ({u_2}^2 - {u_1}^2/2g) + h_f \tag{4.2}$$

Finding optimal internal diameter is a minimization of multi objective optimization problem of Equation (4.3.

Min. C_t

$$C_t = Cc + Cp + (Ce + Co)\left(1 - \frac{1}{(1+i)^T}\right) \times \frac{1}{i} \tag{4.3}$$

Where,
Cc is the capital cost,
Cp is the pump installation cost,
Ce is the annual energy cost,
Co is the pump and pipe maintenance cost,
i is the rate of interest, and
T is the number of years the pipeline will be operated.

Subject to:

$$C_e = C_{kWh} \times O_h \times g\rho \times \frac{Q}{\eta} \times f\frac{u^2 L_e}{2gd_i} \geq 0 \tag{4.4}$$

$$Q = u \times \frac{\pi}{4} d_i^2 = 300 \ {}^{m^3}/_h \tag{4.5}$$

$$1 \leq u \leq 2 \ {}^m/_s \tag{4.6}$$

$$Re = {\rho u d_i}/{\mu} \geq 4000 \tag{4.7}$$

$$0.1 \leq f \leq 0.4 \tag{4.8}$$

Where

$$\frac{1}{\sqrt{f}} 1.14 - 2log_{10}\left(\frac{k}{d_i} + \frac{9.35}{Re\sqrt{f}}\right), \tag{4.9}$$

$$Cc = {C_{osp}}/{d_o} + {C_{in}}/{m^3} \times \pi \times ({r_3}^2 - {r_2}^2), \tag{4.10}$$

k is the pipe roughness,
Re is the Reynolds number,
C_{in} is the cost of insulation per m^3,
${C_{osp}}/{d_o}$ is the cost of pipe per diameter,
C_{kWh} is the cost of electricity per kWh,
d_i is the internal diameter of the steel pipe,
f is the pipe flow frictional factor,
u is the flow velocity,
O_h is the hours the pump is operated per year,
r_1 is the internal radius of the pipe,
r_2 is the outside radius of pipe,
r_3 is the radius of the insulation cladding,
ρ is the fluids density,
Q is the flow rate,
g is the acceleration due to gravity,
η is efficiency of the pump,
L_e is the equivalent length of the pipe, and
μ is the dynamic viscosity.

The price of steel pipes fluctuates with inflation, supply, and demands as well as by geo-locations. Use of updated prices of steel is recommended.

All hot water pipes with diameters above 100 mm and spanning beyond 50 m should be insulated to conserve heat. Table 4.9 shows insulation materials considered in this research.

Table 4.9 Parameters of different insulation materials.

Material	Insulation type	Thermal cond. W/m. °C	Operating temp. °C	Density kg/m3	Cost \$ / m^3

Polypropylene Foam insulation	PPF	Foam	0.17	0 - 130~170	650	124
Calcium Silicate insulation	CSPI	Silica	0.096	-18°C to 650	200 - 500	130
Mineral wool insulation	MW	Rock fiber	0.037	0°C to 650	60 - 160	56
Polyurethane Foam insulation	PUF	Foam	0.03	-160 to 160	30 - 100	85
Fiberglass insulation	FG	Fine glass fibers	0.046	-30 to 540	10 - 14	70
Micro-porous Silica insulation	MPS	Micro ceramic - porous-	0.02	0 - 600	260	90
Aerogel insulation	AI	Nano size silica	0.012	up to 650	200	150

Design of optimal insulation thickness is a function of overall heat transfer coefficient, thermal conductivity of insulation material, insulation material density, and the temperature difference between the insulated surface and air.
This combination of parameters is complicated to model and use of industrial empirical data is advised. Bahadori (2014) developed an empirical model for calculating “economic” insulation thickness based on averaged industrial data, as depicted in Equation (4.11.

$$\ln(\delta) = \alpha + \frac{\beta}{d} + \frac{\gamma}{d^2}\frac{\theta}{d^3}. \tag{4.11}$$

Where,

$$\alpha = A_1 + \frac{B_1}{\lambda} + \frac{C_1}{\lambda^2}\frac{D_1}{\lambda^3}. \tag{4.12}$$

$$\beta = A_2 + \frac{B_2}{\lambda} + \frac{C_2}{\lambda^2}\frac{D_2}{\lambda^3}. \tag{4.13}$$

$$\gamma = A_3 + \frac{B_3}{\lambda} + \frac{C_3}{\lambda^2}\frac{D_3}{\lambda^3}. \tag{4.14}$$

$$\theta = A_4 + \frac{B_4}{\lambda} + \frac{C_4}{\lambda^2}\frac{D_4}{\lambda^3}. \tag{4.15}$$

γ is the thermal conductivity of the insulation material and d is the outside pipe diameter, while parameters A_1 to D_4 are obtained from
Table 4.10.

Table 4.10 Coefficients used in Equations (4.12) to (4.15 to predict optimal economic thickness in metres (Bahadori, 2014).

Factors	Surface Temp = 100°C	Surface Temp = 300°C
A_1	-1.619063838	-1.4673416207
B_1	$-6.0440641629 \times 10^{-2}$	$-9.4579004057 \times 10^{-3}$
C_1	$1.2992412636 \times 10^{-3}$	$-9.0991682769 \times 10^{-4}$
D_1	$-1.0480516067 \times 10^{-5}$	$2.1036093111 \times 10^{-5}$
A_2	$-5.6754247780 \times 10^{-2}$	$5.6420129717 \times 10^{-3}$
B_2	$1.1266206576 \times 10^{-3}$	$-8.1324216389 \times 10^{-3}$
C_2	$-4.5476251244 \times 10^{-5}$	$3.6013086233 \times 10^{-4}$
D_2	$5.4011484658 \times 10^{-7}$	$-5.0991959691 \times 10^{-6}$
A_3	$1.2871451750 \times 10^{-3}$	$-1.0914548287 \times 10^{-3}$
B_3	$-3.1321987972 \times 10^{-5}$	$3.1336503528 \times 10^{-4}$
C_3	$1.3585299744 \times 10^{-6}$	$-1.3704000608 \times 10^{-5}$
D_3	$-1.6951529528 \times 10^{-8}$	$1.9239332368 \times 10^{-7}$
A_4	$-1.1238180847 \times 10^{-5}$	$1.4969220576 \times 10^{-5}$
B_4	$3.5740278360 \times 10^{-7}$	$-3.3674152566 \times 10^{-6}$
C_4	$-1.5140460085 \times 10^{-8}$	$1.4658761606 \times 10^{-7}$
D_4	$1.8649575376 \times 10^{-10}$	$-2.0517177043 \times 10^{-9}$

Working with initial parameters displayed in Table 4.11in Equations (4.2 to (4.15 provides the results in Figure 4.25 and Figure 4.26.

Table 4.11 Working parameters for the hot brine pipeline project at the Olkaria and Menengai geothermal fields.

Parameters
➢ Flow rate 300 t/h
➢ Entry pressure 7 bara
➢ T_{in}, Entry temperature 165°C
➢ Seamless carbon steel, ISO Standards (Heavy gauge)
➢ Air temperature 20°C
➢ Insulation material, Mineral/Rock wool

Rock wool was settled on due to its low thermal conductivity at a reasonable cost. It is also commonly used in Kenyan geothermal fields; hence the suppliers and installers are already established.

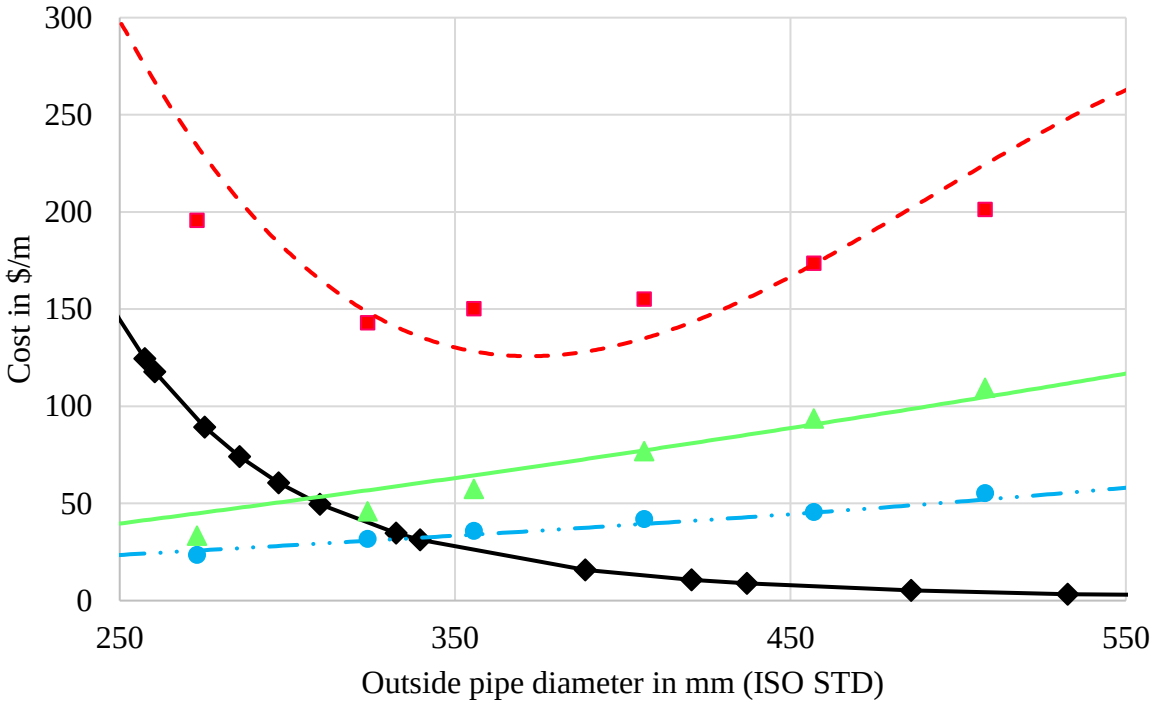

Figure 4.25 The choise of economic external diameter for pipe transmiting hot brine with a flow rate of 300 $^{m^3}/_{h}$.

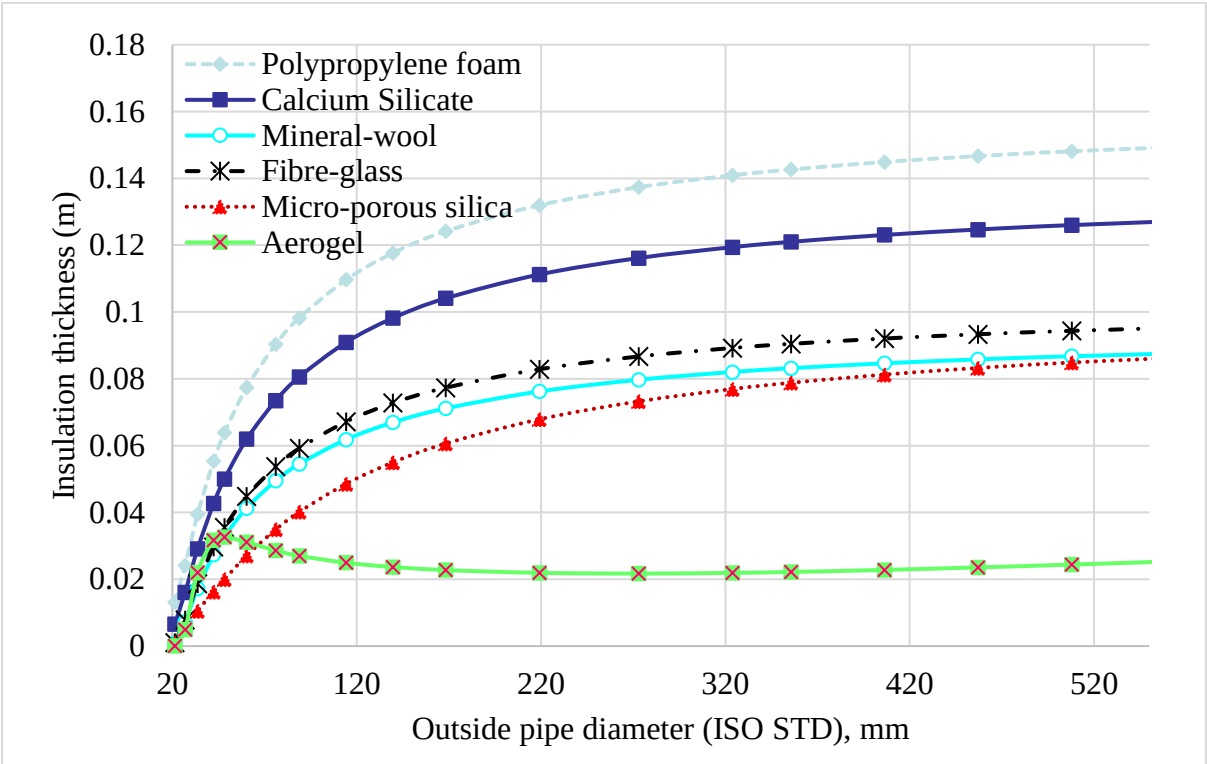

Figure 4.26 The optimal economic insulation thickness for a surface temperature of 150 and outside air temperature of 20°C, for the six insulation materials available in the market.

The optimal economic pipe diameter selected from Figure 4.25 was 355 mm outside diameter. This diameter corresponds to an optimal economic insulation thickness of 83 mm, when rock wool insulation material is used, as indicated in Figure 4.26.

4.13.1 Negating two phase flow in the pipeline.

Saturation conditions in hot water pipes complicates flow of water by increasing pumping costs and pitting of pipes. Once the diameter and insulation thickness are selected, it is prudent to check pumping requirements at every point of the pipe along the route by using Equation (4.2. As topography heavily influences pumping needs, it is paramount to graph brine pressure as it flows along the route against ground elevation and estimate the points to install pumping centres. Figure 4.27 and Figure 4.28 show effect of topology on brine piping for Menengai-Nakuru and Olkaria-Naivasha routes, respectively. However, it is still difficult to estimate whether flashing of brine might occur inside the pipeline.

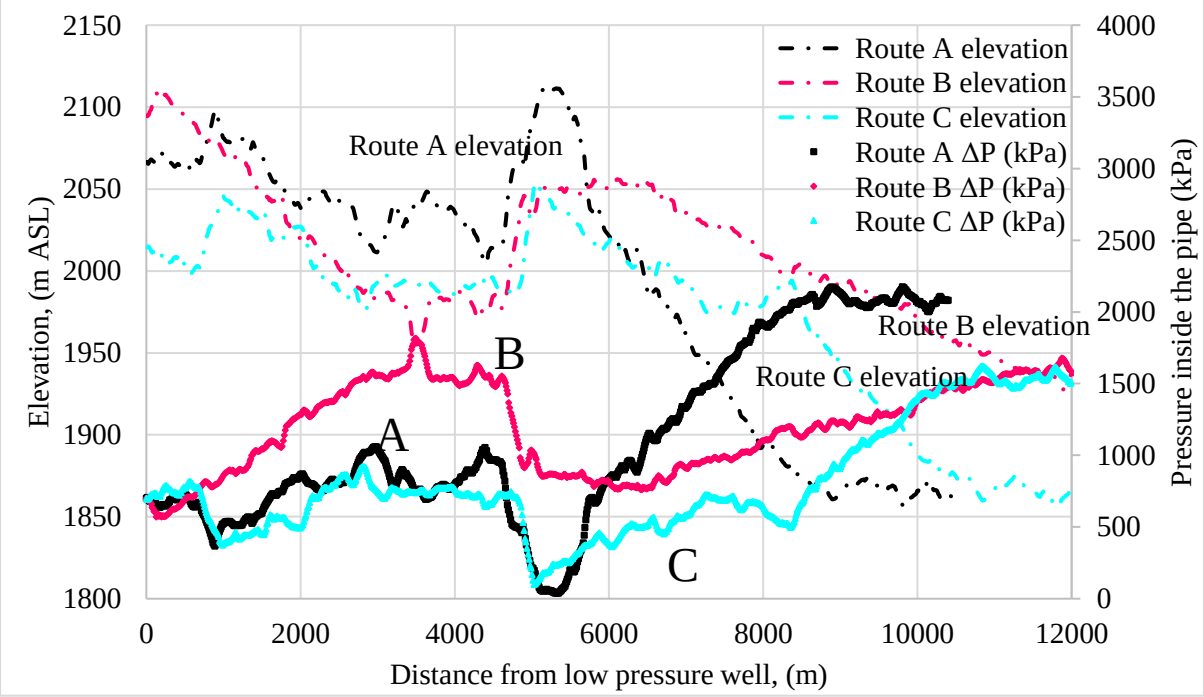

Figure 4.27 Influence of Menengai caldera rim on brine piping pressures along the routes.

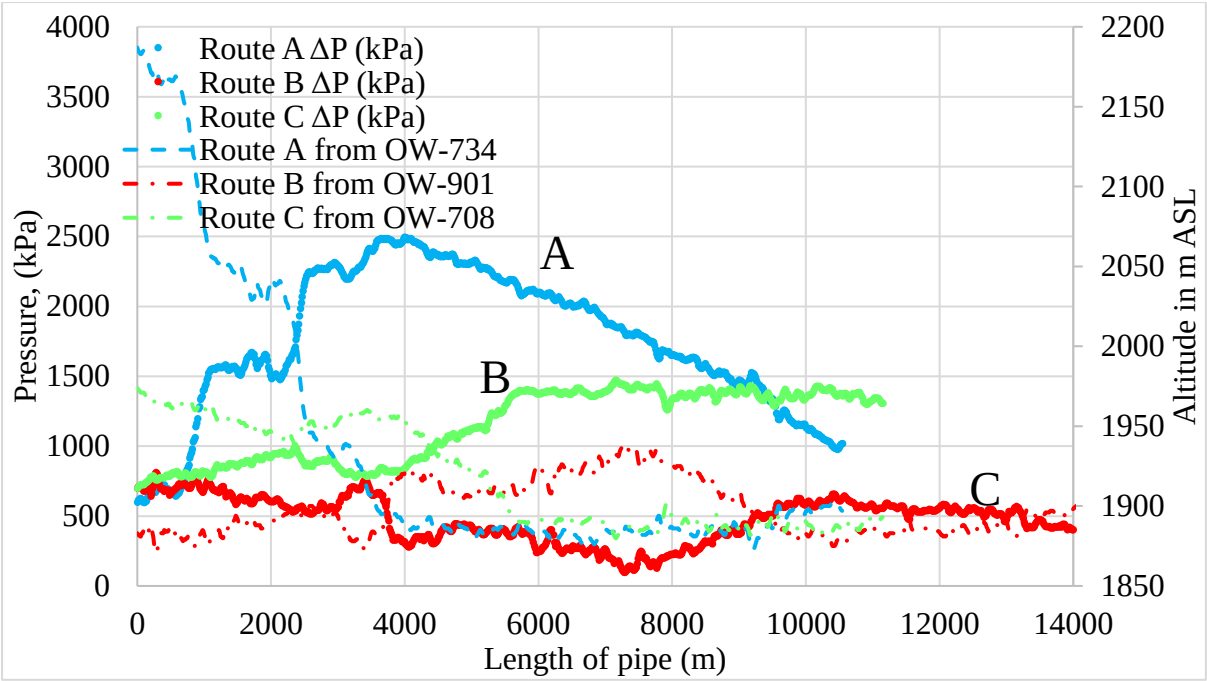

Figure 4.28 Influence of the Olkaria's rugged terrain on piping pressueres from Olkaria northeast to southern shore of Lake Naivasha.

To estimate flashing condition inside the hot water pipe, Joule-Thompson cooling equation is applied, Equation (4.16.

$$T_x = T_{air} + (T_{in} - T_{air})e^{\left(\frac{-xU}{L_e}\right)} + \frac{1}{C_p}\left\{\frac{P_x - P_{in}}{\rho} - g(z_x - z_{in})\right\} \tag{4.16}$$

Where,

$$U = \left[\frac{2\pi}{\frac{1}{r_1 h_{in}} + \frac{ln\left(r_2/r_1\right)}{k_1} + \frac{ln\left(r_3/r_2\right)}{k_2} + \frac{1}{r_3 h_{air}}}\right], \tag{4.17}$$

T_{in} is the pipe entry temperature,
U is the overall heat transfer coefficient of the insulation per metre,
$T_x$is the temperature at any point of the line,
z_{in} is the entry elevation,
P_x is the pipe entry pressure, and
C_p is the heat coefficient of water.

Applying Equation (4.16 on the routes gives results in Figure 4.29 (for Menengai) and Figure 4.30 (for Olkaria).

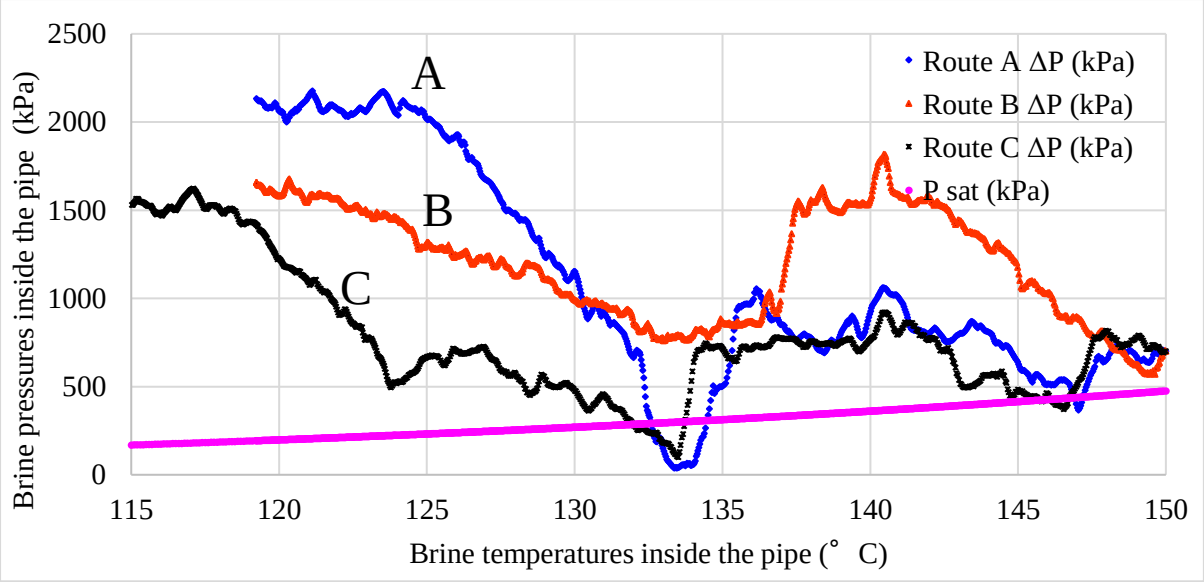

Figure 4.29 Brine flashing conditions for different brine piping routes at the Menengai field (Note flow is from right to left).

Brine flashing is noted at two points along routes A and C, pointing out the locations of pumping centres and pumping pressures of 6 bars. Rooute B can be adopted with no extra pumping center required.

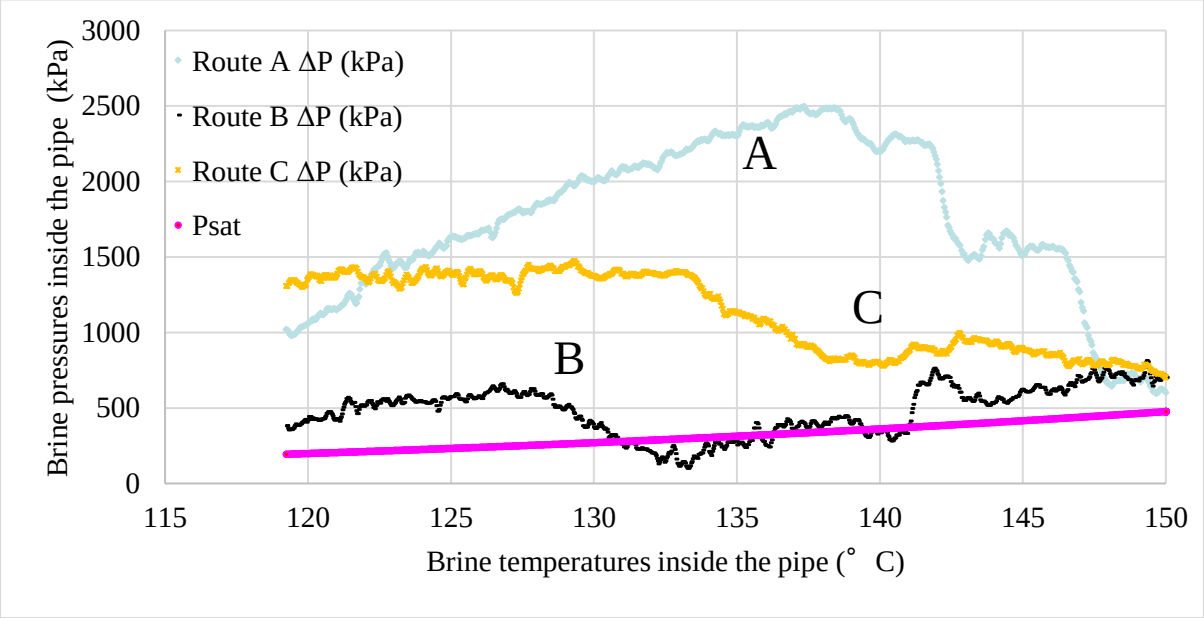

Figure 4.30 The saturation conditions of brine inside the pipes condducting hot brine from northeast of Olkaria field to the southern shore of Lake Naivasha (Note flow is from right to left).

Routes A and C are sufficient to conduct hot brine without the needs of pumping centres. All the routes a heat loss of about 30°C.

4.13.2 Cost of brine per m^3.

Once the optimal brine routes have been chosen, the total pipeline cost, pumping cost, and labour cost can be estimated. Applying amortization formulae, Equation (4.18, on capital and

operation cost, the minimum brine prices at the Menengai and Olkaria geothermal fields were identified as $ 0.68/ m^3 and $ 0.87/ m^3 for hot brine/hot water at 120 °C, respectively.

$$Cbrine = Ct\left(1 - \frac{1}{(1+i)^T}\right) \times \frac{1}{i} \times \frac{1}{8640 \times Q} \quad (4.18)$$

Where, C_t is the capital cost plus operational and maintenance cost for the entire lifetime of the pipeline and$Q$ is the brine flow in cubic metre per hour (300 $^{m^3}/_h$).

4.14 Conclusion

In this chapter, the suitability of high enthalpy geothermal resources for the different direct use scenarios was analyzed, based on Multi Criteria Decision Making (MCDM) methods, Silica Saturation Index (SSI) analysis, remote sensing (RS) of satellite images, Inverse Distance Weighted (IDW) and ordinary kriging interpolation methos, and proximity analysis. The optimum direct usage options for geothermal resources with hot brine and steam were found through investigation. Additionally, the geothermal fields' heat requirements were calculated, and concentrated heat demand areas were discovered. This study disagrees with some prior studies on the viability of direct usage in Kenya since earlier studies neglected to characterize the heat demands as well as the characteristics of the geothermal field. The heat demands at the Olkaria, Eburru, and Menengai geothermal fields were identified as 180 MWt, 650 MWt, and 2050 MWt, respectively. Brine cost at Olkaria and Menengai would start at $ 0.87 and $ 0.68 per m^3 of hot brine at 120 °C.

Finally, the direct use case studies that already exist in the research area and are reported in chapter six confirmed this feasibility model. The model was adjusted to deal with surface manifestations like hot springs for direct use because it strongly described geothermal fields with brine and steam. This modification is detailed in the following chapter (chapter five).

CHAPTER FIVE

5 SELECTION OF BEST DIRECT USE SCENARIOS FOR MEDIUM TO LOW ENTHALPY GEOTHERMAL RESOURCES AND HOT SPRINGS

5.1. Introduction

This chapter describes hot springs' water chemistry for estimating the hydrothermal subsurface temperatures and the selection of the best direct use scenarios for hot spring water. The hydrochemistry analysis includes stable isotope analysis to determine the source of water recharge to the geothermal systems. The geothermometer data helped to reclassify undeveloped medium to low geothermal resources by exergy. The hot springs were further characterized for best direct use scenarios based on their characteristics and economic factors affecting their utilization. The methodology for direct use classification was GIS-based MCDM methods, where AHP was used to weight criteria map layers while QGIS was used to overlay the weighted criteria map layers to obtain suitability map layers.

5.2. Kenyan medium to low enthalpy geothermal resources

Kenyan geothermal resources range from low-medium-high enthalpy. This categorization was based on geochemistry (based geothermometers) during exploration, and the high enthalpy resources were prioritized for further advanced exploration studies (magneto-telluric (MT), transit electro-magnetic (TEM), gravity, micro-gravity, seismic surveys), and development to exploit steam (Kanda, 2010). Generally, medium to low geothermal resources have received low attention from policymakers in the Kenyan energy development sector (Tole, 1988). Besides, several Kenyan geothermal resources, low to high enthalpy, have hot springs and fumaroles which have yet to be characterized for optimal use. Hot springs are precious in promoting volcanic geotourism and spa culture in other countries such as Japan and China (Erfurt, 2021). Currently, hot springs and fumaroles in Kenya are left for community use without protective barriers and remodification to offer better bathing facilities.

All Kenyan geothermal resources are magmatic, originating on orogenic belts of active rifts created by diverging continental plates. The low enthalpy geothermal resources derive their heat sources from partially molten rocks from isolated remnants of Tertiary magma deposits at varying depths. These geothermal resources are hard to distinguish since they lack vigorous surface manifestation, such as fumaroles, though some have self-discharging warm springs. Most of these are located outside the active Kenyan rift valley. The medium enthalpy geothermal resources have hotter and may have more than one hot spring with or without fumaroles and geysers. It is argued that medium geothermal resources such as Lake Bogoria, Homa Hills, Mwananyamala, Lake Magadi and Korosi geothermal fields have high enthalpy reservoirs with a permeable caprock that allows significant heat loss (Mwawasi, 2012). They derive their heat from Quaternary magmatic deposits and heavily rely on fault structures for fluid movement (Mibei et al., 2021).

5.3. Hot springs

The floor of the Kenyan rift is subject to normal faulting, followed by mafic and silicic lava movements, which have allowed meteoric fluid movements and subsequent formation of both high and low enthalpy geothermal resources through hydrothermal activities (Biggs et al., 2021). The magmatic heated fluids ascend to the surface via faults and fissures to form fumaroles, solfataras, hot springs, steaming grounds, and altered grounds. The hot spring

activity might range from weakly seepages to vigorous bubbling of geysers. Kenya has over 150 documented hot/warm springs distributed over 23 geothermal resources. 90% of the hot springs are located within the floor of the East African Rift System (EARS), 5% are to the west of EARS and the remaining hot springs are to the east of EARS. The local communities have used almost all of the accessible springs in Figure 5.1 for different purposes, including bathing, domestic use, drinking, crop drying, salt licks for animals and animal deworming. Some hot springs used for drinking and domestic use have unsafe concentration levels of B, As, and F. This study sought to reclassify these low enthalpy resources with geochemistry analysis and their discharge heat capacity to select the best application scenarios. This work included geochemical study of harmful elements in geofluids such as B, As, Fe, and F to advise the communities that utilize these resources for drinking, watering their animals, or using them as salt licks.

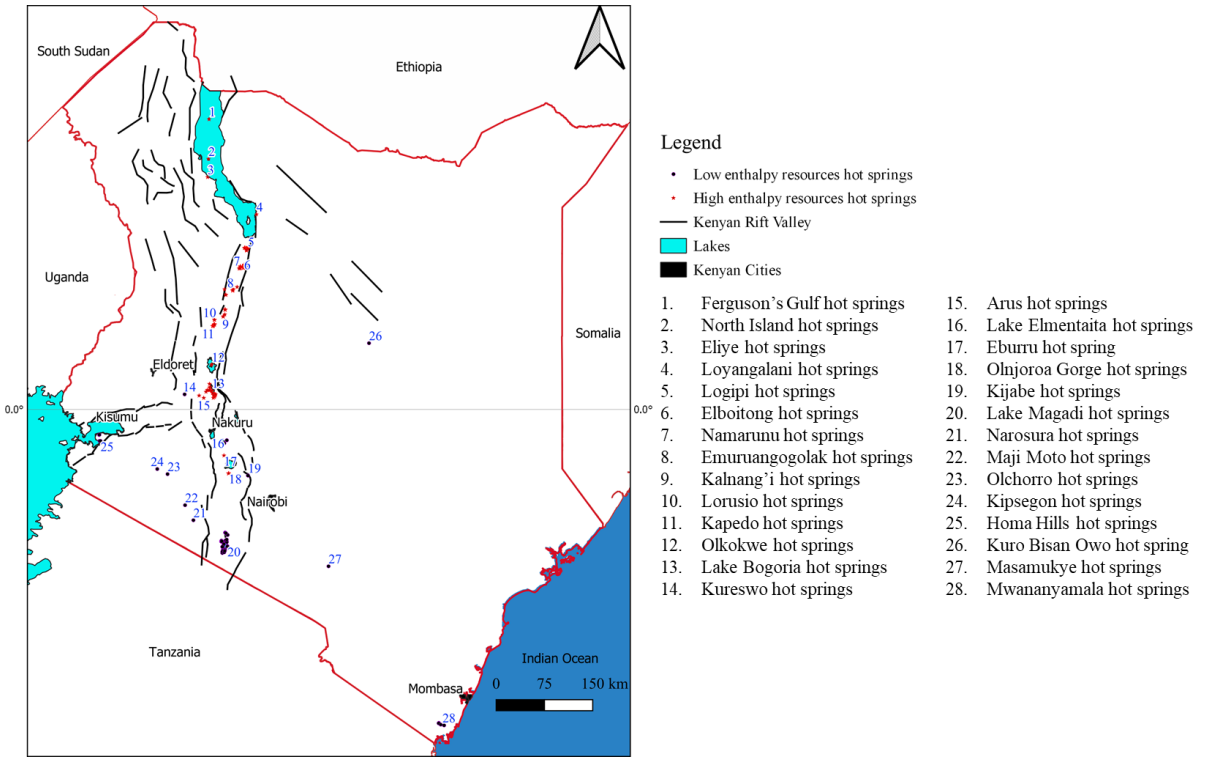

Figure 5.1 Location of hot springs in Kenya (Source of data: Present study with contribution from Dunkley et al., 1993; Kanda et al., 2012; Tole, 1988)

The hot springs are densely distributed within the Kenya Rift Valley floor, with just a few occurring outside this active volcanic graben, as shown in Figure 5.1. The largest group of subaqueous hot springs occur on the banks of lakes Magadi, Bogoria, and Logipi, including along the escarpments leading to Lake Turkana in the north of Kenya.

Hot springs are a type of surface manifestation, along with fumaroles, altered, and steaming grounds, which are signs of subaerial hydrothermal systems. Hot springs are defined as naturally occurring points, pools or seepages, on the earth's surface that discharges a continuous flow of water at temperatures above 25°C, maybe accompanied by steam or other gases (Erfurt, 2021). The discharging points of hot springs may have spectacular carbonate travertines, sulfur, calcite or amorphous silica sinters. Rarely, but occasionally, glorious geysers may be present alongside hot springs (Barrick, 2010). Geysers require a delicate balance of subterranean aquifers plumbed through by proper geometry fissures, allowing groundwater to fill the pipe to reach a high-temperature heat source below (Hurwitz & Manga, 2017). The heated water is then evacuated simultaneously with the help of diffused mantle gases (CO_2 and CH_4) and steam (Ajayi & Ayers, 2021). Hot springs and geysers provide awe-

inspiring sceneries that have long been utilized for bathing, therapeutic healing, spiritual, cultural, and as volcanic geotourism attractions (Barrick, 2010). Besides, hot springs and geysers are ideal for researching thermophiles and hydrothermal mineral systems (Adiguzel et al., 2009; Pirajno, 2020). Their waters mainly carry different minerals and gases from the crust's depths that support the growth of thermophilic microorganism mats with various colours (Barrick, 2010; Jones & Peng, 2012). Additionally, hot springs and geyser waters provide the cheapest geothermal energy exploratory means by estimating hydrothermal reservoir temperatures based on various commonly used geothermometers such as Na-K-Ca, quartz, Na/K ratio, and K/Mg ratio.

Figure 5.2 Photos showing the temperatures and general conditions of hot springs in Kenya: (a) Ol' Kokwe island hot spring in Lake Baringo, (b) Lake Bogoria geyser, (c) Abundu pool type hot spring and (d) A series of seepage hot springs at southern tip of Lake Elementaita.

5.3.1. Origin of hot springs

There are three essential origins of hot spring waters: meteoric, magmatic and connate waters, the primary source being meteoric. Meteoric waters are heated by magmatic intrusions, partially molten rocks, hot rocks heated by natural geothermal gradient or ascending steam from high enthalpy hydrothermal systems. The differences in heat sources categorize hot springs into magmatic and non-magmatic artesian hot springs (Erfurt, 2021). Magmatic hot springs derive their heat source from shallow magma intrusions or partial molten rocks from

solidified magma, while the natural geothermal gradient heats non-magmatic hot springs. Sometimes, chemical reactions such as hydration of peridotite and olivine (serpentinization) of radioactivity in igneous rocks may also provide heat, though rarely (Lamadrid et al., 2017). Figure 5.3 (A) shows a simplified model of magmatic hot springs standard in intra-continental rifting zones such as the East African Rift System (EARS). The majority of the hydrothermal aquifers in Kenya are recharged and fed by meteoric water percolating through normal faults at the edges of rift graben, with some having a mixture of both meteoric and lake waters (Cioni et al., 1992; Dunkley et al., 1993; Kipngok et al., 2019; Nkapiani and Kamunya, 2015).

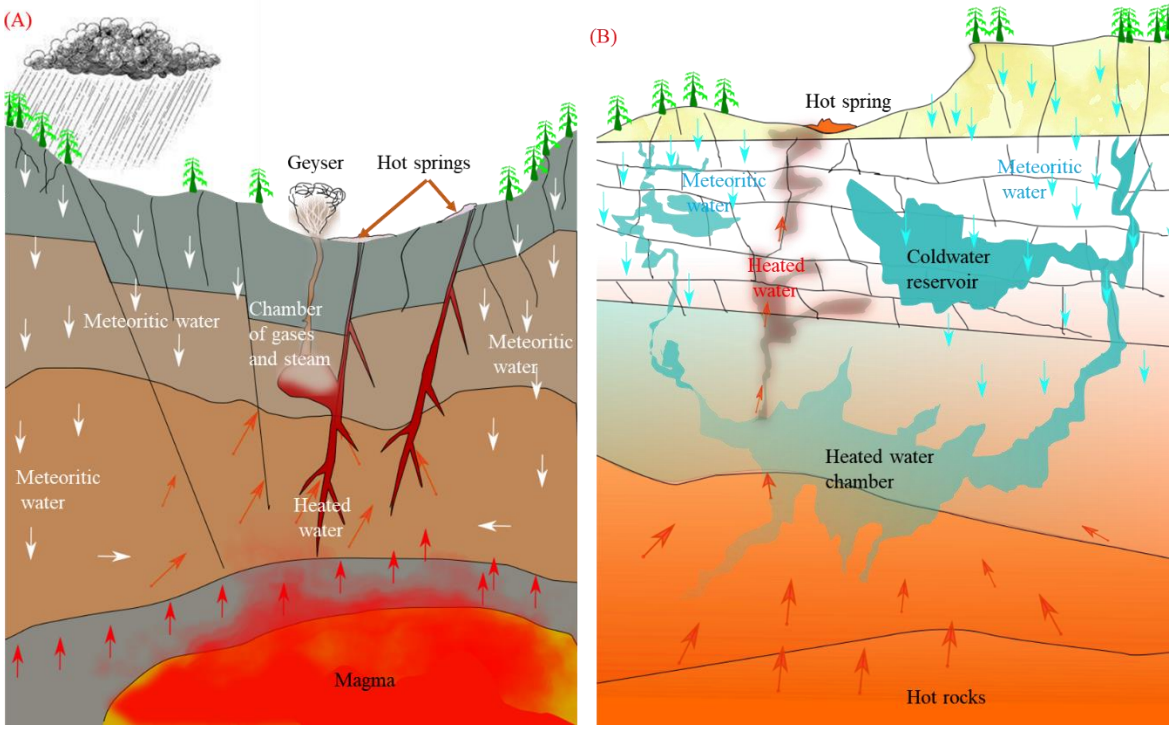

Figure 5.3 A simplified conceptual model of (A) magmatic and (B) craton basin (geothermal gradient heated) artesian hot springs.

Hot springs arising from magmatic-heated hydrothermal systems can be categorized as originating from shallow or deeper thermal aquifers. The shallow aquifer hot springs are generally heated by convective steam and conductively cooling rocks overlaying a non-permeable cap rock of an existing deeper hydrothermal system. These hot springs have lower concentrations of chloride (Cl), boron (B), and other total dissolved substances (TDS) (Karingithi and Wambugu, 2008). The hot springs originating from deeper hydrothermal systems have a longer residence time for water-rock interactions, hence they convey more leached chemical substances; depending on the rock type. Their Cl, B, F and TDS concentrations may be higher. The occurrence of bicarbonate or chloride waters, pH levels, and their chemical properties mainly depend on underlying rocks and the period of water-rock interaction. The alkaline nature of hot springs in the Kenyan Rift Valley is influenced by Quaternary volcanoes that include mildly to hyper-alkaline silicic rocks such as comendites, basalts, rhyolites and trachytes (Karingithi et al., 2010). Most Kenyan hot springs have low sulphate concentrations, <200 ppm except Homa Hills, Logipi, Namarunu, Masamukye, and Lake Magadi, which have a sulphate concentration range of 240 to 1700 ppm. These hot springs exhibit geochemical signatures of deep convecting geothermal reservoirs.

5.3.2. Current community utilization of hot springs

The utilization of hot springs has been going on within Kenyan communities for the last 100 years (Mangi, 2013). Some have utilized the water for medicinal purposes, watering animals, bathing and many other applications (Lagat, 2010). Each application depends on the location of the hot spring, its discharge temperatures, salinity, flow rates and the community living nearby. In regions experiencing water scarcity (Figure 5.4), the hot springs and fumaroles provide much-needed relief but with dire risk to the residents' health if they consume water with high concentrations of B, As, Fe, F and Pb.

The basic traditional direct use schemes of hot springs rarely include remodification of the hot spring water paths or hot spring environment. Such uses include bathing, drinking, spiritual, cultural, and sightseeing. Early usage of hot springs involved scooping out sand and dirt next to the discharge points to make depressions that community members sit in to bathe with hot spring waters (Wightman and Wall, 1985). These primitive bathtubs have minimal environmental impacts. However, the type of utilization depends on the chemical and temperature characteristics of the hot spring and its surrounding environment. In their natural state, shown in Figure 5.4, hot springs are subject to erosion, trampling from animals and people, waste disposal and other destructive activities which limit their utilization and appeal. Most Kenyan hot springs are in this condition hence their contribution to community well-being and economy is limited by their lack of harnessing for commercial exploitation. By harnessing hot springs for direct uses such as bathing, aquaculture, drying, and other uses, the hot spring discharge points are fenced in and protected.

Conventional utilization scenarios of hot springs in Kenya are tabulated in Table 5.1. The applications were recorded during a field survey of the hot springs and the community that resides near them. Just a few hot springs, (two), were noted to be equipped with bathhouses and swimming pools, while most are not protected from trampling by people and animals. The current utilization scenarios are also less guided by the geochemistry of the hot spring waters. Missed opportunities in geotourism, spas, drinking water, heated swimming pools, and aquacultural heated ponds result from the hot springs not being retrofitted with the appropriate channeling and safeguards.

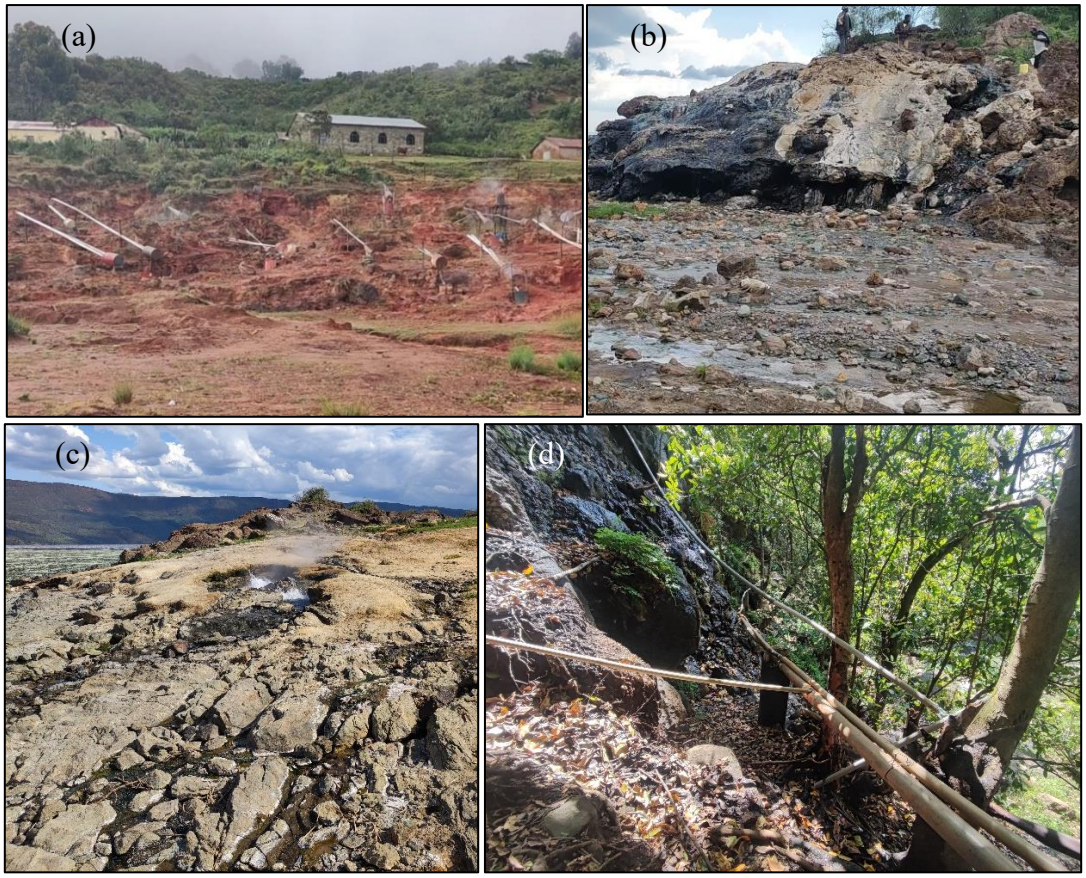

Figure 5.4 (a) Condensing of fumaroles at Eburru and (b) residents collecting hot spring water from Bala (Homa Hills) hot springs, (c) one of the geysers at Lake Bogoria, and (d) piped waters of Kijabe hot springs.

Table 5.1 Specific description and uses of the hot springs in Kenya from field survey.

Hot spring	**Description**	**Uses**
Eliye	Eliye hot springs discharge at the western edge of Lake Turkana.	The hot springs support the nearby community and tourist resort by providing freshwater for domestic use and bathing.
Logipi	Logipi hot springs act as a source of inflow into Lake Logipi.	They recharge lake Logipi. The lake supports millions of Lesser. Flamingoes.
Namarunu	The hot springs discharge water that collects into small tributaries that join the Suguta River.	Recharge Lake Logipi
Kapedo	The hot spring water coalesce into an over 1000.0 m^3/s stream that flow northwest. The streams flow over a cliff forming a spectacular waterfall before joining the Suguta River.	The waters contribute inflow into the Suguta River and forms a beautiful sightseeing attraction.
Ol Kokwe	The hot springs discharge hot water into the Lake Baringo.	The hot springs are the main tourist attractions taking boat rides on Lake Baringo.
Lake Bogoria	Lake Bogoria hot springs discharge as a series of seepages, pools and spectacular geysers	These springs act as the main tourist attraction for the visitors touring Lake Bogoria.

Lake Elementaita hot springs	The hot springs discharge as a series of seepages at the southern edge of Lake Elementaita.	The nearby community has deepened the hot spring discharge points to create bathing points.
Eburru	The hot spring discharges at the bottom of a depression next to near-boiling fumaroles and hot altered grounds.	The water is used for domestic purposes (washing and drinking).
Ol Njorowa Gorge	The hot springs discharge hot water into a ravine.	Wild animals inhabiting the Hells Gate National Park use the cooled hot spring water for drinking.
Kijabe	Kijabe hot spring discharge in a ravine at the bottom of the western escarpment of the Kenyan Rift Valley.	The water is harnessed into pipes and conveyed downhill to Kijabe community for domestic uses (washing and drinking).
Lake Magadi	The Magadi hot springs occur as pools and seepages either at the edge or inside the lake.	The hot spring water recharges Lake Magadi, hence sustaining the Lesser Flamingoes and the Maasai community nearby use them for bathing and swimming.
Homa Hills	The hot springs discharge in a combination of pools and seepages into gulleys and ravines that discharge into Lake Victoria.	The hot springs are used for bathing, Sightseeing and deworming farm animals. The waters are also consumed by humans for medicinal purposes.
Kipsegon	Also located in a ravine, the hot spring discharges neutral water into a pool.	The waters are used for bathing.
Olchorro	The hot spring is located in a valley and discharges water into the one of the tributaries of Mara River.	The hot spring is used for medicinal purposes, bathing, and sightseeing.
Majimoto	The hot springs discharge from a depression with numerous seepages with a total flow rate of 7 m^3/s.	The hot spring water is collected in a dam with a surface area 6000 m^2. The dam provides freshwater to the Majimoto community for domestic use and watering animals.
Narosura	The hot springs discharge from a ravine in the middle of farmland.	The cooling waters are used for bathing and irrigation.
Kuro Bisan Owo	The hot spring has been fenced in and protected by concrete and its waters directed into a watering trough.	The spring is used to provide water for people and animals as a medicinal product.
Masamukye	The hot springs bubble at the Mwooni riverbed, quickly mixing with river water	They serve as sightseeing and tourist attractions. There are several lodges and resorts nearby the hot springs.
Mwananyamala	Occur as a series of pools.	The Mwananyamala site is used as a traditional shrine for rituals as well as an attraction for tourists.
Kariandusi	The hot springs discharge into a small valley with a concrete collection pond.	The water is piped to the nearby hotels for spa and bathing.

5.4 Geochemical analysis of hot spring water from medium and low enthalpy geothermal resources

The water chemistry of subaerial and subaqueous hydrothermal systems is crucial for understanding those systems. The presence of lithium, rubidium, caesium, boron, arsenic, carbon dioxide and hydrogen sulphide is evidence of magmatic high-temperature waters (Ellis and Mahon, 1977; Mwangi, 2013). Mwangi (2013) estimated that the Olkaria temperature is above 230^{o}C using geothermometers. Kanda (2010) estimated Menengai geothermal reservoir temperatures to range from 274 – 304°C by using Thoron – CO_2 ratios from fumaroles gases. These temperatures were later validated by well-logging data to range between 200 - 300°C (Mibei et al., 2016). Hence, in order to reclassify these resources as either medium or low enthalpy, a rigorous geochemical analysis of their hot spring waters is necessary. The geothermometers equations will estimate the reservoir temperatures, especially for the newly discovered fields. The data from the literature will be synchronized to check variations of sub-surface temperatures with time. Thermal reservoir temperatures are crucial in geothermal field evaluation potential. Isotopic analysis is the best tool for hydrological investigations to understand the fluid sources, recharge, infiltration rates, location, depths, temperature, and aquifers location (Ball, 1982). The aqueous concentrations of water (chemical and isotopic components) discharges at the surface are controlled by equilibrium with minerals in aquifers' rocks (Arnorsson, 2000).

Concentration plots and ternary diagrams are generated from the measured and analyzed chemical species. The input values are ppm and stable isotope data per mil (Powell et al., 2010). Charts produced for data analysis and discussion include the famous Giggenbach Na-K-Mg geothermometer ternary, temperature geoindicators, stable isotope, Cl-enthalpy, and trace element ternary plots (Powell et al., 2010).

Geochemical surveys predict the sub-surface temperature and help predict the origin and the flow direction conditions at the depth (Arnorsson, 2000). Conservative constituents are applied in geochemistry to trace the origin of geothermal fluid, whereas reactive substances are helpful for physical reservoir states like temperature (Arnorsson, 2000; Mwangi, 2013).

Geochemistry also quantifies the tendencies of corrosion and scaling challenges in the surface development of geothermal projects (Arnorsson, 1985). Basic ingrained assumptions in sub-surface temperature estimations include (Fournier, 1977;Fournier et al., 1974):

i. Temperature-dependent reactions occur at depth involving rock and water to fix the concentration of dissolved constituents in the water.
ii. The constituents involved in a temperature-dependent reaction are abundant (supply is not a limiting factor).
iii. Water-rock equilibration occurs at the reservoir temperature.
iv. Little or no re-equilibration or change in composition occurs at lower temperatures as the water leaves the reservoir to the surface.

The hot water from deep in the system does not mix with cooler shallow groundwater. The two main temperature-dependent reactions are solubility and exchange reactions (Ellis & Mahon, 1977).

The first three assumptions are probably suitable for a few reactions that occur in many places, while the last two are not valid for many hot-spring systems; therefore, information obtained is for the shallower parts of those systems (Fournier et al., 1974).

5.4.1 Silica geothermometer

In hydrothermal systems, silica occurs in various forms as chalcedony, cristobalite and amorphous silica (gelatinous silica, sinter and opal) (Ellis & Mahon, 1977). Quartz is the stable form of silica with the lowest solubility, unlike the other forms that should rarely have

equilibrium solubility, and the silica content can be correlated with the last temperature of equilibration with quartz using Figure 5.5 (Ellis & Mahon, 1977; Fournier, 1977).

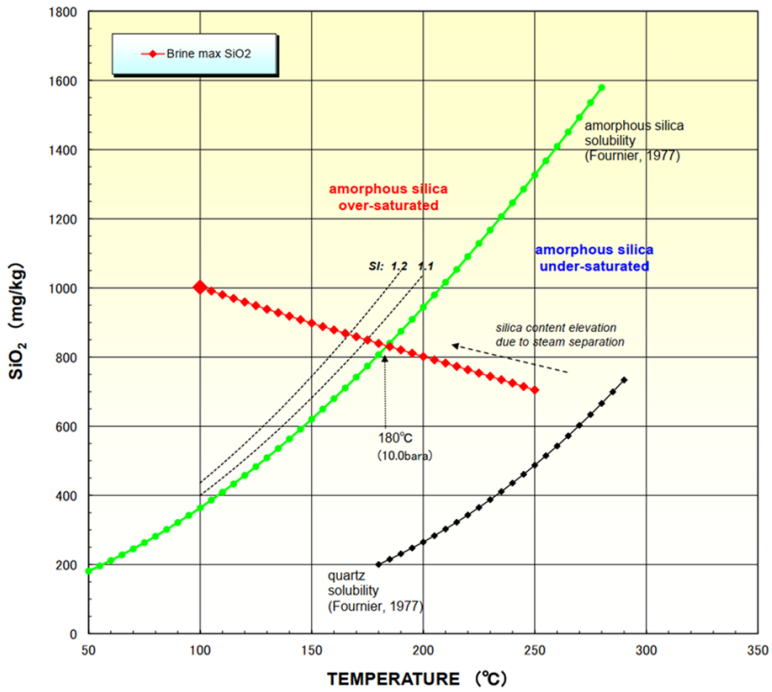

Figure 5.5 Solubility of quartz and amorphous silica as a function of temperature (Zarrouk & Purnanto, 2015).

Quartz geothermometers are excellent predictors of the potential for scaling in the surface facilities and reinjection wells and estimate reservoir temperatures. If cold and hot groundwater are mixed, subsurface solubilities rise; otherwise, they fall. (Ball, 1982). Geothermometry estimation might predict the central up-flow zones depth corresponding to the highest temperatures (Wang et al., 2018a). Water quartz equilibrium is quickly reached, providing accurate predictions for changing reservoirs that are also sensitive to cooling and mixing, making it a good choice for hot springs estimates (Ball, 1982).

5.4.2 Cation geothermometer

The cation geothermometric approach is susceptible to differences in fluid and reservoir compositions (Ball, 1982). Equilibrium constants for exchange and alteration reactions are temperature dependent, and the ratios of dissolved constituents change with changing temperature of equilibration (Fournier, 1977). Low values of Na-K-Ca geothermometer estimates indicate re-equilibration below 100^{o}C evaporative sequence perturbation (Ball, 1982; Fournier, 1977). Due to the retrograde solubility of calcium carbonate, springs supplied directly from hot aquifers have the highest Na/Ca ratios (Fournier, 1977).

5.4.3 Mixing Models

Thermal water usually consists of deep hot water mixed with shallow cold aquifer water. After mixing, partial or complete chemical equilibration may or may not occur (Fournier, 1977). The temperature of the hot-water estimation based on an exchange reaction using a ratio of dissolved constituents is affected by mixing in two ways;

i. The deep hot water is relatively concentrated in the indicator elements than the shallow water.

ii. Little or no chemical reaction occurs after mixing to change the relative concentrations of the indicator elements.

Low Mg on concentration reveals the possibility of extensive mixing with cold water during water movement to the surface(Nouraliee et al., 2014).

5.4.4 O and H Stable Isotopic Analysis

It may be possible to assess subsurface temperatures by using the isotopic composition of geothermal fluid components, in addition to learning about their source, recharge area, and flow patterns (Mutonga, 2015). While demonstrating that the volcanic edifices of the rift floor have different effects on groundwater flow patterns, 0 and H stable isotope ratios can be employed as tracers of infiltration over sometimes large distances (Darling et al., 1996). Analysis of oxygen 18 and deuterium isotopes trace the source of groundwater. The geochemist Craig (1961) developed Equation (5.1) known as the Global Meteoric Water Line (GMWL), which represents the average relationship between hydrogen and oxygen isotope ratios in natural terrestrial waters as a global average.

$$\partial \mathrm{D} = 8\,\partial^{18}O + 10 \tag{5.1}$$

By modifying Equation (5.1), specific baseline equations can be calculated to suit given local areas depending on their averaged field sampled data. Allen et al. (1989) and Armannsson (1994) developed Kenyan Rift Valley Mean Water Line (KRVMWL) and Continental African Rain Line (CARL), respectively, as expressed in Equations (5.2) and (5.3), respectively.

$$\partial \mathrm{D} = 5.56\,\partial^{18}O + 2.04 \tag{5.2}$$

$$\partial \mathrm{D} = 7\,\partial^{18}O + 11 \tag{5.3}$$

The field samples were plotted against these lines to check their sources and effects of evaporation on lake waters with respect to the reservoir water. Stable analysis shows that most geothermal waters in Kenya originated from meteoric water (Kamunya, 2018; Kanda, 2019; Mutonga et al., 2010). Isotope and geochemical data combination give a more reliable and accurate estimation of the available/estimated geothermal resource.

5.5 Results and discussion for hydrogeochemistry analysis

5.5.1 Water chemistry

Table 5.2 summarizes the laboratory geochemical and isotopic analyses results. The chemical composition of the sampled water and the analysis carried out in other fields are relatively investigated in the relative composition of major anions and cations and total silica using ternary diagrams and isotope graphs. From Table 5.2, the samples from Kipsegon, Mulot, Mwananyamala, Majimoto, Narosura, Meru, Homa Hills, Masamukye, Kariandusi, Lake Bogoria, Lake Magadi, Lake Baringo, Kijabe, Lake Elementaita and Silali have near-neutral pH values between 6.16 and 7,84. The Eburru, Magadi and Bogoria samples have pH between 8.18 and 9.8. In the geothermal wells of Olkaria, pH values vary, ranging between 7.43 and 10.28, with most of the wells having pH above 9.

5.5.2 Geochemical geothermometers

The geothermometers make use of dissolved chemical substances in the surface water to estimate temperatures at depth. The water chemistry results were used to estimate the sub-surface temperatures. For the temperature calculation in Table 5.2 and Table 5.3, the geothermometers used are Quartz and cations (Na_K, Na-K-Ca, and Na-K-Ca-Mg).

From Table 5.3 it is noted that there is disagreement in the calculated temperatures from different solute geothermometers. Na/K (Arnórsson, 1983) gave the most pessimistic prediction, with subsurface temperatures ranging lower than or equal to the surface fluid temperature This is an indication of dilution by ground water as the mixing occurs. Hence, the Na/K geothermometers need substantiating with other geothermometers. Quartz (adiabatic), Quartz (conductive), K/Mg (Giggenbach, 1988) and Na – K – Ca gave more consistent readings whose values were averaged to indicate subsurface temperatures. Na/K geothermometers for Kipsegon, Narosura, Olchorro, and Majimoto are way too high to be realistic. This could be that their $\sqrt{M_{Ca}}/M_{Na}$ ratio is greater than 1, an indication of low subsurface temperatures. The same could be said for Eburru hot spring though this assumption is negated by the fact that Eburru reservoir is confirmed to be over 240°C. Hence, it is assumed that Eburru hot spring could be a fumarole cooled by underground water since its temperatures and discharge fluctuate with local precipitation.

It is noted that reservoir temperatures for the Kipsegon, Narosura, Majimoto, and Eliye springs were predicted to be below 100°C. With enthalpy values ≤417 kJ/kg, these four geothermal resources can be classified as low enthalpy. Homa Hills (represented by Abundu, Kakdhimu, and Bala hot springs), Mwananyamala, Lake Magadi, Lake Bogoria, Kijabe, Olchorro, Barrier (represented by Lake Logipi hot springs), and Namarunu geothermal prospects are predicted to have subsurface temperatures between 100 – 150°C. This affords them a subsurface enthalpy range of 417 >h ≤900 kJ/kg as medium enthalpy geothermal fields. However, Lake Bogoria and Barrier related hot springs are largely affected by percolating lake waters and the mixing may give an impression of lower reservoir temperatures (Cioni et al., 1992). Lake Baringo (Ol'Kokwe hot springs), Eburru, and Silali (represented by Kapedo hot springs) hot springs were classified as high enthalpy geothermal prospects with reservoir temperatures and enthalpy above 160 and 852 kJ/kg, respectively. Kapedo hot springs emanate at the bottom of western flanks of Silale/Silali caldera and are suspected to originate from Silali's geothermal reservoir (Dunkley et al., 1993). Eburru's reservoir temperatures have been confirmed through deep drilling to be 249°C and is already producing 2.4 Mwe from a single flash steam turbine.

.

Table 5.2 Total concentration of constituents for the geothermal brine and thermal springs in some of the manifestations in Kenya.

Sample Location (Hot springs)	Lab No.	Temp (°C)	pH	Li	Na	K	Ca	Mg	SiO_2	B	Cl	As	F	SO_4	HCO_3	del ^{18}O	del D
+Kipsegon	KG	33.5	6.58		17	7	8.7	1.71	42	0	2		1	9	73	-3.63	-15.8
+Mulot /Olchorro	ML	46.2	6.16		37	15	25.4	20.50	59	0	15		1	4	293	-4.35	-19.7
+Eburru	EB	49.3	8.18	0.01	71	16	0.7	4.86	107	0	50		1	10	61	-4.61	-26.0
+Narosura	NR	30	6.37		15	6	10.4	4.43	34	0	9		1	21	61	-5.09	-28.5
+Majimoto	MM	56.3	6.66		31	12	18.2	7.50	28	1	50		1	23	61	-5.33	-29.0
+Kakdhimu	KK	74.9	7.84	0.4	6980	54	1.2	91.20	85	7	1900	0.09		2052	12300	-3.48	-12.8
+Abundu	AU	79	8.45		7680	112	66	92.2	90	9.2	1290	0.05	128	1350	14052	-2.1	-11.9
+Bala	BL	72	8.36		7000	82		90.2	70	8.1	1710	0.35	100	1700	11964	-2.5	-12.5
+Mwananyamala (1)	MN1	58	7.18		2170	50.9	8.03	33.4	45	2.8	2503	0.02	58	2	700.5		
+Mwananyamala (2)	MN2	66	7.62	1.89	1428	50.6	128.6	13.6	54	1.9	1860	0.05	35	11	712.1		
+Mwananyamala (3)	MN3	63	7.53	1.94	1394	46	1.38	16.4	55	2.6	2045	0.04	17	8	670.6		
+Mwananyamala (4)	MN4	55	7.74	1.73	1975	56.5	4.48	18.6	49	3.4	2273	0.07	87	23	794		
+Lake Magadi (N)	MGN	44.5	8.8		9700	114	30	287.95	98	3	4828	0.02	112	242	14448	5	27
+Lake Magadi (S)	MGS	44	9.49		14620	144		345	77	0.92	7450	0.019	134	250	13908	11	18
+Masamukye	MY	42.8	7.52														
+ Lake Bogoria	LBG	96	8.95		1770	29	7.8	5.35	135		354	0.02	78	87.3	3372	5.7	29.7
+Kariandusi	KA	45	6.45													-4	-19.7
+Kijabe	KB	43	9.5		80	2.2	1.7	0.256	38		4.8	0	2.7	1.9	144	-4.1	-18.3
+Lake Baringo	LB	95	8.95	0.8	1030	51		0.7	155		276	0.01	20.6	67.9	1968	0.7	3
+Lake Elementaita	LE	44	9.24		1054	36		18.5	124	2.7	492	0.03	110	104	1248	-1.5	-2.1
*Lake Turkana	LT	71	9.45	0.01	621	19	5	2.4	45	0.65	426	0.05	10	40	1580	0.6	11
*Eliye springs	ES	35	8.9	0.01	113	3.5	1.45	0.25	41	0.05	18.4	0.069	2	11.8	302	-3.2	-13
*Logipi	LG	70	8.5		5500	96	0.5	19.9	125.8	5.55	4620	0.05	91	750	5360	2.2	15
*Namarunu	NR	66.2	8.8		5500	113	0.5	18.2	126		3200	0.023	140	814	5860	3.0	14
*Kapedo	KP	50	8.25	0.9	2180	134	3	1.25	245	2.9	890	0.9	28	199	4830	-0.2	-6

Table 5.3 Calculated geothermometers temperatures (ºC) for the geothermal waters from the fields investigated (Samples taken in 2021 and 2022).

Sample Name	Hot spring Temp (℃)	Quartz conductive	Quartz adiabatic	Na-K-Ca	Na/K Fournier 1979	Na/K Giggenbach 1988	Na/K Nieva & Nieva 1987	Na/K Arnorsson 1983	K/Mg Giggenbach 1986	Reservoir temp adopted (℃)
[+]Kipsegon	33.5	94	96	86	380	380	364	407	85	96
[+]Olchorro	46.2	110	109	96	374	375	358	398	100	110
[+]Eburru	49.3	183	170	317	451	440	433	510	172	183
[+]Narosura	30	85	88	77	380	379	364	406	80	85
[+]Majimoto	56.3	77	81	94	364	366	348	384	80	94
[+]Kakdhimu	74.9	128	125	82	15	36	6	-23	124	125
[+]Abundu	79	132	128	138	94	114	83	57	100	128
[+]Bala	72	118	117		83	104	73	46	110	118
[+]Mwanamanyala (1)	58	97	98	157	118	138	107	83	146	118
[+]Mwanamanyala (2)	66	106	106	148	142	161	130	109	140	145
[+]Mwanamanyala (3)	63	107	106	183	137	157	126	104	120	120
[+]Mwanamanyala (4)	55	101	102	171	129	149	118	95	140	149
[+]Lake Magadi (N)	44.5	136	132	138	83	105	73	46	130	138
[+]Lake Magadi (S)	44	123	121		76	97	66	38	110	120
[+]Masamukye	42.8									
[+] Lake Bogoria	96	155	147	138	99	120	89	63	145	145
[+]Kariandusi	45									
[+]Kijabe	43	90	92	94	139	158	127	105	100	140
[+]Lake Baringo	95	164	154		163	182	151	133	152	160
[+]Lake Elememtaita	44	150	143		139	159	128	106	150	150
[*]Lake Turkana	71	97	98	154	133	153	122	99	101	130
[*]Eliye springs	35	77	81	78	67	88	57	29	70	75
[*]Logipi	70	151	144	182	102	123	92	66	118	140
[*]Namarunu	66.2	151	144	191	111	131	100	75	124	140
[*]Kapedo	50	195	180	221	179	196	166	150	177	180

Key for Table 5.2 and Table 5.3.
The suffixes

- + denotes the samples collected during the field visit and data collection (new geothermal manifestations).
- *represents data sampled from literature; these samples do not include isotope analysis. It was one of the motivations to consider the isotopic analysis of new hot springs (already mapped in other studies, e.g., Tole (1992) and (2001).

.

5.5.3 Ternary and enthalpy plots

To understand the extend of reservoir fluid's boiling, fractionation process, equilibration and mixing of geothermal waters with groundwater, Na – K – Mg, Cl-SO_4–HCO_3, Li – Cl – B ternary diagrams are plotted, Figure 5.6 to Figure 5.10. Cooler inflows from shallow aquifers and hotter geothermal waters can mix in varying ratios to yield lower Na/k equilibrium temperatures relative to the measured ones.

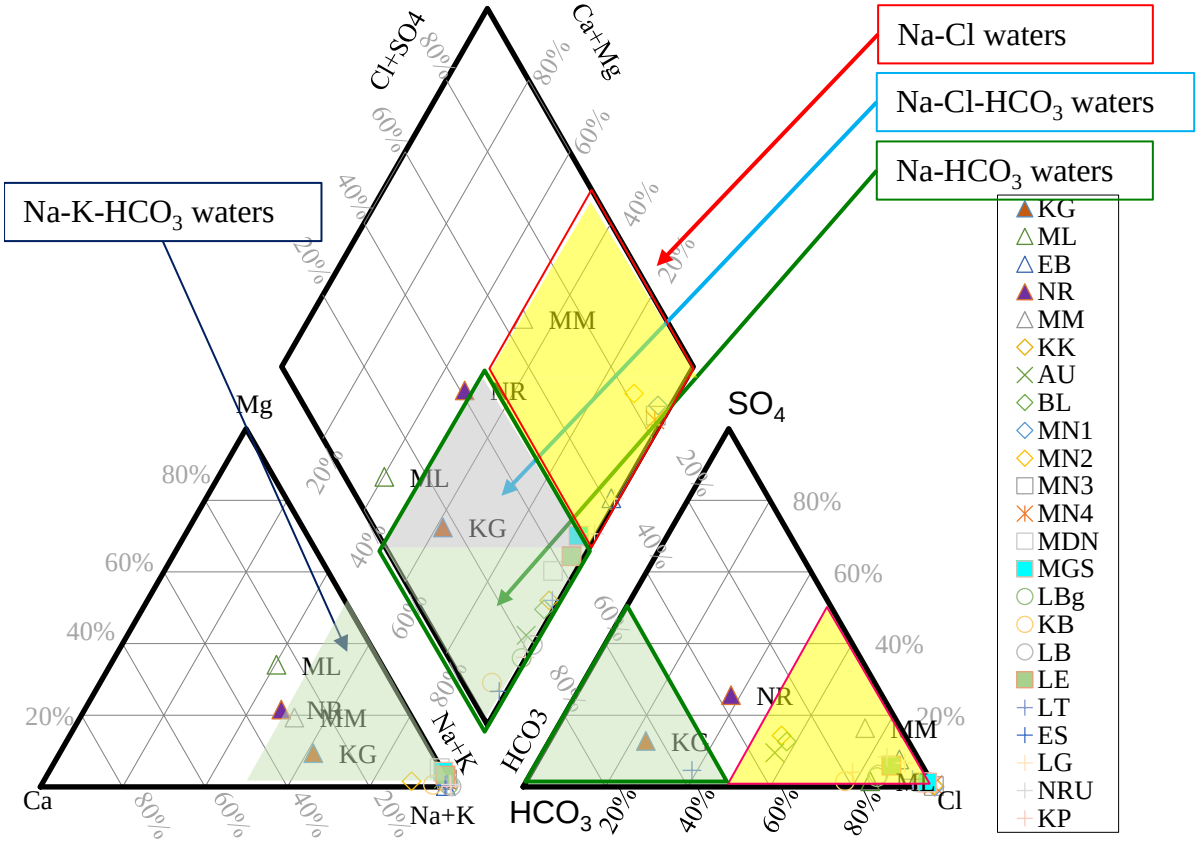

Figure 5.6 Piper plot for the hot springs showing their hydrochemical facies.

From Figure 5.6, it is noted that Olchorro (ML), Kipsegon (KG), Narosora (NR), and Majimoto (MM) plotted like typical neutral - diluted Na – Mg - HCO_3 and Na – Mg - Cl underground waters obtained from boreholes. This indicate that the hot spring water emanating from these hydrothermal systems mix with bigger ratios of underground water, hence the dilution of their solute concentrations. The rest of the hot springs plot on Na – Cl - HCO_3 zones typical of warm and hot spring waters.

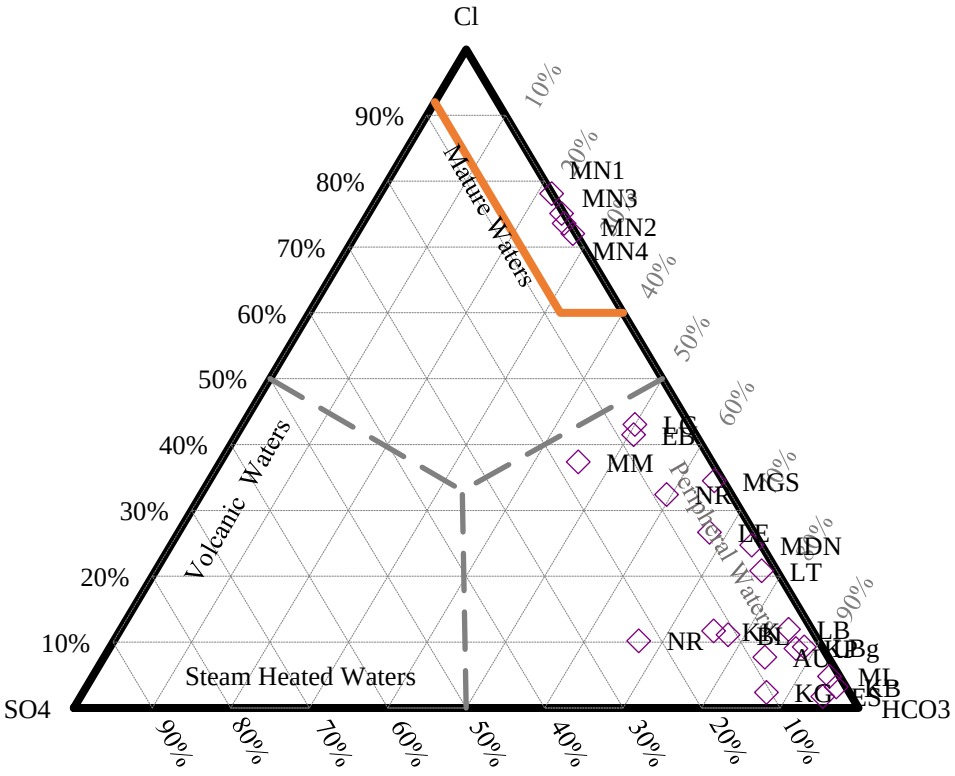

Figure 5.7 Cl - SO_4 – HCO_3 ternary plot (Giggenbach, 1988) showing the the noteworthy distinction of Mwananyamala hot springs from the rest. Mwananyamala plots as mature waters.

From Figure 5.7, it is noted that Mwananyamala hot springs plot close to the chloride apex as mature geothermal waters. Due to their low content of sulphate, they plot along the chloride - bicarbonate line, hence interpreted as emanating from a deeper hydrothermal system (I. Kanda, 2010). The saline hot springs from Lake Magadi, Lake Logipi, and Homa Hills plot on the higher zone of peripheral waters as an indication of their moderately deeper fluids being diluted by underground water. The argument that Lake Bogoria hot springs are shallow aquifers heated by steam from a deeper high enthalpy reservoir underground does not seem to hold since the waters from the geyser plot as peripheral bicarbonate waters due to their low sulphate concentrations (Cioni et al., 1992). The rest of the hot springs can be classified as Na – Cl – HCO_3 waters of varying concentrations of chloride mixed with groundwater.

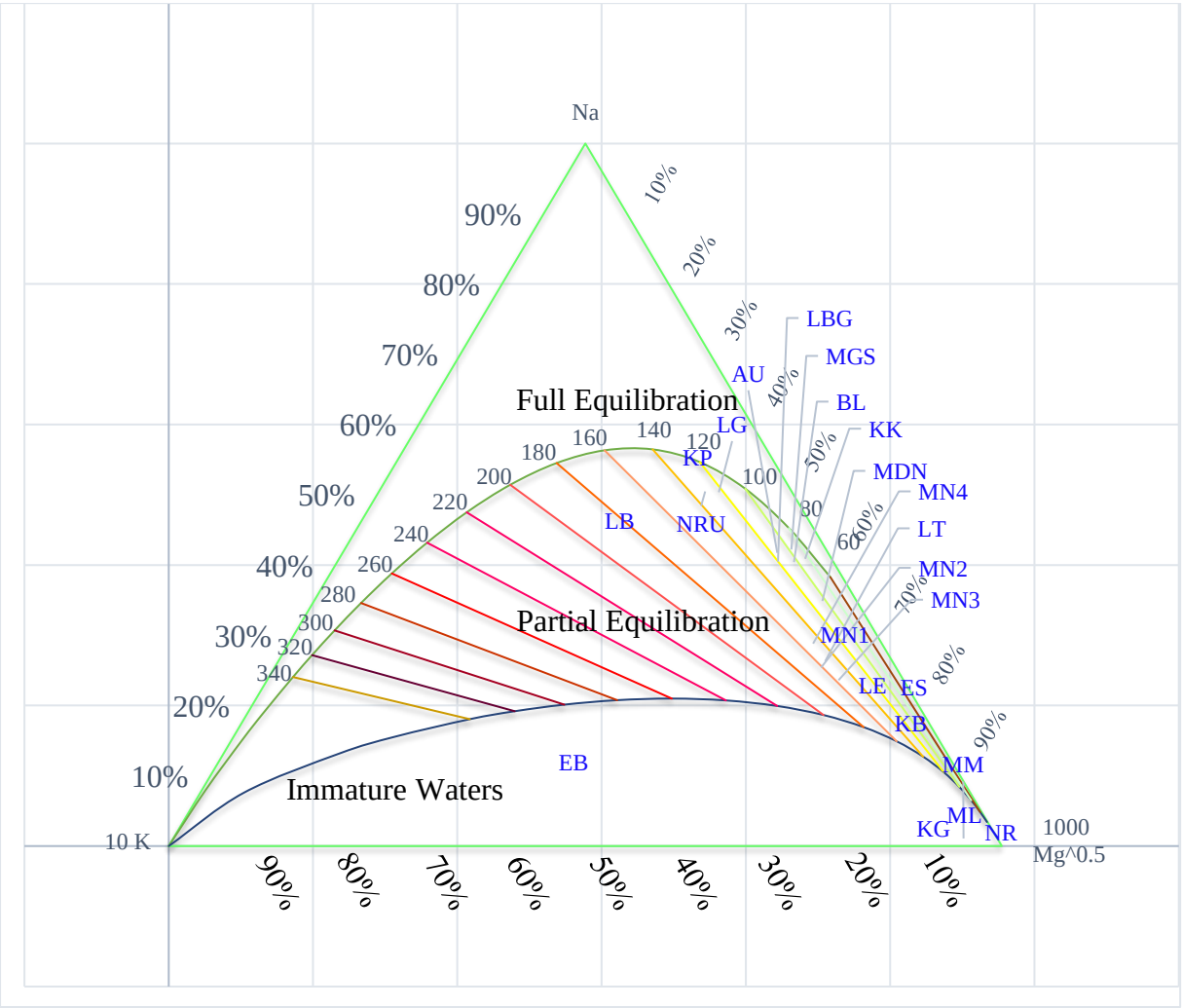

Figure 5.8 Comparative Na – K –Mg (Giggenbach ternary) plot for the hot spring geothermal waters to evaluate the extend of mixing and equilibtation.

The Na – K –Mg plot in Figure 5.8 indicate the extend of equilibration of the thermal waters with ascent to the surface. It is clear that Kipsegon, Olchorro, Narosura and Eburru hot springs are immature and non – equilibrated. The rest of hot springs are partially equilibrated with Kapedo, Lake Logipi, and Narosura being close to equilibrium.

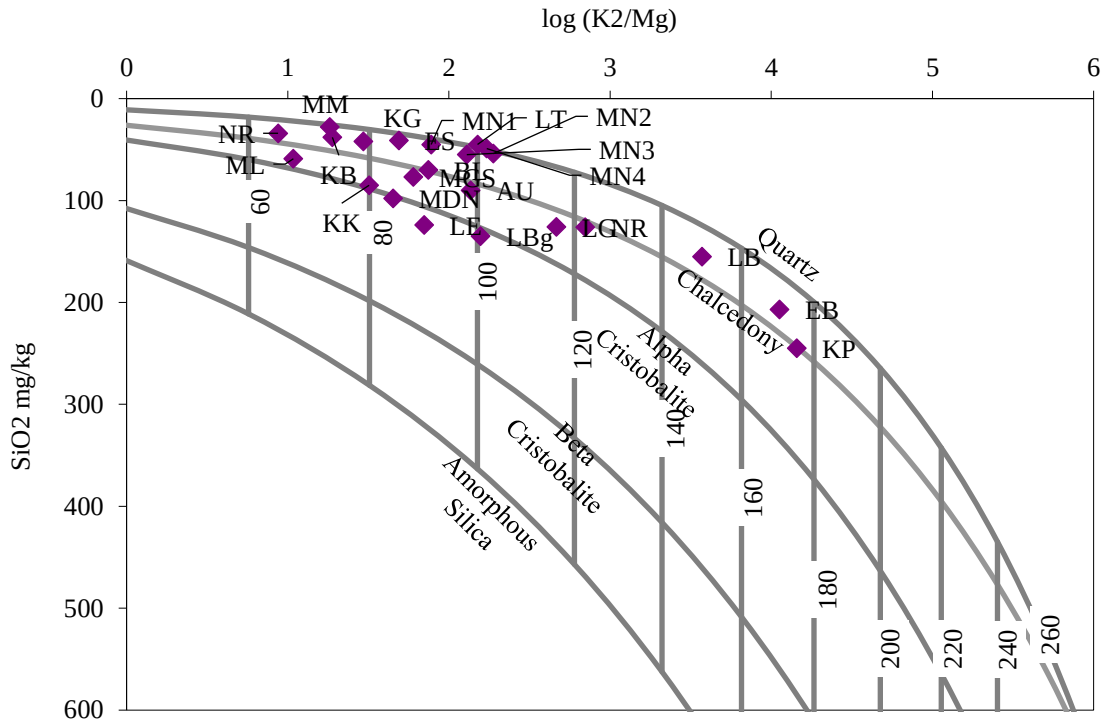

Figure 5.9 Plot of K^2/Mg versus silica geothermometer for the hot spring water samples.

Figure 5.9 shows the suitability of the water samples for the silica geothermometry analysis. Comparing the predictions of Figure 5.9 to Table 5.3 show a good correlation between the cation and silica geothermometers. For the samples to be valid for the test, they have to plot between quartz and amorphous silica solubility lines.

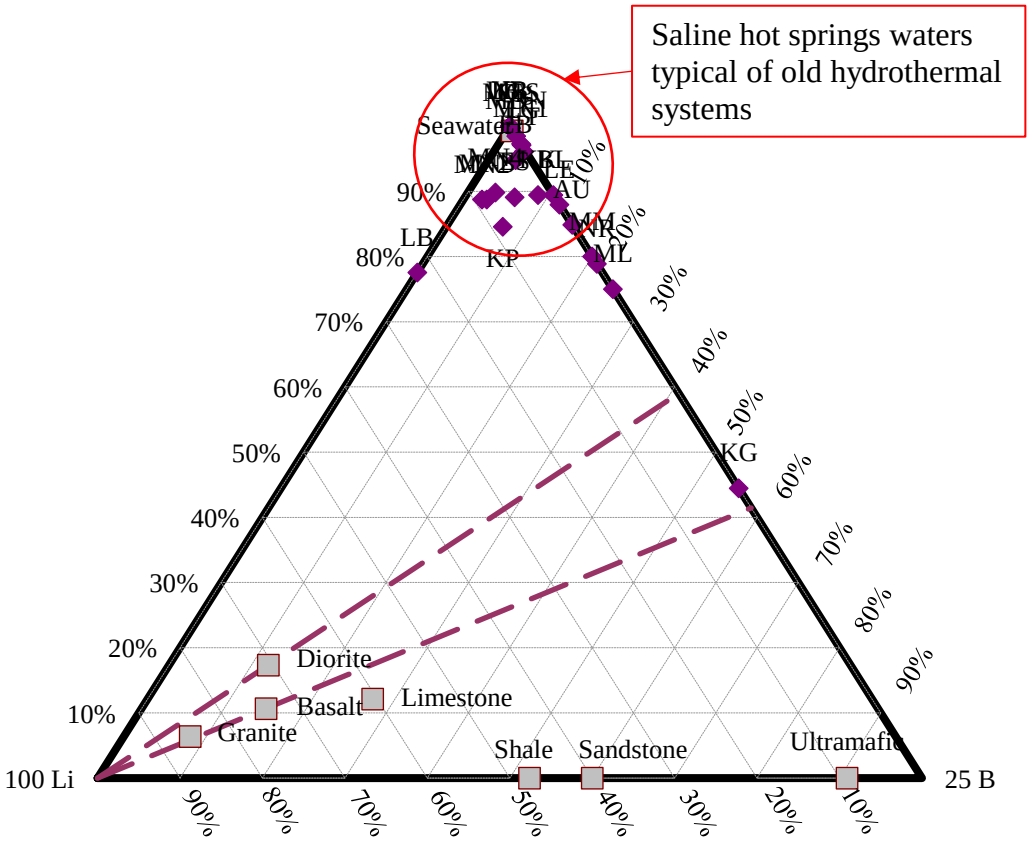

Figure 5.10 Relative Li – Cl – B ternal diagrams for the hot spring waters for distinguishing the mixing and boiling extends of the resevoir fluids.

Figure 5.10 shows that Kapedo and Lake Bogoria hot spring waters are partially equilibrated though the former emanate from a relatively younger hydrothermal system. The rest plot as emanating from older hydrothermal systems and contain minerals that have not attained equilibrium.

5.5.4 O and H stable isotope analysis

Figure 5.11 show that most Kenyan rift lakes, boreholes, hot springs and deep geothermal wells plot along the Kenya Rift Valley Mean Water Line (KRVMWL) with slight differences either brought about by evaporation and reservoir temperatures. All the lakes are enriched with respect to $\partial^{18}O$ and $\partial^{2}H$, especially Lake Bogoria, Lake Turkana and Lake Victoria (Homa Bay) due to high levels of evaporation and the long distances the inflowing rivers travel. Samples from Olkaria, Eburru and Menengai geothermal fields plot along the KRVMWL though the Wells from Olkaria Domes and Olkaria Northeast fields plot closer to the Lakes Naivasha Nakuru and Elementaita. This could imply that in addition to these reservoirs receiving meteoric water, they also have incursion of lake waters. However, it cannot be ignored that isotopic signatures of Olkaria field (East, West and Domes) are quite diverse, implicating different fluid sources, reservoir temperatures and residence time for water rock interactions (Mutonga, 2015; Sekento, 2012). The Lake Elementaita, Lake Bogoria and Ol'Kokwe (Lake Baringo) hot springs plot closer to their respective lakes as an indication of incursion of lake water, though Ol' Kokwe hot springs receive a bigger portion of lake water. The Kariandusi, Narosura, and Majimoto receive meteoric water that is mainly percolating rain. Eburru hot spring plotted on GMWL while Eburru geothermal well (EW-01) plotted on

KRVMWL, indicating their different water sources. Olchorro, Kijabe, Kipsegon and Homa Hills hot springs water plotted on CARL as an indication of their meteoric sources being less affected by the Kenyan rift lakes. It is also interesting to note that despite Homa Hills geothermal reservoir being very close to Lake Victoria, its water plot further from Rift Valley lakes indicating a smaller proportion of lake water recharging the reservoir. However, $\partial^{18}O$ and $\partial^{2}H$of Lake Magadi north and its hot springs have closer resemblance and plot on the KRVMWL. It has long been suspected that Lake Naivasha's water outflow underground to the south, hence rising as hot springs that recharge Lake Magadi north after being heated at Suswa volcano. In a dramatic contrast, the hot springs recharging Lake Magadi south deviate slightly from the KRVMWL, as they have a negative shift with respect to $\partial^{18}O$ and $\partial^{2}H$, implying a different meteoric source. These waters undergo a more accelerated evaporation that enriches the Lake Magadi south with respect to $\partial^{18}O$ and $\partial^{2}H$ to levels greater than any other Kenyan lake. Kapedo hot springs have a varied $\partial^{18}O$ and $\partial^{2}H$ signatures, since some plot on the KRVMWL and the others slightly to the left. The ones which plot on the KRVMWL are suspected to have some contribution from Lake Baringo's subsurface outflow while the others originate from infiltrating rain water on the edges of the Kenya Rift Valley (Darling et al., 1996; Dunkley et al., 1993). Lake Elementaita hot springs were less depleted in isotopes, with a slight shift towards higher $\partial^{18}O$, compared to the Lake Elementaita waters and plotted along the GMWL. This implies their origin is fundamentally meteoric with increased residence time for the rock-water interactions (Montcoudiol et al., 2019). Although both Lake Nakuru and Menengai geothermal wells plotted along KRVMWL with slight deviations, disagreements exist as to whether Lake Nakuru's subsurface outflow contributes to the recharge of Menengai's hydrothermal system (Kanda and Suwai, 2013; Montcoudiol et al., 2019). Menengai geothermal well MW-20A plots intimately with Lake Nakuru isotope signatures. In conclusion, all Kenyan hydrothermal systems plotted on the meteoric line KRVMWL with the exception of Lake Magadi south. Lake Naivasha and Lake Baringo have the greatest effect on various hydrothermal systems within the Kenyan rift valley due to their subsurface outflows in the northerly and/or southerly directions.

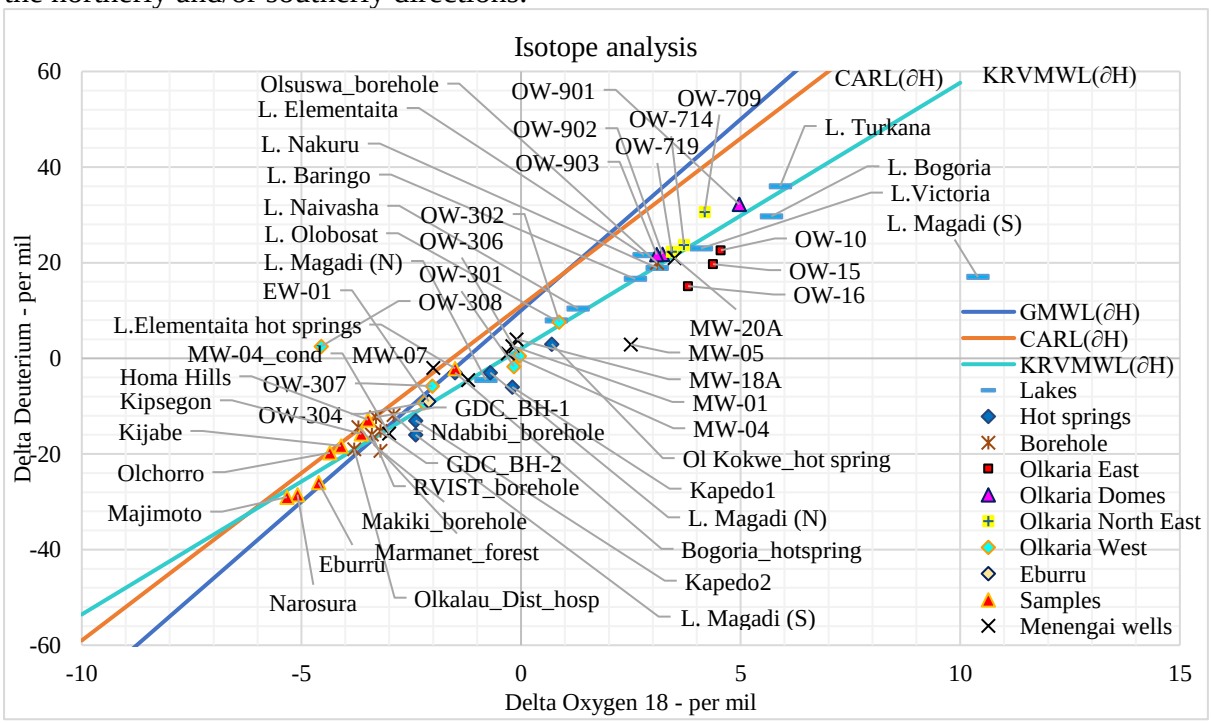

Figure 5.11 $\delta^{18}O$ - $\delta^{2}H$, per mil with respect to Standard Mean Ocean Water (SMOW), plot shows the isotopic composition of hot spring samples. The samples were collected during the field study in 2019 - 2022. (GMWL): Global Mean Water Line. (KRVMWL): Kenya Rift

Valley Mean Water Line. (CARL): Continental African Rain Line. The lakes, borehole (BH), Menengai wells, Olkaria wells and other hot springs data were modified from Darling et al. (1996), Montcoudiol et al. (2019), Mutonga (2015), and Sekento (2012). OW-308 show dilution of thermal waters by highlands (high altitude >1800 m ASL) rainwater. Micro-gravity studies on the field show that cold recharge from north of Olkaria field is directed toward the Olkaria West field (OW-308).

MW-05 show positive ∂^{18} O shift typical of rock-water interactions with longer residence time. This region is mostly recharged by non-thermal ground water. MW-05 and MW-05A are both cold wells drilled at the southeast of Menengai caldera. The wells could be deriving water from cold, heavy, and deep groundwater or metamorphic waters. The magmatic waters plot quite far from MW-05 and their contribution could be assumed to be zero or very minimal.

5.6 Reclassification of Kenyan geothermal resources

Kenya has four high enthalpy geothermal fields with steam producing wells: Eburru, Olkaria, Menengai and Paka. Olkaria is currently producing 863 MWe and Eburru 2.4 MWe. Plans are underway to connect Menengai and Paka to the national grid in the near future. Geological and geochemical characterization of Kenyan geothermal resources has been going on for more than five decades to date (Allen et al., 1989; Clarke et al., 1990; Dunkley et al., 1993; Mibei et al., 2021). This reclassification, represented in Table 5.4, builds on this foundation of previous and current studies, filling in the gaps left by updating the current state of geothermal exploration and measuring the flowrates of hot springs in order to estimate their potential to support direct use. Hot springs, fumaroles and hot altered grounds were

Table 5.4 Reclassification of undeveloped Kenyan High, Medium and Low enthalpy geothermal resources according to geology, geochemistry and the Australian Geothermal Energy Group's Geothermal Lexicon and Canadian Geothermal Code for Public Reporting of geothermal energy resources (AGRCC, 2008). The data was based on field surveys and literature (Dunkley et al., 1993; Igunza and Kanda, 2011; Lagat et al., 2010; Tole, 1988; Tole, 1992: WestJec and JICA, 2017)

No.	Resource	Max surface temperature hot spring / [Fumarole] / (Hot ground) (°C)	Recent trachytic activity (ka) yrs BP	Hot spring (t/h)	Geothermometry estimate of the reservoir (°C) [From this study]	Geothermometry estimate of the reservoir (°C) [From Literature]	Estimated Reservoir capacity MWe	Surveys	Thermal heat from hot springs MWt	Geothermal recovery assessment
1	Silali	51.9/[96.8]/(95.6)	4±2	3600	150-221	260-330	800	Geochemistry, MT, Gravity, TEM	42.0	Measured resource
2	Namarunu	97.1/[100]/(60.3)	3	3000	100-190	250-300	200	Geochemistry	105.0	Measured resource
3	Suswa	[96]	800-0.2			190-310	700	Geochemistry, MT, TEM,		Measured resource
4	Longonot	[96]	200-0.2			200-350	500	Geochemistry, MT, TEM		Measured resource
5	Korosi	[97.3]/(97.4)	104±2			190-200	200	Geochemistry, MT, TEM, Gravity, Exploration wells		Probable reserve
6	Barrier	79.9/[93.3]/(97.7)	58±4	167	120-180	190-320	500	Geochemistry, MT, TEM, Gravity	3.9	Measured resource
7	Mwananyamala	66.5	5000±100	324	100-150	100-160	-	Geochemistry	7.6	Inferred resource
8	Emuruangogolak	69.7/[95.6]/(73.3)	0.1	18.9		310-350	300	Geochemistry	0.4	Indicated resource
9	Bogoria	208±3	104±2	500	120-155	140-180	DU	Geochemistry	17.5	Indicated resource
10	Baringo	95.1/[97.2]/(71.4)	300±20	35	150-181	180-220	200	Geochemistry, Gravity, MT, TEM	0.6	Measured resource

11	Lake Turkana	45		5-15		240-250	200	Geochemistry	0.2	Indicated resource
12	Homa Hills	79	650±10	68	110-140	142-179		Geochemistry, Gravity, MT	0.8	Indicated resource
13	Arus	90/[96]	3	7.9		100-220	100	Geochemistry, Gravity, MT, TEM, Productive borehole	0.2	Probable reserve
14	Elementaita	44/[96]	1000±50	46.25	125-160	-	100	Geochemistry, MT,	0.5	Indicated resource
15	Chepchuk	[96.1]/(88.2)	1130			200-260	70	Geochemistry, MT, TEM, Gravity		Indicated resource
16	Lake Magadi (N)	86	1100 Ma	2500	120-140		-	Geochemistry	58.3	Inferred resource
17	Lake Magadi (S)	44	1100 Ma	2800	80-120		-	Geochemistry	32.7	Inferred resource
18	Narosura	30	1100 Ma	180	80-100	60-80	-	Geochemistry		Inferred resource
19	Majimoto	56.3	1100 Ma	25	85-120	100-110	-	Geochemistry	0.8	Inferred resource
20	Masamukye	42.8	500 Ma	13.76		50-70	-	Geochemistry	0.2	Inferred resource
21	Olchorro	46.2	1100 Ma	21	10-120	-	-	Geochemistry	0.4	Inferred resource
22	Kijabe	44	1100 Ma	5.06	90-150	120-140	-	Geochemistry	0.1	Inferred resource
23	Kariandusi	45	2200	208			-	Geochemistry	3.6	Inferred resource
24	Kipsegon	33.5	1100 Ma	3.1	85-120		-	Geochemistry	0.048	Inferred resource
25	Kuro Bisan Owo	34	800 Ma	0.75		70-110	-	Geochemistry	0.012	Inferred resource

ignored by the previous studies because they have no capacity to generate electricity despite their huge contributions to the direct use sector. From this research, some of the geothermal resources have hot springs with high volumes of warm water (40-60°C) ranging from 1 – 3600 tonne/hour. Using Equation (5.4, the heat recoverable from these hot springs was calculated and summed up to about 200 - 300 MWt. This heat is crucial for various direct use scenarios such as bathing/swimming, aquacultural pond heating and domestic use.

$$\text{Heat} = \frac{\dot{m} \times C_w \times (T_{Av} - 30)}{3.6 \times 1000} \quad \text{MWt}, \tag{5.4}$$

Where $\dot{m}$ is hot water discharge in tonnes/hour, C_w is the specific heat capacity for water between 30 to 60°C (kJ/Kg/°C), and T_{Av} is the hot spring water temperatures in°C. The 30°C was used as the lower side of heat exchange since areas northern and southern Kenyan rift valley experience average temperatures of 25 to 30°C.

The resources were also reclassified according to the Australian Geothermal Energy Group's Geothermal Lexicon and Canadian Geothermal Code for Public Reporting of geothermal energy resources, which helps to systematize reporting of resources based on their different stages of exploration and development (AGRCC, 2008). The differences between the measured and indicated resources were based on the former having magneto telluric (MT) and transient electromagnetics (TEM) surveys which enable a more accurate estimate of recoverable heat. Probable reserve were the measured resources with exploration well. Korosi and Arus were classified as probable resources since both have exploration wells indicating high subsurface temperatures, though Korosi wells produced no steam while the Arus borehole produced steam. Using the data from Table 5.3 and Table 5.4, the resources were reclassified based on exergy according to Lee (2001), Figure 5.12, in order to review whether they fall into high, medium or low enthalpy geothermal resource categories. Unlike previous studies which classified Homa Hills and Mwananyamala as low enthalpy resources (Igunza and Kanda, 2011; Tole, 1988), these resources plot in the medium enthalpy zone closer to the most stable liquid dominated Takigami geothermal field of Japan (Jalilinasrabady et al., 2021). Olchorro, Kipsegon, Narosura, Kijabe, Majimoto, and Lake Magadi south were the only ones plotted as low enthalpy. Lake Bogoria and Lake Baringo were also suspected to be low enthalpy yet plotted as strong medium enthalpy resources. Paka and Korosi which were considered high enthalpy (Mwawasi, 2012), plotted in the medium enthalpy zone.

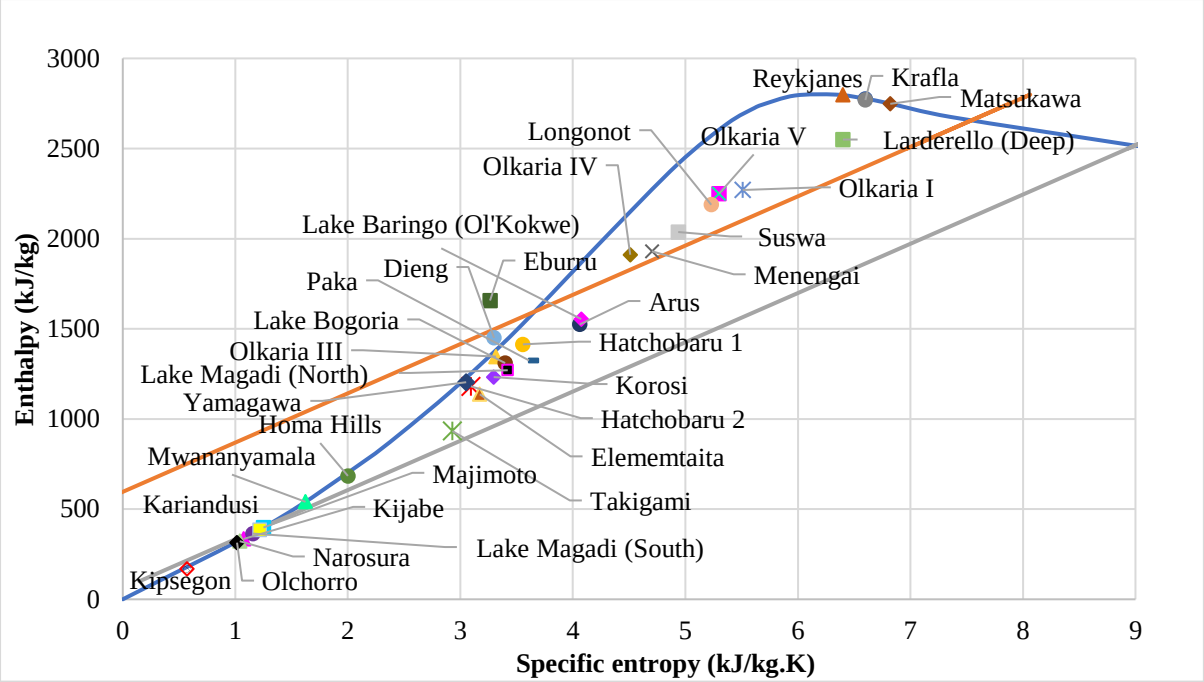

Figure 5.12 Exergetic reclassification of Kenyan geothermal resources.

5.7 Selection of the best direct use scenarios by MCDM analysis of medium and low enthalpy geothermal resources with hot spring in central and southern Kenyan Rift Valley

Currently, there are no studies focusing on characterization of undeveloped medium to low enthalpy geothermal resources with neither productive shallow nor deep geothermal wells. “Productive wells” is conservatively used to denote wells producing hot water above 25°C. This chapter takes advantage of hot springs in these geothermal resources to select their best direct use scenarios. Previous studies only used temperatures to suggest uses for hot springs (Tole, 2002;Roe et al., 2015). The conventional use of hydrogeochemistry is for estimating subsurface temperatures through geothermometers and estimating the source of hydrothermal water via $\partial^{18}O$ and $\partial^{2}H$ isotopes analysis (Tole, 1992; Zhanxue et al., 2010). The optimal use scenarios for hot springs are determined by this study's use of their temperature, flow rates, locations, and concentrations of harmful compounds including fluoride, arsenic, and boron, as well as their salinity levels (Cl concentrations). The best use scenarios being analyzed are domestic use (including drinking), spa/swimming/bathing, aquacultural pond heating and geotourism. To combine these different incommensurate criteria, the multi-criteria decision making (MCDM) methods are used in geospatial information system (GIS) to give a visual synergistic result. This method is superior for selecting both the best direct use locations and the optimal uses for each geothermal resource.

5.7.1 Study area

Kenya shares the East African Rift (EAR) system with Djibouti, Ethiopia, Tanzania, and Uganda. The volcanic activity in this region owes its origin to crustal extension, where the African continent is gradually splitting into two tectonic plates: the Somali plate to the East and the Nubian Plate to the west (Biggs et al., 2021). EAR system is a complex 50 to 90 km wide graben composed of plateaus, domes and step faults of varying magnitude. The volcanism in Kenyan and the greater East African Rift is widely estimated to evolve sequentially, beginning at the Miocene epoch to the recent, less than 300 years, the eruption from satellite-vent flows on Suswa volcano (Johnson, 1969). The erupted mafic and felsic materials are

mainly of alkaline type ranging from trachyte-basalt to nephelinites and phonolites (King and Chapman, 1972). The study area encompasses the main north–south Kenyan Rift Valley and its western branch that terminates into Lake Victoria. This area extends 325 km east to west and 300 km north to south, as shown in Figure 5.13. This area is known as the Kenyan Dome, which hosts caldera volcanoes such as Suswa, Longonot and Menengai and dormant volcanic complexes such as Olkaria, Elementaita and Eburru (Maithya et al., 2020).

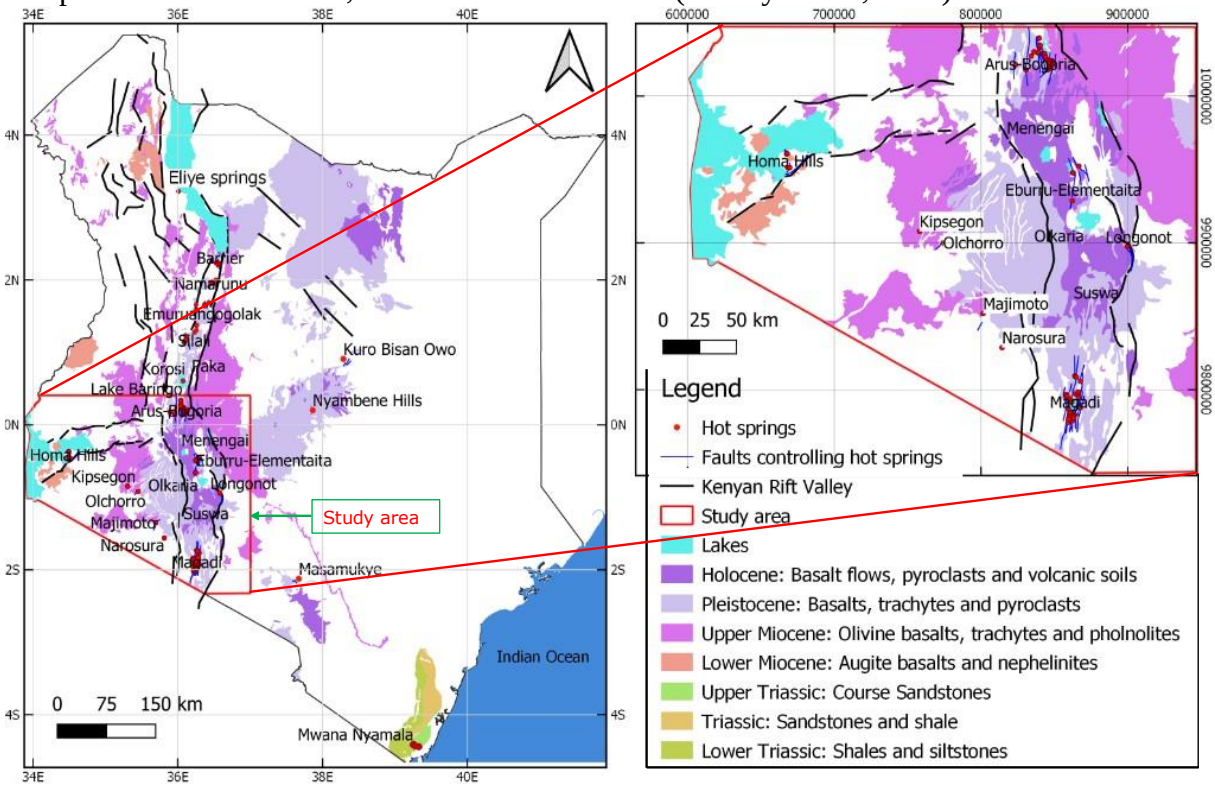

Figure 5.13 Maps of locations of hot springs in Kenya and of the surface geology and structures controlling their hydrothermal systems within the study area (Modified from geological map of Kenya, Ministry of Energy).

From Figure 5.13, the geothermal resources within the Kenyan Rift Valley are controlled by trachytic structures of the Pleistocene to Holocene era, while those out of the valley originate from structures of the Lower to Upper Miocene era. These trachytic eras could have a significant implication on the hydrothermal heat source, though they do not have a linear relationship to the hot springs temperatures of flow rates.

5.7.2 Optimal direct use of hot springs and criteria map layers

Hot springs in the study area had fluid temperatures and flow rates ranging from 30 – 96°C and 0.75 – 208 t/h, respectively. Lindal's diagram, in Figure 1.5, lists direct uses for such temperature ranges as aquacultural pond heating, spa/swimming/bathing, milk pasteurization, space heating/greenhouse warming, and fish drying. However, these uses are fundamentally dependent on the location of the hot spring, its flow rates and the local economic activities such as horticultural farming, fishing, and tourism, to name a few. One everyday use of hot springs and fumaroles in Kenya, though not listed in Lindal's diagram, is the provision of clean water for domestic use (drinking and washing). Hot springs are used for domestic purposes in areas with sparse fresh surface water and deep water-tables (>200 m). The everyday community uses of hot springs, their temperatures, flow rates, and concentrations of fluoride, arsenic, boron and chloride were settled on while selecting the four best uses for analysis: domestic use, spa/swimming/bathing, aquacultural pond heating and geotourism. The GIS-MCDM based

analysis considered several criteria to evaluate the four direct uses as summarized in the Figure 5.14.

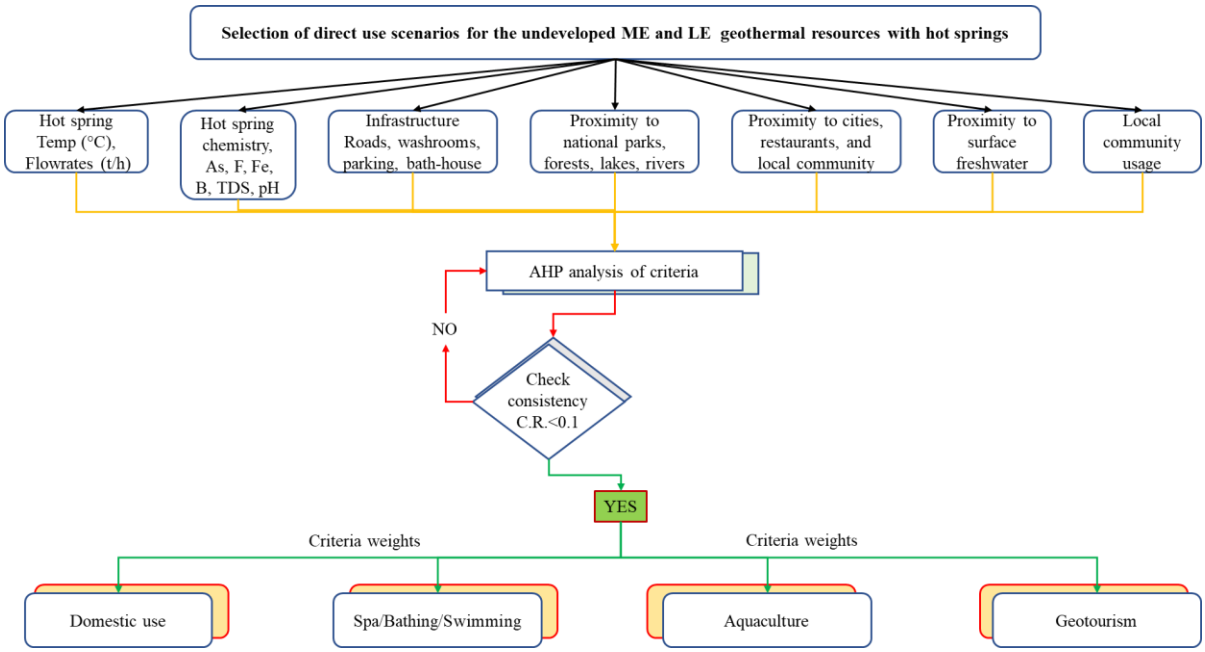

Figure 5.14 GIS-based MCDM analysis of hot springs for best direct use scenarios.

The criteria were hot spring parameters whereas the analytical hierarchy process (AHP) method was used to generate weights assigned to the criteria during selection of the best diret use scenarios for each geothermal resource with a hot spring.
A total of 12 criteria was used in selection analysis. Six from hot spring parameters: temperatures, flow rates and concentrations of arsenic (As), boron (B), fluoride (F), chloride (Cl). And the rest from economic factors: proximity to roads, national parks, lakes, cities, lodges/restaurants and the number of visitors to the hot springs annually. The hot springs temperatures and flow rates represent the heat accessible to the surface while high concentrations of the toxic As, B, and F pose a threat to human consumption. Table 5.5 shows the maximum allowable limits of harmful substances in drinking water. This research used these values to select the best hot springs for drinking and aquacultural uses.

Table 5.5 Limits for harmful elements in geothermal fluid (World Health Organization, 1996).

Drinking water parameters	**pH**	**Mn**	**Ca**	**Mg**	**H_2S**	**F**	**Zn**	**B**	**Fe**	**As**	**Total dissolved substances (TDS)**
Concentrations (ppm)	6.5-8.5	0.05	200	50	10	1.5	1.5	2.4	1.0	0.01	500

The hydrogeochemical data for the hot springs was obtained from laboratory analysis of water samples collected from field surveys of the geothermal resources and some from the literature. The economic data, such as proximity to the roads, cities, national parks, and lakes, was obtained from Google Satellite maps and the Kenyan Ministry of Wildlife and Forestry (Waweru et al., 2021). The number of the visitors to the hot springs were collected during the field surveys.

5.7.2.1 Generation of criteria map layers

The primary step was to represent the hot spring parametric data and economic factors in a GIS platform to understand the objective visually. At this stage, the six parameters of the

hot spring: temperature, flow rates, and concentrations of arsenic, boron, fluoride, and chloride in grams per kilogram of hot spring water were represented in point data format, colour coded in five ranges as shown in Figure 5.15. Similarly, the economic parameters relevant to the direct use of hot spring water, such as the number of visitors to the hot spring, roads, fresh surface water, cities, national parks, and lodges, were represented in as a mixture of point, line and polygon data.

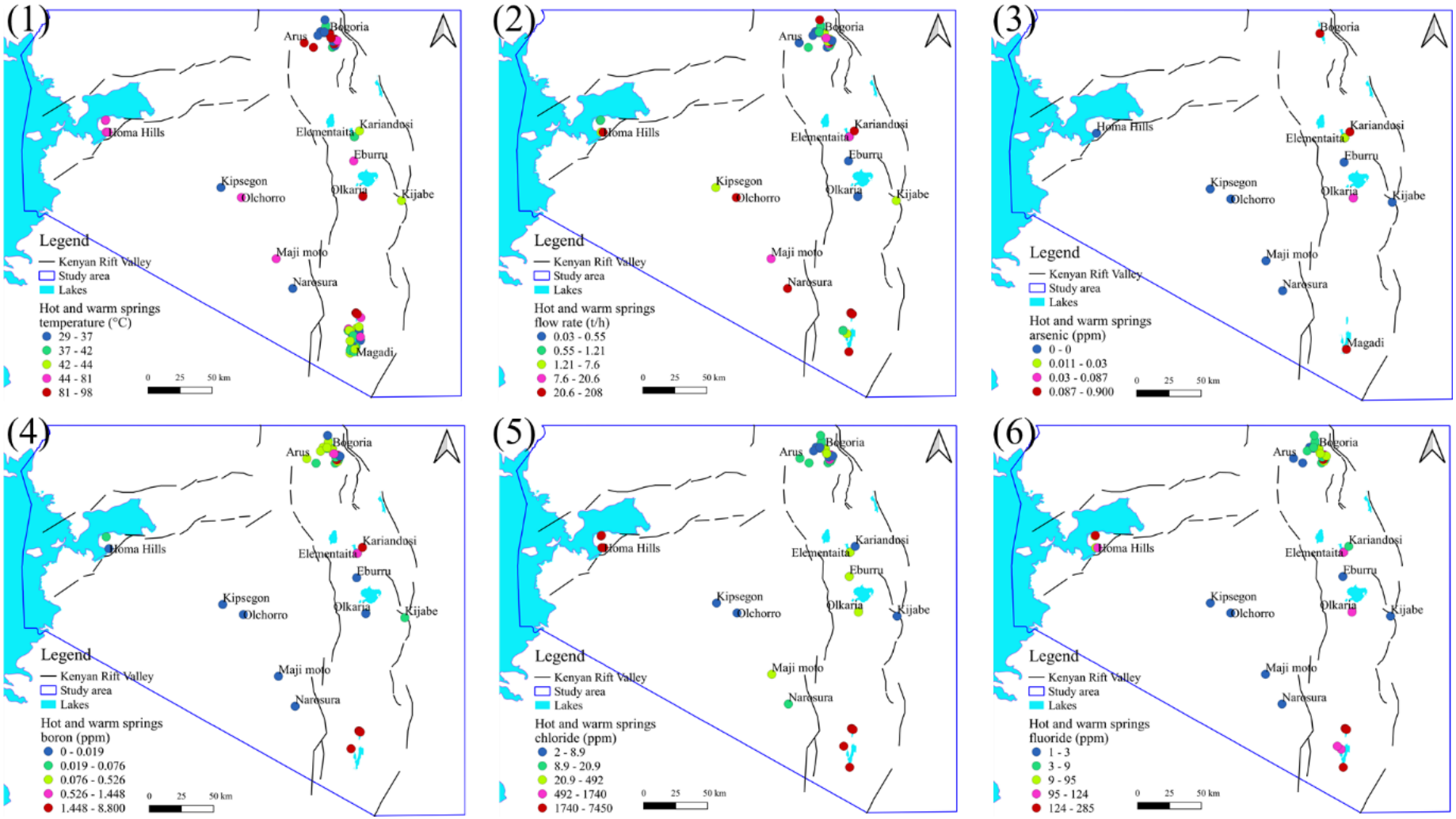

Figure 5.15 Point data representation of hot spring parameters: (1) temperature (°C), (2) flow rates (t/h), (3) concentration of arsenic in mg per kg or litre of hot spring water (ppm), (4) concentration of boron (ppm), (5) concentration of chloride (ppm), and (6) concentration of fluoride (ppm).

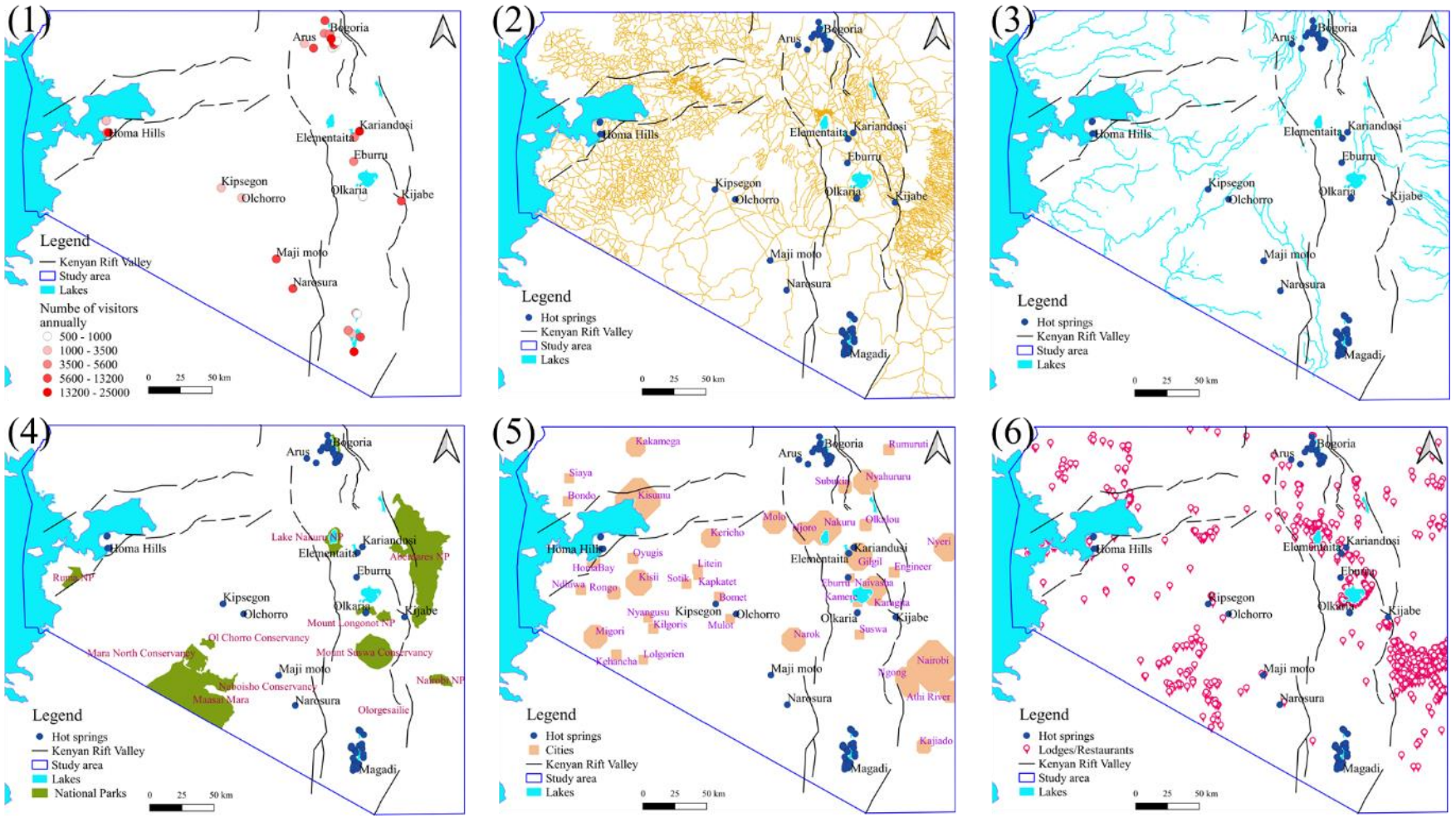

Figure 5.16 Economic data related to direct use of hot spring waters: (1) number of visitors to the hot spring annually, (2) distribution of tarmac roads, (3) distribution of freshwater rivers and and lakes (please note Lakes Nakuru, Magadi, and Bogoria are saline endorheic lakes), (4) distribution of national parks, (5) locations of major cities and minor urban towns, and (6) distribution of lodges/restaurants for providing accommodation or food to visitors and travellers.

5.7.2.1.1 Description of criteria map layers

From the hot spring parametric data shown in Figure 5.15, (1) hot spring temperatures were the crucial factor in their classification since springs' temperatures $\leq 25\,°C$ were considered cold and of no value to heating purposes. Springs with a temperature range of 25 - 45°C were considered warm, while those with temperatures $\geq 45°C$ hot. Figure 5.15 shows that the distribution of warm and hot springs had no trend, though hot springs with temperatures $\geq 80°C$ were situated within the Kenyan Rift Valley at Lakes Bogoria, Olkaria and northern Lake Magadi. These geothermal resources are associated with the trachytic activity of the Pleistocene to the Holocene era, as shown in Figure 5.13. (2) Flow rates of hot springs in terms of m^3/h or t/h were of significant importance to the study since they represented the quantity of subsurface heat reaching the surface via the spring. The spring flow rates failed to show a pattern because of two main reasons: (a) most warm/hot springs are a coalescence of seepages whose flow rate is difficult to measure individually, and the flow rates measurement are the total of several seepages despite their temperature and chemical concentration differences, (b) most sub-aqueous warm/hot springs at Lakes Magadi, Elementaita, Bogoria and Baringo are difficult to measure under the lake surface. Nonetheless, a significant number of hot springs occurring as bubbling pools and seepages with large flow rates were able to be measured. In summary, the sub-aerial hot springs with a flow rates of $\geq 20\,t/h$ were Olchorro, Narosura, Kariandusi, Lake Bogoria spa, and Bala (Homa Hills). The sub-aqueous hot springs with significant flow were found at Lake Magadi (north), Lake Bogoria and Lake Baringo (not within the study area). (3) Concentrations of inorganic arsenic in hot spring waters were of concern due to arsenic's acute toxicity to humans. In ground and hot spring waters, inorganic arsenic is found as arsenite (+3) or arsenate (+5) form depending on oxidation degree of the water and occur at elevated levels of above 0.002 ppm in water that have interacted with volcanic rocks (WHO, 2022). Arsenic has been found to be carcinogenic in addition to causing a myriad of health issues (WHO, 2003). Geothermal resources with unsafe concentrations of arsenic were Olkaria, Kariandusi, Lake Magadi and Lake Bogoria. (4) Boron in the form of borates and borosilicates is found in groundwater and hot spring waters with deep subsurface circulation and long residence time for water-rock interactions (Karingithi and Wambugu, 2008). Boron toxicity inflicts the male reproductive system causing lesions and kidney tumours (WHO, 2022). Hot springs with unsafe concentrations of boron were found to be within Kenyan Rift Valley: Lake Magadi, Lake Bogoria and Kariandusi hot springs. (5) Chloride does not pose health issues to humans and animals. However, chloride concentrations above 250 ppm give rise to a detectable salty taste in water. Salinity also poses accelerated rusting to steel pipes and tanks. Hot springs with high salinity were found at Lake Magadi, Lake Bogoria and Homa Hills geothermal resources. (6) Fluoride in the groundwater and hot spring waters in the Kenyan Rift Valley is associated with weathered rhyolite, dolerite, fluorite, and granitic rocks (Arusei, 1991). Consumption of water with fluoride ranging from 0.9 – 1.2 ppm may give rise to mild dental fluorosis, while elevated concentrations of 3 - 6 ppm may cause skeletal fluorosis (WHO, 2022). From Figure 5.15, only a few hot springs had fluoride concentrations below 1.0 ppm: Olchorro, Kipsegon, Majimoto, Narosura, and Eburru.

The economic data is mapped in Figure 5.16 in points, lines and polygons vector format. The economic factors support the characteristics of the hot springs, making them simple to get to and use. (1) The number of visitors was crucial in establishing the hot springs' popularity. The hot springs of Lake Bogoria were the most visited by over 30,000 – 50,000 visitors annually. The spectacular Chemurkeu and Loburu geysers at Lake Bogoria are among Africa's active geysers. In addition, Lake Bogoria is surrounded by Lake Bogoria National Park and has been designated Ramsar Site since 2003. It acts as one of several lakes habited by millions of Lesser Flamingoes in Kenya. Kariandusi, Lake Elementaita, and Bala hot springs also receive a

significant number of domestic tourists and locals, >10000 annually, for geotourism and bathing. The Lake Bogoria Spa resort is also popular with visitors, and some of the water from a nearby warm spring at 33°C is channeled to the swimming pool for visitors to the hotel. (2 Proximity to passable roads, either tarmac or corrugated, helps visitors access the hot springs. Nearly all hot springs in the study area are located 500 m to 3 km off tarmac roads and are difficult to access during rainy seasons. They also lack car parks, gas filling stations and washroom facilities. Accessing most of the subaerial hot springs in the study area requires a four-wheel drive offroad vehicle. The sub-aqueous hot springs need a boat. From Figure 5.16, the comparatively easily accessible hot springs were those located on the western bank of Lake Bogoria. (3) Proximity to fresh surface water is crucial for human settlement. Over 50% of the world's population lives within 3 km of fresh surface water (Kummu et al., 2011). However, some locations are farther from fresh surface water within the study area and have deeper water tables >200 m. Such places use hot spring water for domestic purposes, such as drinking and washing. Hence this criteria map layer was used to compare the proximity of hot springs to fresh surface water in analyzing their suitability for domestic use. (4) Proximity to national parks has a supportive effect on the number of visitors visiting hot springs for sightseeing. It is common for tourists to bundle their tours together, and hot springs closer to national parks are marketed jointly by tour travel companies. (5) Hot springs near urban areas pool a significant number of their visitors from nearby towns or cities. Most visitors to the Kijabe hot spring come from Kijabe Town, while visitors to Lake Elementaita and Kariandusi hot springs come from Gilgil town. Hot springs farther from urban areas receive fewer visitors, such as Lake Magadi, Majimoto, Narosura and those at northern Homa Hills. (6) Hotels and hot springs operate in a symbiotic relationship (Jiho and Yukio, 2009; Yen et al., 2018). Visitors enjoy hot spring water, food and accommodation in combination or one after another. The hot springs with no restaurants/lodges closeby receive fewer visitors, as evidenced at Lake Magadi and Arus region. Some economic activities helping utilization of hot springs are more site-specific; nonetheless, the ones mentioned above were an excellent representation of the study area.

5.7.2.1.2 Rasterization and normalization of criteria map layers

The GIS platform cannot manipulate the hot spring data because it is supplied in vector point format. In order to rasterize this data, interpolation is required to cover a number of pixels that can be recalculated in the GIS platform (addition, subtraction, multiplication, and division). The interpolation used in this study is the ordinary kriging method since the parameters of the hot springs do not seem to have trends, except at Lake Magadi, where the hot springs in the southern parts have low temperatures and more concentrated substances. The hot springs parameters were interpolated for a 5 km radius buffer since the local community travels to a maximum of 5 km to access the hot springs. Besides, the local community at Kijabe and Kariandusi pipes hot springs water using 2 - 5 inch in diameter PVC pipes for distances of about 3 – 5 km. The interpolated data was cross validated by the measured data, and curve fitting was adjusted to prediction errors below 5.0%. Four classifications of the low, medium, high, and very high colours were assigned to the normalized interpolated point data after it had been rasterized at a $50\ m\ \times\ 50\ m$ pixel size, using the natural breaks Jenkins method (discrete interpolation), as shown in Figure 5.17. The low class for hot spring temperature represents <40°C, while for arsenic, boron, chloride, and fluoride, it represents the values below the WHO allowable limits for human consumption, shown in Table 5.5 Zero represents the lowest, while one represents the maximum value for each normalized criteria map layer. The normalization was carried out as explained in the methodology chapter based on Equations (3.14 and (3.15.
The economic factors contributing to the successful direct use of hot springs, such as the distribution of roads, and restaurants/lodges, were represented as spatial lines and polygons data, as in Figure 5.16 As such, this data is still unmanipulable and needs rasterization. The

roads and rivers were converted into polygon data by assigning them a 1 km buffer. One kilometer accessibility distance for clean water and transportation systems is considered the minimum for the rural community (Kummu et al., 2011; Litman, 2022). The resulting rasters were analyzed for proximity and normalized with maximum criteria values. The normalized criteria map layers were similarly classified into four main discrete classes ranging from zero to one value: low, medium, high and very high, as shown in Figure 5.18. The maximum distance for proximity analysis (for the local community) was arbitrarily fixed at 10.0 km, although both domestic and foreign tourists go farther to tour the locations of their attractions.

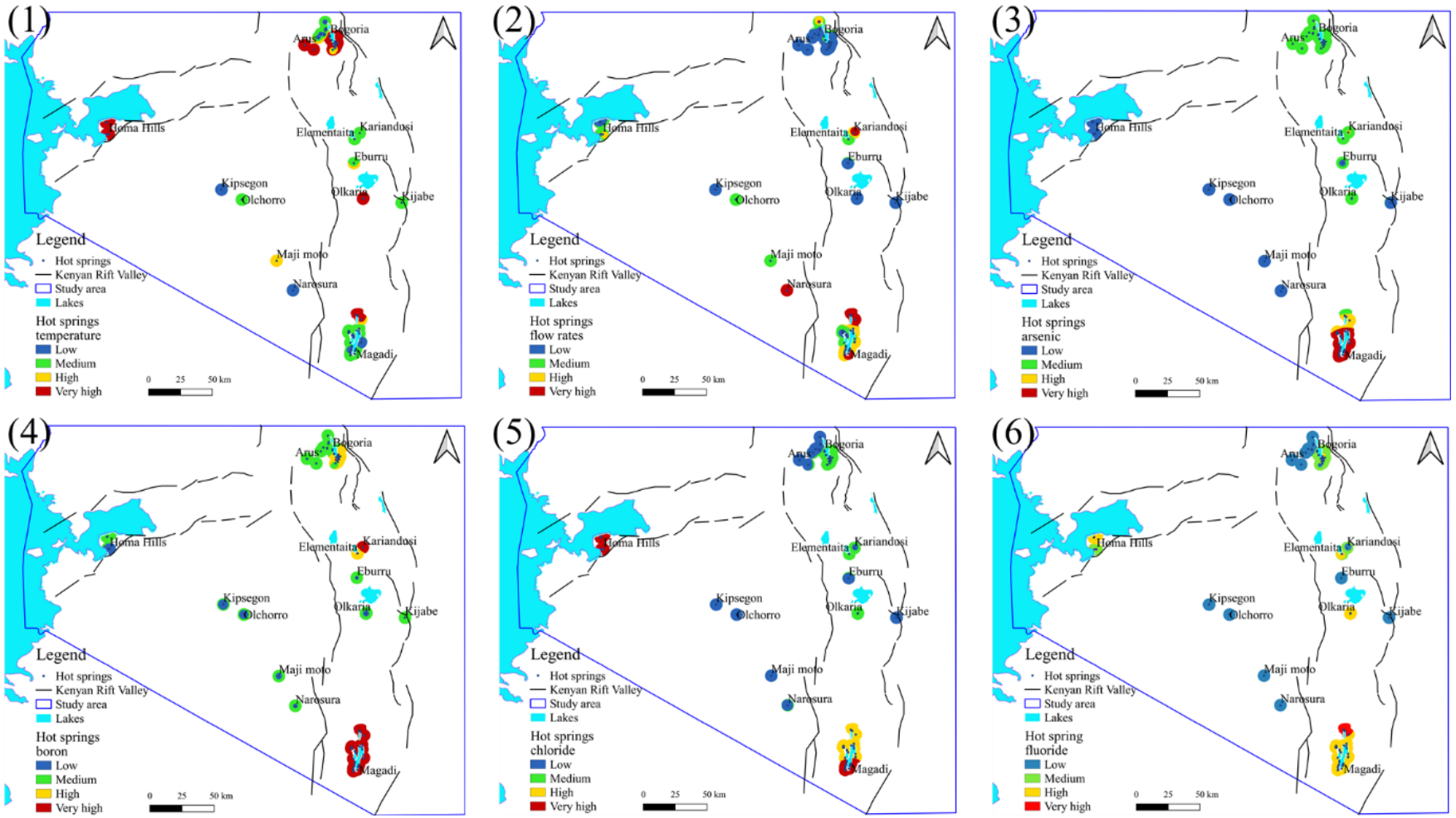

Figure 5.17 Normalized interpolated point data of hot spring parameters: (1) temperature, (2) flow rates, (3) concentration of arsenic, (4) concentration of boron, (5) concentration of boron, and (6) concentration of fluoride. The low class for hot spring temperature represent <40°C, while for arsenic, boron, chloride, and fluoride, it represents the values below the WHO allowable limits for human consumption shown in Table 5.5.

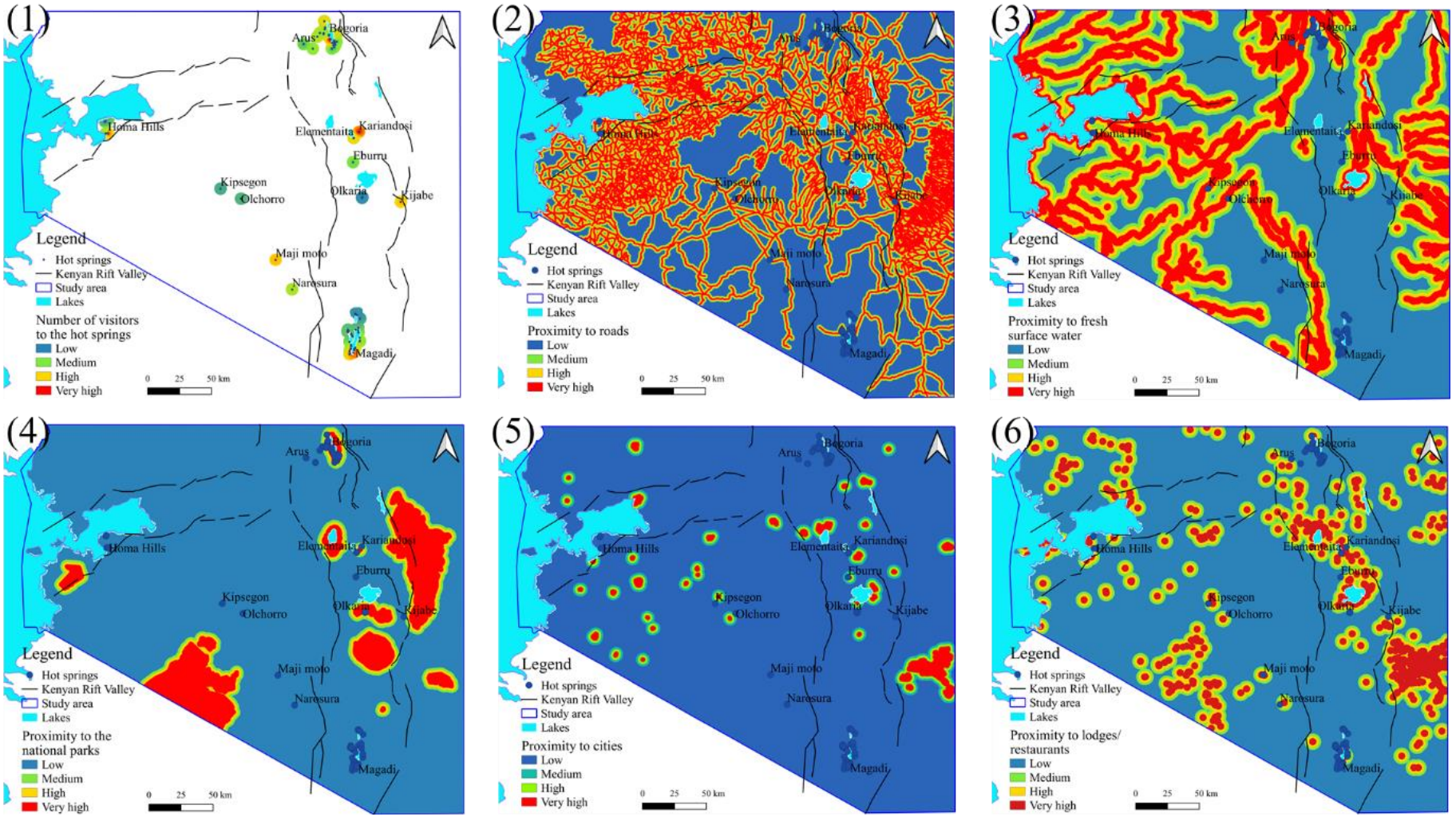

Figure 5.18 Normalized interpolated and proximity maps of economic data related to direct use of hot spring waters: (1) number of visitors to the hot spring annually (generated by ordinary kriging interpolation), (2) distribution of tarmac roads, (3) distribution of freshwater rivers and lakes, (4) distribution of national parks, (5) locations of major cities and minor urban towns, and (6) distribution of lodges/restaurants.

5.7.2.2 Synthesis of best direct use scenario map layers

All the twelve hots spring parameters and economic factors were rasterized into pixels of 50 m by 50 m size and normalized with values ranging from zero to one. Because the pixels' values ranged from 0 to 1, QGIS could overlay these initially incommensurate criteria to produce appropriate maps. The best direct use scenario maps were produced by overlay analysis in Quantum Geographic Information System (QGIS) software, an open-source platform involving addition, division, subtraction, and multiplication of different map layers. Nevertheless, since each criteria map layer does not hold equal weight to the direct use scenarios, meticulous weight assigning is crucial before overlay analysis. This study used the analytical hierarchy process (AHP) to weight criteria map layers. The integrity of criteria map layers were judged by reducing the consistency index (C.I.) close to zero (Saaty and Kearns, 1985). In this study, the Solver add-in in the Excel module of the Microsoft Office was used to minimize C.I. as much as possible by varying the pairwise comparison judgements assigned to the pairwise comparison matrix.

5.7.2.2.1 Best direct use scenario: domestic use of hot spring water

This study aimed to determine which hot springs are acceptable for human consumption and why the local community uses them for drinking and other domestic purposes like washing dishes and clothes. This study found that there were four main reasons local community uses hot springs for domestic purposes: (1) lack of fresh surface water sources such as rivers, cold springs, and lakes, (2) deeper water tables which make subsurface aquifers expensive to access, (3) shallower geothermal upflow zones which make boreholes gush steam and/or hot water (encountered at south of Longonot, Badlands, Suswa and Arus areas), (4) warm hot spring water makes for comfortable washing. For this purpose, the criteria map layers best fitted for this direct use scenario were chosen as proximity to fresh surface water, flow rates of hot springs, and concentrations of harmful substances such as arsenic, boron, fluoride, and chloride.

The criteria map layers were weighted using analytical hierarchy process (AHP) as shown in Table 5.6. Table 5.6 shows that more weight was given to the concentrations of harmful elements arsenic (As), boron (B), fluoride (F) and chloride in hot spring waters. The maximum limits were judged from world health organization (WHO) published data, shown in Table 5.5. The criteria map layer weights were accepted after agreeing with a consistency index values of below 0.1 as stipulated by Saaty (1980).

Table 5.6 Pairwise comparison for criteria map layers constituting domestic use of hot springs and their respective weights and consistency index (CI).

AHP pairwise comparisons							
	Arsenic	Boron	Fluoride	Surface freshwater	Chloride	Flowrates	Criteria weights
Arsenic	1	3.0	2.0	4.0	5.0	5.0	0.388
Boron	0.33	1	1.0	2.0	2.0	2.0	0.164
Fluoride	0.5	1	1	2.0	3.0	2.0	0.188
Surface freshwater	0.25	0.5	0.5	1	2.0	2.0	0.113
Chloride	0.2	0.5	0.33	0.5	1	1	0.071
Flowrates	0.2	0.5	0.5	0.5	1	1	0.076
					Consistency Index (CI)		0.0236

After assigning them with criteria weights, the normalized map layers were overlayed as shown in Figure 5.19 to produce suitability map for domestic use of hot spring water shown in xx (1).

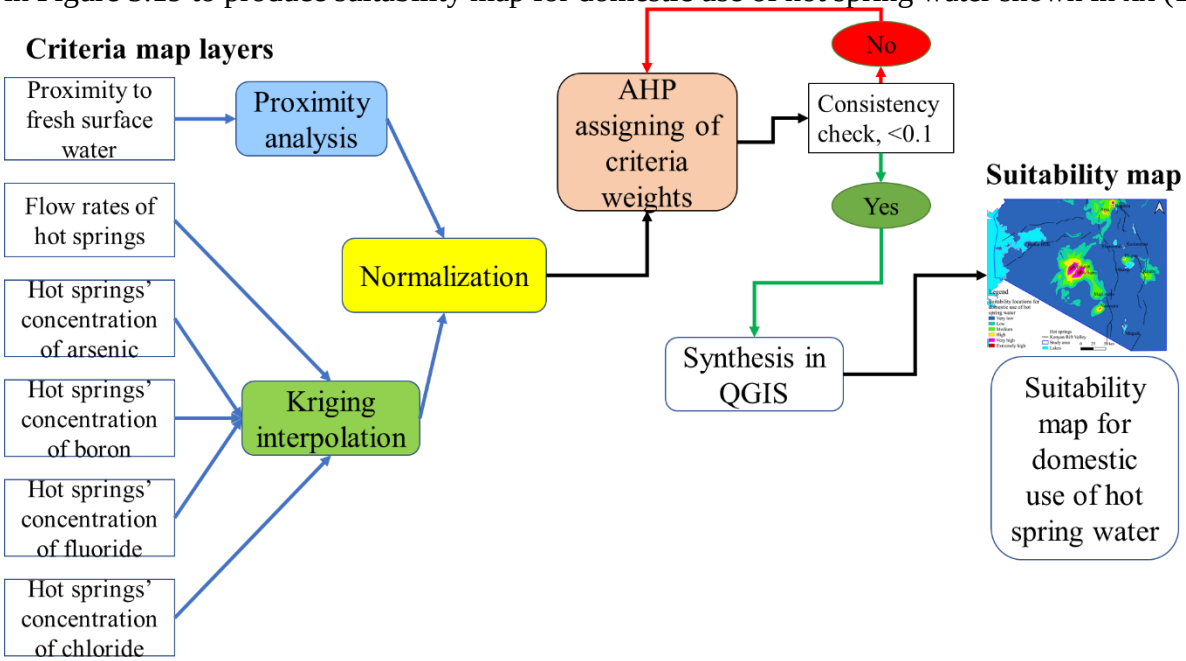

Figure 5.19 AHP-QGIS synyhesis process for suitability map of domestic use of hot spring water.

5.7.2.2.2 Best direct use scenario: commercial use of hot spring water for spa/bathing/swimming pools

The use of hot spring water for spas, bathing and in swimming pools is the most common use of hot springs worldwide (Erfurt, 2021). Figure 5.20 shows how hot springs are re-modified to suit bathing purposes. Except for the hot springs in northern Lake Magadi and those at Lake Bogoria, the rest are used for bathing by locals. However, this use is not commercial since the hot springs are in their natural state and lack bathing facilities. Some have little flow rates and are already harnessed for domestic water or located in remote areas with no infrastructure to support commercial use. The goal was to evaluate which hot springs could sustain a commercial swimming pool/bathing house based on their temperatures, flow rates, and proximity to passable roads, roads, and lodges/restaurants.

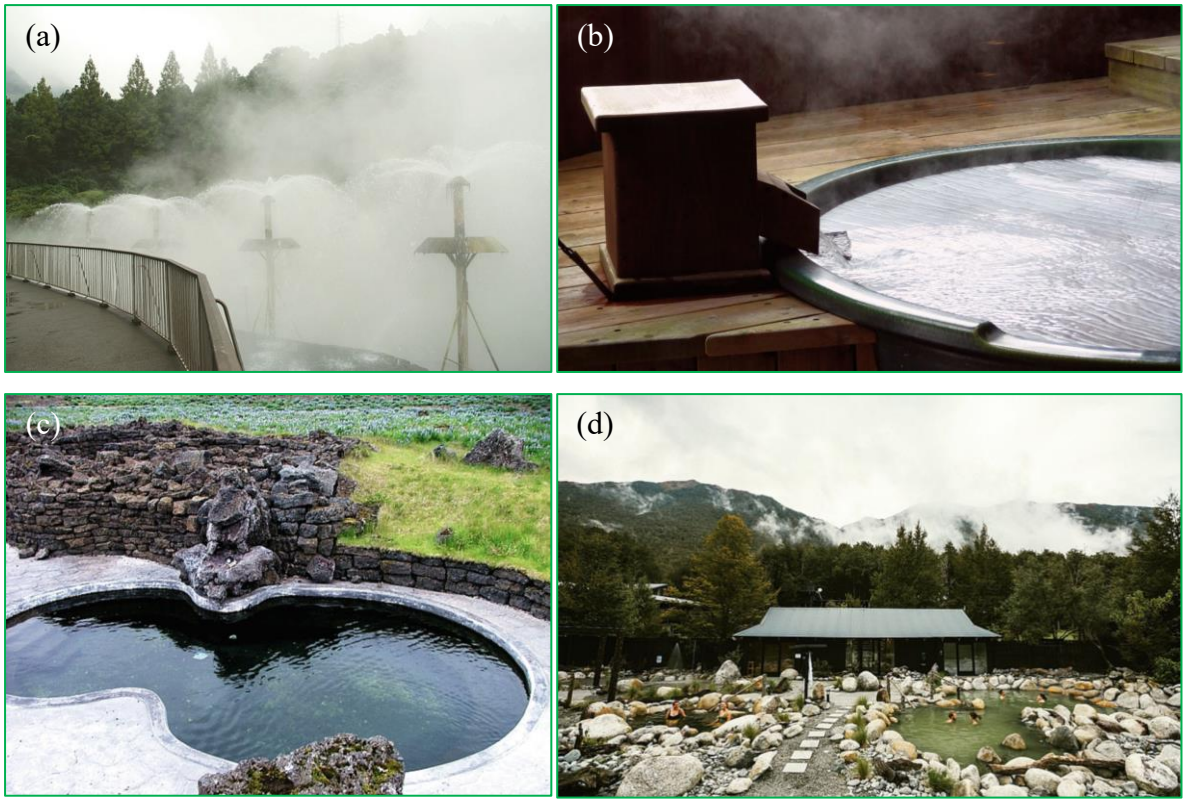

Figure 5.20 (a) A barricated hot spring water spray and (b) a hot spring bath house in Japan. Remodelled pools in Iceland (c) and New Zealand (d) (Erfurt, 2021).

The criteria map layers were weighted as shown in Table 5.7 and overlayed in QGIS as shown in Figure 5.21 to produce a suitability map for commercial use of hot springs for spas or bathing within the study area.

Table 5.7 Pairwise comparison for criteria map layers for commercial use of hot springs water in spas, bathing houses, and swimming pools and their respective weights and consistency index (CI).

Pairwise comparisons						
	Temperature	Flowrates	Proximity to the roads	Proximity to the cities	Proximity to lodges/ restaurants	Criteria weights
Temperature	1.0	1.0	3.0	3.0	3.0	0.328
Flowrates	1.0	1.0	3.0	3.0	3.0	0.328
Proximity to the roads	0.3	0.3	1.0	2.0	2.0	0.149
Proximity to the cities	0.3	0.3	0.5	1.0	1.0	0.097
Proximity to lodges/restaurants	0.3	0.3	0.5	1.0	1.0	0.097
				Consistency Index (CI)		0.0343

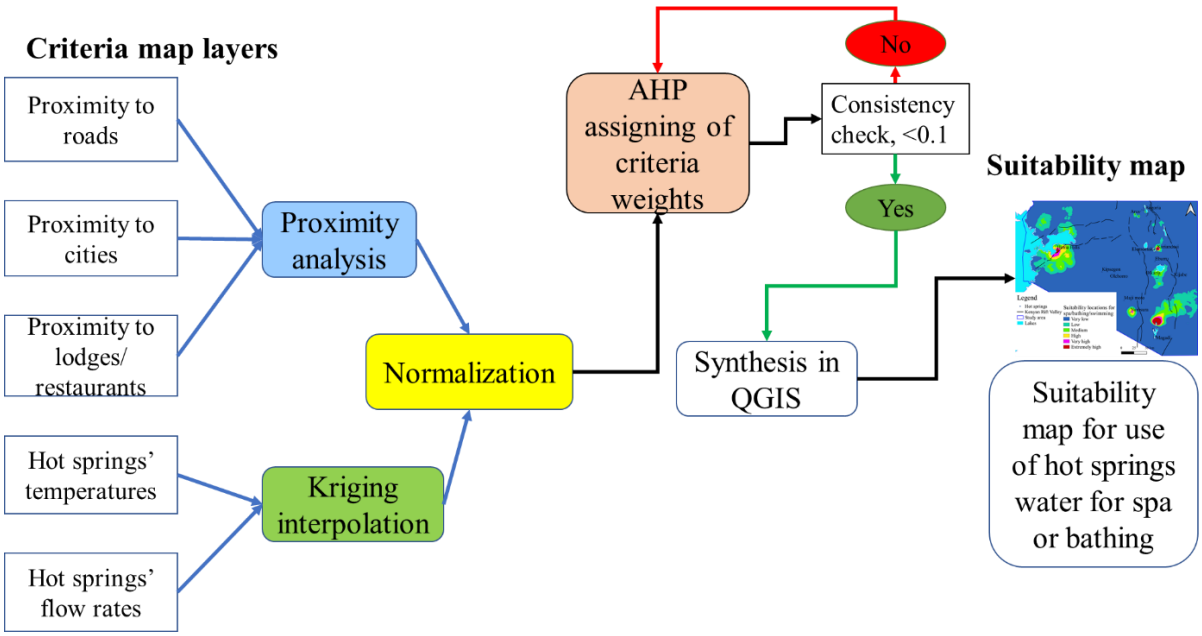

Figure 5.21 AHP-QGIS synyhesis process for suitability map for commercial use of hot spring water in spas, bathing houses and in swimming pools

5.7.2.2.3 Best direct use scenario: commercial use of hot spring water for aquacultural pond heating

Kenyan wild catch resources have been declining over time due to overfishing and deteriorating fish ecosystems at Lake Naivasha, Lake Victoria, Lake Turkana and Lake Baringo. The consequence is annual domestic fish production of 100,000 metric tonnes (MT) against a demand of 700,000 MT (Ngethe, 2021). The deficit is expected to be farmed through aquaculture. Conventionally in Kenya, Nile Tilapia and African Catfish are cultured in fishponds with or without lining and supplied with water at ambient temperatures. So far, aquaculture has only been able to produce up to 25,000 MT annually, leaving a huge deficit to be covered by the importation of fish. Unfortunately, the highland parts of Kenya, elevations ranging from 1000 – 3500 m above sea level, experience temperatures below 25°C at night and much lower temperatures in June and July, which prolong the time required to culture tilapia fish to >500 grams to 12 months. For the aquaculture of tilapia fish to be profitable, the fish culture period must be optimized to 6 – 9 months. This optimization is only possible when fishponds are maintained at 25 – 30°C during the fish-growing period through pond heating. Geothermal fluids from wells and hot springs have been used successfully to culture fish for ages (Ioka and Wakasa, 2021; Land O'Lakes, 2013).

This study sought to characterize the available hot springs for aquacultural pond heating. Similarly, to the domestic use of hot spring water, the concentrations of harmful substances in water, such as arsenic, boron, and fluoride, were vital in selecting the most suitable hot springs. The through-flowing ponds are self-cleaning, so the hot spring flow rates must sustain flow above 1.0 m^3/h. Besides, proximity to roads and cities is beneficial for the quick transportation of fish to the markets in the nearby cities.

The criteria map layers: hot spring temperatures and flow rates, concentration of arsenic, boron, fluoride in mg per liter of hot spring water, and proximity of hot springs to roads and cities, were weighted as shown in Table 5.8 and overlayed in QGIS as shown in Figure 5.22 to produce a suitability map for commercial use of hot springs for aquacultural pond heating within the study area.

Table 5.8 Pairwise comparison for criteria map layers for commercial use of hot springs water for aquacultural pond heating and their respective weights and consistency index (CI).

Pairwise comparisons								
	Temperature	Arsenic	Boron	Flowrates	Fluoride	Proximity to the roads	Proximity to the cities	Criteria weights
Temperature	1.0	1.0	2.0	1.0	3.0	3.0	5.0	0.231
Arsenic	1.0	1.0	2.0	1.0	3.0	5.0	5.0	0.249
Boron	0.5	0.5	1.0	1.0	1.0	2.0	2.0	0.124
Flowrates	1.0	1.0	1.0	1.0	2.0	3.0	3.0	0.186
Fluoride	0.3	0.3	1.0	0.5	1.0	1.0	2.0	0.090
Proximity to the roads	0.3	0.2	0.5	0.3	1.0	1.0	1.0	0.065
Proximity to the cities	0.2	0.2	0.5	0.3	0.5	1.0	1.0	0.054
						Consistency Index (CI)		0.0230

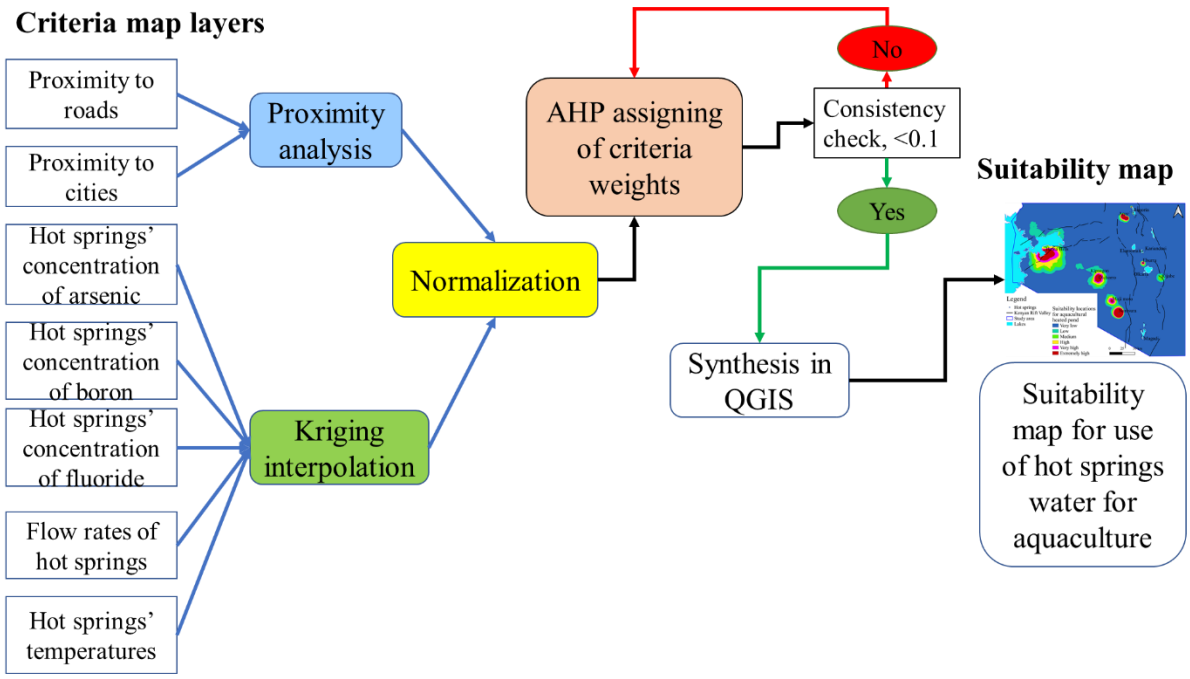

Figure 5.22 Flow map for rasterization, weighting, and overlay analysis of criteria map layers relevant to direct use of hot spring water for aquacultural pond heating.

5.7.2.2.4 Best direct use scenario: use of hot spring for geotourism

Geotourism involves visiting unique landscapes to experience their distinctive environments, aesthetics and heritage. In this study, we pay attention to volcanic geotourism related to hot springs. Erfurt (2021) defines hot spring tourism as visiting a site or facility associated with natural warm/hot mineral springs. Almost all of the accessible hot springs in the study area receive a considerable number of visitors, as shown in Figure 5.16(1). The hot springs on the western bank of Lake Bogoria are more popular as sightseeing attractions. The hot springs of

Lake Magadi are spectacular and popular too, though they are constrained by lack of economic infrastructure such as roads, restaurants, fresh piped water, and electricity.
Geotourism is highly dependent on existence of unique attractions and the enabling infrastructure to access them at an affordable cost. For use to characterize the suitability of hot springs in the study are for volcanic geotourism, we used the following criteria map layers: hot springs temperatures and number of visitors, and its proximity to urban area, roads, lodges/restaurants, and national parks. The proximity to lodges and national parks criteria are very much connected since they support one another and, hence marketed jointly. Presence of tarmac roads enable affordable transportation, while cities contribute a significant number of domestic tourists. These criteria were weighted in AHP as shown in Table 5.9 and later overlayed in QGIS as shown in Figure 5.23.

Table 5.9 AHP Pairwise comparison for criteria map layers for hot springs tourism and their respective weights and consistency index (CI).

Pairwise comparisons							
	Number of visitors	Temp	Proximity to the national parks	Proximity to the lakes	Proximity to the cities	Proximity to the roads	Criteria weights
Number of visitors	1.0	2.0	1.0	2.0	2.0	4.0	0.267
Temp	0.5	1.0	1.0	2.0	2.0	3.0	0.201
Proximity to the national parks	1.0	1.0	1.0	2.0	3.0	3.0	0.239
Proximity to the lakes	0.5	0.5	0.5	1.0	2.0	2.0	0.133
Proximity to the cities	0.5	0.5	0.3	0.5	1.0	1.0	0.089
Proximity to the roads	0.3	0.3	0.3	0.5	1.0	1.0	0.072
				Consistency Index (CI)			0.0300

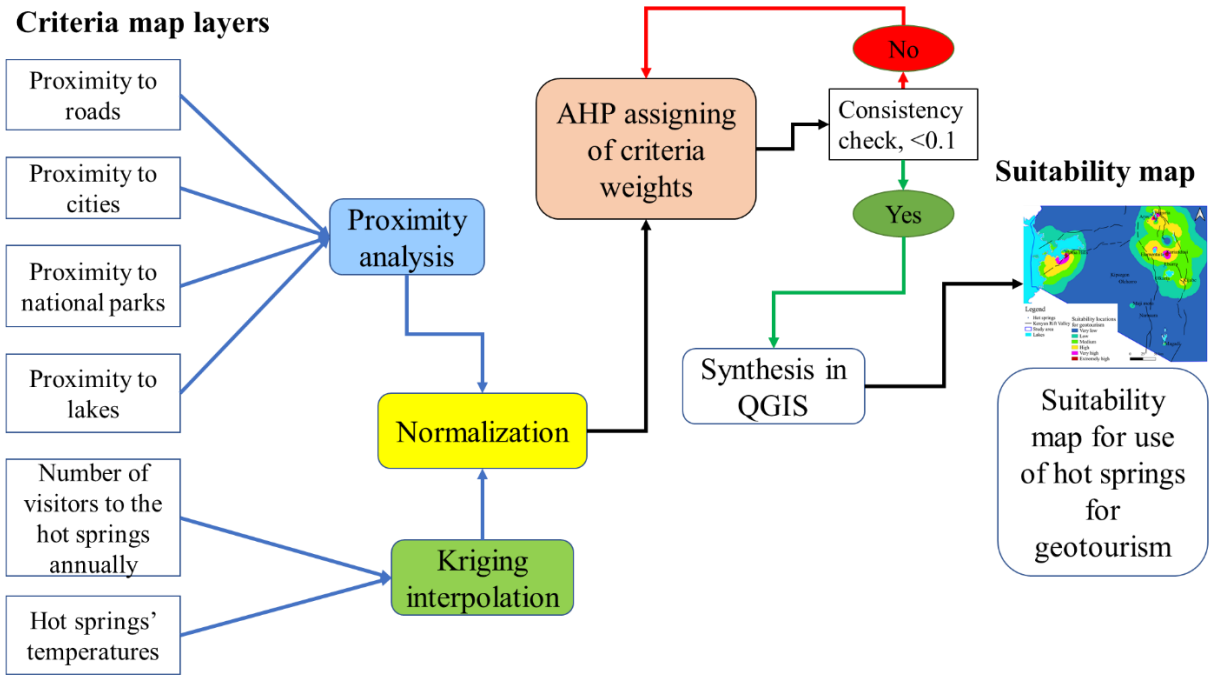

Figure 5.23 Flow map for rasterization, weighting, and overlay analysis of criteria map layers relevant to selection of suitability for hot spring tourism.

5.8 Results and discussion for the selection of the best direct use scenarios by GIS-based MCDM analysis of medium and low enthalpy geothermal resources with hot spring

Japan's "Onsen" culture is grounded on bathing in hot springs for balneological reasons (Serbulea & Payyappallimana, 2012). The Onsen industry has thrived on developing existing hot springs and shallow well drilling in high geothermal gradient locations. Such developmental pathways would unlock the economic potential of Kenyan hot springs and positively impact the visitors' health to the spas and swimming pools. Hot springs are a good tourist attraction, and their present utilization must be relooked at and re-evaluated for possible exploitation of the chances they provide. Kenya has over 150 documented hot springs with varying temperatures, geochemical properties, and flow rates. The current research looked at how quantifying their temperatures, flow rates, salinity, and harmful elements (As, F and B) may help unlock the potential of some of the underutilized hot springs and advise on the best utilization scenario for each hot spring site. The GIS-based MCDM analysis of hot spring parameters and the enabling economic factors relevant to the direct use of hot springs was aimed at creating suitability maps for each direct use scenario.

The results are shown in Figure 5.24. From Figure 5.24, (1) it is seen that hot springs best suited for domestic use were, Narosura, Majimoto, Kijabe, and Eburru, in that order. These hot springs had safe concentrations of As, F and B and were farthest from fresh surface water sources. Besides, Narosura and Majimoto have significant flow rates and temperatures below 45°C. Although Kipsegon and Olchorro share the same qualities, they occur near Mara River tributaries and are not subject to demands for water for domestic purposes. (2) hot springs best suited for spa, bathing or warming swimming pools were selected as those close to northern Lake Magadi, Homa Hills, Narosura, Kariandusi and Arus-Bogoria area. Currently, there are no spas, bathhouses or swimming pools associated with these hot springs. However, the local populations bathe frequently at the hot springs at Kariandusi, Bala (Homa Hills), and Narosura. This implies that providing clean commercial bathhouses and swimming pools would attract more users. In addition, the selected hot springs have flow rates of >20 t/h and could sustain self-cleaning outdoor swimming pools of 12 m by 24 m with a peak occupancy load of 300

persons. Since Lake Bogoria is located inside a national park and designated a Ramsar Site, construction of spas/swimming pools in the location is prohibited.

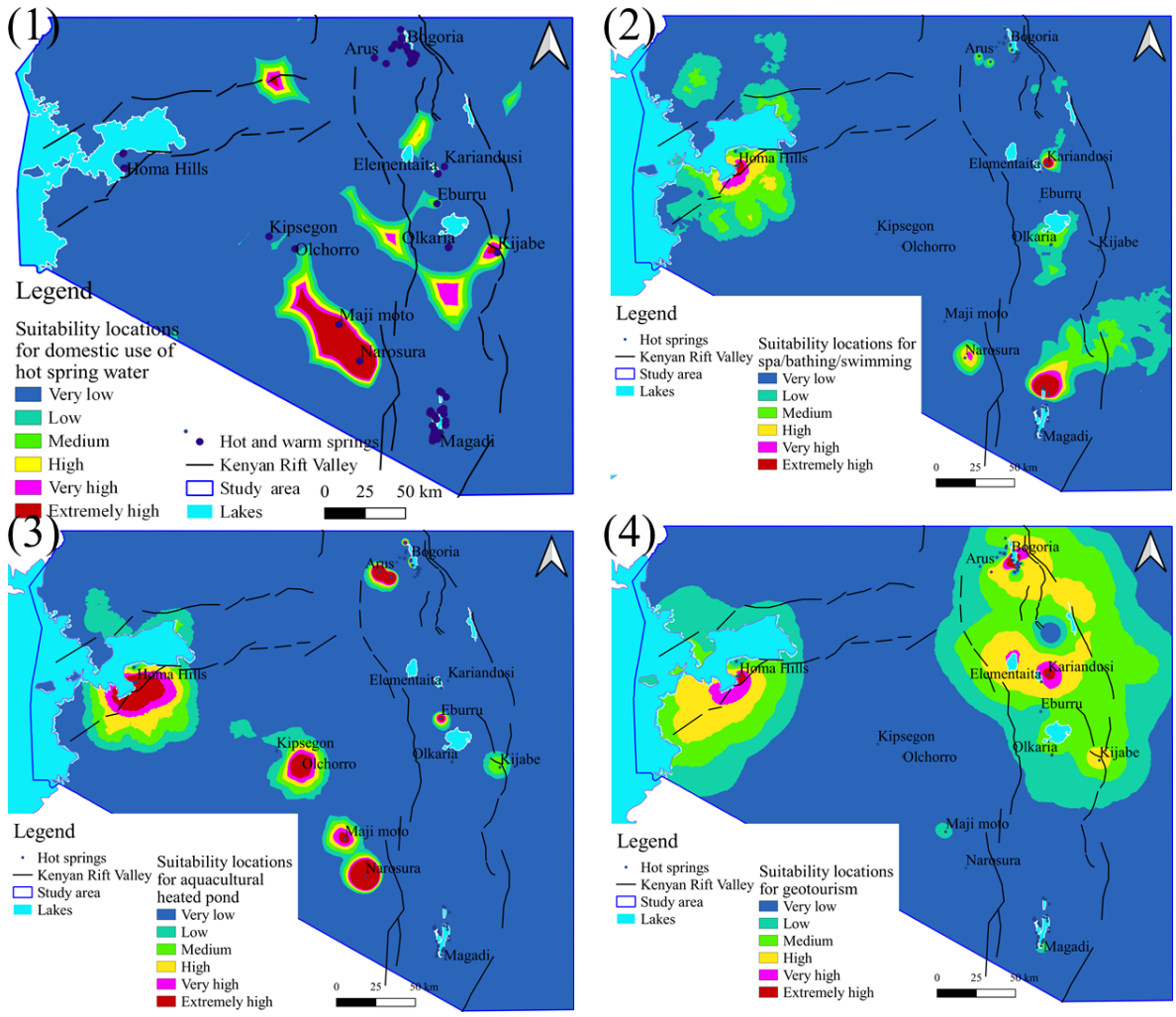

Figure 5.24 Suitability maps for direct use of hot springs for (1) domestic purposes, (2) spa, bathing or in swimming pools, (3) aquacultural pond heating and (4) volcanic geotourism.

From Figure 5.24 (3), it is seen that hot springs selected for commercial aquacultural pond heating were Narosura, Olchorro, Majimoto, Eburru, Kijabe, Arus, and Homa Hills. This selection heavily relied on hot spring parameters such as temperatures, flow rates, concentrations of As, B and F. Olchorro, Homa Hills and Arus hot springs were rated the best since they have little demands for domestic uses. However, Homa Hills hot springs require mixing with nearby river waters to dilute their fluoride concentrations from 90 ppm to below 3 ppm. (4) Hot springs selected as best suited for volcanic geotourism were Lake Bogoria, Kariandusi, Homa Hills, Kijabe, Lake Elementaita and Majimoto. These hot springs are already popular with domestic and international tourists. Their conservation and refurbishment to include car parks, washroom facilities and restaurants has potential to bolster the number of visitors and thus contribute positively to the economics of the local communities. Local community sell their traditional art crafts such as bead bangles and necklaces to tourists.
Table 5.10 ranks the hot springs and summarizes the best direct use of hot springs analyzed in the study area by listing the top two utilization scenarios per hot spring site. Figure 5.25 gives the visual impression of the overall direct use suitability for the hot springs. The figure was generated by overlaying the four suitability maps in Figure 5.24 and normalizing with the maximum score.

Table 5.10 Ranking of hot springs with their suitability to direct use

No	Hot spring site	DU suitability score	DU number 1	DU number 2
1	Lake Bogoria	0.999	Spa	Geotourism
2	Homa Hills (Bala)	0.974	Spa	Aquaculture
3	Narosura	0.996	Domestic use	Aquaculture
4	Arus	0.967	Aquaculture	Geotourism
5	Kariandusi	0.96	Spa	Geotourism
6	Majimoto	0.956	Domestic use	Aquaculture
7	Kijabe	0.941	Domestic use	Geotourism
8	Lake Bogoria Spa	0.940	Aquaculture	Spa
9	Eburru	0.924	Aquaculture	Domestic use
10	Olkaria	0.889	Geotourism	
11	Olchorro	0.872	Aquaculture	Domestic use
12	Kipsegon	0.822	Aquaculture	Geotourism
13	Lake Magadi (N)	0.705	Spa	Geotourism
14	Lake Magadi (S)	0.458	Spa	Geotourism

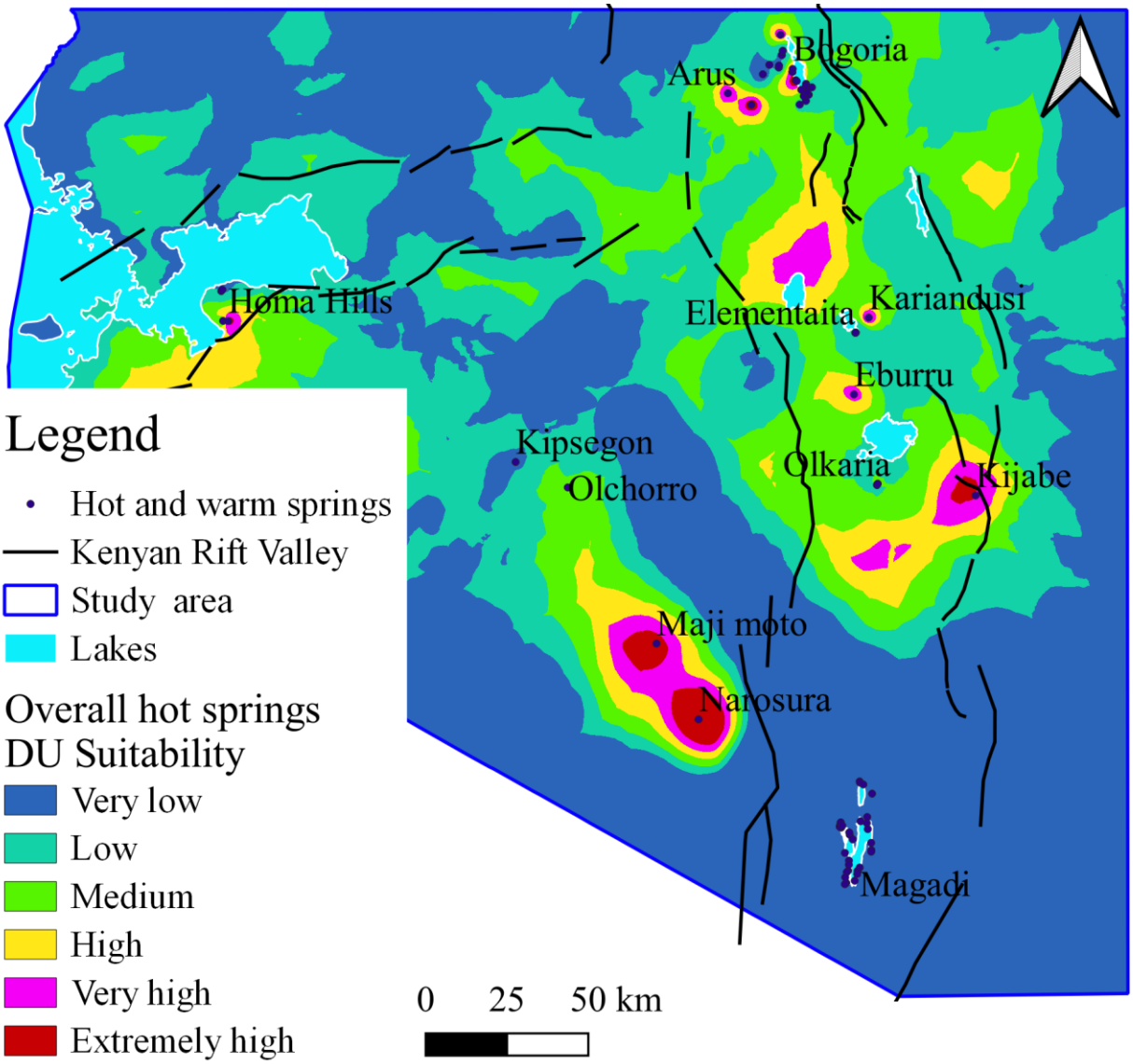

Figure 5.25 Overall map for hot springs' suitability for direct uses in domestic purposes, spa/swimming, aquacultural pond heating and as attractions for volcanic geotourism.

5.9 Conclusion

5.9.2 Water chemistry

The chapter brought to the fore the importance of hot springs to the undeveloped (having neither exploratory nor production wells), medium to low enthalpy geothermal resources. The hot spring waters were subjected to laboratory analysis to ascertain the concentration of various chemical substances which could help characterize their hydrothermal systems. The stable $\partial^{18}O$ and $\partial^{2}H$ analysis enable the source of hydrothermal waters to be investigated.

The water investigated was categorized into three classes; immature, partially equilibrated and fully equilibrated, as depicted in the Na-K-Mg ternary plots. Hydrochemistry was used to estimate subsurface temperatures. Narosura, Majimoto, Kipsegon, Lake Magadi south, and Olchorro were estimated to have reservoir temperatures below 100°C. Kariandusi, Kijabe, Homa Hills and Lake Magadi north were estimated to have reservoir temperatures ranging from 100 - 120°C. At the same time, Arus and Lake Bogoria were estimated to have reservoir temperatures of 150 - 180°C.

According to stable isotopic analysis, the recharge for most of the reservoirs near Kenyan endorheic lakes, such as Olkaria, Menengai and Eburru was found to be a mixture of rain infiltration and lake water. This inference was arrived at due to deep well waters from these geothermal fields plotted on Kenyan Rift Valley Lakes Evaporation Mean Water Line (KRVMWL). However, this was not the case with Homa Hills hot springs, which lie less than a kilometer from Lake Victoria, as they plotted on Continental African Rain Line (CARL). The Lake Magadi hot springs isotopes plotted on KRVMWL with a slight enrichment with respect to oxygen, implying that their sources could be rift Valley lakes located to the north. The waters from Narosura, Olchorro, Kipsegon, Kariandusi and Majimoto had little or no contribution from Kenyan Rift Valley lakes. All the geothermal resources whose stable isotopes were analyzed showed to be recharged by meteoric water.

5.9.3 Classification and selection of best direct use scenarios for the medium to low enthalpy geothermal resources

The geothermal resources arising from satellite magmatic intrusions on the east and west of Kenyan Rift Valley are given a blanket classification of "low enthalpy", while those arising from complex volcanoes within the rift floor are classified as "high enthalpy" (Tole, 1988). Using collected data on highest temperatures from surface manifestations and geothermometer data, these fields were reclassified into three broad categories: high, medium and low enthalpy geothermal resources, as shown in Figure 5.12. Contrary to the previous studies (Kanda, 2010;Tole, 2002), Homa Hills, Lake Magadi north and Mwananyamala were reclassified as medium enthalpy resources together with Arus and Lake Bogoria. Kijabe, Majimoto, Olchorro, Narosura, Kipsegon and Kariandusi maintained their status as low enthalpy geothermal resources.

Using hot spring data, such as temperature, flow rates, and concentrations of As, B, F and Cl, the hot springs' best direct use scenarios were selected by using a GIS-based MCDM framework. The over 150 hot springs in Kenya produce warm to hot water with a thermal capacity of over 275 MWt. Hence, by just harnessing the hot spring resources, Kenya can raise its direct use capacity from the current 18.5 MWt to about 300 MWt without drilling either shallow or deep wells. The hot springs best suited for domestic use and aquacultural pond heating were selected as Narosura, Majimoto, Olchorro, Kipsegon, Kijabe and Eburru. Those best suited for spa, bathing and swimming pools as well as volcanic geotourism, were classified as Lake Bogoria, Arus, Homa Hills, and Kariandusi. Overall, Lake Bogoria, Homa Hills and Narosura hot springs were rated the best for direct use of hot springs.

Validation of this selection was analyzed in the next chapter by analyzing existing case studies for the direct use of hot springs.

CHAPTER SIX

6. CASE STUDIES AND VALIDATION OF THE GIS-BASED MODEL

6.1 Introduction

This chapter will link the selection of direct use sites and scenarios to the existing case studies. All scientific prediction models are rarely without data and analytical uncertainties, which require to be constrained to reality (Wang et al., 2018b). In this research, several requisite steps involved dealing with uncertainty which may affect the results by a certain degree. Remote sensing and interpolation of data inevitably introduce uncertainties, hence the need for validation. Models, hypothesis and simulations are simulated using experimental data or similar studies. In this case, no similar studies exist, hence validation via case studies was the most reasonable way of checking suitability of the model.

6.2 Validation of the method and case studies

Existence of productive geothermal wells in high favourable regions of the suitability maps has been extensively applied as a verification method of the suitability selection maps in previous studies (Meng et al., 2021; Prol-Ledesma, 2000). When GIS-based MCDM methods are used for feasibility studies in exploration of geothermal resources deficient of case studies, surface manifestations such as hot springs serve the purpose of showing consistency of the study (Yalcin & Kilic, 2017). Unlike the previous studies, this study majored on selecting the best sites for nine DU scenarios for the high enthalpy geothermal resources in central and southern Kenyan Rift Valley. Olkaria, Menengai and Eburru geothermal resources have geothermal wells which provide hot brine for DU while the rest either have warm to hot water boreholes and surface manifestations like hot springs and fumaroles. The GIS-based AHP-WASPAS model classified the study area into six categories of DU suitability. With a scale range of 0 for the "Very low" class to 1.0 for the "Extremely high" class of DU favourability, as shown in Figure 4.16. The study area has eight DU case studies shown in Figure 6.1, which were used to validate the consistency of the GIS-based AHP-WASPAS model in carrying out feasibility studies for DU. The consistence is evaluated against the six classes of suitability as shown in the Table 6.1.

Table 6.1 The overlap of existing DU case studies to the six classes of suitability

DU case study	Heat capacity (MWt)	Prediction on suitability map	Scale of 0-1	SSI level
Olkaria spa	8.5	Extremely high	1.000	2.79
Oserian greenhouse warming	5.84	Very high	0.851	3.22
Menengai DU pilot project	4.2	Very high	0.834	1.74
Eburru crop drier	0.3	High	0.680	<0.1
Lake Elementaita hot springs public bath	0.15	Medium	0.504	0.85
Kariandusi hot springs spa	0.1	Low	0.343	0.69
Oreochromis fishpond heating	0.1	High	0.608	<0.1
Piped Kijabe hot springs waters for community use	0.1	Low	0.344	1.56

From Table 6.1, the GIS-based AHP-WASPAS analysis of DU suitability in the study area is consistent with commercial DU case studies such as Olkaria spa, Menengai DU pilot project, and Oserian greenhouse warming, which overlap with regions of high favourability. This could be influenced by availability of brine as well as some of the criteria used in this research.

However, the suitability map highlights Nakuru city (south of Menengai caldera), southern shore of Lake Naivasha and Olkaria domes as highly suitable for DU though they lack case studies. The DU case studies supported by hot springs were categorized in low to medium suitability. The main factor in establishing DU projects in Kenya Rift Valley is highly influenced by availability of hot geofluid as shown by some DU case studies; Kijabe, Kariandusi, Elementaita and Eburru. Since other crucial criteria needed to be included, these projects are limited to thermal usage of less than 0.3 MWt.

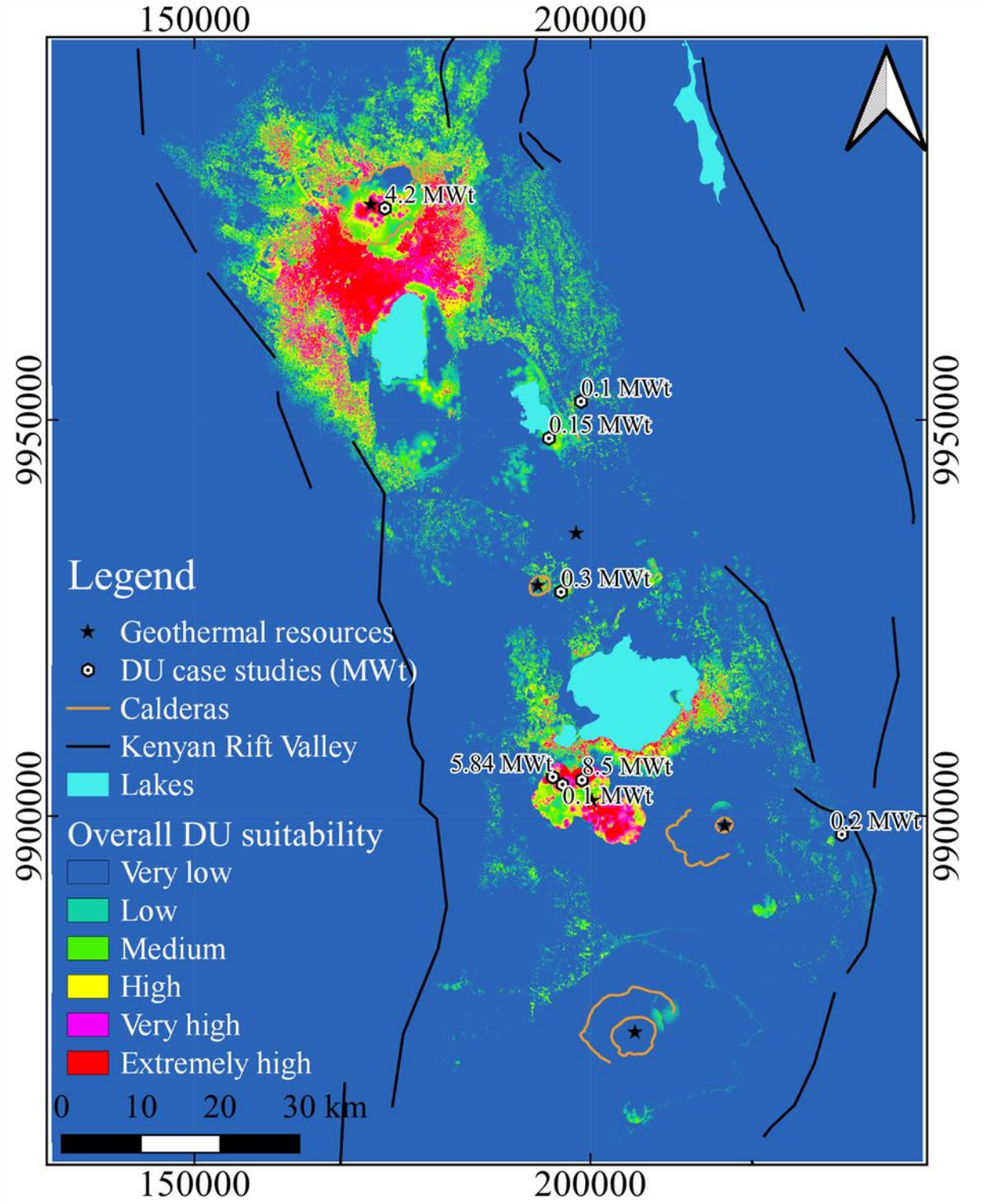

Figure 6.1. Location of DU case studies in central and southern Kenyan Rift Valley with their capacities in MWt.

6.3 Description of some of the case studies

Olkaria Spa and Oserian horticultural greenhouse warming projects trailblaze other commercial-scale DU projects in Kenya (Ngethe & Jalilinasrabady, 2021). They are located at Olkaria geothermal field. Oserian horticultural farm is located to the immediate northwest of Hell's Gate National Park. Hell's Gate National Park hosts Olkaria geothermal field. Oserian Development Company Limited (ODCL) currently exports over 32 varieties of fresh-cut flowers to Europe and the UK. To combat fungi that thrive at relative humidity levels exceeding 85%, such as Botrytis cinerea and Down Mildew, ODCL started heating horticultural greenhouses where roses are grown in 2001. Botrytis cinerea cause petal rotting while Down Mildew spreads fast, at a rate of 1 ha/48h, and affects leaf and stem. By heating the air within the greenhouse, relative humidity is kept below 85% and hence retarding fungal growth and improving growth rates by 25% compared to unheated greenhouses with the same variety of crops. Initially, ODCL used to enrich the greenhouses with CO_2 from well OW-101. However, the accompanying H_2S accelerated rusting of greenhouse structures, and CO_2 enrichment had to be stopped.

ODCL uses two plate heat exchangers (HE) to heat 2.0 million litres of water daily to a target temperature of 88°C near well OW-101 and, in turn, cool the total-flow fluid from 150°C to 45°C depending on well conditions since the well is cyclic, as shown in Figure 6.2. The mixture of steam and brine entering heat exchangers fluctuates between 3.5 to 7 bars, as shown in Figure 6.2. It exits at a pressure range of 0.88-2.85 bars before being dumped in a 4400 m^2 evaporation pond located 30 m from the wellhead. The heated water is then taken to a storage tank before being circulated to the greenhouses depending on relative humidity, which dictates the heating demand at the Oserian flower farm. The 60 t/h well, OW-101, currently heats about 48 ha of roses using hot water at 55°C that is passed in looped ¾" galvanized iron (GI) pipes positioned in the middle of the flower beds. Since relative humidity depends on rainfall and temperature, heating is done for 24 hours during June, July, and August and mostly at night during the remainder of the year. In addition to leasing well OW-01, ODCL also leases wells OW-202 and OW-306 from KenGen, which it uses to produce 1.3 MWe and 1.6 MWe, respectively, to run water pumps, refrigeration systems and other auxiliary systems on the farm. The heat exchangers at Oserian well OW-101 cool a mixture of brine and steam with a silica content of 600 ppm and pH 9.5 from an average of 140°C to 45°C without experiencing heavy silica scaling on the plates. Therefore, the plates are cleaned for silica scaling once per year, shown as two weeks of downtime in Figure 6.2 (days 330 to 345).

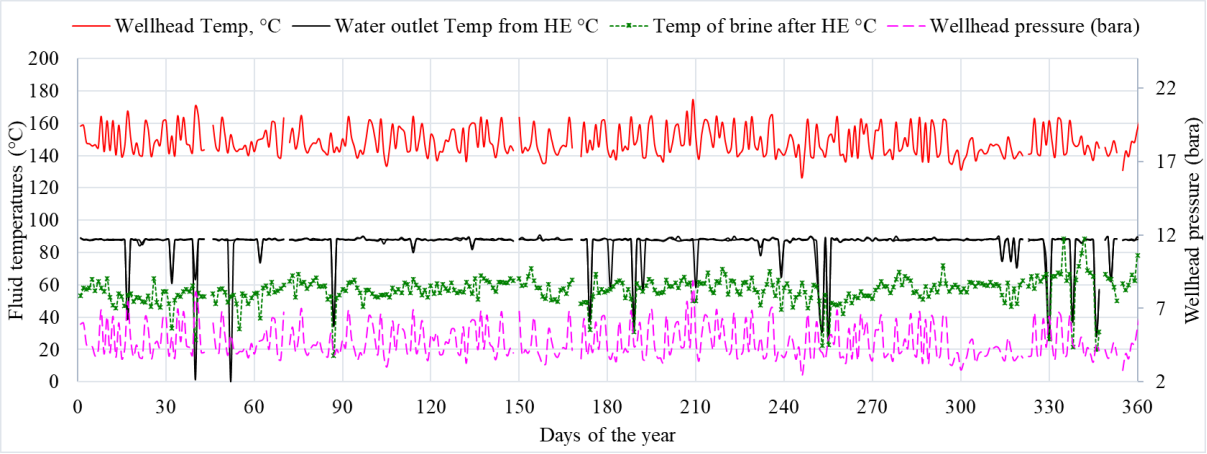

Figure 6.2. Temperatures at heat exchanger system of ODCL for 2019 (well OW-101).

In addition, ODCL uses condensate from well OW-202 to wash off the dust from a 1MW solar panels farm and heat 12 fishponds with a total area of 3091 m^2 for an aquaculture company, Oreochromis Kenya.
Olkaria Spa's 2800 m^2 swimming pool of geothermal brine had seen tremendous success with over 43,041 visitors in 2019 before Covid-19 restrictions affected the attendance to public facilities, as shown in Figure 6.4. Olkaria spa project was initiated in 2010 and commissioned in October 2013 at $1.2868 million. The spa has three lagoons with an area of 435 m^2, 500 m^2 and 2800 m^2 for Lagoon 1, Lagoon 2 and Lagoon 3, respectively and a kids' pool with an area of 250m^2. Figure 6.3 shows an infrared thermal image of the lagoons depicting temperature variations as brine flows from main brine line to the cold reinjection well. Lagoon 1 and Lagoon 2 serve as evaporation ponds with brine temperatures above 60°C; hence are restricted from visitors. At the same time, Lagoon 3 can accommodate 500-700 people at a go. Since 2014, the spa has been enjoying growing popularity to account for 30% of the visitors entering Hell's Gate National Park by 2019, as shown in Figure 6.4.

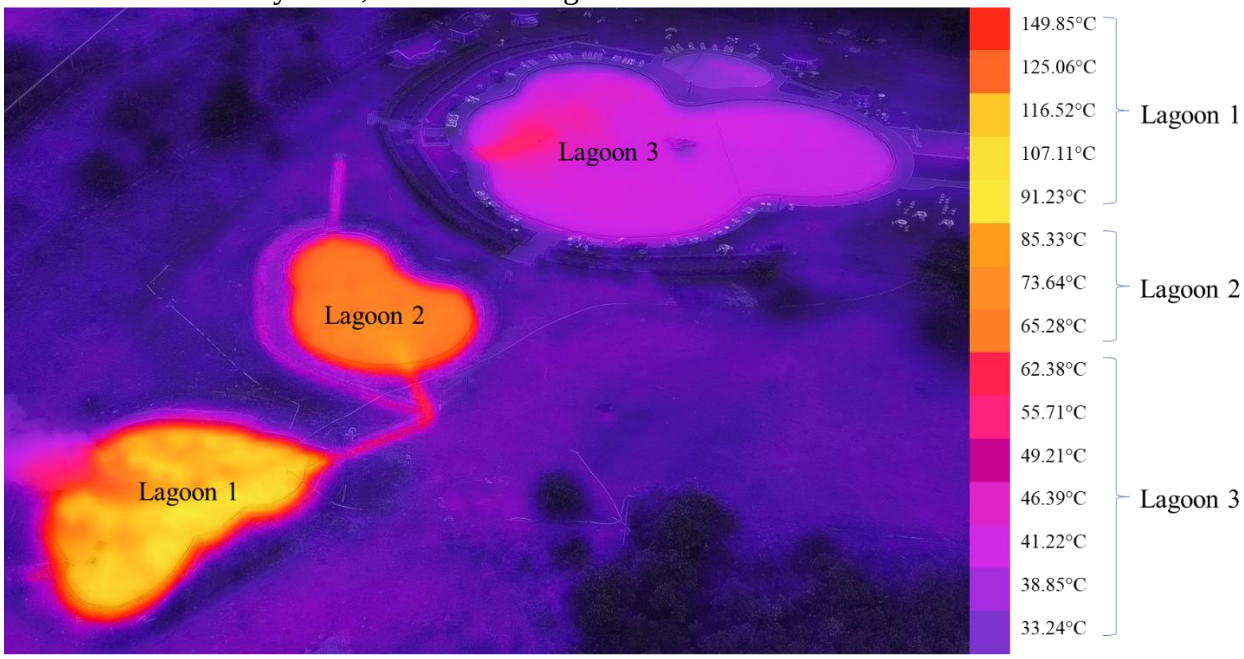

Figure 6.3. Thermal image of Olkaria spa showing temperature distribution in the lagoons. The infrared photo was taken at $\varepsilon = 0.93$ and 60° from zenith.

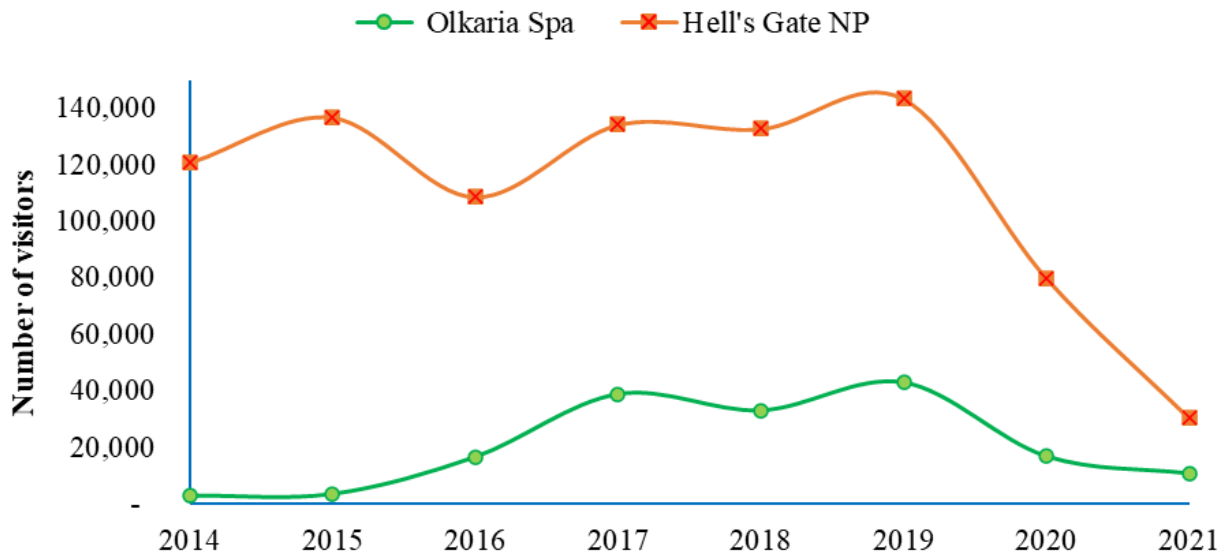

Figure 6.4. Number of visitors to both Olkaria Spa and the encompassing Hell's Gate National Park.

Olkaria geothermal spa is supplied by brine from a reinjection line en route to reinjection well OW-708 from separators providing the Olkaria II power plant with steam. 140 t/h of brine is tapped from the brine line and introduced at Lagoon 1 at 149.85℃, where 10-15% flash off to the atmosphere, thus cooling the brine to 93℃. The remaining brine evaporates in Lagoons 1 and 2 to exit at 85℃ and 63℃, respectively. Lagoon 3, accessible to visitors, receives brine at 62℃ that quickly mixes with existing brine to maintain a temperature range of 33-45℃ depending on the distance from the brine exit point. Evaporation from all the lagoons and a drop in temperature encourages both silica concentration and polymerization, resulting in high pH values, 9.93 at Lagoon 1 to 9.97 at Lagoon 3. Despite the Olkaria lagoons' evaporation and temperature drop from 150℃ to 33℃, the solubility of monomeric silica increases marginally downstream as the pH rises from 9.5 to 9.97 at Lagoon 3. The high pH nature of Olkaria fluids seems to affect the ionization of monomeric silica, thus retarding silica polymerization and deposition rate.

Menengai field has staged a DU pilot project where horticultural greenhouse warming of horticultural products such as capsicum and tomatoes has been successfully practised by using a low enthalpy well MW-03. Besides, they pasteurize milk, wash clothes for Geothermal Development Company (GDC) staff, and practice geothermally heated tilapia aquaculture. In 2019, a 6-tonne batch grain drier was introduced, with a capacity to dry 20-24 tonnes of grains per day. In 2021, GDC invited expression of interest from companies willing to carry out industrial heating by offering cheap geothermal energy in the form of 200 t/h of steam at 7 bara and up to 500 t/h of brine at 165℃. Besides the GDC pilot project, Nakuru city has grain dryers, milk pasteurization and cooking oil refineries located to the immediate southeast of Menengai caldera. These facilities are a testament to the commercial thermal needs available in the area. They also reinforce the sustainability of Nakuru county by providing raw materials and a market for milk processing and crop dryers.

Eburru geothermal field has also excelled in DU, with the oldest pyrethrum drier in Kenyan, which began operation in 1937. The drier is versatile, as it dries both vegetables, pyrethrum, and grains. It is powered by a shallow 30 m deep well that produces only steam. The condensate from the drier and many other fumaroles in the area are harnessed for domestic use.

Fumaroles in Elementaita are harnessed for domestic use, while the local community uses the hot springs for bathing and balneotherapy. Similarly, the water-scarce regions of Suswa also witness fumarole harnessing for domestic and irrigation use.

6.4 Conclusion

This model well predicted these case studies, implying its robustness as a planning and feasibility tool for direct utilization of geothermal energy. This method relies on the characteristics of a geothermal resource and the economic activities within its proximity which offer thermal demands that can be augmented by geothermal energy. By further matching these thermal needs to the available resource and the existing infrastructure such as roads, surface water, and the topographical traits of the area, the best direct utilization scenarios were chosen for each geothermal resource. As demonstrated by Figure 4.16 each DU scenario is site-specific. By specific matching of criteria to the attributes of the resource, most sustainable DU scenarios can be ranked for each geothermal resource site. However, to validate this matching, existing utilization case studies are necessary. This research used several DU case studies in Kenya to ascertain whether the model is in line with reality.

CHAPTER SEVEN

7. CONCLUSION AND RECOMMENDATIONS ON OPTIMISATION OF GEOTHERMAL RESOURCES IN KENYA

7.1 General conclusions

The present study majored in the selection of best direct use scenarios for Kenyan high, medium, and low enthalpy geothermal resources located in the central and southern Rift Valley. The main objectives were to select the best suited sites and direct scenarios to sustain economically viable utilization. Due to the huge disparity in volumes and temperatures of the fluids at high enthalpy and low enthalpy geothermal resources, the study was divided into two: high enthalpy and medium to low enthalpy geothermal resources.

For high enthalpy geothermal resources, the research applied a GIS-based MCDM model where AHP and WASPAS methods were hybridized for synergistic benefits. AHP provided decision weighting of criteria, while WASPAS provided the methodology of synthesizing different criteria map layers to obtain the best DU scenarios. Nine utilization scenarios and eleven criteria were chosen to represent the DU of geothermal energy in the study area. Firstly, the geothermal fluid's silica saturation index (SSI) in each site was analyzed, and the lowest heat extraction temperature was set. Then spatial topological data representing criteria maps were first mapped as vector layers and then interpolated using kriging and IDW methods to fill in missing data before being rasterized and normalized for proximity and suitability. The normalized criteria map layers were combined through the WASPAS method to obtain the best DU scenarios and best DU sites. The results were validated using existing DU case studies. The “Very high” and “Extremely high” zones were used to estimate heat demands and hence propose hot brine/water pipeline routes.

From this research, accurate matching of geothermal resource characteristics to economic activities in its proximity to thermal needs and existing infrastructure such as roads, water, and topography is the most influential stage of analyzing and precisely predicting the best DU scenarios. Each geothermal resource has different DU scenarios that match its resource traits, such as fluid volume, temperature, pH, and silica content. SSI limits utilization of a geothermal field, and careful analysis is crucial before brine utilization to inform the correct remedial steps necessary to deter silica scaling, such as pH modification. This research found SSI$\leq$2.0 to be safer in avoiding silica scaling without chemical remediation. Higher values of SSI allowed more geothermal wells to be utilized in DU.

For the low enthalpy geothermal, deep wells were a missing factor hence the hot spring fluids’ temperatures were less than 96°C. At these temperatures, high temperature direct use scenarios such as greenhouse warming, crop drying, water desalination, industrial heating and milk pasteurization were impossible. Therefore, the medium to low enthalpy geothermal resources were analyzed for domestic use, aquaculture, spa/bathing and hot spring tourism. Hence the silica saturation index (SSI) analysis and remote sensing of grain farms were removed from the GIS-based MCDM analysis. The steps began by carrying out of laboratory hydrogeochemistry analysis of sampled hot spring waters. The data was used to check the origin of hydrothermal recharge and for geothermometry of reservoir temperatures. The temperatures were used to classify the resources as high, medium or low enthalpy. This research used six characteristics of the hot spring to assess suitability for direct use: temperature, flow rate, concentrations of arsenic, boron, fluoride, chloride. And further six economic enabling factors for a successful direct use project: proximity to a road network, fresh surface water, national parks, cities, lakes and the number of visitors to the hot springs. These twelve criteria were analyzed in a QGIS-

based AHP framework to select the best direct use scenarios for the hot springs. The results reveal that hot springs provide a thermal heat of 275 – 300 MWt.
In conclusion, Olkaria, Menengai and Eburru were currently the best sites for DU as far as high enthalpy resources are concerned. Lake Bogoria, Homa Hills and Narosura were found to be the best suited for direct use in the category of medium to low enthalpy resources. Olkaria's best DU scenarios were found to be greenhouse warming, aquacultural pond heating and spa and bathing, while for Menengai, crop drying, and industrial processing came top. Eburru's DU scenarios were crop drying and milk pasteurization. These utilization scenarios confirm the immense contribution of agriculture and tourism to Kenya's economy and the need to optimize these utilization scenarios for more gains by expanding them to other undeveloped geothermal resources throughout Kenya. The validation of DU scenarios by existing case studies signifies that this model can be applied in other regions with geothermal resources as a planning and feasibility tool. Sensitivity analysis done on the parameters showed geothermal brine flow rate and temperature had the greatest impact in selection and ranking with maximum values of 17% and 11%.

7.2 Recommendation and future work

As a result of characterizing geothermal resources for direct use, several lost opportunities were identified:

- The separation pressures based on total amount of dissolved silica in a geothermal deep well need to be re-evaluated to account for pH.
- The Geothermal Development Company (GDC) has clearly documented the number of low pressure productive wells at menengai geothermal field and dedicated them for direct use. The number and locations of low pressures wells at Olkaria is obscure, yet it has more than 300 deep wells and higher seperation pressures than Menengai.
- The Geothermal Development Company (GDC) has set up a 4.2 MWt pilot project inside the Menengai crater, however, this research identifies high thermal demands and suitability for direct use outside the caldera, towards the Nakuru city. Hence, the economic viability of the direct use facilities (crop dryer, horticultural greenhouses, heated aquacultural ponds) need to be evaluated.
- More than 600 t/h of brine is not reinjected at the greater Olkaria geothermal field, This brine has the cpacity to drive a cascaded direct use project of 78 MWt.
- Kenya lacks a policy mandating hot springs to a central management body. Similar to Kengen and GDC, which manage high enthalpy resources. This is required to protect them from destruction, market them for volcanic tourism, and facilitate commercial exploitation.
- The local community which consumes hot spring water without being aware of the As, B, and F in in the water need to be sensitized.

  This research was limited by lack of data on geothermal gradients in the floor Kenyan rift valley. This is crucial for direct use facilitated by warm to hot shallow boreholes. In addition, the distribution maps for aquacultural ponds significantly affected this direct use scenario. This will be sought and incorporated in future studies.

.

References

Adiguzel, A., Ozkan, H., Baris, O., Inan, K., Gulluce, M., & Sahin, F. (2009). Identi fi cation and characterization of thermophilic bacteria isolated from hot springs in Turkey. *Journal of Microbiological Methods*, *79*(3), 321–328. https://doi.org/10.1016/j.mimet.2009.09.026

AGRCC. (2008). *Australian Code for Reporting of Exploration Results, Geothermal Resources and Geothermal Reserves*.

Ajayi, M., & Ayers, J. C. (2021). CH 4 and CO 2 diffuse gas emissions before , during and after a Steamboat Geyser eruption. *Journal of Volcanology and Geothermal Research*, *414*(June 2019), 107233. https://doi.org/10.1016/j.jvolgeores.2021.107233

Alexander, G. B., Heston, W. M., & Iler, R. K. (1954). The Solubility of Amorphous Silica in Water. *Journal of American Chemical Society*, *75*, 453–455.

Allen, D. J., Darling, W. G., & Burgess, W. G. (1989). *Geothermics and hydrogeology of the southern part of the Kenya Rift Valley with emphasis on MAgadi-Nakuru are*.

Ambunya, M. N. (2017). *Processing and inverting resistivity soundings from Mt. Longonot field, kenya. An interpretation of the subsurface resistivity structure in the context of the geothermal field*. United Nations University.

Arabameri, A., Rezaei, K., Cerda, A., Lombardo, L., & Rodrigo-Comino, J. (2019). GIS-based groundwater potential mapping in Shahroud plain, Iran. A comparison among statistical (bivariate and multivariate), data mining and MCDM approaches. *Science of the Total Environment*, *658*, 160–177. https://doi.org/10.1016/j.scitotenv.2018.12.115

Armannsson, H. (1994). *Geochemical Studies on three geothermal areas in West and Southwest, Uganda*.

Arnorsson, S. (1985). The use of mixing models and chemical geothermometers for estimating underground temperatures in geothermal systems. *Journal of Volcanology and Geothermal Research*, *23*, 299–335.

Arnorsson, S. (Ed.). (2000). *Isotopic and Chemical Techniques in Geothermal Exploration, Development and Use*. International Atomic Energy Agency.

Arnórsson, S. (1983). Chemical equilibria in icelandic geothermal systems-Implications for chemical geothermometry investigations. In *Geothermics* (Vol. 12, Issues 2–3, pp. 119–128). https://doi.org/10.1016/0375-6505(83)90022-6

Arusei, M. K. (1991). *Hydrochemistry of Olkaria and Eburru Geothermal Fields , Kenyan Rift Valley* (Vol. 2).

Baba, A., Bundschuh, J., & Chandrasekharam, D. (Eds.). (n.d.). *Geothermal systems and energy Resources: Turkey and Greece* (7th ed.). Taylor & Francis.

Bahadori, A. (2014). *Thermal Insulation for Oil, Gas, and Petrochemical industries* (One). Gulf Professional Publishing.

Ball, L. (1982). *Handbook of Geothermal Energy* (G. V Chilingar, L. M. Edwards, H. H. Rieke III, & F. W. H (Eds.)). Gulf Publishing Company.

Barrick, K. A. (2010). Environmental review of geyser basins: Resources, scarcity, threats, and benefits. *Environmental Reviews*, *18*(1), 209–238. https://doi.org/10.1139/A10-008

Bett, A. K., Dyson, M., Jalilinasrabady, S., & Shimada, H. (2019). Optimization of geothermal Binary Unit by Energy, Exergy and Sustainability Index: Comparative study of Olkaria Geothermal Field in Kenya and Chiweta Geothermal field in Malawi. *International Symposium on Earth Science and Technology*, 19–24.

Bett, A. K., & Jalilinasrabady, S. (2021a). Exergoeconomic Analysis for Optimized Combined Wet and Dry Cooling BinaryPower Plant at Olkaria I, Kenya. *Geothermics*, *95*(June), 102160. https://doi.org/10.1016/j.geothermics.2021.102160

Bett, A. K., & Jalilinasrabady, S. (2021b). Exergoeconomic Analysis for Optimized

Combined Wet and Dry Cooling BinaryPower Plant at Olkaria I, Kenya. *Geothermics*, *95*(May), 102160. https://doi.org/10.1016/j.geothermics.2021.102160
Biggs, J., Ayele, A., Fischer, T. P., Fontijn, K., Hutchison, W., Kazimoto, E., Whaler, K., & Wright, T. J. (2021). Volcanic activity and hazard in the East African Rift Zone. *Nature Communications*, *12*(1), 1–12. https://doi.org/10.1038/s41467-021-27166-y
Bilewu, S., & Sule, B. (2015). Selection of an Appropriate Interpolation Method for Rainfall Data In Central Nigeria. *Ethiopian Journal of Environmental Studies and Management*, *8*(4), 423. https://doi.org/10.4314/ejesm.v8i4.7
Bodvarsson, G. S., Pruess, K., Stefansson, V., Bjornsson, S., & Ojiambo, S. B. (1987). East Olkaria geothermal field, Kenya. 2. Predictions of well performance and reservoir depletion. *Journal of Geophysical Research*, *92*(B1), 541–554. https://doi.org/10.1029/JB092iB01p00541
Bonyo, E. A. (2020). *Scaling and Corrosion Mitigation in Olkaria Using Brine and Condensate Mixing Method*. *10*, 1–22.
Bozorg-Haddad, O., Zolghadr-Asli, B., & Loáiciga, H. A. (2021). *A Handbook on Multi Attribute Decision Making Methods* (1st ed.).
Brooker, D. B., Bakker-Arkema, F. W., & Hall, W. H. (1981). *Drying Cereals and Grains* (1st ed.). The Avi Publishing Company.
Brown, K. (2011). Thermodynamics and kinetics of silica scaling. *Proceedings International Workshop on Mineral Scaling 2011*, *May*, 1–9. https://doi.org/10.1002/jcc.21990
Budak, G., Chen, X., Celik, S., & Ozturk, B. (2019). A systematic approach for assessment of renewable energy using analytic hierarchy process. *Energy, Sustainability and Society*, *9*(1). https://doi.org/10.1186/s13705-019-0219-y
Chastain, R., Housman, I., Goldstein, J., Finco, M., & Tenneson, K. (2019). Remote Sensing of Environment Empirical cross sensor comparison of Sentinel-2A and 2B MSI , Landsat-8 OLI , and Landsat-7 ETM + top of atmosphere spectral characteristics over the conterminous United States. *Remote Sensing of Environment*, *221*(November 2018), 274–285. https://doi.org/10.1016/j.rse.2018.11.012
Cioni, R., Fanelli, G., Guidi, M., Kinyariro, J. K., & Marini, L. (1992). Lake Bogoria hot springs (Kenya): geochemical features and geothermal implications. *Journal of Volcanology and Geothermal Research*, *50*(3), 231–246. https://doi.org/10.1016/0377-0273(92)90095-U
Clarke, M. C. G., Woodhall, D. G., Allen, D., & Darling, G. (1990). *Geological, volcanological and hydrogeological controls on the occurrence of geothermal activity in the area surrounging Lake Naivasha, Kenya*.
Corrado, S., Aldega, L., Celano, A. S., De Benedetti, A. A., & Giordano, G. (2014). Cap rock efficiency and fluid circulation of natural hydrothermal systems by means of XRD on clay minerals (Sutri, Northern Latium, Italy). *Geothermics*, *50*, 180–188. https://doi.org/10.1016/j.geothermics.2013.09.011
Craig, H. (1961). Isotopic Variations in Meteoric Waters. *Science*, *133*(3465), 1702–1703.
Cressie, N. (1989). Spatial prediction and ordinary kriging. *Mathematical Geology*, *21*(4), 493–494. https://doi.org/10.1007/BF00897332
Darling, W. G., Gizaw, B., & Arusei, K. M. (1996). Lake-groundwater relationships and fluid rock interactions in the East African Rift Valley : isotopic evidence I. *Journal of African Earth Sciences*, *22*(4), 423–431.
Deibert, L., Hjartarson, A., McDonald, I., McIlveen, J., Thomson, A., Toohey, B., & Yang, D. (2010). *The Canadian Geothermal Code for Public Reporting: Reporting of Exploration Results, Geothermal Resources and Geothermal Reserves*.
DiPippo, R. (2008). Geothermal Power Generating Systems. In *Geothermal Power Plants*. https://doi.org/10.1016/b978-075068620-4.50009-5

DiPippo, R. (2012). Geothermal power plants. In *Comprehensive Renewable Energy*. https://doi.org/10.1016/B978-0-08-087872-0.00708-3

DiPippo, R. (2016). Geothermal Power Plants. In *Geothermal Power Plants: Principles, Applications, Case Studies and Environmental Impact: Fourth Edition* (4th ed.). Elsevier. https://doi.org/10.1016/C2014-0-02885-7

Dong, J., He, P., Liu, H., Guan, Y., Liu, H., Xia, W., & Dong, J. (2022). AHP-Based Evaluation of the Suitability of Shallow Geothermal Energy Utilization in GSHP System. *Frontiers in Energy Research*, *10*(March), 1–9. https://doi.org/10.3389/fenrg.2022.859454

Duan, Z., Pang, Z., & Wang, X. (2011). Sustainability evaluation of limestone geothermal reservoirs with extended production histories in Beijing and Tianjin, China. *Geothermics*, *40*(2), 125–135. https://doi.org/10.1016/j.geothermics.2011.02.001

Dudi, J. A. (2014). *Assessment of post harvest grain management operations and their effects on food security of smallholder households in Kisumu county, Kenya.* University of Nairobi.

Dunkley, P. N., Smith, M., Allen, D. J., & Darling, W. J. (1993). *The Geothermal Activity and Geology of Nothern Sector of the Kenya Rift Valley*. Nairobi

Elbarbary, S., Abdel Zaher, M., Saibi, H., Fowler, A.-R., & Saibi, K. (2022). Geothermal renewable energy prospects of the African continent using GIS. *Geothermal Energy*, *10*(1), 1–19. https://doi.org/10.1186/s40517-022-00219-1

Ellis, A. J., & Mahon, J. W. . (1977). *Chemistry and Geothermal Systems* (J. Denton (Ed.)). Academic Press.

Erfurt, P. (2021). *The Geoheritage of Hot Springs* (1st ed.). Springer Nature.

Erol, Ö., & Kilkiş, B. (2012). An energy source policy assessment using analytical hierarchy process. *Energy Conversion and Management*, *63*, 245–252. https://doi.org/10.1016/j.enconman.2012.01.040

Falcone, G., Antics, M., Baria, R., Bayrante, L., Conti, P., Grant, M., Hogarth, R., Juiliusson, E., Mijnlieff, H., & Nador, A. (2017). *Application of the United Nations Framework Classication for Resources (UNFC) to Geothermal Energy Resources - Selected case studies*.

Feizizadeh, B., Kienberger, S., & Kamran, K. V. (2015). Sensitivity and Uncertainty Analysis Approach for GIS-MCDA Based Economic Vulnerability Assessment. *Geographic Information Science*, *1*, 81–89. https://doi.org/10.1553/giscience2015s81

Firozjaei, M. K., Nematollahi, O., Mijani, N., Shorabeh, S. N., Firozjaei, H. K., & Toomanian, A. (2019). An integrated GIS-based Ordered Weighted Averaging analysis for solar energy evaluation in Iran: Current conditions and future planning. *Renewable Energy*, *136*, 1130–1146. https://doi.org/10.1016/j.renene.2018.09.090

Fleming, B. A., & Crerar, D. A. (1982). Silicic acid ionization and calculation of silica solubility at elevated temperature and pH application to geothermal fluid processing and reinjection. *Geothermics*, *11*(1), 15–29. https://doi.org/10.1016/0375-6505(82)90004-9

Fournier, R. ., White, D. E., & Truesdell, A. H. (1974). Geochemical indicators of subsurface temperature Part 1, Basic assumptions. *Journal of Research of the U.S Geological Survey*, *2*(3), 259–262.

Fournier, R. O. (1977). Chemical geothermometers and mixing models for geothermal systems. *Geothermics*, *5*, 41–50.

Fournier, R. O., & Rowe, J. J. (1977). The solubility of amorphous silica in water at high temperatures and high pressure. *Zeitschrift Fur Physikalische Chemie*, *62*, 1052–1056. https://doi.org/10.1524/zpch.1992.177.Part_2.225

Giggenbach, W. F. (1988). *Geothermal solute equilibria. Derivation of Na-K-Mg-Ca geoindicators* (Vol. 52).

Gitonga, G. (2016). *Model Organic Rankine Cycle for Brine at Olkaria Geothermal Field, Kenya*.

Gitonga, K., & Snyder, M. (2022). *Grain and Feed Annual*.

Glassley, W. E. (2012). Geothermal Energygeothermalenergy, Geologygeothermalenergygeologyand Hydrologygeothermalenergyhydrologyof. In R. A. Meyers (Ed.), *Encyclopedia of Sustainability Science and Technology* (pp. 4179–4190). Springer New York. https://doi.org/10.1007/978-1-4419-0851-3_230

GreenMax. (2020). *Technical Assistance to Identify The Most Suitable Direct Use Applications and Technologies in Low-To-Medium Temperature Geothermal Systems in Six African Countries*.

Gudni Axelsson et al. (2013). Updated Conceptual Model and Capacity Estimates for the Greater. *Thirty-Eighth Workshop on Geothermal Reservoir Engineering Stanford University, February 11-13, 2013*. https://pangea.stanford.edu/ERE/pdf/IGAstandard/SGW/2013/Axelsson.pdf

Gunnarsson, I., & Arnórsson, S. (2005). Treatment of Geothermal Waste Water to Prevent Silica Scaling. *Proceedings World Geothermal Congress 2005, April*, 24–29.

Hermant, B., Bellanger, M., Colas, E., Patriarche, D., & Auxiètre, J.-L. (2019). New Classification of High Temperature Geothermal Systems Based on 110 Geothermal Fields Worldwide. *European Geothermal Congress, June*, 11–14. https://www.researchgate.net/publication/333774574

Hottenroth, H., Sutardhio, C., Weidlich, A., Tietze, I., Simon, S., Hauser, W., Naegler, T., Becker, L., Buchgeister, J., Junne, T., Lehr, U., Scheel, O., Schmidt-Scheele, R., Ulrich, P., & Viere, T. (2022). Beyond climate change. Multi-attribute decision making for a sustainability assessment of energy system transformation pathways. *Renewable and Sustainable Energy Reviews*, *156*(August 2021), 111996. https://doi.org/10.1016/j.rser.2021.111996

Huenges, E. (2010). *Geothermal Energy Systems* (1st ed.). WILEY-VCH Verlag GmbH & Co. KGaA.

Hurwitz, S., & Manga, M. (2017). The Fascinating and Complex Dynamics of Geyser Eruptions. *Annual Review of Earth and Planetary Sciences*, *45*, 31–59.

IEA. (n.d.). *Kenya primary energy demand and GDP in the Africa Case, 2010-2040, IEA, Paris*.

Igunza, G., & Kanda, I. (2011). Geochemical Characteristics of the Mwananyamala Geothermal Prospect in the Kenyan Coast. *GRC Transactions Vol 35*.

Ioka, S., & Wakasa, S. (2021). Land-based aquaculture as a geothermal direct use and change of hot springs water quality. *Journal of the Japan Hydrological Society*, *51*(1), 3–5.

Jalilinasrabady, S. (2011). *Optimum Utilization of Geothermal Energy Employing Exergy Analysis and Reservoir Simulation*. Kyushu University.

Jalilinasrabady, S. (2022). Geothermal Resources Classification – A Review. *Geothermal Rising (GRC 2022)At: Reno - USA*.

Jalilinasrabady, S., & Itoi, R. (2013). Classification of Geothermal Energy Resources in Japan Applying Exergy Concept. *International Journal of Energy Research*, *37*(14), 1842–1850. https://doi.org/10.1002/er.3002

Jalilinasrabady, S., Tanaka, T., Itoi, R., & Goto, H. (2021). Numerical simulation and production prediction assessment of Takigami geothermal reservoir. *Energy*, *236*, 121503. https://doi.org/10.1016/j.energy.2021.121503

Jenicka, S. (2021). *Land Cover Classification of Remotely Sensed Images* (1st ed.). Springer Nature.

Jiho, H., & Yukio, Y. (2009). The Trends Regarding Foreign Tourists to Beppu, Oita Prefecture in Japan. *Journal of Ritsumeikan Social Sciences and Humanities*, *291*(1st),

61–72.
Jin, Z., Azzari, G., You, C., Di Tommaso, S., Aston, S., Burke, M., & Lobell, D. B. (2019). Smallholder maize area and yield mapping at national scales with Google Earth Engine. *Remote Sensing of Environment*, *228*(April), 115–128. https://doi.org/10.1016/j.rse.2019.04.016
Jones, B., & Peng, X. (2012). Amorphous calcium carbonate associated with biofilms in hot spring deposits. *Sedimentary Geology*, *269–270*, 58–68. https://doi.org/10.1016/j.sedgeo.2012.05.019
Kabak, M., Erbaş, M., Çetinkaya, C., & Özceylan, E. (2018). A GIS-based MCDM approach for the evaluation of bike-share stations. *Journal of Cleaner Production*, *201*, 49–60. https://doi.org/10.1016/j.jclepro.2018.08.033
Kamar, M., Wetangula, M., Langat, C., Mbito, M., Kabaka, B., Mogeni, E., Seneta, M., Lokorio, P., & Cherarkey, S. (2018). *Ad-hoc Senate Committee on the Maize Crisi in The Country: Report on Maize Crisis in Kenya*.
Kamunya, K. M. (2018). *δD and δ 18 O systematics in geothermal fluids, Olkaria Geothermal system, Kenya* (Issue November).
Kanda, I. (2010). *Geochemical Exploration of Geothermal Prospects : a Case Study of Menengai , Kenya*.
Kanda, I., Fujimitsu, Y., & Nishijima, J. (2019). Geological structures controlling the placement and geometry of heat sources within the Menengai geothermal field, Kenya as evidenced by gravity study. *Geothermics*, *79*(December 2018), 67–81. https://doi.org/10.1016/j.geothermics.2018.12.012
Kanda, I. K. (2019). *Geological, geophysical and geochemical studies on the hydrothermal system of Menengai geothermal field, Kenya*. Kyushu.
Kanda, I., Njue, L., & Suwai, J. (2012). Opportunities for Direct Use of Medium Enthalpy Geothermal Resources in Mwananyamala Geothermal Prospect, Kenya. *Proceedings of the 4th African Rift Geothermal Conference 2012, November*, 21–23.
Kanda, I., & Suwai, J. (2013). *Hydrogeochemistry of Shallow and Deep Water Aquifers of Menengai Geothermal Area , Kenya Rift Valley*. *37*, 403–410.
Karaşan, A., & Kahraman, C. (2020). Selection of the Most Appropriate Renewable Energy Alternatives by Using a Novel Interval-Valued Neutrosophic ELECTRE I Method. *Informatica (Netherlands)*, *31*(2), 225–248. https://doi.org/10.15388/20-INFOR388
Karingithi, C. W., Arnórsson, S., & Gródienvold, K. (2010a). Processes controlling aquifer fluid compositions in the Olkaria geothermal system, Kenya. *Journal of Volcanology and Geothermal Research*, *196*(1–2), 57–76. https://doi.org/10.1016/j.jvolgeores.2010.07.008
Karingithi, C. W., Arnórsson, S., & Gródienvold, K. (2010b). Processes controlling aquifer fluid compositions in the Olkaria geothermal system, Kenya. *Journal of Volcanology and Geothermal Research*, *196*(1–2), 57–76. https://doi.org/10.1016/j.jvolgeores.2010.07.008
Karingithi, C., & Wambugu, J. (2008). Geochemical Survey Case Study of Arus and Bogoria Geothermal Prospects. In *Short Course II on Surface Exploration for Geothermal Resources*. http://www.os.is/gogn/flytja/JHS-Skjol/Kenya 2007/Papers/25_Karinghiti and Wambugu.pdf
Kazimierczuk, A. H. (2019). Wind energy in Kenya: A status and policy framework review. *Renewable and Sustainable Energy Reviews*, *107*(December 2018), 434–445. https://doi.org/10.1016/j.rser.2018.12.061
Kenya Forest Service. (2021). *National Forest Resources Assessment (NFRA) Report 2021*.
Khaemba, A. W. (2015). Well design and well workover to land deep production casings in the Menengai field. *Transactions - Geothermal Resources Council*, *39*, 191–196.

Khanal, S., Fulton, J., & Shearer, S. (2017). An overview of current and potential applications of thermal remote sensing in precision agriculture. *Computers and Electronics in Agriculture*, *139*, 22–32. https://doi.org/10.1016/j.compag.2017.05.001

Kiavarz, M., & Jelokhani-Niaraki, M. (2017). Geothermal prospectivity mapping using GIS-based Ordered Weighted Averaging approach: A case study in Japan's Akita and Iwate provinces. *Geothermics*, *70*(July), 295–304. https://doi.org/10.1016/j.geothermics.2017.06.015

Kiende, R., & Kandie, R. (2015). Structural Geology of Eburru Volcano and Badlands Geothermal Prospects in Kenya. *Fourtieth Workshop on Geothermal Reservoir Engineering*, *1997*, 1–10.

Kinyanjui, S. (2014). *Direct use of geothermal energy in Menengai, Kenya: proposed geothermal spa and crop drying* (Issue 9). https://orkustofnun.is/gogn/unu-gtp-report/UNU-GTP-2013-09

Kiplagat, J. K., Wang, R. Z., & Li, T. X. (2011). Renewable energy in Kenya: Resource potential and status of exploitation. *Renewable and Sustainable Energy Reviews*, *15*(6), 2960–2973. https://doi.org/10.1016/j.rser.2011.03.023

Kipngok, J., Auko, L., Malimo, S., Igunza, G., Kangogo, S., Ranka, L., Bett, E., & Suwai, J. (2019). Geochemical characteristics of the Menengai geothermal Reservoir, Kenya: An overview. *Transactions - Geothermal Resources Council*, *43*, 674–689.

Kipngok, J., Magnússon, R., Melosh, G., Haizlip, J., Cumming, W., Hinz, N., Harvey, M., Alexander, K., Lopeyok, T., Mwakirani, R., Wamalwa, A. M., Malimo, S. J., & Auko, L. O. (2017). Geothermal conceptual model of Suswa Volcano, Kenya. *Transactions - Geothermal Resources Council*, *41*(Figure 1), 1153–1171.

Kiruja, J. (2017). *The viability of supplying an industrial park with thermal energy from Menengai geothermal field, Kenya* (Issue February). United Nations University.

Kiyota, Y., & Uchiyama, N. (2011). Silica scale prevention effects of brine pH modification at Hatchobaru power station , Japan. *Proceedings International Workshop on Mineral Scaling 2011 Manila, Philippines, May*, 25–27.

Krauskopf, K. B. (1956). Dissolution and precipitation of silica at low temperatures. *Geochimica et Cosmochimica Acta*, *10*, 1–26. https://doi.org/10.1016/0016-7037(56)90009-6

Kulakowski, K. (2021). *Understanding the Analytic Hierarchy Process* (1st ed.). Taylor & Francis Group, LLC.

Kummu, M., de Moel, H., Ward, P. J., & Varis, O. (2011). How close do we live to water? a global analysis of population distance to freshwater bodies. *PLoS ONE*, *6*(6). https://doi.org/10.1371/journal.pone.0020578

Kwambai, C. B. (2010). Exergy Analysis for Olkaria I Geothermal Power Plant, Kenya. *Worl Geothermal Congress*.

Lagat, J. (2010). Direct utilization of geothermal energy. *World Geothermal Congress*, 1–7. https://doi.org/10.3390/en3081443

Lagat, J., Muturia, C., Omondi, C., & Malimo, S. (2010). *Homa Hills Geothermal Prospect: A geothermal resource assessment project*.

Lamadrid, H. M., Rimstidt, J. D., Schwarzenbach, E. M., Klein, F., Ulrich, S., Dolocan, A., & Bodnar, R. J. (2017). Effect of water activity on rates of serpentinization of olivine. *Nature Communications*, *8*(May), 1–9. https://doi.org/10.1038/ncomms16107

Land O' Lakes. (2013). *Priority Geothermal Direct-Use Applications for Kenya : A Pre-Feasibility Study for Greenhouses*.

Land O' Lakes. (2014). *Priority Geothermal Direct-Use Applications for Kenya : A Pre-Feasibility Study for Crop Drying*.

Land O'Lakes. (2013). *Priority Geothermal Direct-Use Applications for Kenya : A Pre-*

Feasibility Study for Aquaculture.
Langat, R. K. (2015). *Topping Unit at Olkaria IV geothermal power plant, Naivasha Kenya* (Issue 18). The United Nations University (UNU).
Lawless, J. V, Ward, M., & Beardsmore, G. (2010). The Australian code for geothermal reserves and resources reporting : Practical experience. *Proceedings World Geothermal Congress*, 1–5. http://www.geothermal-energy.org/pdf/IGAstandard/WGC/2010/0406.pdf?
Lee, K. C. (2001). Classification of geothermal resources by exergy. *Geothermics*, *30*(4), 431–442. https://doi.org/10.1016/S0375-6505(00)00056-0
Lemenkova, P. (2020). Sentinel-2 for High Resolution Mapping of Slope-Based Vegetation Indices Using Machine Learning by SAGA GIS. *Transylvanian Review of Systematical and Ecological Research*, *22*(3), 17–34.
Lepuschitz, E. (2015). Geographic information systems in mountain risk and disaster management. *Applied Geography*, *63*, 212–219. https://doi.org/10.1016/j.apgeog.2015.06.014
Litman, T. (2022). *Evaluating Accessibility for Transport Planning: Measuring peoples' ability to reach desired services and activities*.
Lowell, R. P., & Rona, P. A. (2005). Hydrothermal Activity. In *Encyclopedia of Geology : Vol 5* (1st ed., pp. 362–372). Elservier Academic Press.
Lowry, J. H., Miller, H. J., & Hepnel, G. F. (1995). ARTICIE A GIS-Based Analysis of Gommunity Sensitivity Vulnerability to Hazardous on the Contaminants Mexi Border co / U . S . *Society*.
Lund, J. W., & Boyd, T. L. (2016). Direct utilization of geothermal energy 2015 worldwide review. *Geothermics*, *60*, 66–93. https://doi.org/10.1016/j.geothermics.2015.11.004
Lund, J. W., & Freeston, D. H. (2001). World-wide direct uses of geothermal energy 2000. *Geothermics*, *30*(1), 29–68. https://doi.org/10.1016/S0375-6505(00)00044-4
Lund, J. W., Freeston, D. H., & Boyd, T. L. (2005). Direct application of geothermal energy: 2005 Worldwide review. *Geothermics*, *34*(6), 691–727. https://doi.org/10.1016/j.geothermics.2005.09.003
Lund, J. W., Freeston, D. H., Boyd, T. L., & Rica, C. (2011). Direct utilization of geothermal energy 2010 worldwide review. *Geothermics*, *40*(3), 159–180. https://doi.org/10.1016/j.geothermics.2011.07.004
Lund, J. W., & Toth, A. N. (2021a). Direct utilization of geothermal energy 2020 worldwide review. *Proceedings World Geothermal Congress 2020*, 1–39. https://doi.org/10.1016/j.geothermics.2020.101915
Lund, J. W., & Toth, A. N. (2021b). Direct utilization of geothermal energy 2020 worldwide review. *Geothermics*, *90*(November). https://doi.org/10.1016/j.geothermics.2020.101915
Macarringue, L. S., Bolfe, É. L., Roberto, P., & Pereira, M. (2022). Developments in Land Use and Land Cover Classification Techniques in Remote Sensing : A Review. *Journal of Geographic Information System*, *14*, 1–28. https://doi.org/10.4236/jgis.2022.141001
Magnus, G., & Victor, L. (2012). *Geothermal Handbook: Planning and Financing Power Generation. Energy Sector Management Assistance Program (ESMAP)*.
Maier, D., & Bakker-Arkema, F. W. (2002). Grain drying systems. *Grain Elevator And Processing Society Facility Design Conference*, 53.
Maithya, J., & Fujimitsu, Y. (2019). Analysis and interpretation of magnetotelluric data in characterization of geothermal resource in Eburru geothermal field, Kenya. *Geothermics*, *81*(September 2018), 12–31. https://doi.org/10.1016/j.geothermics.2019.04.003
Maithya, J., Fujimitsu, Y., & Nishijima, J. (2020). Analysis of gravity data to delineate structural features controlling the Eburru geothermal system in Kenya. *Geothermics*,

85(December 2019), 101795. https://doi.org/10.1016/j.geothermics.2019.101795
Mangi, P. (2013). Direct Utilisation in Kenya : a Case of a Geothermal Spa and Demonstration Centre At Olkaria. *Short Course VIII on Exploration for Geothermal Resources*, 1–14.
Masum, M., & Akbar, A. M. (2019). The Pacific Ring of Fire is Working as a Home Country of Geothermal Resources in the World. *IOP Conference Series: Earth and Environmental Science*, *249*(1). https://doi.org/10.1088/1755-1315/249/1/012020
Mburu, M. (2010). Feasibility Study on Direct Utilisation of Energy from Geothermal Brine – A Case Study of Olkaria Geothermal Power Plant , Kenya. *Proceedings World Geothermal Congress 2010*, *April*, 9.
Meng, F., Liang, X., Changlai, X., & Wang, G. (2021). Geothermal resource potential assessment utilizing GIS - based multi criteria decision analysis method. *Geothermics*, *89*.
Mibei, G., Harðarson, B. S., Franzson, H., Bali, E., Geirsson, H., & Guðfinnsson, G. H. (2021). Eruptive history and volcano-tectonic evolution of Paka volcanic complex in the northern Kenya rift: Insights into the geothermal heat source. *Journal of African Earth Sciences*, *173*(January 2020). https://doi.org/10.1016/j.jafrearsci.2020.103951
Mibei, G., Mutua, J., Njue, L., & Ndongoli, C. (2016). Conceptual Model of the Menengai Geothermal Field. *Proceedings, 6th African Rift Geothermal Conference*, *November*, 1–13.
Mohamud, Y. N. (2013). *1D Joint Inversion of TEM and MT Data : Suswa Geothermal Field, Rift Valley, Kenya* (Issue 19). United Nations University.
Montcoudiol, N., Burnside, N. M., Györe, D., Mariita, N., Mutia, T., & Boyce, A. (2019). Surface and Groundwater Hydrochemistry of the Menengai Caldera Geothermal Field and Surrounding Nakuru County, Kenya. *Energies*, *12*(3131), 22.
Mostafaeipour, A., Dehshiri, S. J. H., Dehshiri, S. S. H., Jahangiri, M., & Techato, K. (2020). A thorough analysis of potential geothermal project locations in afghanistan. *Sustainability*, *12*(20), 1–17. https://doi.org/10.3390/su12208397
Murage, M. W., & Anderson, C. L. (2014). Contribution of pumped hydro storage to integration of wind power in Kenya: An optimal control approach. *Renewable Energy*, *63*(2014), 698–707. https://doi.org/10.1016/j.renene.2013.10.026
Mutonga, M. W. (2015). Stable isotopic composition of geothermal fields in Kenya ; The relationship between geothermal fields and Kenya Rift lakes waters. *World Geothermal Congress*, 9.
Mutonga, M. W., Sveinbjornsdottir, A., Gislason, G., & Amannsson, H. (2010). The Isotopic and Chemical Characteristics of Geothermal Fluids in Hengill Area, SW-Iceland (Hellisheidi, Hveragerdi and Nesjavellir Fields). *Proceedings World Geothermal Congress*, *April*, 25–29.
Mwangi, S. M. (2013). Application of Geochemical Methods in Geothermal Exploration in Kenya. *Procedia Earth and Planetary Science*, *7*(12), 602–606. https://doi.org/10.1016/j.proeps.2013.03.220
Mwarania, F. M. (2014). *Reservoir Evaluation and Modelling of the Eburru Geothermal System , Kenya* (Issue December). University of Iceland.
Mwaura, E., Bukker-Arkema, F. W., Guillaumon, M., Kulchik, S., & Ee, V. (1982). *Corn drying with biomass energy*. *82*(3520).
Mwaura, F. (2000). A Spatio-Chemical Survey of Hydrogeothermal Springs in Lake Elementaita, Kenya. *Discovery and Innovation*, *12*(1–2), 73–79. https://doi.org/10.1007/bf02442126
Mwawasi, H. M. (2012). Heat loss assessment of selected Kenyan geothermal prospects. *Transactions - Geothermal Resources Council*, *36 1*, 717–721.

Ngethe, J. (2021). Potential of Cascaded Use of Geothermal Energy to Uplift Fish Production in Kenyan Aquaculture. *GRC Transactions, Vol. 45, 2021*, 486–498.

Ngethe, J., & Jalilinasrabady, S. (2020). Considering future feasible agricultural projects for direct use of geothermal energy at eburru geothermal field. *Geothermal Resources Council Virtual Annual Meeting and Expo: Clean, Renewable and Always On, GRC 2020*, 268–283.

Ngethe, J., & Jalilinasrabady, S. (2021). Optimization of Geothermal Greenhouses Design for Kenyan Fresh-cut Flowers Source : KNBS 2020. *PROCEEDINGS, 46th Workshop on Geothermal Reservoir Engineering Stanford University, Stanford, California, February 15-17, 2021 SGP-TR-218*, 1–8.

Njenga, M., Gitau, J. K., & Mendum, R. (2021). Women's work is never done: Lifting the gendered burden of firewood collection and household energy use in Kenya. *Energy Research and Social Science*, *77*. https://doi.org/10.1016/j.erss.2021.102071

Nkapiani, M. N., & Kamunya, K. M. (2015). Application of Stable Isotope Geochemistry to Tracing Recharge and Flow Systems of Fluids in. *PROCEEDINGS, Fourtieth Workshop on Geothermal Reservoir Engineering Stanford University, Stanford, California, January 26-28, 2015*.

Noorollahi, Y., Ghasempour, R., & Jalilinasrabady, S. (2015). A GIS based integration method for geothermal resources exploration and site selection. *Energy Exploration and Exploitation*, *33*(2), 243–258. https://doi.org/10.1260/0144-5987.33.2.243

Noorollahi, Y., Itoi, R., Fujii, H., & Tanaka, T. (2008). GIS integration model for geothermal exploration and well siting. *Geothermics*, *37*(2), 107–131. https://doi.org/10.1016/j.geothermics.2007.12.001

Nouraliee, J., Porkhial, S., Ebrahimi, D., & Rahmani, M. R. (2014). Chemical studies on warm springs of West Azarbaijan province in the north west of Iran. *Journal of Scientific Research and Studies*, *1*(4), 65–72.

Ofwona, C. (2000). Recent Reservoir Studies of the Olkaria Geothermal Field, Kenya. *Proceedings World Geothermal Congress 2000*, 2767–2772.

Ofwona, C. (2010). Reservoir response to 28 years of production at Olkaria I - Kenya. *Transactions - Geothermal Resources Council*, *34 1*(April), 186–190.

Okamoto, G., Okura, T., & Goto, K. (1957). Properties of silica in water. *Geochimica et Cosmochimica Acta*, *12*(1–2), 123–132. https://doi.org/10.1016/0016-7037(57)90023-6

Okwiri, L. (2017). *Risk Assessment and Risk Modelling in Geothermal Drilling* (Issue February). United Nations University.

Omenda, P. A. (2010). Status of geothermal exploration in Kenya and future plans for its development. *World Geothermal Congress*, *April*.

Omenda, P., Mangi, P., Ofwona, C., & Mwangi, M. (2020). *Country Update Report for Kenya 2015-2019*. *4*.

Onono, P. A., Wawire, N. W. H., & Ombuki, C. (2013). The response of maize production in Kenya to economic incentives. *International Journal of Development and Sustainability*, *2*(2), 530–543.

Opondo, K. M. (2015). Carbonate Scale Formed in Well Ow-202 in Olkaria Central Field , Kenya. *Proceedings World Geothermal Congress 2015*, *April*, 10.

Oukil, A., & Govindaluri, S. M. (2020). A hybrid multi-attribute decision-making procedure for ranking project proposals: A historical data perspective. *Managerial and Decision Economics*, *41*(3), 461–472. https://doi.org/10.1002/mde.3113

Ouko, B., & Mangi, P. (2020). Increased utilization of the lagoon spa water in making skin care products. *Proceedings World Geothermal Congress 2020*, 1–6.

Özkan, B., Özceylan, E., & Sarıçiçek, İ. (2019). GIS-based MCDM modeling for landfill site suitability analysis: A comprehensive review of the literature. *Environmental Science*

and Pollution Research, *26*(30), 30711–30730. https://doi.org/10.1007/s11356-019-06298-1

Park, H., Choi, J., Park, N., & Choi, S. (2017). Sharpening the VNIR and SWIR bands of Sentinel-2A imagery through modified selected and synthesized band schemes. *Remote Sensing*, *9*(10), 1–20. https://doi.org/10.3390/rs9101080

Pirajno, F. (2020). Subaerial hot springs and near-surface hydrothermal mineral systems past and present, and possible extraterrestrial analogues. *Geoscience Frontiers*, *11*(5), 1549–1569. https://doi.org/10.1016/j.gsf.2020.04.001

Powell, T., Cumming, W., & Zealand, N. (2010). *SPREADSHEETS FOR GEOTHERMAL WATER AND GAS GEOCHEMISTRY*.

Power Africa. (2016). Development ot Kenya's power sector 2015-2020. In *Power Africa*. Power Africa.

Prol-Ledesma, R. M. (2000). Evaluation of the reconnaissance results in geothermal exploration using GIS. *Geothermics*, *29*(1), 83–103. https://doi.org/10.1016/S0375-6505(99)00051-6

Ragnarsson, Á. (2021). Geothermal Development in Iceland. *Proceedings World Geothermal Congress 2020+1 Reykjavik, Iceland, October*, 1–15. https://www.geothermal-energy.org/pdf/IGAstandard/WGC/2015/01077.pdf

Ramos-Escudero, A., García-Cascales, M. S., Cuevas, J. M., Sanner, B., & Urchueguía, J. F. (2021). Spatial analysis of indicators affecting the exploitation of shallow geothermal energy at European scale. *Renewable Energy*, *167*, 266–281. https://doi.org/10.1016/j.renene.2020.11.081

Raos, S., Hranić, J., Rajšl, I., & Bär, K. (2022). An extended methodology for multi-criteria decision-making process focused on enhanced geothermal systems. *Energy Conversion and Management*, *258*(December 2021), 115253. https://doi.org/10.1016/j.enconman.2022.115253

REN21. (2021). *Renewables 2021 Global Status Report*.

REN21. (2022). *Renewables 2022 Global Status Report*. https://www.ren21.net/reports/global-status-report/

Rezaie, M., & Aghajani, H. (2013). A New Combinational Terminology for Geothermal Systems. *International Journal of Geosciences*, *04*(01), 43–48. https://doi.org/10.4236/ijg.2013.41005

Robertson, E., Biggs, J., Edmonds, M., Clor, L., Fischer, T. P., Vye-Brown, C., Kianji, G., Koros, W., & Kandie, R. (2016). Diffuse degassing at Longonot volcano, Kenya: Implications for CO2 flux in continental rifts. *Journal of Volcanology and Geothermal Research*, *327*, 208–222. https://doi.org/10.1016/j.jvolgeores.2016.06.016

Roe, G., Benoit, D., & Pike, C. (2015). *Study of Direct Use Options for Hot Springs in Adak, Akutan & Atka*.

Ronoh, I. J. (2020). Geothermal Fluid for Industrial Use in the KenGen Green Energy Park , Kenya. *45th Workshop on Geothermal Reservoir Engineering*, 1–11.

Rybach, L. (2015). Classification of geothermal resources by potential. *Geothermal Energy Science*, *3*(1), 13–17. https://doi.org/10.5194/gtes-3-13-2015

Saaty, T. L. (1980). *The Analytic Hierarchy Process: Planning, Priority Setting, Resource Allocation* (1st ed.). McGraw-Hill Book Company, New York.

Saaty, T. L., & Kearns, K. P. (1985). *Analytical Planning; The Organization of Systems* (1st ed.). Pergamon Press Ltd.

Saaty, T. L., & Müjgan, O. S. (2005). *The Encyclicon: A dictionary of decisions with dependence and feedback based on the anlytic network process* (1st ed.). RWS Publications.

Sadeghi, A., Larimian, T., & Molabashi, A. (2012). Evaluation of Renewable Energy Sources

for Generating Electricity in Province of Yazd: A Fuzzy Mcdm Approach. *Procedia - Social and Behavioral Sciences*, *62*, 1095–1099. https://doi.org/10.1016/j.sbspro.2012.09.187

Saitet, D., & Rop, E. (2015). *Use of Feed Zones to Interpret Subsurface Permeability Controls : A Case Study of Olkaria Geothermal System*. 1–11.

Saraswat, S. K., Digalwar, A. K., Yadav, S. S., & Kumar, G. (2021). MCDM and GIS based modelling technique for assessment of solar and wind farm locations in India. *Renewable Energy*, *169*, 865–884. https://doi.org/10.1016/j.renene.2021.01.056

Sekento, R. (2012). Geochemical and Isotopic Study of the Menengai Geothermal Field, Kenya. In *Geothermal Trainning Programme* (Issue 31).

Senapathi, V., Viswanathan, P. M., & Chung, S. Y. (2019). *GIS and Geostatistical Techniques for Groundwater Science* (1st ed.). Elservier.

Şener, E., & Şener, Ş. (2021). Exploration of geothermal potential using integrated fuzzy logic and analytic hierarchy process (AHP) in Ağrı , Eastern Turkey. *Turkish J Earth Sci*, *30*, 1134–1150. https://doi.org/10.3906/yer-2105-18

Serbulea, M., & Payyappallimana, U. (2012). Onsen (Hot Springs) in Japan – Transforming terrain into healing landscapes. *Health and Place*, *18*(6), 1366–1373. https://doi.org/10.1016/j.healthplace.2012.06.020

Setianto, A., & Triandini, T. (2015). Comparison of Kriging and Inverse Distance Weighted (Idw) Interpolation Methods in Lineament Extraction and Analysis. *Journal of Southeast Asian Applied Geology*, *5*(1), 21–29. https://doi.org/10.22146/jag.7204

Setiawan, F. A., Rahayuningsih, E., Petrus, H. T. B. M., Nurpratama, M. I., & Perdana, I. (2019). Kinetics of silica precipitation in geothermal brine with seeds addition: minimizing silica scaling in a cold re-injection system. In *Geothermal Energy* (Vol. 7, Issue 1). https://doi.org/10.1186/s40517-019-0138-3

Shortall, R., Davidsdottir, B., & Axelsson, G. (2015). Geothermal energy for sustainable development: A review of sustainability impacts and assessment frameworks. In *Renewable and Sustainable Energy Reviews* (Vol. 44, pp. 391–406). Elsevier Ltd. https://doi.org/10.1016/j.rser.2014.12.020

Simić, V., Lazarević, D., & Dobrodolac, M. (2021). Picture fuzzy WASPAS method for selecting last-mile delivery mode: a case study of Belgrade. *European Transport Research Review,Springer*, *13*(43).

Slocum, M., & Kessler, H. (2014). *Thematic Cartography and Geovisualization* (3rd ed.). Pearson Education Limited.

Stein, E. W. (2013). A comprehensive multi-criteria model to rank electric energy production technologies. *Renewable and Sustainable Energy Reviews*, *22*, 640–654. https://doi.org/10.1016/j.rser.2013.02.001

Takase, M., Kipkoech, R., & Essandoh, P. K. (2021). A comprehensive review of energy scenario and sustainable energy in Kenya. *Fuel Communications*, *7*, 100015. https://doi.org/10.1016/j.jfueco.2021.100015

Tasri, A., & Susilawati, A. (2014). Selection among renewable energy alternatives based on a fuzzy analytic hierarchy process in Indonesia. *Sustainable Energy Technologies and Assessments*, *7*, 34–44. https://doi.org/10.1016/j.seta.2014.02.008

Tchobsala, Haman, B., Gilbert, H., Paul, K., Danra, D. D., & Denis, K. (2022). Socio-economic and environmental influences of firewood exploitation in Bongor and its surroundings (Chad). *Environmental Challenges*, *6*(October 2021), 100406. https://doi.org/10.1016/j.envc.2021.100406

Thráinn Fridriksson and Halldór Ármannsson. (2007). *APPLICATION OF GEOCHEMISTRY IN GEOTHERMAL RESOURCE*.

Tinti, F., Kasmaee, S., Elkarmoty, M., Bonduà, S., & Bortolotti, V. (2018). Suitability

evaluation of specific shallow geothermal technologies using a GIS-Based multi criteria decision analysis implementing the analytic hierarchic process. *Energies*, *11*(2). https://doi.org/10.3390/en11020457
Tole, M. P. (1988). Low enthalpy geothermal systems in Kenya. *Geothermics*, *17*(5–6), 777–783. https://doi.org/10.1016/0375-6505(88)90037-5
Tole, M. P. (2002). The potential of geothermal systems in Kenya for balneological use. *Environmental Geochemistry and Health*, *24*(2), 103–110. https://doi.org/10.1023/A:1014208705778
Tole, P. M. (1992). Geochemical studies of the geothermal systems in Kenya: II. The Majimoto geothermal field. *Journal of African Earth Sciences, 14*(3), 387–391.
Traineau, H., Sanjuan, B., & Lasne, E. (2015). Main results of a long-term monitoring of the Bouillante geothermal reservoir during its exploitation. *Proceedings World Geothermal Congress 2015 Melbourne, Australia, 19-25 April 2015*, *November 2015*.
Varma, M. K. S. (2016). Pixel-based Classification Using Support Vector Machine Classifier. *2016 IEEE 6th International Conference on Advanced Computing*, 51–55. https://doi.org/10.1109/IACC.2016.20
Wamalwa, A. M., Mickus, K. L., & Serpa, L. F. (2013). Geophysical characterization of the menengai volcano, central kenya rift from the analysis of magnetotelluric and gravity data. *Geophysics*, *78*(4). https://doi.org/10.1190/geo2011-0419.1
Wamalwa, R. N., Waswa, A. K., Nyamai, C. N., Mulwa, J., & Ambusso, W. J. (2016). Evaluation of the Factors Controlling Concentration of Non-Condensable Gases and Their Possible Impact on the Performance of Geothermal Systems: Case Study of Olkaria Wells in the Kenyan Rift Valley. *International Journal of Geosciences*, *07*(03), 257–279. https://doi.org/10.4236/ijg.2016.73021
Wang, X., Wang, G. L., Gan, H. N., Liu, Z., & Nan, D. W. (2018). Hydrochemical Characteristics and Evolution of Geothermal Fluids in the Chabu High-Temperature Geothermal System, Southern Tibet. *Geofluids*, *2018*, 1–15. https://doi.org/10.1155/2018/8532840
Wang, Z., Deng, Y., & Fan, Y. (2018). Validation plays the role of a “bridge” in connecting remote sensing research and applications. *Advances in Space Research*, *62*(1), 55–64. https://doi.org/10.1016/j.asr.2018.04.018
Watson, A. (2013). *Geothermal Engineering* (1st ed.). Springer New York. https://doi.org/10.1007/978-1-4614-8569-8
Waweru, J., Omondi, P., Ngene, S., Mukeka, J., Wanyonyi, E., Ngoru, B., Mwiu, S., Daniel, M., & Fredrick, L. (2021). *National Wildlife Census 2021 Report*.
WestJec, & JICA. (2017). *Project for reviewing GDC’s geothermal development strategy in the Republic of Kenya final report*.
WHO. (2003). *Arsenic in drinking water*.
WHO. (2022). *Guidelines for drinking water quality*.
Wightman, D., & Wall, G. (1985). The spa experience at Radium hot springs. *Annals of Tourism Research*, *12*, 393–416.
Williams, C. F., Reed, M. J., & Anderson, A. F. (2011). Updating the Classification of Geothermal Resources. *Proceedings, Thirty-Sixth Workshop on Geothermal Reservoir Engineering, Stanford University, Stanford, California, January 31 - February 2, 2011*, SGP-TR-191.
Witter, J. B., Trainor-Guitton, W. J., & Siler, D. L. (2019). Uncertainty and risk evaluation during the exploration stage of geothermal development: A review. *Geothermics*, *78*(October 2018), 233–242. https://doi.org/10.1016/j.geothermics.2018.12.011
World Health Organization. (1996). *Trace Elements in Human Nutrition and Health*.
Xu, D., Ren, J., Dong, L., & Yang, Y. (2020). Portfolio selection of renewable energy-

powered desalination systems with sustainability perspective: A novel MADM-based framework under data uncertainties. *Journal of Cleaner Production*, *275*. https://doi.org/10.1016/j.jclepro.2020.124114

Yalcin, M., & Kilic, G. F. (2017). A GIS-based multi criteria decision analysis approach for exploring geothermal resources: Akarcay basin (Afyonkarahisar). *Geothermics*, *67*, 18–28. https://doi.org/10.1016/j.geothermics.2017.01.002

Yen, C. L. (Alan), Kyutoku, Y., & Dan, I. (2018). Exploring Tourists' Perceptions of Traditional and Contemporary Hot Springs Hotels in Japan. *International Journal of Hospitality and Tourism Administration*, *19*(3), 336–360. https://doi.org/10.1080/15256480.2017.1324341

Zarrouk, S. J., & Purnanto, M. H. (2015). Geothermal steam-water separators: Design overview. *Geothermics*, *53*, 236–254. https://doi.org/10.1016/j.geothermics.2014.05.009

Zavadskas, E. K., Antucheviciene, J., Turskis, Z., & Adeli, H. (2016). Hybrid multiple-criteria decision-making methods: A review of applications in engineering. *Scientia Iranica*, *23*(1), 1–20. https://doi.org/10.24200/sci.2016.2093

Zavadskas, E. K., Turskis, Z., Antucheviciene, J., & Zakarevicius, A. (2012). Optimizationation of Weighte ed Aggre egated Sum Pro duct Ass sessment t. *Electronics and Electrical Engineering*, *2012.No.6*(122), 3–6.

Zhanxue, S., Jinhui, L., & Bai, G. (2010). Hydrogeochemistry and Direct Use of Hot Springs in Jiangxi Province , SE-China. *Proceedings World Geothermal Congress 2010 Bali, Indonesia, 25-29 April 2010*, *April*, 1–5.

Zimmerman, L. D., & Zimmerman, M. B. (1991). A Comparison of Spatial Semivariogram Estimators and Corresponding Ordinary Kriging Predictors. *Technometrics*, *33*(1), 77–91.

Appendix

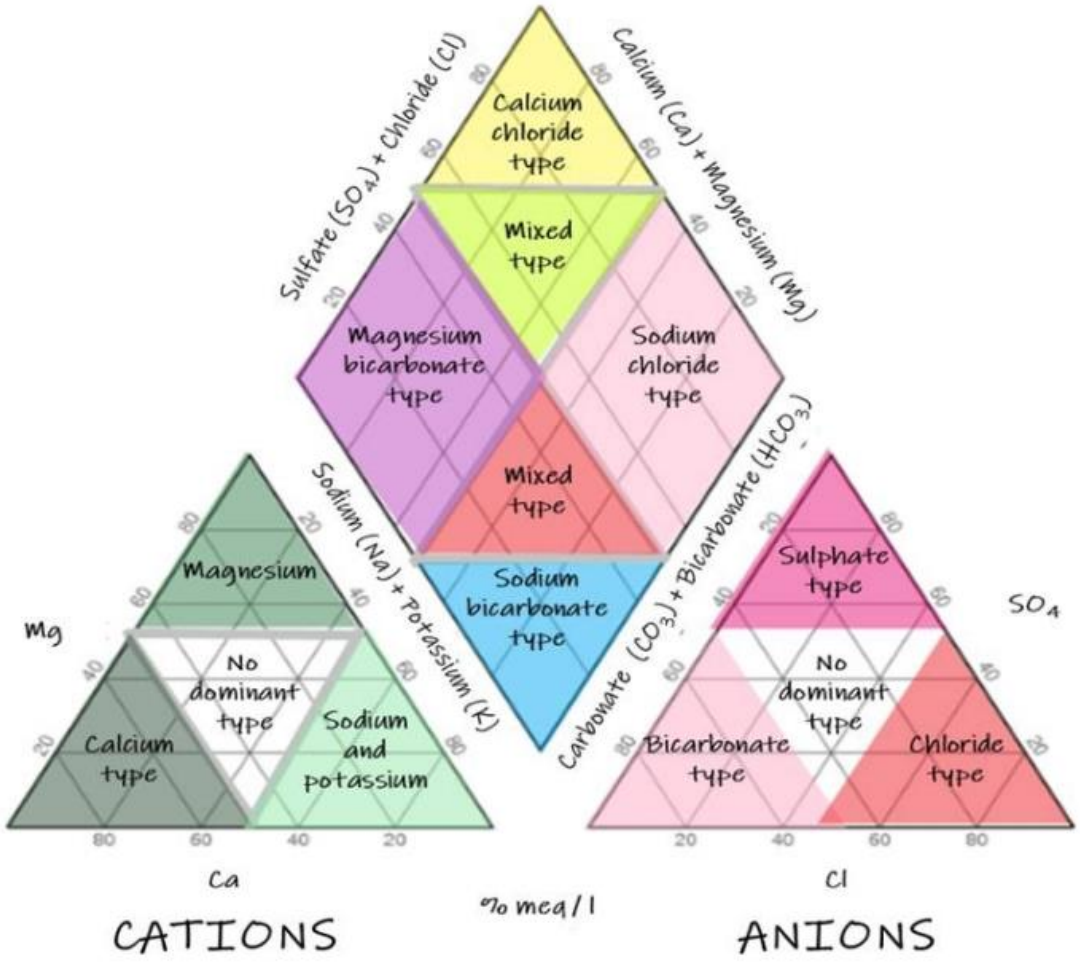

Piper diagram for classifying the types of geochemical waters

(https://hatarilabs.com/ih-en/what-is-a-piper-diagram-and-how-to-create-one)

Cation geothermometry equations (Arnorsson, 2000; Baba et al., n.d.; DiPippo, 2008).

Geothermometer	Equations (concentration of Na, K mg/L)	
Na–K (100–275°C)	$T = 856 / (\log Na/K + 0.857) - 273.15$	Truesdell (1976)
Na–K	$T = 883 / (\log Na/K + 0.780) - 273.15$	Tonani (1980)
Na–K (25–250°C)	$T = 933 / (\log Na/K + 0.993) - 273.15$	Arnorsson *et al*. (1983)
Na–K (250–350°C)	$T = 1319 / (\log Na/K + 1.699) - 273.15$	Arnorsson *et al*. (1983)
Na–K	$T = 1217 / (\log Na/K + 1.483) - 273.15$	Fournier (1979)
Na–K	$T = 1178 / (\log Na/K + 1.470) - 273.15$	Nieva and Nieva (1987)
Na–K	$T = 1390 / (\log Na/K + 1.750) - 273.15$	Giggenbach (1988)
K–Mg	$T = 2330 / (\log K^2/Mg + 7.35) - 273.15$	Fournier (1991)
K–Mg	$T = 1077 / (\log K^2/Mg + 4.033) - 273.15$	Fournier (1991)
K–Mg	$T = 4410 / (\log K/Mg + 14.0) - 273.15$	Giggenbach (1988)
K–Li	$T = 2200 / (\log Li/Mg + 5.470) - 273.15$	Kharaka and Mariner (1989)
Na–Li	$T = 1590 / (\log Na/Li + 0.779) - 273.15$	Kharaka *et al*. (1982)
Na–Li (Cl > 0.3 M)	$T = 1195 / (\log Na/Li + 0.130) - 273.15$	Fouillac and Michard (1981)
Na–Li (Cl < 0.3 M)	$T = 1000 / (\log Na/Li + 0.389) - 273.15$	Fouillac and Michard (1981)
Na–Li	$T = 1267 / (\log Na/Li + 0.07) - 273.15$	Verma and Santoya (1997)
Li–Mg	$T = 2200 / (\log Li/(Mg)^{1/2} + 5.47) - 273.15$	Kharaka and Mariner (1989)
Na–Ca	$T = 1096.7 / (\log Na/\sqrt{Ca} + 2.37) - 273.15$	Tonani (1980)
K–Ca	$T = 1930 / (\log K/\sqrt{Ca} + 2.920) - 273.15$	Tonani (1980)
Na–K–Ca	$T = 1647 / (\log(Na/K) + \beta[\log(\sqrt{Ca}/Na) + 2.06 + 2.47) - 273.15$ $\beta = 4/3$ for $T < 100°C$; $= 1/3$ for $> 100°C$	Fournier and Truesdell (1973)

Production wells connected to Olkaria IV power plant

No	Well No	Location	Plant	Year production started	Separator Station	Current Status
1	OW-901A	Domes	Olkaria IV	2019	OW-921	Producing
2	OW-901B	Domes	Olkaria IV	2019	OW-921	Producing
3	OW-903A	Domes	Olkaria IV	2014	SD1	Producing
4	OW-903B	Domes	Olkaria IV	2014	SD1	Producing
5	OW-904	Domes	Olkaria IV	2014	SD1	Producing
6	OW-904A	Domes	Olkaria IV	2014	SD1	Producing
7	OW-904B	Domes	Olkaria IV	2014	SD1	Producing
8	OW-907A	Domes	Olkaria IV	2014	SD4	Producing
9	OW-908	Domes	Olkaria IV	2014	SD2	Producing
10	OW-908A	Domes	Olkaria IV	2014	SD2	Producing
11	OW-908B	Domes	Olkaria IV	2015	SD2	Producing
12	OW-909	Domes	Olkaria IV	2015	SD2	Producing
13	OW-909A	Domes	Olkaria IV	2015	SD2	Producing
14	OW-910	Domes	Olkaria IV	2015	SD2	Producing
15	OW-910A	Domes	Olkaria IV	2015	SD2	Producing
16	OW-910B	Domes	Olkaria IV	2015	SD2	Producing
17	OW-914	Domes	KWG 06 & 07	2014	OW-914	Producing
18	OW-914A	Domes	KWG 04	2014	OW-914A	Producing
19	OW-914B	Domes	KWG 05	2014	OW-914B	Producing
21	OW-921	Domes	Olkaria IV	2019	OW-921	Producing
22	OW-921A	Domes	Olkaria IV	2019	OW-921	Producing
23	OW-926A	Domes	Olkaria IV	2019	OW-926	Producing
24	OW-926B	Domes	Olkaria IV	2019	OW-926	Producing

Reinjection wells for Olkaria IV.

No	Well	Location	Year Inj. Started	Remarks
1	OW-906A	Domes	2015	Brine Reinjection
2	OW-911	Domes	2015	Brine Reinjection
3	OW-911A	Domes	2015	Brine Reinjection
4	OW-913A	Domes	2015	Brine Reinjection
5	OW-902A	Domes	2015	Condensate Reinjection
6	OW-921B	Domes	2019	Hot Reinjection

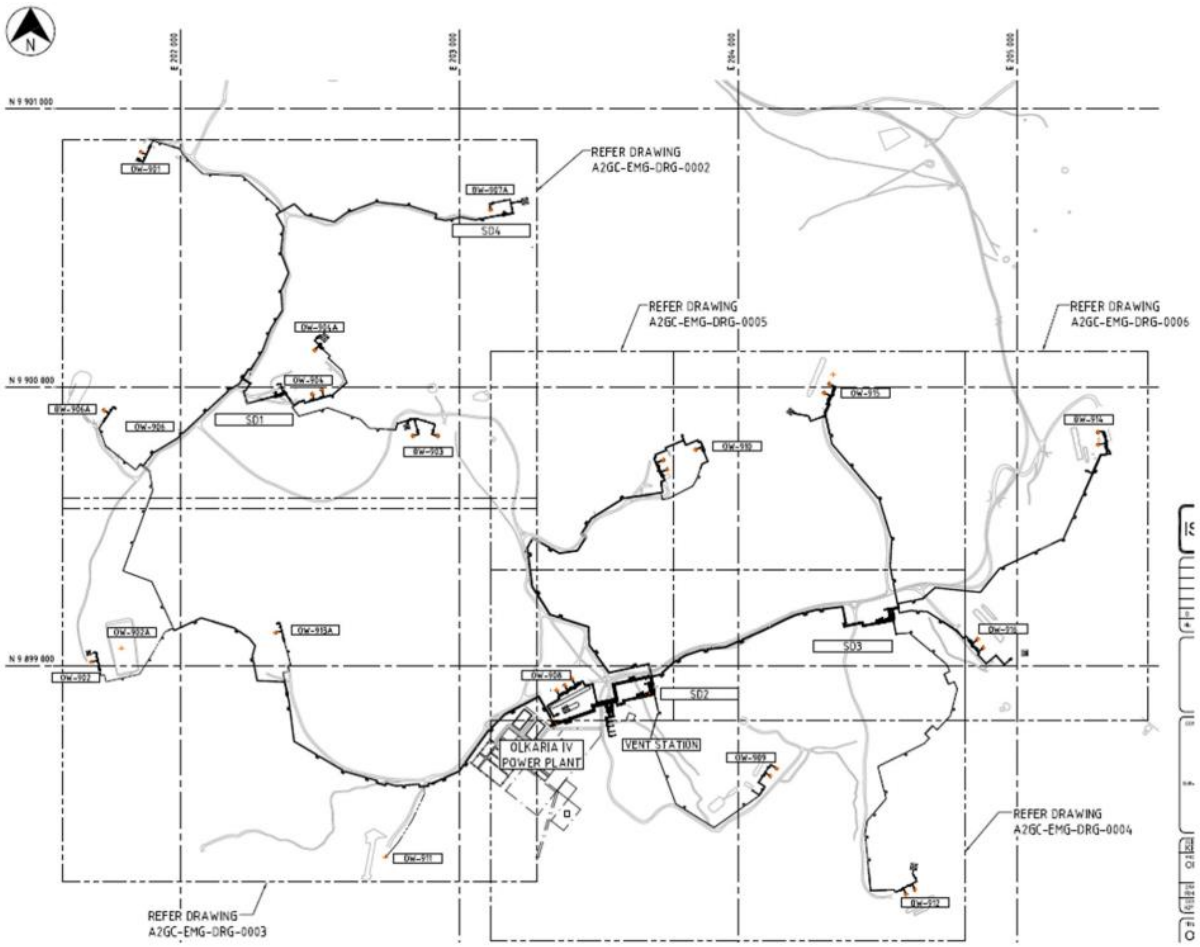

Pipe line connection and well locations supplying steam to Olkaria IV power plant (Langat, 2015).